STUDIES ON WALL-SLIP IN ENTANGLED POLYMERIC LIQUIDS

Submitted in partial fulfillment of the requirements
for the degree of

DOCTOR OF PHILOSOPHY

by

YOGESH MORESHWAR JOSHI

DEPARTMENT OF CHEMICAL ENGINEERING
INDIAN INSTITUTE OF TECHNOLOGY, BOMBAY

2001

Thesis entitled **STUDIES ON WALL-SLIP IN ENTANGLED POLYMERIC LIQUIDS**,

By **YOGESH MORESHWAR JOSHI**

is approved for the degree of **DOCTOR OF PHILOSOPHY**.

Examiners

_____

_____

_____

Supervisors

_____

_____

Chairman

_____

Date:_____

Place:_____

INDIAN INSTITUTE OF TECHNOLOGY, BOMBAY, INDIA

Certificate of Course Work

This is to certify that Mr. Yogesh Moreshwar Joshi was admitted to the candidacy of the Ph.D. Degree on August 1997, after successfully completing all the courses required for Ph.D. programme. The details of the course work are given below.

Sr. No	Course No.	Course Name	Credits
1	CL 601	Advanced Transport Phenomena	6
2	CL 602	Mathematical and Statistical Methods in Chemical Engineering	6
3	CL 603	Optimization	6
4	CL 629	Natural and Synthetic Polymers	6
5	CL 691	Experimental and Numerical Methods Lab	10
6	ME 613	Finite Element and Boundary Element Methods	6
7	CLS801	Seminar	4

I. I. T. Bombay Dy. Registrar (Academic)

Dated: 27/07/1998

ACKNOWLEDGMENT

I would like to express my sincere gratitude to Dr. R. A. Mashelkar for his invaluable guidance. His continuous encouragement and support has always been an inspiration and a source of energy for me. He has not only guided in just technical matters but has always taught several important points to gain maturity in the field of academics through minor incidences. His vision, his capacity to work and his nature of thinking has always influenced me in many ways. I thank him for all his efforts and help

I would also like to thank Dr. Ashish Lele for his patient guidance. The success of our association lies only in his calm and understanding nature. There were several incidences when we had a conflict on technical issues, but thanks to him that it NEVER caused any bitterness in our relationship. I haven t yet seen so close guide-student relationship anywhere, like the way he keeps with his students. More than a guide, he is always like a friend for all of us. I sincerely thank Dr. Lele for all his well wishes, help and guidance. I think it was my great fortune that I could work so closely with a trio Dr. Mashelkar, Dr. Khakhar and Dr. Lele. I also like to thank Mrs. Ashwini Lele for her patience and help. She was one of the sufferers of my association with sir. I must have spoiled her countless Sunday evenings by suddenly appearing and taking hold of sir for some crude technical discussions that may go on for hours.

I take this opportunity to thank Prof. Devang Khakhar. I have always been a great admirer of his innocence, sincerity and dedication. I have seen very few people like him who live science. It is my pleasure for being associated with him. I sincerely thank him for all the trouble and efforts he has taken for me.

I am grateful to Dr. Paul Ratnasamy, Director, NCL for giving me an opportunity to work in NCL. I would like to thank Dr. B. D. Kulkarni for his support and interest in my work throughout my stay in NCL. I thank Dr. Sivram for his just presence (because unfortunately I was not associated with him in any way) in NCL that is an inspiration for me. Further, I also thank Dr. M. G. Kulkarni for his readily rendered help.

Many thanks are due to Dr. Badiger, Dr. Vivek Ranade, Dr. Premnath, Dr. (Mrs.) Jog, Dr. Ramesh, Dr. R. A. Kulkarni, Dr. Ravikumar, Mr. Deodhar, Mr. Daibhate for their help and support. I would like to acknowledge the efforts taken by RPC members, Prof. Juvekar, Prof. Shenoy and Prof. Nanawati. In the course of this work, they have given many useful suggestions, which has helped to improve the quality of the work.

In this thesis several figures have been incorporated that have been published elsewhere. I would like to thank various institutes and publishers namely Society of Rheology, American Chemical Society, American Institute of Physics and Elsevier Science and various individuals namely Prof. E. B. Bagley, Prof. de Vargas, Prof. Hatzikiriakos and Prof. Morton Denn for allowing me to use the copyrighted figures in my thesis.

A very special note of thanks is due to Prof. G. Marrucci and Dr. G Ianniruberto for an insightful remark on our approach (chapter 6), which helped us improve the analysis of our molecular model substantially. I am also grateful to anonymous referees of our publications, which have helped us to improve the quality of our work.

Its my pleasure to thank all the past and present PPCites namely, Sunil, Vivek, Sandeep, Madhuri, Shyni, Nitin, Rajendra, Arpita, Harsha, Nivedita, Abhijeet, Prashant, Girish, Ajit, Leena, Shailesh and Bakul. Special thanks are due to Shyni for her association for last four years. She has always taken care of lab and each of us like an elder sister. At their respective periods in PPC, all of them have helped me in every possible way and kept

the cherish atmosphere in the lab. Thanks are also due to Mr. Shukla and Mr. Dhupe for their help.

Special thanks are also due to various friends in IIT namely, Ashok, Arup, Ashish, Milind Mhalgi and Hemant Joshi for helping me in various ways. I would also like to thank the Academic office of IIT for their prompt help.

I would like to acknowledge the financial assistance of The British Society of Rheology for partially sponsoring my visit to Cambridge for attending an International Congress of Rheology. Finally, last but not the least, I greatly acknowledge the financial assistance from Council of Scientific and Industrial Research for providing a research fellowship for carrying out the doctoral work.

Table of Contents

Chapter No. **Title** **Page No.**

List of Figures and Tables

NOMENCLATURE

a	Entanglement distance or tube diameter, m
a	Arbitrary parameter in equation (3.25), *dimensionless*
a'	Monomeric length scale, m
A	Parameter in equation 4.5, *dimensionless*
b	Arbitrary parameter in equation (3.26), *dimensionless*
c	Number of chains per unit volume, $chains/m^3$
C^*	Critical (overlap) concentration, kg/m^3
D	Diameter of the capillary, m
D_{rep}	Reptative or longitudinal diffusivity, m^2/s
D_I	Diffusivity due to dominant relaxation mode in the interfacial region, m^2/s
$\underset{\approx}{E}$	Deformation or strain tensor, *dimensionless*
ΔE_{adh}	Adhesive energy, $(\Delta E_d - \Delta E_a)$, J
ΔE_a	Activation energy for adsorption, J
ΔE_d	Activation energy for desorption, J
ΔE_m	Elastic free energy of the attached molecule relative to the equilibrium (no-flow) state, J
E_H	Energy of hydrogen bonding, J
f	Rate of creation of segments, *dimensionless*
$f(q)$	Switch function, *dimensionless*
F_H	Force of adsorption, N
F_T	Tension in freely joined chain, N
F_f, F_g	Arbitrary parameter in equation (3.28) and (3.29), *dimensionless*
g	Rate of loss of segments, *dimensionless*
G	Segment renewal probability, *dimensionless*
G_N^0	$(15G_0/4)$, Plateau modulus, N/m^2
G_0	Elastic modulus, N/m^2
h	Plank's constant, 6.62×10^{-34} $J\,sec$

i	Number of a type of segment, *dimensionless*
$\underset{\approx}{I}$	Unit tensor, *dimensionless*
$k_1,\ k_2$	Kinetic rate constants of entanglement –disentanglement process, sec^{-1}
k'	Friction coefficient, $m^3/(N\ sec)$
k_a	Kinetic rate constants of adsorption process, $m^2/(molecules\ sec)$
k_d	Kinetic rate constants of desorption process, sec^{-1}
k_B	Boltzmann's constant, $1.38\times10^{-23}\ (J/molecule)\ K$
L_{iN}	Probability of segment creation per unit time per unit volume. (at equilibrium L_i^{eq}), $1/(m^3\ sec)$
L	Contour length of the deformed tube, m
L_0	Contour length of the tube at equilibrium or no-flow condition, m
M	Molecular weight, $gm/mole$
M_e	Entanglement molecular weight, $gm/mole$
n	Psudoplasticity index of power law model, *dimensionless*
n	Number of segments per unit volume normalized with equilibrium number of segments per unit volume, *dimensionless*
N	Number of segments in the tethered molecule, *dimensionless*
N_A	Avogrado number, $6.023\times10^{23}\ molecules/mole$
N_c	Critical number of segments, *dimensionless*
N_0	Number of entanglements (segments) per chain, *dimensionless*
P	Pressure, N/m^2
P	Number of segments in the bulk molecule, *dimensionless*
P	Number of bulk chains in the vicinity of wall, $molecules/m^2$
P_w	Chains attached to the wall, $molecules/m^2$
P_w^e	Entangled with bulk but attached to the wall, $molecules/m^2$
P_w^d	Disentangled with bulk but attached to the wall, $molecules/m^2$
q	ds/ds_0 , *dimensionless*
$\underset{\sim}{Q}$	Segment vector, m
$\underset{\approx}{Q}$	Geometric universal tensor, *dimensionless*
Q	Flow rate m^3/sec

R	Radius of capillary, m
R	Universal gas constant, 8.314×10^{3} $kg\ m^2/(sec^2\ kg\ m\text{-}mole\ K)$
R	Mean square end to end distance of a chain, m^2
s	Contour length variable of the deformed chain, m
s_0	Contour length variable of the undeformed chain, m
$\dot{s}$	$\partial s/\partial t$, m/sec
$\underset{\approx}{S}$	Orientational order parameter tensor, *dimensionless*
t	Current time, *sec*
t'	Initial time, *sec*
T	Absolute temperature, K
$\underset{\sim}{u}$	Unit vector represent ting segment in primitive path, m
V_s	Slip velocity, m/sec
$\underset{\sim}{w}$	Unit vector represent ting segment in primitive path, m
w	Free sites on wall, m^{-2}
We	Weissenberg number, $\left(\frac{\lambda v_m}{\mathrm{R}}\right)$, *dimensionless*

Greek letters

α_f , α_g	Arbitrary parameter in equation (3.28) and (3.29), *dimensionless*
β	Cone angle in cone and plate rheometer, *radian*
δ	Dimension of the interfacial region (molecular scale), m
ϕ	Fraction of surface coverage of molecules attached to the wall (ϕ_{eq} under equilibrium), *dimensionless*
γ_e	Effective strain, *dimensionless*
$\dot{\gamma}_a$	Apparent shear rate, sec^{-1}
$\underset{\approx}{\dot{\gamma}}$	Rate of strain tensor. $\left(\underset{\sim}{\nabla}\underset{\sim}{\boldsymbol{v}}\right)+\left(\underset{\sim}{\nabla}\underset{\sim}{\boldsymbol{v}}\right)^{\mathrm{T}}$, sec^{-1}
η	Viscosity, $N\ sec/m^2$
η_B	Viscosity in the bulk region, $N\ sec/m^2$
η_I	Viscosity in the interfacial region, $N\ sec/m^2$
η_0	Zero shear viscosity, $N\ sec/m^2$

φ	Fraction of surface coverage of molecules entangled with the bulk and attached to the wall, *dimensionless*
κ_I	Shear rate in the interfacial region, sec^{-1}
κ_B	Shear rate in the bulk region, sec^{-1}
$\underset{\approx}{\kappa}$	Rate of strain tensor, sec^{-1}
λ	Relaxation time, *sec*
λ_{iN}	Probability of segment loss per unit time per unit volume. (at equilibrium λ_i^{eq}), *dimensionless*
$\underset{\approx}{\pi}$	Total stress tensor, N/m^2
θ_f, θ_g	Arbitrary parameters in equation (3.28) and (3.29), *dimensionless*
θ	Time, $t-t'$, *sec*
ϑ	Exponent in expression for fluctuation time, *dimensionless*
Σ	Surface coverage, $Chains/m^2$
σ_w	Wall shear stress, N/m^2
$\underset{\approx}{\sigma}$	Stress tensor, N/m^2
τ_I	Dominant relaxation mode in the interfacial region, *sec*
τ_{AR}	Arm retraction timescale, *sec*
τ	Dominating relaxation time of the entangled system, *sec*
τ_ξ	Fluctuation timescale, *sec*
$\tau_{cr,I}$	Relaxation time due to constrain release of a tethered molecule, *sec*
τ_d	Reptation time, *sec*
τ_r	Rouse relaxation time or retraction time, *sec*
τ_w	Local jump time of a segment, *sec*
υ_1	Velocity of the tube (mesh) with respect to respective segment of test chain, m/sec
υ_2	Velocity of the chain end of the bulk chain towards its center due to continuous retraction, m/sec
υ_m	Maximum velocity, m/sec
$\underset{\sim}{\upsilon}$	Velocity, m/sec

υ	Tangential velocity towards the center of the chain, which arises due to the continuous retraction, m/sec
ω	Angular velocity, rad/sec
ξ	$\left(1-2\left\|s(s_0)\right\|/L\right)$, $dimensionless$
ψ_1	First normal stress coefficient, $N\,sec^2/m^2$
Ψ	Configuration distribution function, $segments/m^3$

Subscripts

I	Corresponding variable related either to interfacial region or to tethered molecule.
B	Corresponding variable either related to bulk region or to bulk molecule
CR	Constraint Release
AR	Arm retraction
CCR	Convective constraint release

$\overset{\nabla}{\mathrm{B}}$	Upper convected derivative of arbitrary variable..
$\langle \mathrm{B} \rangle$	Average over configuration distribution function

Acronyms

HDPE	High Density Polyethylene
LDPE	Low Density Polyethylene
LLDPE	Linear Low Density Polyethylene
PAm	Polyacrylamide
PDMS	Polydimethylsiloxane
PEO	Poly ethylene oxide
PS	Polystyrene
PVC	Polyvinylchloride

CHAPTER 1

INTRODUCTION

The no-slip boundary condition at the fluid–solid interface has been a textbook prescription for students of fluid mechanics. However, the occurrence of sudden slippage at the wall for structured fluids under certain conditions has been a challenging problem in fluid mechanics. Flow instabilities occurring in entangled polymer solutions and melts in particular, has been a subject of intense investigation for the past several decades. A non-zero velocity at the boundary or a very high velocity gradient near the boundary gives rise to several instabilities in shear flow. Experimentally, only some polymeric fluids seem to undergo a distinct and dramatic wall-slip, the characteristics of which depend on the nature of the wall. Although slip is observed in most of the shear geometries, the slip-instabilities are more prone to occur in case of pressure flow since very high values of shear rates and wall stresses are achievable in this flow field. Also, since pressure flow is more commonly used in the polymer processing industry, these instabilities limit the processing speed to a great extent and therefore demand detailed investigation.

Slipping fluids exhibit many typical characteristics such as a drastic reduction of resistance to flow, diameter dependence of flow curves, surface distortions of the extrudate and (apparent) violation of no-slip boundary condition close to the wall [Wang *et al.*, 1999]. The critical value of wall shear stress for the onset of gross distortion as observed in many experiments varies usually between 0.01 MPa to 1 MPa for most of the tested polymers and its variation is much less than a decade within a particular polymer homologous series [Adewale and Leonov, 1997].

Several different molecular interpretations exist for wall slip. In the case of polymer solutions, apparent wall slip has been attributed to migration of macromolecules away from the wall under the influence of a stress gradient. This was believed to create a polymer-depleted layer of low viscosity near the boundary and cause apparent slip [Agarwal *et al.*, 1994; Barnes, 1995]. For entangled melts, the mechanism of constitutive

(bulk) instability (non-monotonic shear stress-shear rate curves) was considered to be responsible for the observed instabilities [Denn, 1990]. Recently, two important mechanisms that have been proposed for wall-slip are the disentanglement mechanism and the debonding mechanism. When a polymeric liquid comes in contact with the bare wall, some of the chains get adsorbed onto the wall. These grafted chains get entangled with the free bulk chains and resist their movement. This causes the no-slip boundary condition to prevail even for such structured fluids. There are then two ways by which the polymeric liquid can slip past the wall. One is by chain desorption from wall [Denn, 1990] and the other is by chain disentanglement at wall [Wang, 1999]. If the adhesive energy is not high enough to sustain the stress in the grafted chains created by the flowing bulk chains then at a critical stress the adsorbed chains would desorb from the wall and the bulk liquid can slip on the bare wall. This mechanism is known as debonding or adhesive failure. On the other hand, if the adsorption energy is high enough then at a critical stress the adsorbed chains could get oriented in the direction of the flow without desorbing so that the bulk chains can disentangle from them and slip. This is the so-called disentanglement mechanism.

Theoretical formulations of each of these mechanisms differ considerably, thus making it difficult to ascribe the experimentally observed slip to any of the mechanisms exclusively. Several years of research in this subject has indeed developed some consensus regarding the mechanisms. It is now generally accepted that for entangled polymeric fluids, slip is caused by either disentanglement or debonding mechanisms rather than by constitutive instability.

We propose to look at the problem of entanglement dynamics near the solid boundary and its implications on wall slip from a theoretical standpoint. The literature survey described in the next chapter points to the need for developing a rheological flow model that can unify several experimental observations under one common theoretical framework.

Thus, a primary scope of this work is to develop a unified slip model. The word ‘unified’ has several dimensions. Unification is proposed to be achieved in terms of the nature of the slipping fluid (i.e., concentrated solution or melt), the mechanisms of slip (i.e., disentanglement and debonding) and the different theoretical frameworks that have been used for describing slip. As discussed in literature review, several characteristics of

slip observed in entangled polymer solutions and in melts are similar in nature. Slip in a polymer solution results in a continuous but large increase in flow rate and in diameter dependent flow curves. In a slipping polymer melt a discontinuous increase in flow rate and diameter dependent flow curves are observed. A unified model should be able to predict such differences. The literature review also describes how a polymeric fluid can show different slip characteristics when flowing on dies of different materials of construction. A unified model should be able to naturally account for the effect wall-polymer interactions. The theoretical frameworks for describing slip occurring on low adhesive energy surfaces (by debonding) are considerably different than those that describe slip on high adhesive energy surfaces (i.e., by disentanglement). A unified model should be able to successfully combine such mechanisms into one consistent framework. The same model should be applicable for various slip regimes without any extra assumptions.

Finally, the success of a model describing wall-slip will be determined by whether it can predict several experimentally observed slip effects such as diameter dependence for smaller die diameters, diameter independence for larger diameters, first order transitions in flow rate, flow oscillations, hysteresis, etc. Since slip is generally observed in concentrated solutions and melts, the dynamics of which can be successfully predicted by the transient network theory, we develop a unified model on this theoretical framework. Although the transient network model is 'molecular' in nature, it requires some empirical fitting parameters. The incorporation of the empiricism simplifies the model substantially. However, such a model is unable to answer several fundamental issues that are at the heart of the physics of slip phenomenon. Thus there is also a need for a truly molecular model for describing the dynamics of polymer molecules near a wall. Another important scope of this work is to develop a fully predictive molecular model for wall-slip in highly entangled polymers.

All of the previous molecular theories for slip are essentially based on scaling models, which while providing a molecular understanding for wall slip cannot quantitatively predict the slip data. In this work, we propose a parameter free molecular constitutive equation based on the tube model for predicting slip on a high-energy wall. Our motivation is to develop an understanding of the molecular mechanisms that are responsible for slip due to disentanglement and to quantitatively predict various characteristic features of wall-slip.

Indeed, the choice between phenomenological and molecular models depends on the ends to be achieved. Phenomenological models are more suitable for engineering calculations of complex flows in complex geometries because of their relative mathematical simplicity. Molecular models, on the other hand, are insightful and fully predictive but are mathematically more complex and hence difficult to use in predictions on complex flows.

This thesis is organized as follows. In the next chapter we provide a detailed account of the literature, its critical review and the current status of the problem. In the chapter 3, we propose a disentanglement model that is based on transient network theory. In the chapter 4 the analysis in the previous chapter (chapter 3) is extended to include the debonding mechanism, thus proposing a unified model. In chapter 5, we discuss an experimental work aimed at testing an important prediction of the unified slip model namely, the temperature dependence of the critical stress for debonding-driven slip. In chapter 6, we develop a molecular model for slip phenomena, which is based on the tube theory, and is free from any arbitrary fitting parameters. Finally, the summary and the various conclusions arrived out of our work are discussed along with the scope for future work.

CHAPTER 2

LITERATURE SURVEY

2.1. Introduction:

Whenever a flowing fluid comes in contact with a solid boundary (wall) the magnitude of the macroscopic (slip) velocity of the fluid element next to the wall is given by the Navier's slip boundary condition [de-Gennes, 1979], $V_s = \sigma_{12}/\beta$, where σ_{12} is the wall shear stress and β is an interfacial friction coefficient. It is assumed that an interfacial region of the order of molecular dimensions a' exists near the wall, which connects the solid boundary to the bulk fluid. The stress in the bulk under steady shear flow is given by $\sigma_{12} = \eta\kappa_{12}$, where η is the bulk viscosity and κ_{12} is the shear rate. A similar relationship can also be written for the interfacial region as, $\sigma_{12} = \eta_I \kappa_{12,I}$, where η_I and $\kappa_{12,I}$ are the viscosity and the shear rate in the interfacial region respectively. Since the velocity changes from the stationary wall to macroscopic velocity V_s over a length scale equal to molecular dimensions a', $V_s = \sigma_{12}/\beta = a'\kappa_{12,I}$. Thus, the Navier's relation $V_s\beta = \eta\kappa_{12} = \eta_I \kappa_{12,I}$ introduces a length scale called the extrapolation length b, given by, [de-Gennes, 1979; Wang 1999]

$$b = \frac{V_s}{\kappa_{12}} = \frac{\eta}{\beta} = \frac{\eta}{\eta_I} a' \qquad (2.1)$$

The physical interpretation of the extrapolation length (b) is shown in figure (2.1). The extrapolation length b is widely used to quantify the slip in the flowing fluids. When $b > a'$, the fluid is said to be slipping on the wall. For monomeric liquids, the interfacial and bulk viscosities are of similar magnitude since both involve monomer-monomer interactions, hence b is of the order of a'. For polymeric liquids flowing on bare wall, i.e., a molecularly smooth non-adhering wall, the interfacial viscosity η_I is still equal to the monomeric viscosity while η increases by several orders of magnitude depending on the molecular weight of the flowing liquid ($\eta \sim M^{3.4}$). Hence $b >> a'$ and the polymer slips on the wall. However, if the wall is not bare, i.e., if it can adsorb polymer chains on

to its surface to form a grafted layer that can entangle with the flowing bulk, then $\eta_I \sim \eta$ and hence $b \sim a'$. Thus, slip is considerably suppressed in this case.

As discussed in the previous chapter, slip instabilities play a very important role in polymer processing industry. In extrusion-based industries, these instabilities limit the processing speed up to a great extent, as at higher flow rates the system shows extrudate distortion and pressure oscillations. Due to such high industrial importance, this area has been explored extensively for last five decades. The main aim behind such studies is to understand the molecular mechanisms behind these phenomena and to suggest the remedies to remove the extrusion instabilities. Further, the task to uncover the molecular origins of these phenomena has been considered as one of the few uncompleted challenges in the field of polymer Rheology. Roughly, this subject has invited over three thousand publications from 1950s up to 1990s [Wang, 1999]. We divide the literature on wall slip broadly into two parts: (i) experimental studies which are aimed at measuring wall slip and understanding the influence of various parameters that can affect slip, and (ii) theoretical investigations which are aimed at understanding the mechanisms of slip and predicting the observed flow behavior. Correspondingly, this chapter contains two main sections. In the first section, we present a detailed survey of the various experimental observations made in last few decades. In the second section, we provide a detailed account of the various theoretical interpretations and mathematical models that have been proposed in order to explain the observed experimental behavior. Figure (2.2) shows a schematic of the various issues discussed in this chapter.

2.2. Experimental Observations:

When polymeric liquids are sheared in viscometers and processing equipment, the phenomenon of wall slip manifests itself in various ways. Slip is seen in pressure flows (such as in extrusion or in capillary and slit rheometers) as well as in drag flows (such as in cone and plate, plate and plate, couette and sliding plate rheometers). Interestingly, the characteristics of slip behavior differ from apparatus to apparatus, since they explore different range of shear rates (or shear stresses). The occurrence of slip in some rheometers can also masked by other effects such as secondary flows and other instabilities. We will first discuss various experimental observations in the

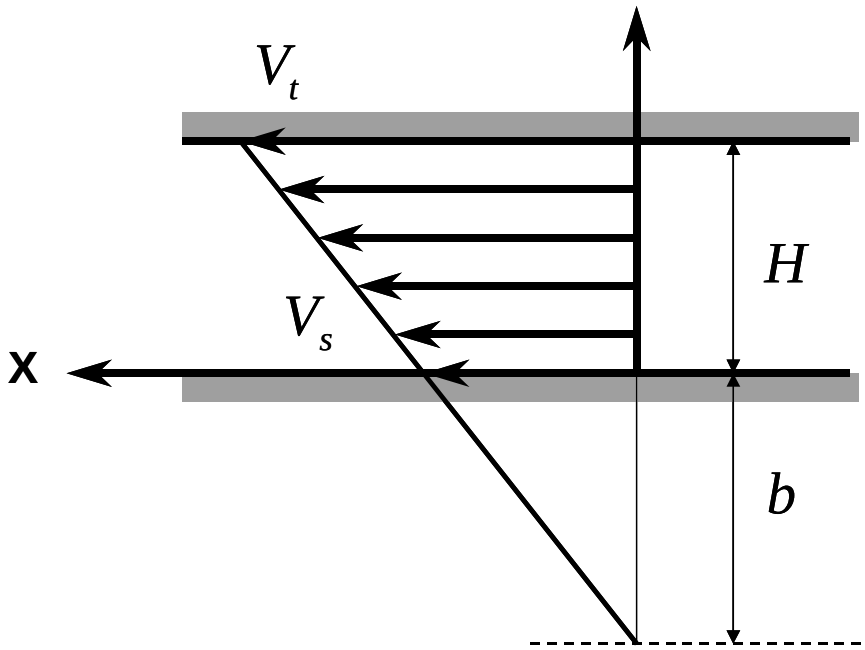

Figure 2.1 A schematic of a simple shear geometry. The two plates are separated by distance H. Top plate moves with velocity V_t, while bottom plate is stationary. The shear rate in the bulk is $\kappa_{12} = (V_t - V_s)/H$. The velocity profile extrapolates to zero at a distance b below the interface, with extrapolation length $b = V_s/\kappa_{12}$.

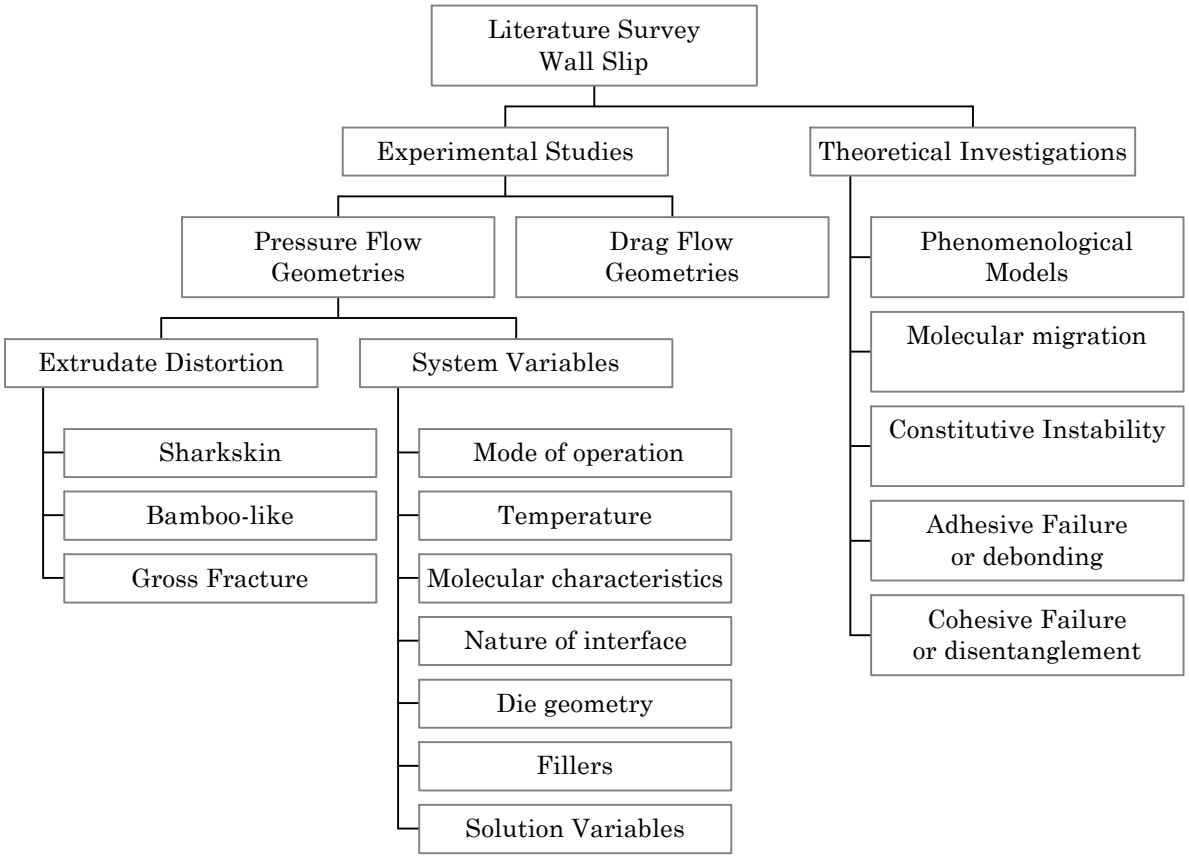

Figure 2.2 A schematic of the various issues discussed in literature survey

pressure flow viscometers followed by a survey of the experimental observations for the drag flow viscometers.

2.2.1. Pressure flow

Pressure flow rheometers (e. g. capillary viscometer and slit viscometer) are the most popular apparatus for studying slip. An important reason for this is that these rheometers explore a shear rate range that is observed in many of the extrusion processing techniques such as film blowing, casting, profile extrusion and spinning, which are most susceptible to slip instabilities.

2.2.1.1 Manifestations of slip

When a polymeric liquid is extruded through a capillary or a slit die at low shear rates (or low shear stresses), a smooth extrudate with die swell is observed. At higher rates, small ripples on the extrudate surface are observed. These ripples are popularly known as sharkskin. This behavior is observed in some polymers such as high density polyethylene [Tordella, 1969], linear low density polyethylene [Deeprasertkul *et al.*, 1998; Pudjijanto and Denn, 1994], polydimethylsiloxane (PDMS) [Piau *et al.*, 1990], etc. At still higher shear rates in a typical rate-controlled extrusion process, one observes significant pressure drop and flow rate oscillations, though the input flow rate (feed) is maintained at a constant value. In this regime, the extrudate shows alternating bands of smooth and distorted surface [Kissi and Piau, 1990]. This flow regime is called "stick-slip" or "spurt flow". If the shear rate is increased even further a grossly distorted extrudate is observed [Wang, 1999]. This is typically called as "gross melt fracture".

If the polymer is extruded in a stress controlled process then sharkskin is observed at the same stress (or shear rate) as that in the rate-controlled process. However, at a higher shear stress corresponding approximately to the stress at which stick-slip is observed in a rate-controlled process, the apparent shear rate (or flow rate) jumps discontinuously by as much as one order of magnitude [Bagley *et al.*, 1958; Tordella, 1963; Wang and Drda, 1996a]. There are no pressure-drop and flow rate oscillations accompanying the stick-slip instability in a stress-controlled process. Interestingly, the extrudate after the discontinuous jump has a smooth surface [Tordella, 1963; Wang and Drda, 1996a], but this behavior changes with change in polymer-wall pair. If the stress

is increased further then the extrudate surface becomes grossly distorted in a manner similar to that observed in a rate-controlled extrusion process. On gradually decreasing the stress, the apparent shear rate (or flow rate) decreases discontinuously at a critical shear stress, which is generally lower than the stress at which the sudden increase was seen. Thus, a hysteresis is observed [Bagley *et al.*, 1958; Kissi and Piau, 1990; Yang *et al.*, 1998c]. Further, if the extrusion is carried out using dies of different diameter, the discontinuous increase in apparent shear rate increases with decrease in diameter thus showing the diameter dependent flow curves [Wang and Drda, 1996a]. However, such diameter dependence is seen to be decreasing with increase in diameter of the capillary in such a way that the capillaries with large diameter do not show any diameter dependence [Cohen and Metzner, 1982].

In polymers such as isotactic polypropylene or low density polyethylene, the sharkskin and stick-slip instabilities are completely absent even at very high stress levels [Yang *et al.*, 1998a], but sometimes at very high flow rates the glossy spirals or macroscopic screw-like extrudate appears through the capillary [Kissi and Piau, 1990]. Such effect has been sometimes confused with the spurt phenomenon. However, now it has been accepted that such behavior is observed because of entry instability [Wang, 1999].

2.2.1.1. Extrudate distortion

To the best of our knowledge, the first experimental observation of surface defect during extrusion dates back to 1942. Garvey and coworkers (1942) observed the extrudate distortion while extruding the synthetic rubber compound through tire thread die at 110°C. Nason (1945) used a gas driven extrusion capillary rheometer for extrusion of polystyrene and cellulose acetate and observed that the extrudate of the polystyrene became wavy when the Reynolds number was in the range 800-1000. He found that the waviness of the extrudate increased further with increasing the extrusion pressure. After these early observations, several research groups have investigated similar phenomenon in other polymers. Many terms have been used in literature (as mentioned in the review of Boudreaux and Cuculo, 1977) to describe this phenomenon, namely melt fracture, elastic turbulence, waviness, ripples, bamboo effect, sharkskin, etc. The various details of the extrudate distortion phenomenon as investigated by several research groups have been reviewed extensively [White, 1973; Petrie and Denn, 1976; Boudreaux and Cuculo, 1977; Denn, 1990; Larson, 1992; Graham, 1999; Wang, 1999;

Denn, 2001]. In the following, we will summarize only some of the very important observations.

Three types of extrudate distortions are generally observed during extrusion [Wang, 1999]. At lower shear rates, ripples are observed on the surface of the extrudate. This behavior is seen irrespective of the mode of operation (either pressure controlled or the rate controlled). Such ripples are popularly known as sharkskin or sometimes called as surface fracture. The second type of distortion occurs only in rate-controlled mode, when periodic pressure and flow rate oscillations are seen. The emerging extrudate appears to be bamboo-like, where periodic rough and smooth bands on the surface can be seen. The third type of distortion is the gross distortion of the extrudate or the smooth spirals. The intensity and/or presence of any of the above instability depend on the various characteristics of polymer melt as well as its interactions with the die wall.

2.2.1.1.1. Surface fracture: Sharkskin

Sharkskin or surface fracture is the first indication of an instability and it occurs at a comparatively lower shear stress. As the name suggests the extrudate surface shows ripples perpendicular to the flow direction as shown in figure (2.3). Piau *et al.* (1990) defined sharkskin as 'a surface defect characterized by a small scale and high frequency rugosity of the free surface due to relaxation of strain at the die outlet'. In the early days of research in this area, the gross distortion was often confused with sharkskin behavior. Benbow and Lamb (1963) demonstrated the distinct differences between the gross fracture and sharkskin. While gross distortions occur as a result of melt fracture due to entry instability, sharkskin distortions are localized only at the surface and are also called surface instabilities. Generally, sharkskin is seen mainly in polyolefins like HDPE [Tordella, 1969], LLDPE [Deeprasertkul *et al.*, 1998; Pudjijanto and Denn; 1994], polybutadine [Shaw and Wang, 2000] and PDMS [Piau *et al.*, 1990] while other polymers directly show either stick slip transition or gross distortion (or spirals), with out showing sharkskin effect.

In most of the cases it is found that coating the die surface with a fluoropolymer can eliminate the sharkskin [Moynihan *et al.*, 1990; Hatzikiriakos and Dealy, 1993; Kissi *et al.*, 1994; Kazachkov *et al.*, 1995; Kissi and Piau, 1996b; Wang *et al.*, 1996]. However, in some cases, sharkskin is seen to persist even after the coating the die with

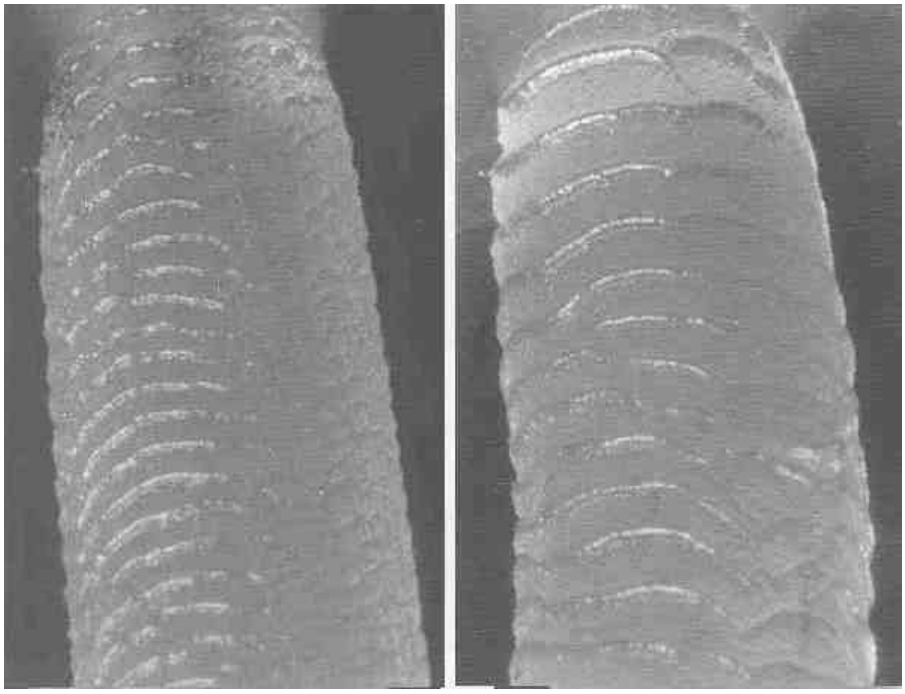

Figure 2.3 Sharkskin on the extrudate of PDMS melt through an orifice die. It can be seen that the ripples on the surface are perpendicular to the axial direction. (Reproduced with permission. From Kissi and Piau, 1996b; © 1996, Elsevier Science B. V.).

fluoropolymer [Person and Denn, 1997]. Instead of coating the entire die, Moynihan *et al.* (1990) coated only the entry and the exit regions of the slit die independently and observed the suppression of the sharkskin in both the cases. Similar observations of vanishing of sharkskin due to die lip (exit) coating have been made by others also [Kazachkov *et al.*, 1995; Wang *et al.*, 1996]. Moynihan *et al.* (1990) also varied the length to diameter ratio (L/D) of the capillary and observed that the sharkskin was delayed and occurred at higher shear rates with increase in L/D. Similar behavior has also been observed by Sornberger *et al.* (1987). Although Moynihan *et al.* (1990) and Sornberger *et al.* (1987) observed a substantial influence of die geometry on sharkskin; Venet and Vergnes (1997), Constantin (1984) and Beaufils *et al.* (1989) reported only a weak dependence of sharkskin on (L/D). Sornberger *et al.* (1987) also observed that sharkskin appears at a critical value of shear rate, and this critical shear rate increases with increase in temperature. They further observed that mixing a lubricant with LLDPE attenuates the severity of the sharkskin. Similar observations of reducing sharkskin by mixing lubricants or fluoropolymers have been made by Nam (1987), Rudin *et al.* (1990) and Hatzikiriakos (2000).

Kurtz (1984) was the first to observe a distinct change in slope of the shear rate - shear stress flow curve at the onset of sharkskin. Ramamurthy (1986), Kalika and Denn (1987) and Wang *et al.* (1996) have also made similar observations for LLDPE at various temperatures. Wang *et al.* (1996) also used a die with 60^{o} exit taper. The effect of this less abrupt exit leads to a smaller slope change. In general, though a change in slope of the flow curve is visible at the onset of sharkskin, it is not as severe as that observed during the stick slip instability regime at higher stress. Figure (2.4) shows various regions of extrudate distortions on the flow curve. The change in slope in the sharkskin region can be clearly seen in the figure.

Molecular structure significantly affects the sharkskin behavior. Not all polymers, which show stick-slip behavior show sharkskin and vise a versa. As discussed earlier, sharkskin is mainly seen in polyolefins and PDMS. Amongst polyolefins, sharkskin is mainly observed in polymers with linear chain structure like HDPE and LLDPE. Commercial LDPE, which has long branches and high polydispersity, does not show sharkskin [Wang *et al.*, 1996; Venet and Vergnes, 1997; Yang *et al.*, 1998a]. Contrary to this, Mackley *et al.* (1998) indeed observed the surface instability for LDPE at low temperature around 140^{o}C. However, the same vanished at higher temperatures. They

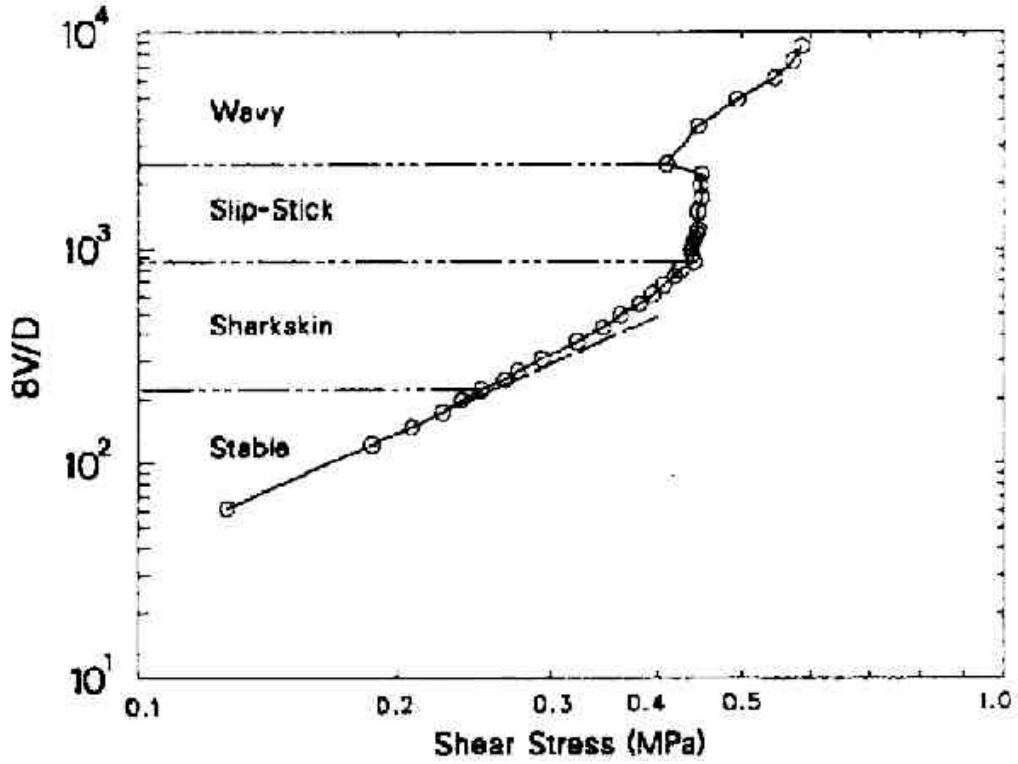

Figure 2.4 Flow curve for LLDPE at 215°C. Various regions of extrudate distortion are mentioned on the curve. (Reproduced with permission. From Kalika and Denn, 1987; © 1987, Society of Rheology)

also found the severe sharkskin for LLDPE. Interestingly, when they blended LLDPE and LDPE, they found that the blend shows enhanced sharkskin than LLDPE at normal processing temperatures.

It is generally observed that lower the polydispersity higher is the severity of sharkskin [Graham, 1999]. Kazatchkov and coworkers (1999) studied various LLDPEs with same weight average molecular weight and different polydispersity. They observed that an apparent shear rate at the onset of sharkskin goes on increasing with the polydispersity. After a critical polydispersity (~9.6) sharkskin vanished and spirally distorted extrudate appeared out of the die. Hatzikiriakos *et al.* (1997) observed an absence of sharkskin while extruding single site catalyzed metallocene LLDPE. They argued that though these metallocene LLDPE are less polydisperse, they have higher long chain branching than conventional LLDPE. However, contrary to the observation made by Hatzikiriakos *et al.* (1997), Deeprasertkul and coworkers (1998) observed the sharkskin for metallocene LLDPE. Stereoregularity is also shown to be influencing the sharkskin behavior. Tapadia *et al.* (2000) observed sharkskin in syndiotactic polypropylene (PP) while for isotactic polypropylene sharkskin was completely absent.

Various mechanisms have been proposed to explain this behavior. Benbow and Lamb (1963) argued that sharkskin is initiated at the die exit. Based on birefringence studies, Vinogradov *et al.* (1972) argued that the high stresses at the die exit cause the sharkskin like surface distortion. Cogswell (1977) proposed that the stress singularity near the die exit could cause the local stress to exceed the melt strength of the polymer. This causes rupture of the polymer melt, which results in the sharkskin. On similar lines, Venet and Vergnes (1997) claimed that since LDPE has a strong strain-hardening elongational behavior (i.e., higher melt strength), it is resistant to rupture and hence does not show sharkskin. Rutgers and coworkers (1998) supported the argument of random crack formation under the influence of high tensile stress at the die exit by analyzing the flow field by means of optical stress birefringence. Rutgers and Mackley (2000) present a numerical simulation of a slit die for two grades of LLDPEs. They also calculate the critical stress at which melt ruptures in a uniaxial elongation flow for both the grades. They show that the onset of the surface fracture (exit tensile stress) correlates the critical stress level for melt rapture. They argue that as the critical extentional stress in reached, the periodical crack formation occurs in the emerging extrudate. The depth of the crack can be correlated to the depth of the material at the

die exit in which the tensile stress exceeds the critical level. Venet and Vergnes (2000) have also carried out a numerical study of the flow conditions at the die exit. They observe an existence of small traction zone located at the periphery of the die exit where the tensile stress grows with increase in flow rate. They further observe that the intensity and the dimensions of the traction zone remains unaffected due to die geometry. Based on these observations they argue that the tangential stress cannot be a unique parameter to explain the sharkskin phenomena and the history of deformation should also be taken into account. Moynihan *et al.* (1990), based on their observations from the capillary as well as slit die, proposed a similar mechanism to explain and locate the site for initiation of sharkskin. They proposed that the first requirement for surface melt fracture to occur is that the material be pre-stressed, which they visualized as occurring in the land region of the die and the second requirement is the acceleration of the melt as it exits the die. Ramamurthy (1986) and Kalika and Denn (1987) reported that the origin of the sharkskin is due to the loss of adhesion between the polymer and die wall. Dhori *et al.* (1997) proposed a molecular mechanism, in which they attribute the sharkskin to the wetting-dewetting (adsorption-desorption of the polymer molecules) process at the die lip (exit). The dewetting occurred as a result of the elastic energy in the tethered molecule exceeding the adhesion energy, while the wetting process was due to relaxation of the free (i.e., slipping) molecules at the die lip.

Barone and coworkers (1998) proposed an interfacial molecular instability (IMI) mechanism to explain the sharkskin phenomenon. They proposed a mechanism that is in some sense similar to that proposed by Dhori *et al.* (1997). A crucial difference, however, is that the wetting-dewetting dynamics is replaced by entanglement-disentanglement dynamics. They argue that due to higher exit stresses and/or elongational flow component near the die exit, the molecules tethered in the die lip region undergo a reversible coil to stretch transition much earlier than those in the die land. The coil state represents the entanglement state while the stretch state represents disentanglement. This results in cycles of local stress relaxation and growth, which produces a periodic perturbation of the extrudate swell that appears like sharkskin roughening on the extrudate surface. They estimated the sharkskin period using the average distance between two ripples and the velocity of the cooled extrudate. They found that the sharkskin period follows the WLF like temperature dependence in a manner similar to that exhibited by the melt viscosity (or the molecular relaxation time). Wang *et al.* (1996) showed that the frequency of sharkskin correlates well with

the characteristic molecular relaxation time determined by linear viscoelastic measurements. They argued that this observation correlates the sharkskin to a molecular relaxation process triggered by a reversible coil to stretch transition. Recently Barone and Wang (2001) have carried out the rheo-optical observations to show the presence of tethered chains in the die exit region to be the necessary criteria to generate the sharkskin on the extrudate. They coated the die exit using ethanol to assure no adsorption of polymer chains in the die lip region. They found the extrudate to be smooth even when the stress levels obtained by birefringence substantially exceed the onset value for sharkskin formation for a bare die.

2.2.1.1.2. Bamboo-like extrudate.

During a controlled-rate extrusion process a second critical stress is observed [see figure (2.4)], above which periodic flow rate and pressure oscillations take place and emerging extrudate shows alternate bands of smooth and sharkskin regions [see figure (2.5)] [Kissi and Piau, 1990; Denn, 1990]. Since the input flow rate into the die is constant, the oscillating output from the die must clearly be a result of the finite compressibility of the melt [Molenaar and Koopmans, 1994; Ranganathan *et al.*, 1999]. The widths of the smooth and sharkskin regions of the extrudate depend on the frequency of the flow rate oscillations, which in turn depends on the compressibility of the melt and the material in the barrel (i.e. reservoir volume) [Wang, 1999; Pearson, 1985]. The bamboo-like distortions are not always visible in a controlled stress extrusion process. Indeed, in such a mode of operation, the shear rate (or flow rate) jumps discontinuously and the accompanying extrudate is typically smooth.

As discussed earlier, only some polymers show stick slip behavior. Whether a polymer will show stick slip behavior or not depends mainly on its molecular characteristics and its interactions with the die surface. Further only highly entangled polymeric liquids show stick-slip instability [Wang, 1999], we will discuss this issue in more detail later in this chapter. Several observations of bamboo like extrudate for various polymers are reported in literature and can be found in various review papers [Wang, 1999; Denn, 1990; Boudreaux and Cuculo, 1977; Petrie and Denn, 1976]. Further, similar to sharkskin behavior it is observed that the stick-slip behavior also vanishes on coating the die with a fluoropolymer [Hatzikiriakos *et al.*, 1995; Piau *et al.*, 1995]. Various details of such observations are discussed later in this chapter.

Some reports describe a second stable flow region for linear polyethylene after the stick-slip instability (Schreiber *et al.*, 1960; Tordella, 1969; Pudjijanto and Denn, 1994). Pudjijanto and Denn (1994) observed that such a stable region for LLDPE, when processed between 140 to 146 ^{0}C. It is claimed that a linear polyethylene requires low temperatures, large diameter capillaries to attain the second region of stability [Boudreaux and Cuculo (1977); Tordella (1969)].

2.2.1.1.3. Gross fracture or spirals

Gross fracture or spirals are observed in mostly all entangled polymeric liquids irrespective of their slip behavior. Figures (2.6a) to (2.6c) show photographs of a grossly fractured extrudate of LLDPE while figure (2.6d) shows a photograph of a extrudate of PDMS distorted in the form of spirals. It has been suggested that such spirals or the gross distortion arise from the formation of secondary flow (vortices) in the barrel due to the strong converging flow near die entry [White, 1973; Wang, 1999]. White (1973) argued that the size of the vortices increases with the increase in flow rate. The streamlines in the die entry eventually break and material with different deformation history alternatively surge in to the capillary to give rise to gross distortion of the extrudate [White, 1973]. Perez-Gonzalez *et al.* (1997) observed that pressure fluctuations accompany gross distortion. They further observed that the severity of the extrudate distortion decreases with decrease in entrance angle of the capillary die. The phenomenon of entry instability and gross distortion is out of the scope of present work and hence will not be discussed in more detail here.

2.2.1.2. Slip characteristics and system variables

In this subsection, we will discuss the effect of various system variables on the stick-slip phenomena and the wall-slip phenomena occurring over a die land. Although some of the system variables are implicitly inter-related, we try to take account of each one independently.

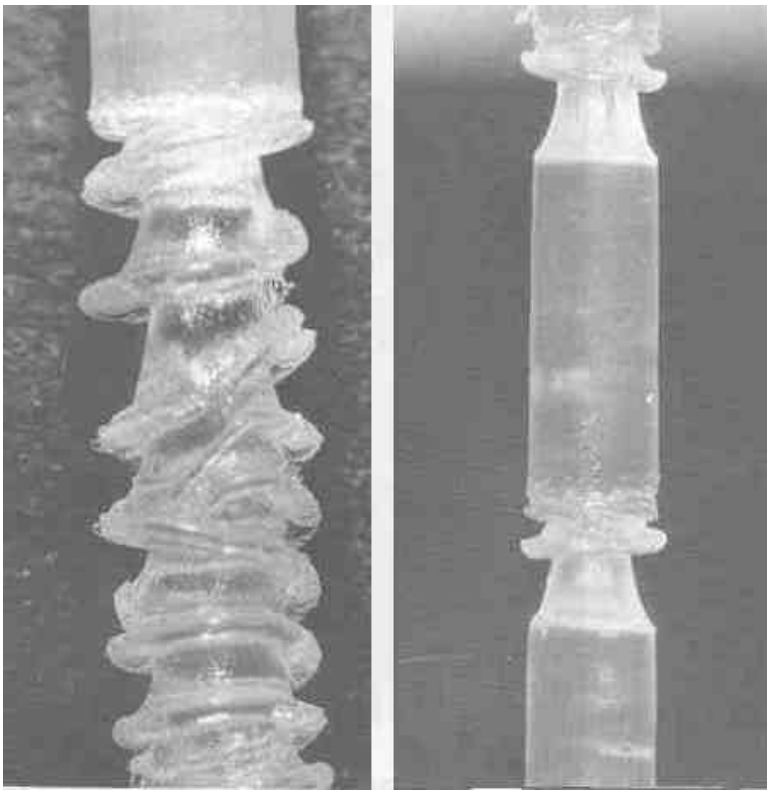

Figure 2.5 Bamboo like extrudate distortion for PBD during the oscillatory region. (Reproduced with permission. From Kissi and Piau, 1996b; © 1996, Elsevier Science B. V.)

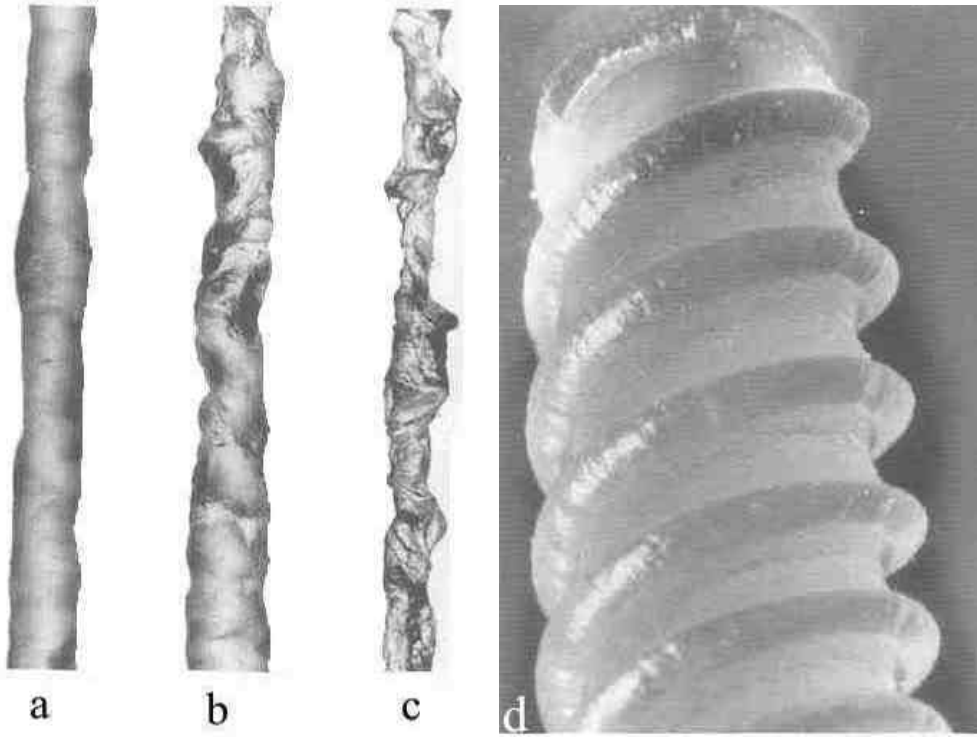

Figure 2.6 Gross extrudate distortion (a-c) can be seen for LLDPE melt through 0.5 mm capillary die, while d is the spiral distortion observed for PDMS through orifice die. (Reproduced with permission. From Kissi and Piau, 1996b; © 1996, Elsevier Science B. V.)

2.2.1.2.1. Mode of operation and flow curve

The mode of operation of the extrusion process has a significant effect on the slip characteristics as well as on the flow curve. As mentioned earlier, the extrusion rheometer can be operated in two modes; a rate-controlled mode, in which the piston speed or the net flow rate of the material through the extruder is controlled, and a stress-controlled mode, in which the pressure drop across the die is controlled. In principle, the relationship between the shear stress and shear rate (i. e., the apparent viscosity) is a material property and should be independent of the mode of operation. However, in the case of highly entangled polymeric liquids the flow curves observed in the two modes differ whenever stick-slip occurs.

At low shear rates and up, until a critical shear rate (or shear stress) the flow curves of the rate controlled and stress controlled modes match identically. After the critical shear rate (or stress) is crossed, the flow in the rate-controlled mode becomes erratic; the pressure drop across the die and the flow rate through the die show periodic oscillations [Denn, 1990]. Figure (2.7) shows the pressure or stress oscillations of HDPE melt when extruded from a rate-controlled capillary rheometer. The frequency and the amplitude of the oscillations depend on the compressibility as well as the volume of the material remaining in the barrel (Pearson, 1985). Above the stick-slip instability, the pressure drop and the flow rate once again become monotonically increasing functions of each other.

If the extrusion rheometer is operated under controlled pressure-drop model, the flow rate discontinuously increases at a critical pressure drop. The magnitude of the jump in the flow rate (or the apparent shear rate) depends on the molecular characteristics of the polymer. Above the discontinuity, the flow curve again becomes monotonic. While decreasing the pressure drop gradually system shows hysteresis as shown in figure (2.8). [Bagley *et al.*, 1958; Kissi and Piau, 1990; Yang *et al.*, 1998c].

Recently Munstedt *et al.* (2000) measured the velocity profile of the PE melt in a slit die using laser-Doppler velocimetry. They observed pronounced wall slip velocities at low shear rates. They further measured the velocity fluctuations along with the pressure fluctuations while the system is undergoing the stick-slip instability. Although they found that the frequencies of the oscillations for both velocity and pressure were same,

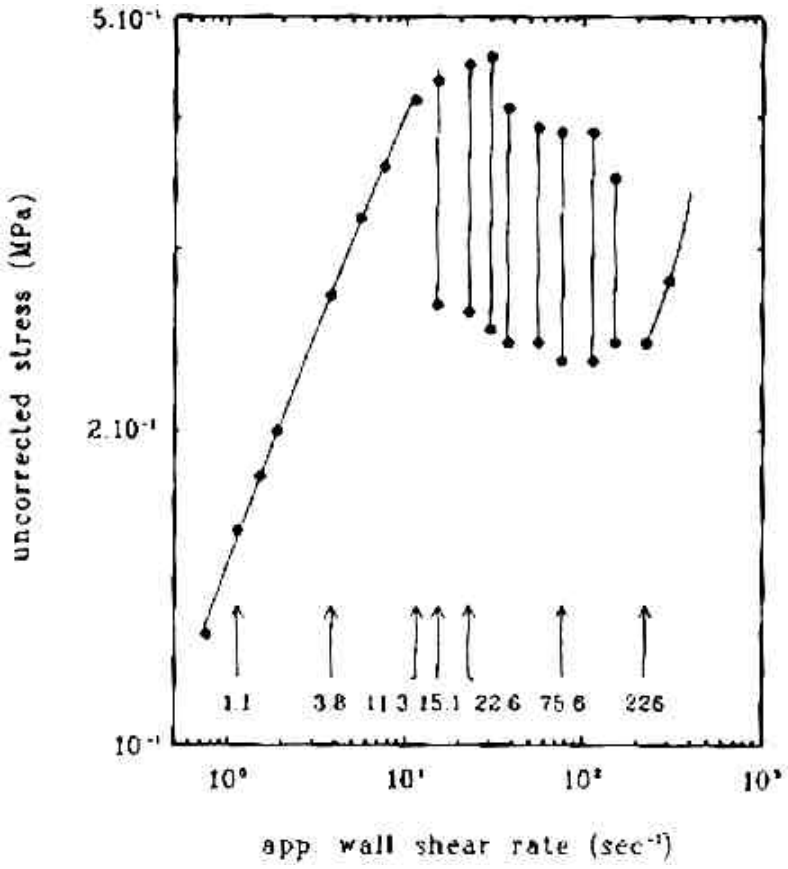

Figure 2.7 The flow curve for linear polyethylene at 180 °C in a rate controlled rheometer. The vertical line denotes the pressure oscillations. (Reproduced with permission. From Kolnaar and Keller, 1996; © 1996, Elsevier Science B. V.)

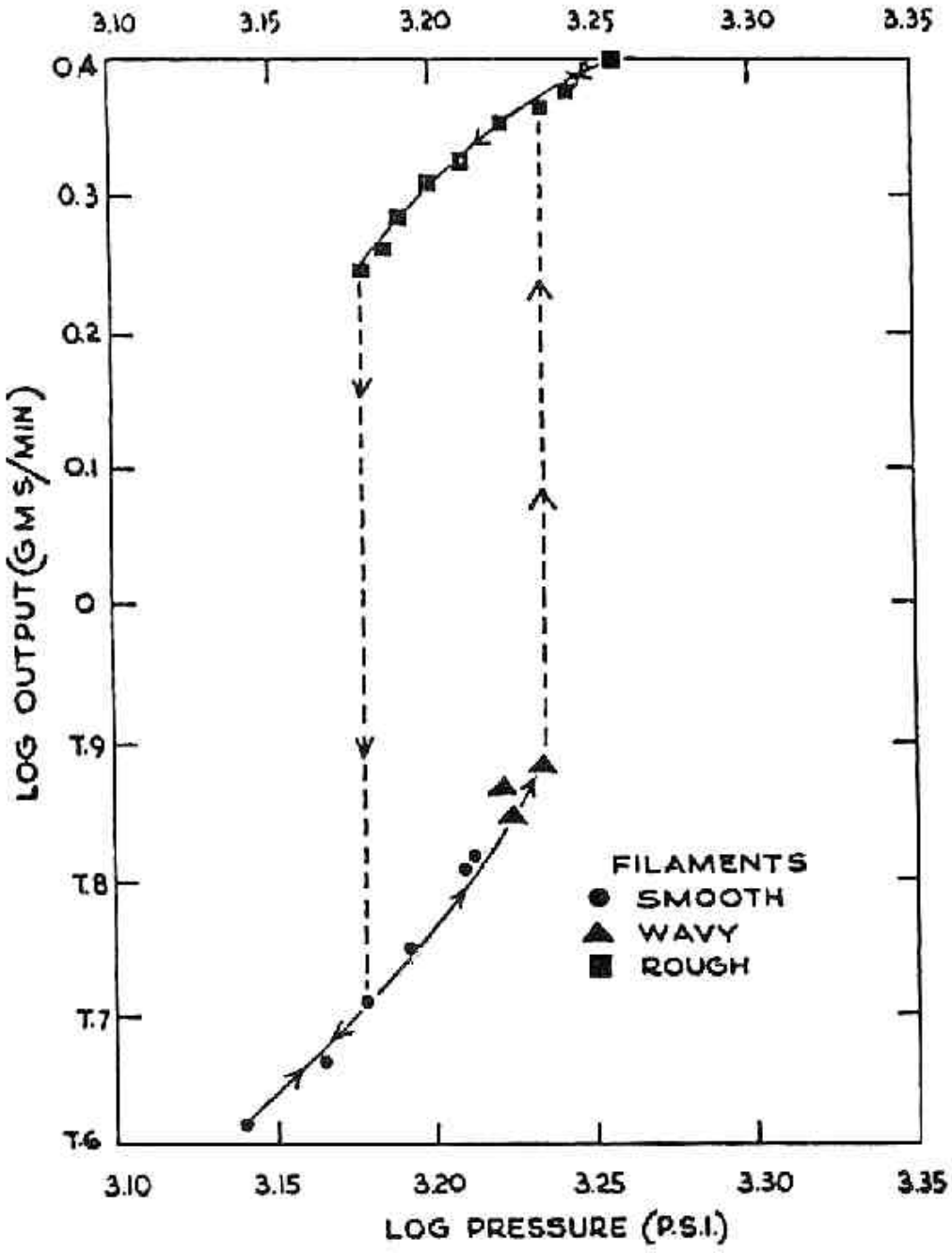

Figure 2.8 Flow of linear polyethylene through a flat entry capillary. Polymer melt shows hysteresis while undergoing discontinous stick-slip transition. (Reproduced with permission. From Bagley *et al.*, 1958; © 1958, American Institute of Physics)

the shapes of the amplitude were completely different. They explained this behavior based on the entanglement-disentanglement model.

Following the first discontinuity in flow rate in a stress-controlled mode of operation, Wang and Drda (1997b) reported a second critical stress for LLDPE, at which the flow rate again increased discontinuously. The flow curves after this second critical stress did not show diameter dependence, unlike those after the first critical stress. The authors claimed that the second criticality might arise out of disentanglement within the bulk chains (Constitutive instability).

2.2.1.2.2. Temperature

The influence of temperature on stick-slip has been extensively investigated. Even the earliest studies as reviewed by Boudreaux and Cuculo (1977) have reported that, in general, the critical stress for stick-slip is found to increase slightly with temperature. They further added that the observed increase was so slight that many investigators claimed the critical stress to be temperature independent.

In 1992 in a seminal contribution Brochard and de Gennes proposed a scaling model, which showed that the critical stress for stick-slip should increase with temperature, provided slip occurs by the so-called "disentanglement mechanism". Based on this premise, Wang and Drda (1996a) revisited the temperature dependence problem. While extruding HDPE through steel capillaries in a stress-controlled mode, they indeed found a small but definite increase in critical stress with increase in temperature [see figure (2.9)] They further observed that the slip length (b) remains constant with respect to temperature in the explored temperature range. They found that the chains experience the same extent of stretching and its magnitude is same at all the temperatures. Since the ratio of critical shear stress to temperature was found out to be a constant, they argued that the transition is not an activation process (debonding) and hence the polyethylene melt slips on steel due to the disentanglement mechanism.

In an interesting observation, Kolnaar and Keller (1994, 1997) have reported the existence of a narrow temperature window in which flow resistance drops significantly. While extruding the HDPE, they found a temperature range (146^{o}C-152^{o}C) in which, above a certain piston speed, the extrusion pressure decreased significantly with a small

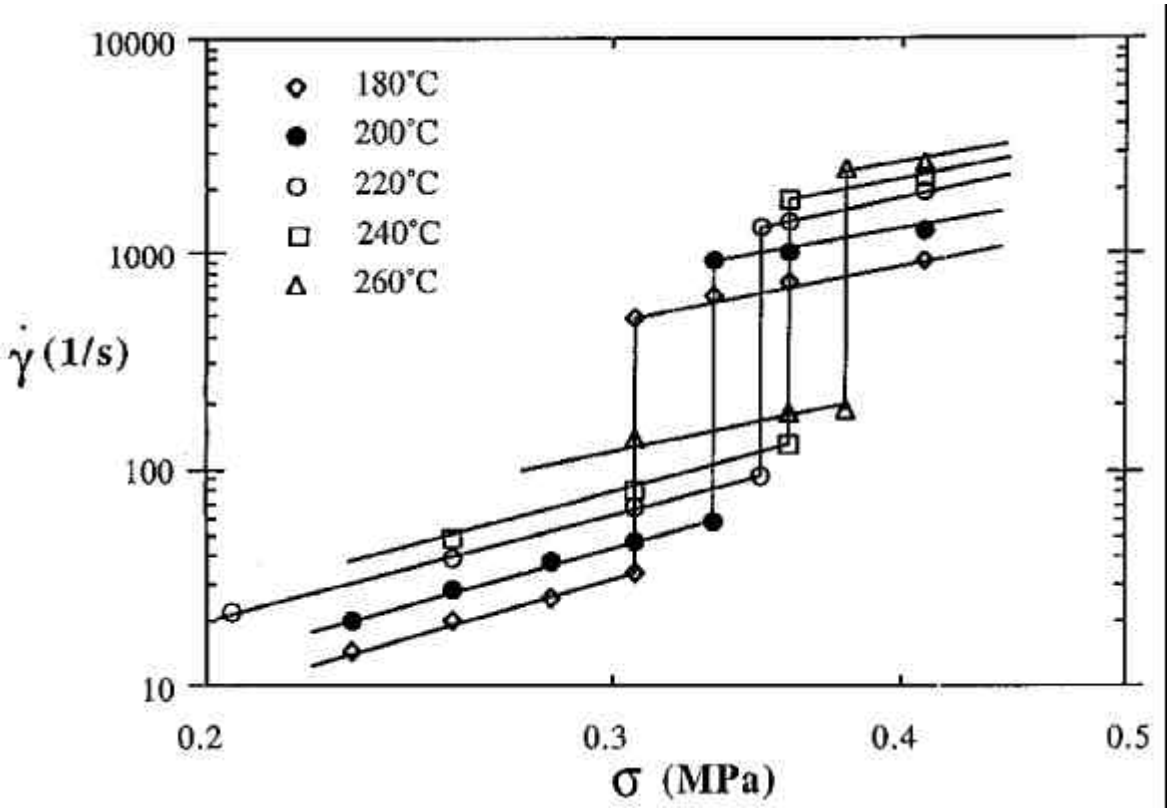

Figure 2.9 The flow curve for linear polyethylene for various temperatures. It can be seen that as temperature increases the critical stress for stick slip transition also increases. (Reproduced with permission. From Wang and Drda, 1996a; © 1996, American Chemical Society)

increase in temperature. Above this temperature window, the pressure increased and showed oscillations accompanied by melt fracture. In-situ wide angle X-ray diffraction results showed an anomalous hexagonal phase near the capillary wall (Van Bislen *et al.*, 1995). The authors proposed that such a hexagonal phase is responsible for the slippage of polymer molecules at the wall causing a decrease in pressure. Until this day, this remains the only direct experimental observation so far on chain stretching at the wall accompanying wall slip. Recently Perez-Gonzalez *et al.* (2000) have also reported the existence of similar temperature window for metallocene LLDPE. They observed a non-linear temperature dependence of the critical stress at the onset of slip. They found that up to 140^{o}C the critical stress decreases with increase in temperature and above 140^{o}C it increases with increase in temperature. They argue that the former behavior is the result of a flow induced phase change due to crystallization of the melt, while the later behavior can be explained based on the disentanglement model of Brochard and de Gennes (1992).

Myerholtz (1967) observed that the critical shear rate at the onset of pressure and flow rate oscillations shifted to the higher values with increase in temperature. Vinogradov *et al.* (1984) and Wang and Drda (1996a) observed that the jump in the flow rate to be independent of temperature.

2.2.1.2.3. Molecular characteristics

Various molecular features of polymeric liquids are responsible for their slip characteristics. These include molecular weight, molecular weight distribution, entanglement molecular weight or plateau modulus and several molecular architectural characteristics like long and short chain branching and their distribution, stereoregularity, etc. Although it is understood that all these parameters are interrelated in a complex manner with the rheological response, they are also known to influence the slip behavior independently as discussed below.

Several investigators have studied the effect of molecular weight on the slip characteristics. Vinogradov *et al.* (1972) used a controlled rate as well as a controlled stress capillary rheometer for studying various grades of polybutadine (PB) and polyisoperene (PI) of narrow molecular weight distribution. For various grades of both polymers the critical shear stress at which slip occurred was found out to be

independent of molecular weight. They also showed that sudden slip was seen only if the molecular weight was above some threshold value. Vinogradov *et al.* (1984) reported that the threshold molecular weight for slip instability (transition) to occur should be $M_w > 5M_e$, where M_e is the molecular weight between two entanglements. They further observed that the magnitude of the jump in flow rate has a 3.4 power law dependence on the molecular weight of the flowing polymer. Similar observations have been made by various other investigators [Kissi and Piau; 1990; Yang *et al.*, 1998b]. It can be seen from figure (2.10) that as molecular weight increases the jump in shear rate also increases.

For some polymers an inverse dependence of critical stress with respect to molecular weight is seen. Bagley (1961) reported that for linear polyethylene and polystyrene the product of molecular weight and critical shear stress is constant and could be related to recoverable shear strain. Tordella (1969) also observed inverse dependence of critical stress on molecular weight. Wang and Drda (1996b) extruded HDPE resin of various molecular weights in a controlled stress rheometer. They found that the critical stress scales as $\sigma_c \propto M_w^{-0.5}$ irrespective of the molecular weight distribution [see figure (2.10)]. They explained this behavior based on the scaling theory of Brochard and de Gennes (1992). We will discuss the details of this scaling in the next section.

A broader molecular weight distribution is known to reduce the severity of the fracture. In 1962, Sabia and Mullier observed that as the polydispersity increases, the hysteresis loop becomes shallower. Similar behavior was also observed by Myerholtz (1967). Vinogradov *et al.* (1984) observed that with increasing polydispersity the transition from lower curve to the slip branch occurred continuously (smoothly).

To the best of our knowledge Den Otter (1970, 1971) was the first to report on the absence of melt fracture in LDPE. He observed pressure drop oscillations for linear polyethylene in a rate controlled rheometer, but reported that no such pressure fluctuations occurred for branched polyethylene (LDPE). Similar observations about the long chain branched polyethylene (LDPE) have been made by many investigators [for e.g., see Utracki and Gendron, 1984; Yang *et al.*, 1998a]

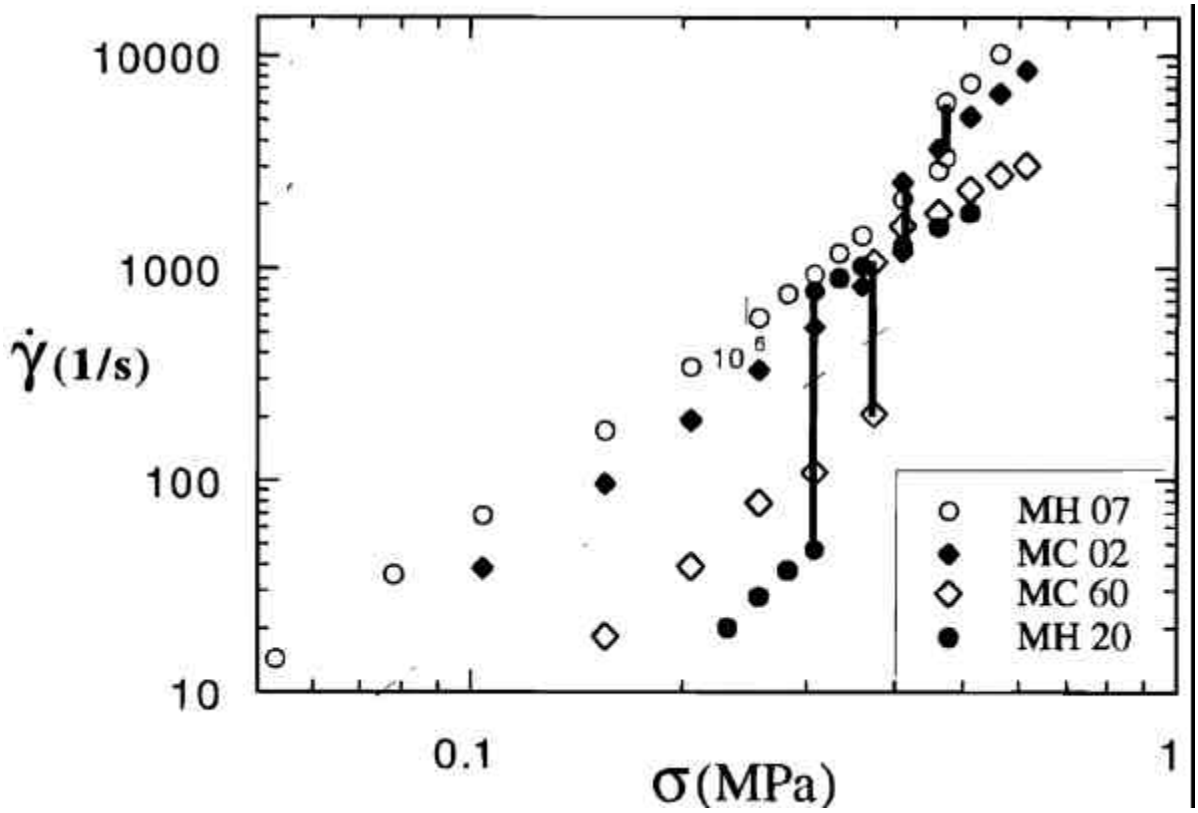

Figure 2.10 The flow curves for linear polyethylene of various molecular weights. Molecular weight increases as MH07<MC02<MC60<MH20. It can be seen that as molecular weight increases the jump in the apparent shear rate also increases. Further the critical wall shear stress can be seen to be decreasing with increase in molecular weight. (Reproduced with permission. From Wang and Drda, 1996b; © 1996, American Chemical Society)

The entanglement molecular weight is one of the most important parameters that decide the fracture behavior of the polymer melt in the shear flow. As discussed earlier, the polymeric liquid does not show stick-slip behavior unless its molecular weight is above some threshold value, which is related to the entanglement molecular weight (Vinogradov *et al.,* 1984). An interesting effect of the entanglement molecular weight on slip in polymer solutions is discussed later in this section. Tapadia *et al.* (2000) showed that syndiotactic polypropylene (s-PP) showed the sharkskin instability but the isotactic polypropylene (i-PP) of the same molecular weight and polydispersity failed to show any instability. Based on the sharkskin theory of Barone *et al.* (1998) they argue that since the entanglement molecular weight of s-PP is lesser than that of i-PP, s-PP is more prone to sharkskin instability for comparative molecular weight.

2.2.1.2.4. Nature of polymer-wall interface

The effect of die material on slip has indeed been a very important issue in discerning the mechanism of slip. One of the first reports on the effects of die material on slip characteristics is by Clegg (1957), in which he extruded polyethylene through roughened as well as smooth glass dies and found no difference in the slip behavior. Similarly Tordella (1963) extruded linear polyethylene through steel, glass, graphite and fluoropolymer dies and found no difference in critical stress for extrudate distortion. Vinogradov *et al.* (1984) studied various grades of PB of different molecular weights and polydispersity. They used steel, glass, teflon and teflon coated steel capillaries. Contrary to Clegg's observations, they observed that the flow curves for teflon and teflon coated capillaries bifurcated much before the point at which slip was observed in steel and glass capillaries. Also, the shear rate increase in teflon and teflon coated capillaries was seen to be much faster than that compared to the inorganic surfaces

In 1986, Ramamurthy revisited the effect of die material on slip behavior. He extruded an LLDPE resin through dies of various materials and observed that although the critical stress at the onset of surface distortions did show a dependence on the die material, the critical stress at the onset of the flow fluctuations showed a comparatively poor dependence. He noted that the onset of the melt fracture can be eliminated in film extrusion by using an alpha brass (a copper-zinc alloy with more than 20% zinc) die. Based on these results he argued that the slip occurred due to adhesive failure between the wall and the polymer melt. Halley and Mackay (1994) extruded LLDPE through dies

containing inserts made up of various metals located at the die exit. They observed that the viscosity was independent of the die exit material except for the brass insert where a significant increase in exit pressure was observed. They argued that the porous, copper-rich brass surface increased adhesion between the LLDPE and die exit, which subsequently increased the pressure drop. Person and Denn (1997) also observed a decrease in shear rate at same shear stress with the α-brass dies as compared to stainless steel. They argued that the different adhesive energies of steel-LLDPE and α-brass-LLDPE were responsible for such behavior. Chen *et al.* (1993) studied the effect of material of construction and surface roughness on the slip behavior of LLDPE. They found comparatively high slip velocities for stainless-steel die and lowest slip velocity for aluminum die. Further, they also observed an increase in slip velocity by decreasing the surface roughness.

Several investigators have studied the effect of organic coatings (e.g. fluoropolymer) on the slip behavior. Most of them have shown a massive enhancement of slip even at lower shear stresses along with the complete elimination of extrusion instabilities [Hatzikiriakos *et al.*, 1995; Piau *et al.*, 1995; Wang and Drda, 1997a]. Figure (2.11) shows that the flow curve corresponding to a fluoropolymer coated die bifurcates from the flow curve for a steel capillary at a lower pressure drop, indicating massive slip. Recently Barone and Wang (2000) extruded a carbon black filled polyethylene and polybutadine through a slit die with only the lower half coated with fluoropolymer. By visual inspection they show that the colored polymer sticks to the bare half of the die while slips on the coated die. Contrary to this Person and Denn (1997) observed no effect of fluoropolymer coating when compared with stainless steel coating. They argued that massive slip was seen only when the fluoropolymer was vapor deposited on the wall and not when it was solution-deposited.

Wang and Drda (1997a) investigated slip in a threaded die. It was believed that the bulk molecules entangle with the stagnant molecules to give rise to no-slip boundary condition. Compared to the smooth die, the sudden increase in flow rate occurred at higher wall shear stress for the case of the threaded die. Wang and Drda (1997a) postulate that the slip occurs due the sudden disentanglement between the chains stagnant in the threaded portion and the flowing bulk molecules.

2.2.1.2.5. Die geometry

The variables associated with the die geometry are the length of the die, its diameter, and the entry angle. It is generally observed that increasing the capillary length and decreasing the entry angle tend to lower the severity of the instability by apparently increasing the critical stress and the rate at the onset of the distortion, while the critical stress at the onset of distortion is observed to be independent of capillary diameter [Boudreaux and Cuculo, 1977]. Tordella (1963, 1969) observed that the jump in apparent shear rate, $32Q/\pi D^3$, (where Q is flow rate and D is the diameter of capillary) increases with increase in L/D of the capillary but occurs at the same critical wall shear stress. Den Otter (1971) observed that the extent of the hysteresis increases with increase in capillary length. Vinogradov *et al.* (1984) observed that the jump in flow rate increases with increase in L/D of the capillary. Similar results of increase in jump of apparent shear rate with a decrease in diameter or an increase in L/D have also been shown by Wang and Drda (1996a, 1997b) [see figure (2.12)]. Recently Lee and Mackley (2000) analyzed the flow behavior of LLDPE by using their multipass rheometer [Mackley *et al.*, 1995] using capillaries of different L/D. They simulated this flow numerically keeping a no slip boundary condition. They observed that the simulation predicted the observed behavior quantitatively for lower L/D but required to account for slip at higher L/D. Contrary to these observations Person and Denn (1997) observed that the flow curves for LLDPE extruding through a steel die are independent of the gap spacing. Based on the theory of Hill *et al.* (1990), they argued that the measurable gap dependence is not a necessary consequence of wall slip. If the slip velocity is pressure dependent then its combined effect with slip can mask the gap dependence [Person and Denn, 1997].

Wales (1969) reported the absence of fracture in slit dies for LDPE, while fracture was observed in the case of capillary dies at similar stress. However, no difference between the two geometries was observed for HDPE. Various investigators have studied the comparative effect of slit versus capillary geometry on the slip characteristics. While some studies indeed show a difference, others show no effect of such geometry change. All such observations up to 1976 have been reviewed by Petrie and Denn (1976).

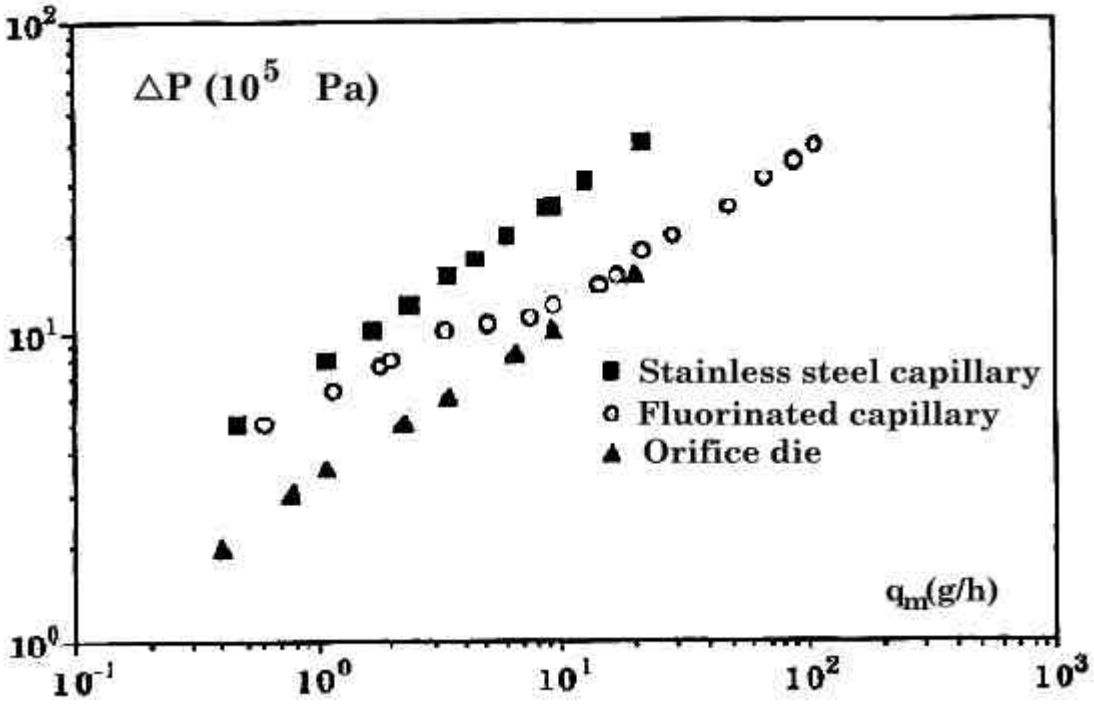

Figure 2.11 The flow curves for PBD for various dies. The ordinate is flow rate while the abscissa is pressure drop. It can be seen that the flow curve for the fluorinated capillary shows a massive slip as compared to stainless capillary after a critical pressure drop. (Reproduced with permission. From Kissi and Piau, 1996a; © 1996, Elsevier Science B. V.)

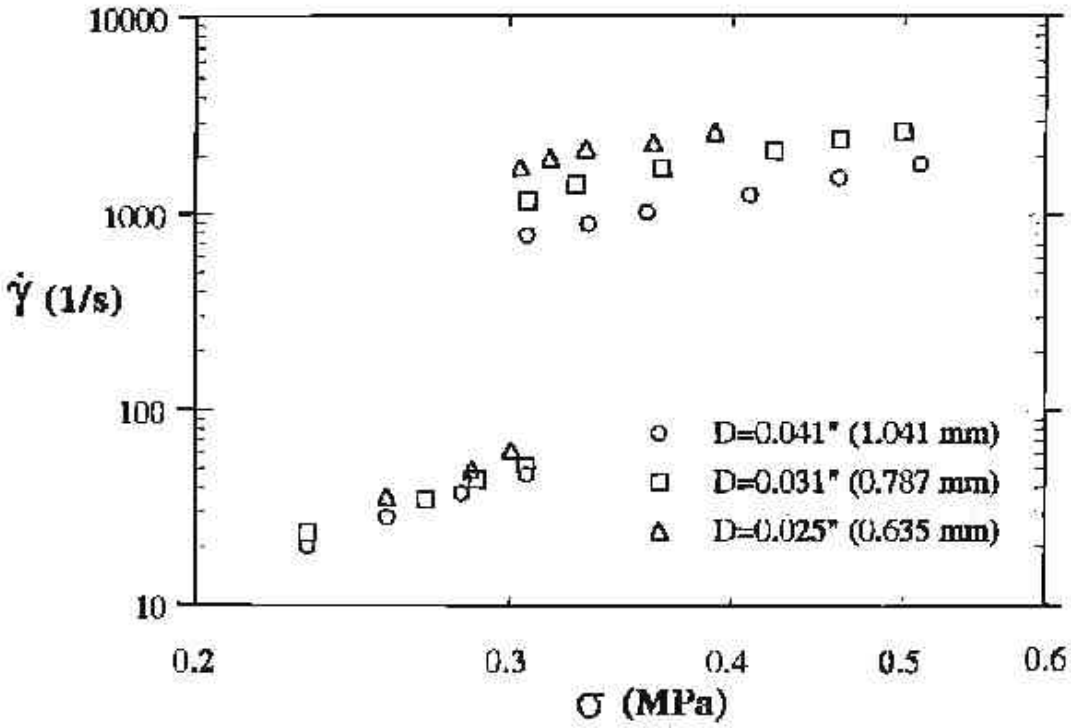

Figure 2.12 The flow curves for the linear polyethylene for various capillary diameters. It can be seen that after a discontinuous jump the flow curves show diameter dependence. (Reproduced with permission. From Wang and Drda, 1996a; © 1996, American Chemical Society)

It is generally observed that a conical entry into the die delays the extrudate distortion. [Boudreaux and Cuculo, 1977] Schreiber *et al.* (1960) and Bagley and Schreiber (1961) argue that the value of critical shear stress and shear rate increases with taper since the deformation of fluid in various regions above capillary inlet becomes homogeneous. Ballanger *et al.* (1971) reported that the effect of the tapered entry decreased the severity of distortion. Piau *et al.* (2000) studied the effect of various porous media placed at the entrance of an extrusion die, on the slip characteristics of HDPE as well as PDMS resin. Although they observed a significant increase in pressure drop, the flow curve did not show any discontinuity or hysteresis. Recently Liang and Mackley (2001) have reported an application of gas-assisted extrusion process. They inject a gas at the metal die-molten polymer interface, which gives the full slip boundary condition. The formation of a low viscosity gas layer at the wall substantially reduces the overall stress level of the polymer at the exit of the die. Such massive slip and reduction of overall stress level also shows a significant reduction in the die swell of the emerging extrudate.

2.2.1.2.6. Fillers

Various fillers and additives are known to influence slip behavior. Plasticizers are commonly used to enhance slip at the extruder wall in case of polyvinylchloride [Todd, 1972]. There are not many observations on the effect of fillers on the slip behavior in polymeric liquids. Bagley and Schreiber (1969) have reported that the addition of titaniumdioxide increased the critical stress for the onset of instability. They further noted that above 10 % addition of titaniumdioxide, the extrusion instability completely disappeared. Vinogradov *et al.* (1984) observed that when 100:30 PB-carbon black was extruded, the critical shear stress for the onset of instability increased and the jump in flow rate decreased as compared to the unfilled PB. The appearance of the extrudate after the transition was found out to be regular and smooth than that observed in the unfilled PB. Recently Rosenbaum *et al.* (2000) and Hatzikiriakos (2000) compounded small amount of boron nitrate with various polyolefin resins. They observed that typically 200-1000 ppm of boron nitrate not only eliminated the surface melt fracture (sharkskin) but also postponed the onset of gross melt fracture to significantly higher shear rate values depending on the resin, boron nitrate type, temperature, and additive content. Akay (1983) studied glass fiber filled PP in an injection capillary rheometer in which he forced the material through multiple capillaries. He found that the glass filled PP shows pressure as well as flow rate oscillations while calcium carbonate filled PP

does not. The fiber orientation studies showed a very high orientation of the glass fiber in the axial direction while flowing through the capillary.

Fluoropolymer based processing aids are commonly used in polyolefins for improving their flow properties. De Smedt and Nam (1987) used fluoropolymer-based rubber processing aid in LLDPE. They argued that the fluoroelastomer moves towards the wall-polymer interface, and acts as a lubricant. This enhances the slip and removes the processing instabilities. Lo *et al.* (1999) extruded the blend of HDPE and the fluoropolymer processing aid (Dynamar) through slit die and found the improvement in the flow behavior of HDPE. After the extrusion, they examined the slit die blocks using X-ray photoelectron spectroscopy (XPS), secondary ion mass spectroscopy and scanning electronic microscope. They indeed found the presence of a lubricating layer with the thickness in the range 5 to 15 μm, which tends to increase with shear rate at high Dynamar concentration. They found that the efficiency of viscosity reduction is independent of thickness of lubricating layer. Similar results are also discussed by Focquet and Blong (1998) and Chen and Feng (1997).

2.2.1.2.7. Wall slip in polymer solutions

Tomos (1949) reported the first observation of wall slip in a 2.5-gm/lit solution of PMMA in chlorobenzene. Ramamurthy (1974) extruded a highly elastic polyacrylamide solution [1.49% solution of Separan AP 30 in a 50% by weight water-glycerol mixture] through a capillary rheometer. He observed that at higher flow rate the exit stream alternately accelerated and decelerated, showing oscillations. Further increasing the flow rates made the stream chaotic. Interestingly, at very high flow rates, he observed a second stable regime, where the flow field abruptly changed from oscillating flow to a smooth steady flow. Cohen and Metzner (1982, 1985) extruded the 0.5% aqueous Separan AP 30 solution through a capillary and observed diameter dependent flow curves. Cohen and Metzner (1985) found a flow rate enhancement with decrease in capillary diameter. Similarly Metzner *et al.* (1979) and Cohen and Metzner (1982, 1985) found a decrease in viscosity with decrease in capillary diameter. Cohen and Metzner (1982) and De Vargas and Manero (1989) found an enhancement in flow rate over that of predicted by a no-slip theory with increasing pressure drop. Similar effects were seen by Chauveteauet (1982), Chauveteauet *et al.* (1984), Omari *et al.* (1989a, b), Kalashnikov and Vlasov (1978), Perez-Gonzalez *et al.* (1992). At a microscopic level slip has been observed by measuring

the velocity profile or the concentration profile near the wall. Muller-Mohnssen *et al.* (1987, 1990) measured velocity profile of aqueous solution of polyacrylamide through a capillary up to a distance of 0.15 μm from the wall. They observed a rapid increase in velocity from zero (no slip) velocity at wall, which occurred in a low viscosity boundary layer of thickness smaller than 0.15 μm. Rofe *et al.* (1996) also measured the velocity profile of a capillary flow of xanthan gum using nuclear magnetic resonance imaging. Figure 2.13 shows the velocity profile at various shear rates.

Recently Pluctaveesak *et al.* (1999) studied the flow behavior of entangled PB solution through the pressure controlled capillary rheometer. They observed a sudden increase in flow rate at a critical stress. They further observed that with increase in the concentration of solution, the critical stress as well as the jump in flow rate increases (see figure 2.14). Similar to the observation in melts, they observed the rise in critical stress with increase in temperature. The critical stress was seen to be proportional to the plateau modulus, which increases with temperature as well as concentration. They explain this behavior based on the scaling theory of Brochard and de Gennes (1992), which we will discuss in next section.

2.2.2. Drag flow

2.2.2.1. General observations

Most of the commercially used drag flow apparatus are based on the simple shear flow geometry shown in figure 2.1. These include cone and plate rheometer, plate and plate rheometer, couette rheometer and sliding plate rheometer. Several investigators have reported stick-slip instability in drag flow rheometers. The general observation is a discontinuous increase in shear rate [Mhetar and Archer, 1998b], gap dependent flow curves in the plate and plate rheometers [Hatzikiriakos *et al.*, 1993], and a substantial increase in slip length (b) with increase in shear stress [Mhetar and Archer, 1998a] or shear rate [Leger *et al.*, 1997b]. Observations of wall slip in drag flow apparatus are affected by various other instabilities such as inertial instabilities, secondary flow and meniscus distortion. The different instabilities are discussed in various review papers and books (Larson, 1992; Petrie and Denn, 1976; Dealy and Giacomin, 1998; Powell, 1998). In this section, we will summarize only those observations related to slip in drag flow geometry.

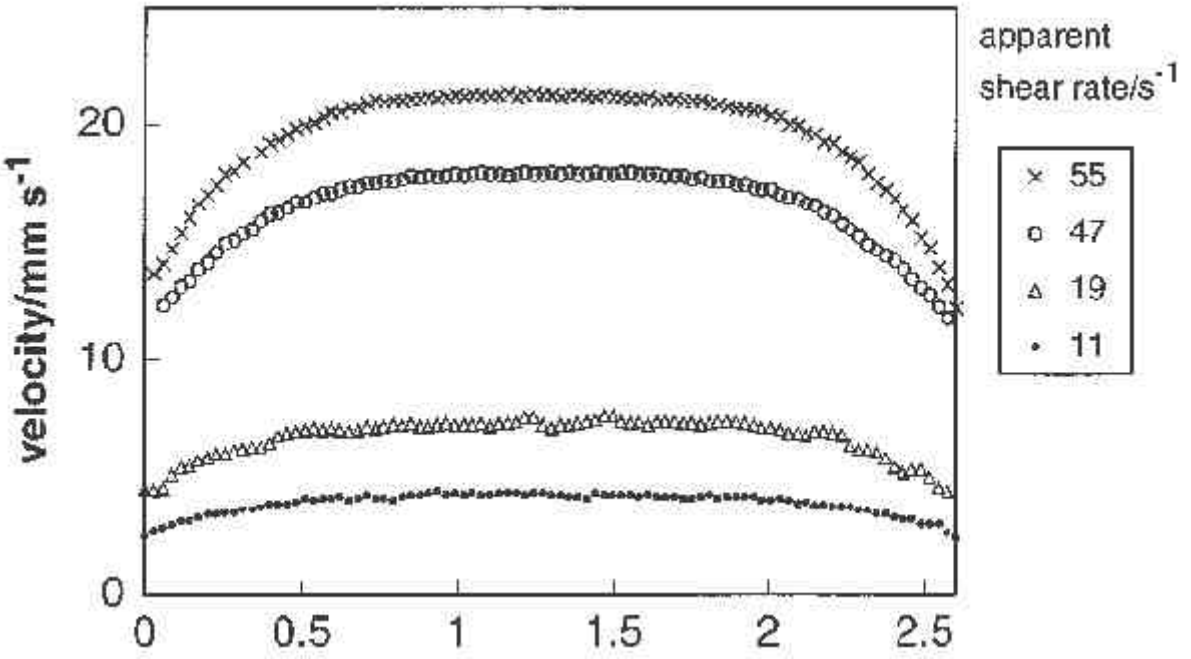

Figure 2.13 Velocity profile for xanthan solution in 2.6 mm capillary at various shear rates. (Reproduced with permission. From Rofe *et al.*, 1996, © 1996, Society of Rheology)

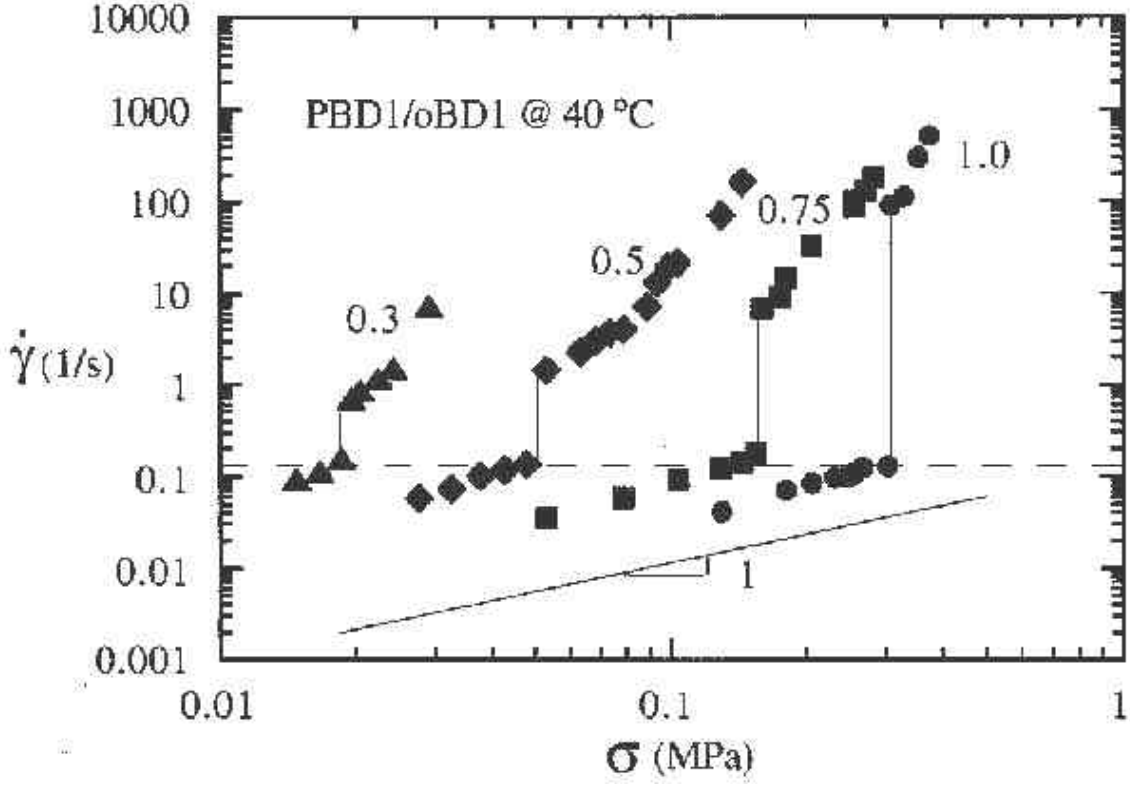

Figure 2.14 The flow curves for PBD solutions (in oligomeric PBD). The figure next to the curve shows volume fraction of the high molecular weight PBD. It can be seen that as the concentration (that is plateau modulus) increases from left to right the jump in shear rate as well as the critical stress for transition also increases. (Reproduced with permission. From, Plucktaveesak *et al.*, 1999; © 1999, American Chemical Society)

Burton *et al.* (1983) analyzed polystyrene (PS) melt of various molecular weights using the parallel plate geometry. They observed that the torque required for maintaining a particular shear rate increases with increase in the gap separation. This effect was evident for samples having molecular weights in the entangled region. Two explanations were suggested. The first was the possibility of higher orientation of the tethered chains leading to severe shear thinning locally in the vicinity of the wall. The other explanation concerned the possibility of a stagnant adsorption layer of thickness of the order of 20 μm near the wall, which decreased the effective thickness of the gap. Henson and Mackay (1995) also observed similar behavior for polystyrene samples on steel and titanium surfaces. They argued that the observed effect was due to true slip of the melt on the wall (chain sliding along the surface) and observed the molecular weight dependence of the slip length to be $b \propto M^{1.1}$. Laun (1982) used a short-time sandwich rheometer (SSR) developed in their laboratory, to measure high shear transient properties of the polyethylene melt. He observed that the stick-slip transition (change in boundary condition from no slip to slip) occurred over the time scale of the few miliseconds. He concluded that for the stick-slip transition to occur not only a specific critical stress but also a certain amount of orientation in the melt is needed to be achieved.

Hatzikiriakos and Dealy (1991) used their novel sliding plate rheometer (Giacomin *et al.*, 1989) to study the flow behavior of high density polyethylene (HDPE) melt on various surfaces. On a bare surface they found that slip occurred at a critical shear stress of 0.09 MPa. They used two fluoropolymer coatings of which one showed no change in critical shear stress, but lowered the slip velocity, while the other lowered the critical stress along with enhancing the slip velocity. From the observed results they concluded that wall slip was a result of an adhesive failure occurring at the wall-polymer interface. Hatzikiriakos *et al.* (1993) studied the effect of surface coating on slip behavior of LLDPE melt using the sliding plate rheometer. They observed that the flow curves became gap dependent after some critical stress was reached, which could be interpreted in terms of slip at the interface. They found that for various organic coatings the critical stress at the onset of slip, increased linearly with work of adhesion of the wall (coating)-polymer pair. Again, adhesive failure was inferred from the data.

Koran and Dealy (1999a) developed a high pressure sliding plate rheometer, which can operate up to the pressure 70 MPa and used the same to study the wall slip behavior of

polyisobutelene (Koran and Dealy, 1999b). They found that whenever the slip occurred due to disentanglement (cohesive failure) mechanism, the flow curves at different mean pressures superposed on each other after applying the necessary pressure correction. However, the corrected flow curves did not superpose when slip occurred by adhesive failure. They inferred that the various characteristics of slip due to cohesive failure scale with respect to pressure in a manner similar to the way in which the viscosity scales with pressure. However, this does not happen for the case of slip by adhesive failure. They did not observe a discontinuous shear rate jump from no-slip to slip branch at ambient as well as higher pressures. They argued that the discontinuous spurt phenomena might not be an intrinsic property of the polymer but could arise from various complications in the pressure driven flow (Koran and Dealy, 1999b).

Leger and coworkers [Migler *et al.*, 1994; Leger *et al.*, 1996b; 1997a; 1999] developed a new optical technique called near field velocimetry (N. F. V.) for the determination of velocity at the wall (i.e., up to 70 nm away from the wall). This technique requires the polymer molecules to be labeled with an easily photobleachable fluoroscent probe. The material is sheared between two surfaces of silica separated by a few microns by moving the top plate with a known velocity. They studied various polydimethylsiloxane (PDMS) grades of different molecular weights and various silica surfaces that were tailored to produce grafted layers of different surface coverage; different grafted layer thickness and end grafted surfaces with tethered PDMS chains of different molecular weights. In general for all the combinations they found an increase in slip velocity with increase in top plate velocity. For low surface coverage of strongly grafted chains, the slip velocity became almost comparable to the top plate velocity. They estimated the slip length (b) for various combinations of surfaces and PDMS grades. The slip velocity vs. slip length plot showed three distinct flow regimes. In the first regime of low slip velocity, the slip length was found to be independent of top plate velocity (or shear rate) and rather small. Above a critical velocity in the second regime, slip length increased with a power law dependence on slip velocity. At higher slip velocity in the third regime, the slip length again became independent of slip velocity and the magnitude of b was found to be a few order of magnitude higher than the molecular dimensions [see figure (2.15)] [Leger *et al.*, 1997b]. The value of critical velocity (at which slip length starts increasing) was seen to be dependent on the molecular weight of the flowing polymer and the nature of surface [Leger *et al.*, 1996; Leger *et al.*, 1999].

They further found that the critical shear rate shows a maximum when plotted with respect to surface grafting density. The critical shear rate increases linearly with surface grafting density at low values of grafting density and then starts decreasing with grafting density at higher values of grafting density. They inferred that the critical shear rate increases initially because of the additive effect of friction on each of the tethered chains, which act independently at the low surface coverage (the so-called "mushroom regime"). At high surface coverage the critical shear rate decreases because of collective behavior of the tethered chains [Durliat *et al.*, 1997]. They measured the dependence of critical slip velocity on the molecular weight of the bulk chains and that of the tethered chains. Their experimental data showed $V_s^* \propto M_P^{-3.3} M_N^{-1}$, where M_P is the molecular weight of the bulk chains and M_N is the molecular weight of the tethered polymer [see figure (2.16)]. These observations are in excellent agreement with the predictions of the disentanglement model proposed by Brochard and de Gennes (1992). We will discuss this model and related work in detail in the second section of the literature survey.

Mhetar and Archer (1998a) investigated wall-slip behavior of a concentrated solution of narrow molecular weight distribution polystyrene in diethyl phthalate. A plane-couette flow apparatus was used in their experiments. On bare silica surface the slip velocity vs. shear stress plot showed various power law regimes while slip length vs. shear stress plot showed four distinct flow regimes. For low stresses (no-slip), the slip length was independent of shear stress. After a critical stress was crossed, the slip length showed a power law dependence with respect to the shear stress and increased up to factor of three depending on the concentration of the solution. In the third region, the slip length again remained constant while in the fourth region the slip length decreased with respect to the shear stress [see figure (2.17)]. They also studied slip behavior on an Octadecyltrichlorosilane grafted silica surface. This organic surface showed about an order of magnitude increase in the slip length at low stresses than that compared with the bare silica surface. They proposed a scaling model, which explained the various power regimes observed by them. This model was based on the disentanglement mechanism and will be discussed in the next section. Mhetar and Archer (1998b, 1998c) studied the slip behavior for various polybutadine resins with narrow molecular weight distribution in a plain couette apparatus. On a clean silica glass surface, they found a discontinuity in the slip velocity at a critical stress when the hydrodynamic boundary

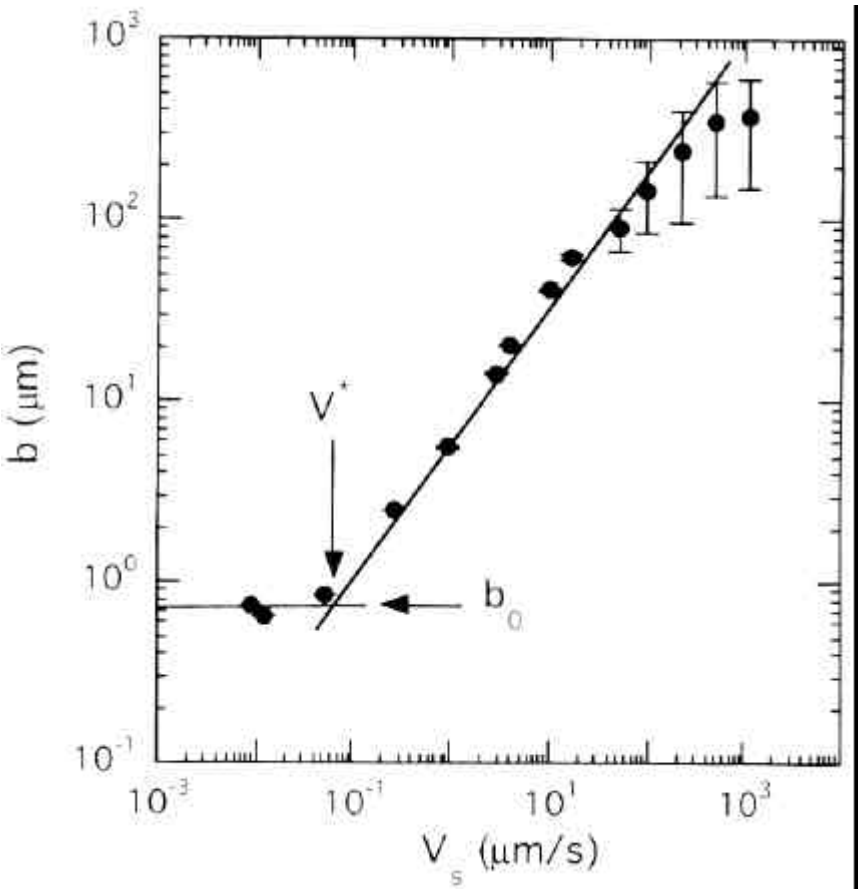

Figure 2.15 Slip length b plotted slip velocity. Three regions of slip length can be clearly seen. (Reproduced with permission. From Leger *et al.*, 1996b; © 1996, Elsevier Science B. V.)

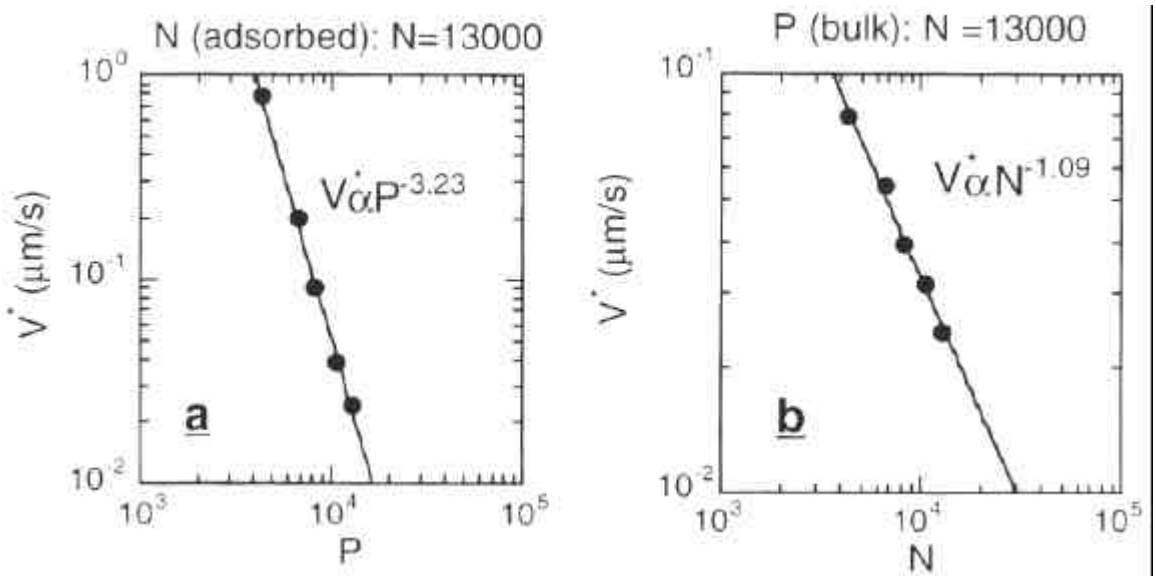

Figure 2.16 Dependence of critical slip velocity on the molecular weight of bulk as well as the tethered chain for nearly monodispersed PDMS melt. N represents number of monomers in tethered chain while P represents number of monomers in bulk chain. (Reproduced with permission. From Leger *et al.*, 1996b; © 1996, Elsevier Science B. V.)

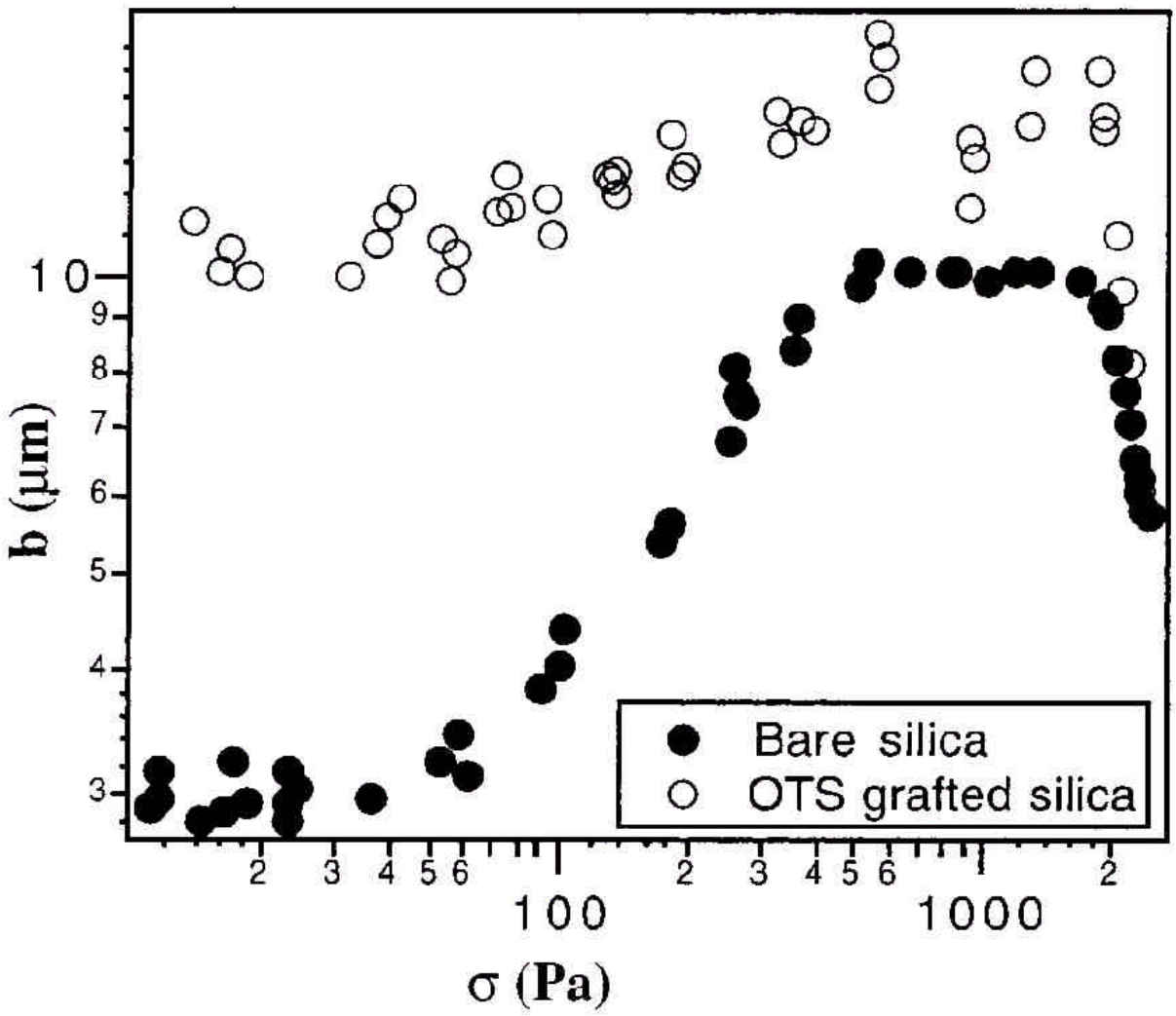

Figure 2.17 The slip length b is plotted with the wall shear stress. The forth region where the slip length decrease with stress can be clearly seen. Further it can be seen that the octadecyltrichlorosilane grafted silica surface shows massive surface as compared to bare silica at very low shear stress also. (Reproduced with permission. From, Mhetar and Archer, 1998a; © 1998, American Chemical Society)

condition changed from no-slip to slip. In addition, the critical shear stress was found to scale linearly with plateau modulus, $\sigma_c \approx 0.22 G_N^0$. They argued that this dependence is consistent with the scaling model for the disentanglement proposed by them in an earlier work [Mhetar and Archer, 1999a]. They used various treated silica surfaces and noted the change in slip behavior, depending on the energies as well as roughness of the surfaces.

2.3. **Theoretical analysis:**

The various experimental observations summarized in the previous section show the rich behavior of the wall-slip phenomenon. Several mechanisms and models have been proposed to describe wall slip. These include inertial instability, shear wave instability, entry instability, viscous heating, stress induced migration, constitutive instability, disentanglement (cohesive failure) and debonding (adhesive failure). Some of these mechanisms are contradictory to each other, while some are probably exclusively operative under different experimental conditions. In this section, we will summarize some of the important mechanisms relevant to the present work. The details of the other mechanisms can be found in various review papers [White, 1973; Petrie and Denn, 1976; Boudreaux and Cuculo, 1977; Denn, 1990; Larson, 1992; Agarwal *et al.*, 1994]. The different theoretical mechanisms for sharkskin and the controversial issues regarding them are not discussed in this chapter in detail because they are out of scope of the work presented in this thesis.

2.3.1 Stress induced migration:

The phenomenon of stress induced migration and its implication on apparent wall-slip has been investigated extensively [Agarwal *et al.*, 1994; Barnes, 1995]. Metzner *et al.* (1979) predicted slip by considering the diffusion of polymer molecules in the direction of stress gradient and by calculating the depletion layer thickness (slip layer thickness) δ. Tirrel and Malone (1977) solved the uncoupled diffusion and momentum equation by ignoring the dependence of viscosity on concentration. They estimated that the length to diameter ratio L/D required to achieve 63 % of fully developed concentration profile was 5000 and thus concluded that this mechanism cannot predict slip seen in capillaries with much lower L/D ratio. Janssen (1980) coupled viscosity and concentration and proposed an *instability mechanism*, which predicted that concentration redistribution, is

completed in a relatively short time. Dutta and Mashelkar (1983) extended this analysis to channel flow but the predictions showed considerable difference with experimental data, which casts doubt on the instability mechanism. Cohen and Metzner (1982) found that though it takes a long time for concentration profile to develop fully, depletion near the wall is rapid, which was sufficient for slip to occur. Dutta *et al.* (1987) estimated flow length required for stress induced diffusion in capillary flows, and found it to be considerably less than the previous analysis done by neglecting viscosity and concentration dependence. Recently Mendez-Sanchez *et al.* (1999) developed a two-fluid model, which considers the capillary flow field to be consisting of two concentric regions filled with immiscible fluids. The core is the polymeric solution (bulk) while the small annular region is the polymer-depleted layer. They consider a power law model with different parameters in both the layers. The two fluid model predicts an apparent slip and shows that the slip velocity calculated by Mooney [Mooney, 1931] method is dependent on flow geometry.

However, the stress induced migration theories suffer from four main drawbacks. Firstly, there is a fundamental difficulty in introducing thermodynamic arguments for stress induced migration in a flowing (non-equilibrium) system. Secondly, different theories predict contradictory trends for migration in capillary flows. [Agarwal *et al.*, 1994]. Thirdly, there is no convincing experimental evidence for radial migration of polymer molecules in pipe flow. Finally, the predicted L/D for slip to occur is still too long compared to experimental data.

2.3.2 Constitutive instability

Constitutive instability of the bulk fluid was proposed as another mechanism for wall slip. This mechanism is related to a non-monotonic shear stress-shear rate relationship. The idea was first proposed by Huseby (1966), who then developed a constitutive equation based on Pao's theory [Pao, 1962; Pao, 1964] for predicting a non-monotonic flow curve. He argued that the behavior observed by Bagley *et al.* (1958) and Tordella (1963) is constitutive in nature. He added that the flow rate discontinuity occurs due to the non-monotonic shear stress-shear rate behavior of the polymer melt [see figure (2.18)]. Because of the convincing predictions of this hypothesis the constitutive (bulk) instability idea gained a lot of popularity in later years.

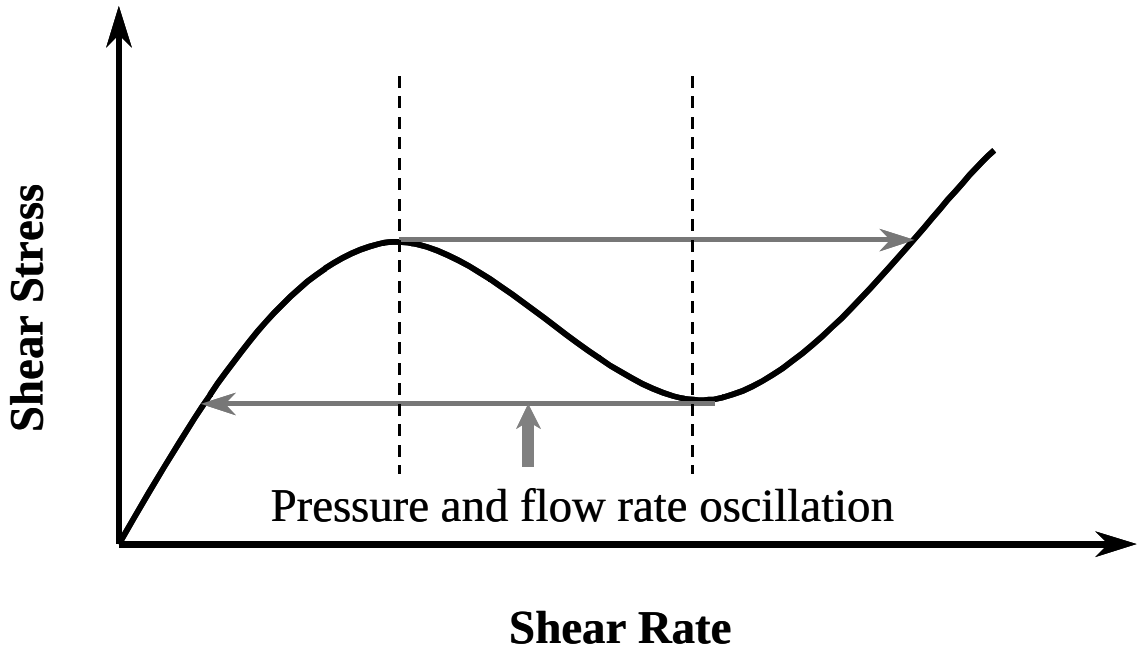

Figure 2.18 A non-monotonic flow curve represents a constitutive instability. A hysteresis loop under controlled stress mode can be clearly seen. The part of the flow curve with negative slope is argued to give rise to pressure and flow rate under rate controlled extrusion mode.

In 1978, Doi and Edwards (1978a, 1978b, 1978c) proposed a systematic approach towards the modeling of the dynamics of entangled polymeric liquids. In their theory, a polymer chain was considered to be confined to the tube formed by constraints posed by the surrounding molecules. It was proposed that the confined molecule undergoes a longitudinal motion along the tube to relax its orientation. This snake-like motion along the contour was called the reptation. Although this model was highly successful in predicting various experimental observations in the linear viscoelastic region, it predicted a maximum in shear stress under steady shear flow. The cause of this non-monotonic nature was hinted to the lack of effective relaxation modes for fast flows [Doi and Edwards, 1979]. The shear stress shows maximum when the shear rate is of the order of $1/\tau_d$, where τ_d is the reptation time. They argued that the predicted response might correspond with the melt fracture behavior seen in polymer melt [Doi and Edwards, 1979]. Doi (1980a) extended their earlier model to incorporate the short time relaxation modes. Lin (1985) made use of this model and predicted a stress minimum following the a stress maximum of the original Doi-Edwards model. He showed that the discontinuous jump in the flow rate at a critical stress increases with increase in molecular weight and that increasing the polydispersity can eliminate the dip in the shear stress-rate plot. He concluded that the melt fracture phenomena were related to the bulk instability of linear polymers of high molecular weight and low polydispersity.

McLeish and Ball (1986) extended Doi-Edwards theory by incorporating two distinct relaxation mechanisms. These were the reptation time (τ_d) and the other contour length equilibrium time (τ_{eq}). The latter involves random fluctuation of Rouse chain. Similar to the Lin (1985) model, the McLeish-Ball model predicted a stress maximum followed by a stress minimum for polymer of a molecular weight above a threshold value. McLeish (1987) extended the earlier model and showed that the stability of the interface between the low shear and high shear regions is determined by the normal stresses. Several empirical models such as the KBKZ model, the Jonhson-Segalman model, the corotational Maxwell model and the Giesekus model also show a non-monotonic flow curve for a particular set of fitting parameters [Bird *et al.*, 1987a]. Kolkka *et al.* (1987) and Malkus *et al.* (1990) predicted a non-monotonic flow curve for the Jonhson-Segalman and Giesekus models and argued that the experimentally observed phenomenon that gives an appearance of slip could in fact be governed solely by material properties of the fluid. Deiber and Schowalter (1991) also showed the non-

monotonic curve for Doi-Edwards, Jonhson-Segalman and corotational Maxwell model. They showed that the predictions of these models fit the spurt data of Lim and Schowalter (1989) quantitatively. Effects such as a first order transition in flow rate, hysteresis and the possibility of pressure drop oscillations can be successfully explained with a non-monotonic flow curve [Hunter and Slemrod, 1983; McLeish and Ball, 1986; Deiber and Schowalter, 1991].

There are several drawbacks of this hypothesis. Firstly, it fails to show any diameter dependence of flow curves, which is a distinct feature of wall-slip observed experimentally. Further, bulk instability hypothesis predicts that the interface of shear rate discontinuity propagates towards the center as pressure drop increases, which is not observed experimentally. Recently Yang *et al.*, (1998b) related the hysteresis seen in the spurt flow to the history of the sample being sheared. They argued that since the sample from the barrel is constantly being brought into the die, sample under investigation cannot visit its history upon the discontinuous transition. Hence, it is not possible to observe any hysteresis phenomenon in capillary flow if the mechanism is intrinsic (that is constitutive instability). They further argued that the hysteresis would only be seen if the phenomenon is interfacial in nature since the chains at the interface that are adsorbed on the wall remain in the die and hence can revisit their history.

2.3.3 Adhesive failure (debonding) mechanism:

Adhesive failure at the wall has been proposed to be responsible for slip in melt extrusion, since the energy of the wall-polymer interface is known to dramatically influence slip behavior [Ramamurthy, 1986; Kalika and Denn, 1987]. The adhesive failure hypothesis proposes that polymer molecules adsorbed on the wall undergo a sudden desorption above a critical shear stress and hence slip at the wall. Vinogradov *et al.* (1972) argued that this phenomenon occurs due to a transition from a fluid state to a highly elastic state at higher shear rates. In the high elastic state polymer melts behave similar to a crosslinked polymer, and hence detach from the wall (surface) and slip. They further argued that the hysteresis loop in the flow curve is due to transition of the material into another physical state, which along with the bulk compression, gives rise to pressure and flow rate oscillations [Vinogradov *et al.* 1972; 1984]. They proposed that for such transition to occur the critical shear rate should correspond to the maximum of the loss modulus ($G''_{\max}$) [Vinogradov *et al.*, 1977]. Extending Vinogradov *et al.*'s, (1984)

argument Denn (1990) argued that there is a critical stress at which the tethered chain suddenly desorps from the surface. These desorped chains at the wall are under a high degree of orientation. Since the orientation causes substantial change in free energy, re-adsorption is unlikely. Re-adsorption can only occur by either diffusion of chains from the bulk or after the relaxation of the chains in the vicinity of the wall. Since both these processes are slow, the period of stick-slip should be of the order of residence time of the melt in the capillary as experimentally observed by Kalika and Denn (1987).

Lau and Schowalter (1986) where the first to propose a kinetic rate model of surface-bulk exchange of free and bonded macromolecules. They predicted a power law dependence of slip velocity and wall shear stress above a critical stress. Stewart (1993) modified the above model, which is based on the concept of activation rate theory of kinetics of chemical reactions and showed the dependence of slip velocity on normal stresses. Hill *et al.* (1990) showed that the stress dependence of slip velocity could be correlated with peel experiments of polymer on metal surface. Hatzikiriakos and Kalogerakis (1994) solved a transient network model for special case of polymer/wall interface. They suggested that whenever the end-to-end length of a segment that is attached to the wall was less than a critical segment length, the slip velocity was zero. When such a length crosses critical length, the segment breaks and system obeys an empirical slip equation. Hatzikiriakos (1995) modified above model to incorporate multiple relaxation modes.

Black and Graham (1996) proposed a semi-empirical model based on unsteady state kinetics of wall-polymer interactions. The model takes into account both shear and normal stresses and shows that the slip leads to instability in the viscoelastic shear flow. Hill (1998) proposed a quasi-chemical model in which polymer chains near the wall undergo a dynamic adsorption-desorption process, which is influenced by the flow. He argued that even under strong slip condition, the polymer melt-solid interface is always under the equilibrium. The model predicted a critical wall shear stress at which large slip occurs naturally by sudden desorption of the chains from the wall. Recently Yarin and Graham (1998) have proposed a slip model based on the proposition that the lifetime of a tethered chain under shear flow is proportional to the excess energy gained by the tethered molecule due to the flow. In the case, where the detachment of tethered chains precedes disentanglement, they predict that the shear stress-slip velocity relationship becomes non-monotonic due to the desorption of tethered chains. They also

predict that when slip occurs by debonding, the slip length is independent of temperature. They argue that the temperature independence of the slip length may not be an appropriate criterion for assigning the slip mechanism to be disentanglement driven. Anastasiadis and Hatzikiriakos (1998) measured the adhesive energy for various wall-polymer pairs using the pendent drop method. Figure (2.19) shows the critical shear stress plotted against adhesive energies calculated using above method. From the linear relationship between the adhesive energy and critical shear stress, they argued that the adhesive failure was the governing mechanism for slip.

Chain desorption mechanism has an important limitation. The theory is applicable only when the wall-polymer melt adhesive energy is low so that the molecule could be detached from the wall under flow. Although the experiments of Ramamurthy (1986) and Person and Denn (1997) show the effect of die material on critical shear stress, this is an indirect evidence of possibility of wall slip by debonding mechanism. However, the effect of die material indeed influences the configuration of the tethered molecule and thus can change the critical stress for disentanglement as well. Although there is a strong debate on whether polymer slips on metal surface by adhesive failure or by cohesive failure, it is generally accepted that polymer melt slips on organic surfaces by adhesive failure and that of on inorganic surface by cohesive failure [Wang, 1999].

2.3.3 Cohesive failure (disentanglement) mechanism:

It is generally believed that chains, which are strongly tethered to a high-energy wall, disentangle from the bulk chains at a critical stress leading to discontinuous slip by a 'disentanglement' mechanism. This picture was first conceptualized by Bergam (1976) when he argued that “the temporary network of entangled chain molecules yields through sudden disentanglement when shear stress is increased to a definite value, thus providing a thin layer of low-viscosity polymer where this value first is reached, i. .e. at the die periphery of the die entrance, and subsequently over the whole inner surface of the die”.

Although the concept of disentanglement was proposed way back in 1976, it couldn’t attract much attention until early 90s when the wall slip problem in melts was re-visited by Brochard and de-Gennes (1992). In a seminal contribution, they developed a scaling model for the flow of a polymer melt along the wall on which the chains of the

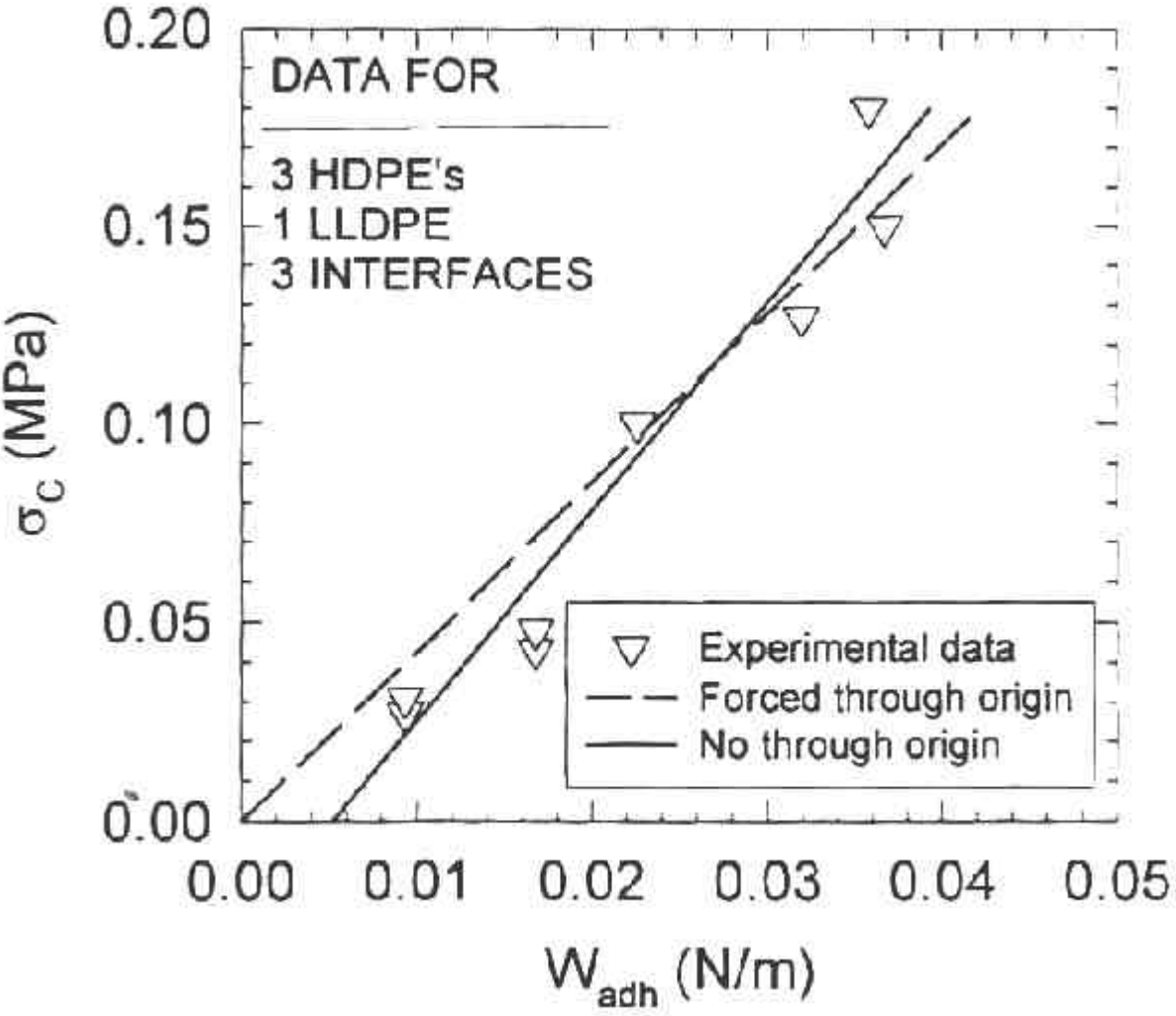

Figure 2.19 The critical shear stress for the onset of slip as a function of work of adhesion for different polyolefins on various interfaces. The authors claimed the adhesive failure to the governing mechanism for slip from above plot. (Reproduced with permission. From Anastasiadis and Hatzikiriakos, 1998; © 1998, Society of Rheology)

same polymer are tethered and entangled with the bulk chains. The model was developed for the case of low grafting density of tethered chains in the so-called 'mushroom' region, in which different tethered chains do not overlap with each other. They argued that under the influence of flow a tethered polymer chain deforms into a 'cigar' shaped coil and when the diameter of the deforming cylindrical coil of a tethered molecule decreases below the entanglement spacing the bulk chains suddenly disentangle from the tethered chains causing discontinuous slip. They proposed that polymer chains adsorbed on the wall undergo a coil to stretch transition at a critical shear stress. Since stretched molecules cannot entangle with the bulk molecules, the bulk slips past the stretched chains. They showed that the critical shear stress is given by,

$$\sigma_w^* = \Sigma\, k_B T / a \qquad (2.2)$$

where Σ is the number of chains per unit area grafted to the wall, a is the segment length or the entanglement distance (average distance between two entanglements). Equation (2.2) indicates that the critical wall shear stress σ_w^* increases with temperature and grafting density (in mushroom regime). As discussed in the earlier section, Wang and Drda (1996a) indeed observed an increase in critical stress with temperature [see figure (2.9)]. Recently Pluctaveesak *et al.* (1999) showed that the critical shear stress also increases with increase in concentration of the solution [see figure (2.14)]. Since increasing concentration or plateau modulus is equivalent to decreasing the segment length a, this behavior is also successfully predicted by the model. The Brochard-de Gennes model theoretically predicts three regions of slip as seen by Leger *et al.* (1997b) except in the first region, where the theory predicts small decreases in the slip length with slip velocity [see figure (2.16)]. Based on Brochard and de Gennes's (1992) calculations Wang (1999) showed that $\Sigma \sim M^{-0.5}$ and since all other parameters in equation (2.2) are independent of molecular weight, σ_w^* varies as $M^{-0.5}$ as observed by his group experimentally [Wang and Drda, 1996b].

Ajdari *et al.*, (1994) extended the Brochard and de Gennes (1992) model for various values of the bulk molecular weight. Further, they considered a probe chain (tethered chain) as being pulled through a stationary bulk of different molecular weight, which is equivalent to considering the bulk flowing past a stationary wall. They consider the non-uniform (trumpet-like) deformation of the probe chain. They argue that the probe chain relaxes its stress similar to that of an arm of a star polymer. The usual reptational

diffusion is not possible because of tethering at one end. The various other modes of relaxation, which they consider are arm retraction and constraint release. They predict that at low slip velocities the friction of the undeformed probe chain is very strong. As the slip velocity increases, the probe chain deforms and above a certain threshold stress becomes almost velocity independent. They further predict that as the molecular weight of the bulk chain increases, the jump in slip velocity at the critical stress, goes on increasing. Brochard-Wyart *et al.* (1996) considered the effect of different grafting densities (surface coverage) on the slip phenomena. They showed that at lower grafting densities the friction of the mushroom is additive. Above a threshold, since all the bulk chains near the wall are trapped, the low velocity friction becomes independent of surface coverage. They further showed that the critical slip velocity depends on molecular weight of tethered and bulk polymer as,

$$V_s^* \propto M_P^{-3} M_N^{-1} \qquad (2.3)$$

They observed that above a threshold surface coverage, the critical slip velocity increases linearly with the surface coverage. Recently Mhetar and Archer (1998a) developed a scaling model for the case of mushroom region. They also consider arm retraction and constraint release to be the relaxation modes of the tethered chain. They considered the conformational changes of the tethered molecule under flow and predicted various friction laws in different slip velocity regions, which qualitatively agreed with their experimental data.

2.3.4 Phenomenological Models.

Apart from molecular theories, various empirical theories have also been proposed to model slip behavior. Shore *et al.* (1996) proposed a slip model for a capillary flow of polymer melt, which incorporates the stick-slip boundary condition, describing the kinetics of the first order transition. They solve the momentum balance using Maxwell model and the stick-slip boundary condition. The model predicts spurt flow, periodic oscillations and complicated spatiotemporal structures, which they argue to be similar to sharkskin. Adewale and Levnov (1997) proposed a flow model, which consists of a viscoelastic constitutive equation, along with a hardening effect. They propose an empirical stick-slip boundary condition and also take into account the compressibility effect. They successfully predict various features of slip including onset of critical condition for slip, proper description of hysteresis, frequencies of the pressure oscillations, etc. Brassur *et al.* (1998) proposed a slip equation, which shows non-

monotonic slip velocity-wall shear stress relationship. They argued that multivaluedness of the constitutive equation is not required and multivaluedness of shear stress-slip velocity relationship can explain the observed spurt phenomena.

Molenaar and Koopmans (1994) proposed an empirical model, which predicts the pressure and flow rate oscillations in the stick-slip region. They argued that the *sawtooth* like pressure signal in this region resembles the relaxation oscillations phenomenon. They further argued that this phenomenon can be described only in terms of second–order differential equation or two coupled first order equations. They construct such equations by performing the mass balance across the capillary taking into account the compressibility and volume of the polymeric liquid remaining in the barrel. They predict the flow rate and pressure drop fluctuations using above system and argue that the compressibility of the material is an essential parameter in describing the polymer melt from instability. Ranganathan *et al.* (1999) extended the Molenaar and Koopmans (1994) model for applying it to the multipass rheometer (MPR) [Mackley *et al.*, 1995]. They generate the pressure vs. flow rate data for HDPE over a range of shear rates using MPR. They assumed an empirical relation between pressure and flow rate and predicted the flow oscillation data quantitatively. They argue that the pressure relaxation upon cessation of flow can be entirely attributed to the compressibility of the melt.

2.4 Concluding Remarks

Although wall slip, and in particular, the extrusion instabilities in melt, were first observed nearly five decades ago, the various distinguishing features of this complex phenomenon are still being explored experimentally and theoretically. Several decades of research in this field has indeed brought some consensus regarding the understanding of the underlying physics. However, some controversial issues still remain unresolved and often contradictory arguments are made by various groups to explain the same phenomenon. A critical review of the literature brings forth the existing gaps in understanding of the wall-slip phenomenon, which we will attempt to highlight in this section.

Adewale and Leonov (1997) have pointed out some flaws in the then available literature. They had argued that none of the models predict onset of spurt (drastic change from slip

to non-slip boundary condition). In addition, slip models proposed in general are highly empirical and operate with many fitting constants. Further, the viscoelastic properties of melt in bulk flow are ignored in most of the models. Finally, role of compressibility effect in spurt flows is poorly understood. The first two points highlight the need for a more molecular approach than the empirical one. While last two point out the need for considering the polymeric system as a whole rather than concentrating on individual issues.

From the discussion in the theoretical section it is evident that different mechanisms such as migration, desorption, constitutive instability and disentanglement exist to explain the observed instabilities associated with wall-slip. It is safe to assume that polymer migration may be ruled out for the case of concentrated polymer solutions and melts because of the problems listed earlier. Further it is clearly observed that over a wide range of shear rates, above the inverse of reptation time, the shear stress is nearly constant for very highly entangled melts or solutions or increases slowly with shear rate for less highly entangled ones [Mead *et al.*, 1998]. Apart from this, some distinct drawbacks of constitutive instability theory are discussed earlier. Hence, it is safe to assume that the observed instability is indeed interfacial in nature and complex dynamics of the tethered chains is responsible for the same. We believe that the mechanisms of debonding and disentanglement are both active and occurrence of any of them depends on the nature of polymer-wall interface. This is an important premise for the work presented in this thesis.

Although there is some consensus on the molecular origin of the mechanism, (that is interfacial) there is still some confusion as to whether the polymer slips on metal surface by debonding or disentanglement. The physical manifestation of slip shows up in terms of experimental observations of existence of a critical wall-shear stress, flow oscillations, extrudate distortion, hysteresis and temperature dependence of critical wall-shear stress. However, by merely observing a given manifestation in a given set of experimental data, it has not been possible so far to *a priori* assign a mechanism, be it debonding or disentanglement. Indeed the same experimental data on slip for the same polymer have been interpreted in terms of both disentanglement as well as debonding. For example, the experimental data on wall slip for common systems such as polyethylene in steel capillaries has been described by theoretical arguments of debonding [Hill, 1998; Yarin and Graham, 1998] as well as disentanglement [Wang and

Drda, 1997b]. It is important to recognize that the physical basis and the mathematical frameworks for debonding and disentanglement are completely different. It is generally believed that the magnitude of the energy of adhesion between the wall and the adsorbed polymer chains will determine the governing mechanism of slip. We believe that a unified model, which can predict slip by both debonding and disentanglement mechanisms and which can distinguish between the two mechanisms on basis of the relative role of adhesive energy will be helpful in ascribing the correct mechanism to given experimental slip data. In this work, we develop a unified slip model to address this issue.

As discussed earlier, Wang and Drda (1996a) measured the temperature dependence of critical shear stress while extruding a linear polyethylene through steel die. They observed a positive dependence of critical stress on temperature. Based on the Brochard and de Gennes (1992) model they argued that the mechanism of stick-slip was disentanglement. Wang and Drda (1997b) argued that if the mechanism were debonding then, the critical stress should show inverse temperature dependence. To the best of our knowledge, no study has reported on the temperature dependence of critical shear stress for slip occurring by debonding. In this work, we plan to investigate the temperature dependence of critical shear stress for a surface with organic coating like fluoropolymer coating, on which the polyethylene is known to show the stick-slip transition by debonding mechanism.

As seen, various molecular interpretations provided until now are at scaling level. These scaling models provide the relationship between the slip velocity and the applied stress by considering various relaxation modes of the grafted chain like arm retraction and constraint release. Although the scaling models provide very handy relationship between various controlling parameters, they fail to quantitatively predict the slip data. We believe that a constitutive equation based on the molecular theories would be useful in predicting the data quantitatively. Since the tube theories have been known to be the most successful molecular theories for entangled polymeric liquids, we feel that the tube model will provide a better framework to model the dynamics of the tethered molecules. Over a last two decade since the original tube model was proposed, several modifications have been suggested to improve the predictions of the tube model to quantitatively match the experimental data. Various relaxation mechanisms other than reptation have been proposed so as to model the dynamics of entangled liquids under *fast flow*

conditions. Some of these recently identified relaxation mechanisms are also active for the case of grafted chain. In this work, we provide further molecular insights by using one of the most refined tube models, into the complex phenomenon of wall slip with an emphasis on modeling towards a more quantitative prediction, something that has been lacking so far.

CHAPTER 3

A TRANSIENT NETWORK DISENTANGLEMENT MODEL

3.1 Introduction:

In this chapter we present a disentanglement model for wall slip. This model is based on the transient network theory, which provides a suitable physical description for deformation and stresses in entangled polymeric liquids such as concentrated solutions and melts. This chapter is organized as follows. As background information we present the basic outline of the transient network theory along with the various details relevant to the current problem. This is followed by the development of the disentanglement model. The main predictions of the disentanglement model are presented followed by discussions and conclusions.

3.2 The transient network (TN) theory

An entangled polymeric liquid can be considered as a liquefied rubber, in which the permanent chemical junctions of a covalently crosslinked rubber are replaced by the entanglements between chains [Bird *et al.*, 1987b]. The resistance to flow principally comes from the frictional polymer-polymer interactions at the entanglements. Green and Tobolsky (1946) first proposed a molecular theory for polymer melt, which was based on rubber elasticity theory. In this model the chemically crosslinked permanent network in the theory of rubber elasticity was replaced by a physically crosslinked 'transient' network. The physical crosslinks or the entanglements were allowed to break and reform within an average lifetime of a junction. Green and Tobolsky (1946) considered the rate of disentanglement to be equal to the rate of re-entanglement. This model predicted a constitutive equation that was identical to the upper convective Maxwell (UCM) model [Larson, 1988]. Several modifications have been proposed to the Green-Tobolsky's network model so as to predict the various observed rheological behaviors of entangled polymeric fluids. In this section we will briefly summarize the transient network theory and its various modifications, which are relevant to the problem at

hand. A more detailed discussion on the TN theory can be found elsewhere [Bird *et al.*, 1987b; Larson, 1988].

In transient network models, the contribution to stress is considered to be localized at entanglement points called junctions. A segment, which joins two junction points, is assumed to be a Gaussian spring. If the number of segments of type i and length Q that are created per unit time per unit volume at time t are denoted by $L_i(Q,t)$, and the probability that the segments are destroyed is $\lambda_i^{-1}(Q,t)$, then the diffusion equation which determines the distribution function of such segments is given by (Bird *et al.*, 1987b),

$$\frac{\partial \psi_{iN}}{\partial t} = -\left(\frac{\partial}{\partial \underset{\sim}{Q}} \cdot \left[\left[\underset{\approx}{\kappa} \cdot \underset{\sim}{Q} \right] \psi_{iN} \right] \right) + L_{iN}(Q,t) - \frac{\psi_{iN}}{\lambda_{iN}(Q,t)} \tag{3.1}$$

where $\underset{\sim}{Q}$ is the segment vector and $\underset{\approx}{\hat{e}} = (\nabla \cdot \underset{\sim}{\upsilon})^{T}$ is the deformation gradient tensor. $\Psi_{iN}(\underset{\sim}{Q},t)d\underset{\sim}{Q}$ represents the number of segments per unit volume at time t that have end-to-end vector in the range of $d\underset{\sim}{Q}$ at $\underset{\sim}{Q}$. In the transient network model the total stress is assumed to be the sum of contributions from individual segments. The expression for the total stress is given by

$$\underset{\approx}{\pi} = \sum_i H \left\langle \underset{\sim}{Q}\underset{\sim}{Q} \right\rangle \tag{3.2}$$

where H is a spring constant.

The constitutive equation obtained from equations (3.1) and (3.2) is given by

$$\underset{\approx}{\sigma}_i + \lambda_i \overset{\nabla}{\underset{\approx}{\sigma}}_i = -k_B T \hat{L}_i^{eq} \lambda_i^{eq} \lambda_i(t) \underset{\approx}{\dot{\gamma}} - k_B T \left[\hat{L}_i(t) \lambda_i(t) - \hat{L}_i^{eq} \lambda_i^{eq} \right] \underset{\approx}{I} \tag{3.3}$$

and $$\underset{\approx}{\sigma} = \sum_i \underset{\approx}{\sigma}_i \tag{3.4}$$

Here $\underset{\approx}{\sigma}$ is the stress tensor, $\hat{L}_i^{eq}$ and l_i^{eq} are the equilibrium creation and loss terms and $\overset{\nabla}{\underset{\approx}{\sigma}}_i$ is the upper convected derivative of the stress tensor. The modulus G_{0i} is defined as

$$G_{0i} = k_B T \hat{L}_i^{eq} \lambda_i^{eq} \tag{3.5}$$

Next, the creation and loss functions can be defined as

$$\hat{L}_i(t) = f(t)\hat{L}_i^{eq}(t)$$
$$\lambda_i(t) = \lambda_i^{eq} / g(t) \tag{3.6}$$

where $f(t)$ and $g(t)$ are dimensionless rates of creation and loss of entanglements.

Under steady state, the dimensionless number of segments (normalized by the equilibrium number of segments), the shear viscosity and the first normal stress coefficient can be obtained as [Ahn and Osaki, 1995],

$$n = \frac{f}{g} \tag{3.7}$$

$$\eta = \frac{G_0 \lambda f}{g^2} \tag{3.8}$$

$$\psi_1 = \frac{G_0 \lambda^2 f}{g^3} \tag{3.9}$$

In the original Green-Tobolsky or Lodge's network models, $f = g$ so that the number of entanglements remain unchanged and the fluid had a constant viscosity irrespective of the magnitude and rate of deformation. Thus, this is a linear viscoelastic constitutive equation. Several modifications to the original network theory have been proposed in order to account for the observed non-linear visco-elastic behavior such as shear thinning. It can be seen from equation (3.8) that with increasing shear rate if f increases more rapidly than g^2 then the model predicts shear thickening, otherwise it predicts shear-thinning. Interestingly, if f increases more rapidly than g as a function of shear rate, then the model predicts an increasing number of entanglements with shear rate, however, it may not predict shear thickening unless f increases rapidly than g^2.

The different modifications to the transient network model essentially use different physical arguments for the creation and loss of network segments. Several forms of f and g have been proposed in literature and are reviewed by Ahn and Osaki (1995). The modified network models can be classified into basically two types: phenomenological and molecular, depending on the manner in which the segment creation and loss functions are related to either macroscopic or molecular deformation parameters,

respectively. In a molecular approach the segment loss rate is typically considered constant while the creation rate is related to the end-to-end distance Q of Gaussian network segments [Tanaka and Edwards, 1992]. The change in the end-to-end distance is usually related to the macroscopic deformation by the affine deformation assumption. Vrahopoulou and McHugh (1987) proposed that the creation rate is proportional to $\exp(-u(r)/k_BT)$, where $u(r)$ is free energy of non-gaussian chain and r is the end-to-end distance. Tanaka and Edwards (1992) and Wang (1992) argued that the rate of creation is proportional to the dangling chain density. Marrucci *et al.* (1993) postulated that the chain tension due to large deformation causes chains to break off from junctions more frequently than in absence of flow. The constitutive equations that arise from such molecular arguments are mathematically complex and often require sophisticated numerical solution procedures [Petruccione and Biller, 1988]. Indeed, the Doi-Edwards tube model [Doi and Edwards, 1978a, b, c, 1979] was also developed from the picture of a transient network. The modifications of the tube models provide even more complex constitutive equations. These will be discussed later in chapter 6 in greater detail.

Phenomenological network models on the other hand, result in much simpler constitutive equations. Indeed closed form solutions can often be obtained from such models. In 1972, Carreau proposed a model in which the loss rate and the creation rate of the segments are dependent on second invariant of rate of deformation tensor. This Carreau B model has in all six fitting parameters of which three are determined from the linear viscoelastic measurements, while the other three are determined from the non-linear behavior. This model shows a very good fit to the various experimental data in both linear and non-linear regimes [Bird *et al.*, 1977]. Phan-Thien and Tanner (1977) proposed a similar modification to the model and assumed the rate of creation and loss of segment to be proportional to mean squared segment vector $\langle Q^2 \rangle$. This model requires two parameters and two spectrums to be fitted. The two spectrums are fitted to linear viscoelastic data while the two parameters are fitted to non-linear material functions. Ahn and Osaki (1994) proposed a particularly simple network model using purely empirical forms of the rates of formation and loss of segments. In their model f and g are functions of the macroscopic variable, effective strain, which is defined as $\gamma_e = (\sigma_{11} - \sigma_{22})/2\sigma_{12}$. The use of this particular measure of macroscopic deformation enables derivation of closed form solutions to viscometric flows. In fact, most of the observed rheological responses of entangled fluids can be predicted by the Ahn-Osaki

model through proper choice of model parameters. We develop the disentanglement model in this chapter starting from the Ahn-Osaki model.

3.3 Model development

3.3.1 Polymer chains near wall

We begin by outlining the framework of the disentanglement model based on the transient network concept. Consider the physical picture near the wall as depicted in the schematic shown in figure (3.1). Bulk polymer chains that are in the close vicinity to the wall adsorb on the wall strongly or weakly depending on the polymer-wall interactions. The segments of adsorbed molecules entangle with segments of the bulk molecules to form a transient network. The transient network has two types of junctions: the entanglements between adsorbed and bulk chains, and the adsorption points on the wall. The segments can break away from the network by either disentangling from the bulk chains or by desorbing (debonding) from the wall. In either case, the bulk of the fluid will then slip on the wall with a massive velocity. For simplicity of the analysis, it is assumed that a polymer molecule attaches to the wall at only a single site. If P_w are the number of chains per unit area attached to the wall, P are number of bulk polymer molecules per unit area coming in contact with the bare wall and w are number of bare sites per unit area on the wall on which a molecule can be bonded, then the reaction of adsorption-desorption can be written as,

$$P_w \underset{k_a}{\overset{k_d}{\rightleftharpoons}} P + w \tag{3.10}$$

where, k_a and k_d are kinetic rate constants for adsorption and desorption reaction, respectively. From equation (3.10),

$$\frac{d[P_w]}{dt} = k_a[P][w] - k_d[P_w] \tag{3.11}$$

Since the kinetics of adsorption and desorption are extremely fast compared to the rheological time scale, the reaction (3.10) can be considered to be under quasi equilibrium [Hill, 1998]. Hence we can define the fraction of adsorbed sites as,

$$\phi = \frac{[P_w]}{[w_t]} = \frac{k_a[P]}{k_a[P] + k_d} \tag{3.12}$$

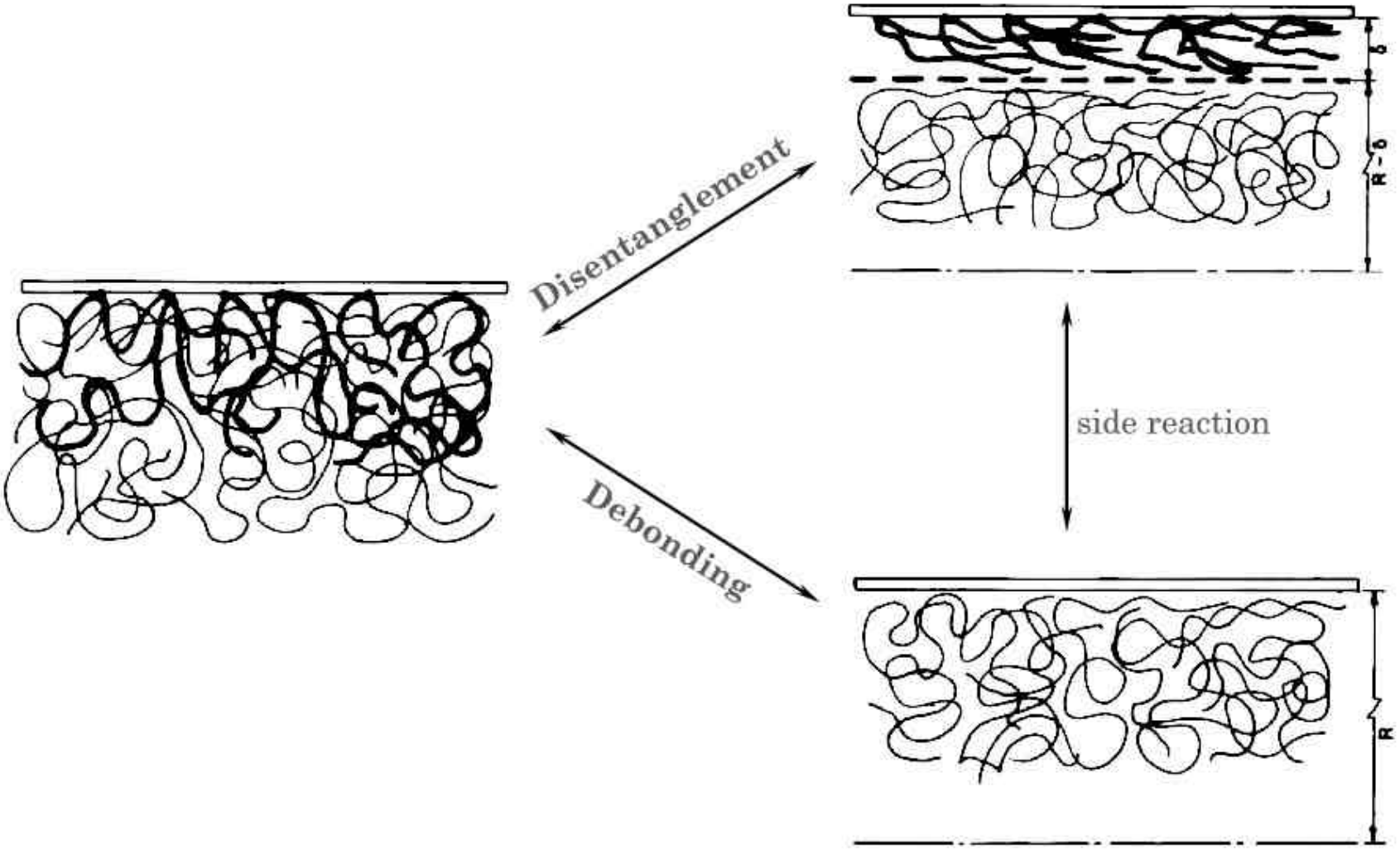

Figure 3.1. Schematic representing flow induced disentanglement and debonding of polymer molecules attached to the wall. In case of disentanglement, the flow domain can be divided into two regions as shown in the figure.

where ϕ is fraction of surface coverage. w_t are total number of sites per unit area to which polymer molecules can attach ($w_t = P_w + w$). $[P]$ can be assumed to be constant because it is a very high value. It is assumed in this chapter that the adsorbed molecules do not detach from the wall ($\phi = \text{Constant}$). More specifically, we consider the case where the polymer is strongly adsorbed on the wall so as the occupy most of the sites on the wall, i.e., $\phi = 1$.

Consider the case of polymer molecules strongly adsorbed on the wall, say by hydrogen bonding. Flow induced desorption would require that the tension in the segment should exceed the adsorption force. The tension in the freely joined segment can be estimated as $F_T \sim \frac{k_B T}{a'\sqrt{N_e}} \sim \frac{k_B T}{10a'}$ [Brochard and de Gennes, 1992]. Here, N_e is the entanglement length, a' is monomeric length scale. The force of adsorption can be estimated to be $F_H \sim \frac{E_H}{a'}$, where the energy of hydrogen bonding $E_H \sim O(k_B T)$. Thus $F_T << F_H$ and it is expected that chain stretching by flow would not significantly affect the adsorption-desorption dynamics. The above discussion also suggests that the 'side reaction' of desorption of disentangled chains in figure 1 can be neglected. This is because strongly adsorbed chains (e.g. PDMS on mica) have to be stretched much beyond the disentangled state to be desorbed by flow. Therefore, it is assumed in this chapter that the entanglement-disentanglement process governs the network dynamics.

For the case of weak adsorption, for which $E_H << O(k_B T)$, the flow can significantly affect the adsorption-desorption kinetics, making it the governing mechanism for network dynamics. We will consider the case of debonding along with disentanglement in the next chapter.

3.3.2 Transient network model for capillary flow

As discussed in chapter 2, most of the experimental evidence for wall slip exists for pressure driven capillary flows. We will now start solving the network model through the capillary. We will therefore solve the network model for flow through capillary. However, our model leads to identical results for wall slip in the case of simple shear (drag) flows as demonstrated in Appendix I For sake of simplicity we begin by assuming

that the network segments are of only one type (i=1) and henceforth drop the subscript i. Inserting equation (3.5) and (3.6) into equation (3.3) and non-dimensionalising it by following parameters for capillary flow,

$$\underset{\approx}{\sigma}^{*} = \frac{\underset{\approx}{\sigma}}{G_0},\ t^{*} = \frac{\upsilon_m}{R}t,\ r^{*} = \frac{r}{R},\ \underset{\approx}{\tilde{a}}^{*} = \lambda \underset{\approx}{\tilde{a}},\ z^{*} = \frac{z}{R},\ \underset{\sim}{\nabla}^{*} = R\underset{\sim}{\nabla},\ \overset{\nabla}{\underset{\approx}{\sigma}}^{*} = \frac{G_0\upsilon_m}{R}\overset{\nabla}{\underset{\approx}{\sigma}} \tag{3.15}$$

we get,

$$g\,\underset{\approx}{\sigma}^{*} + We\,\overset{\nabla}{\underset{\approx}{\sigma}}^{*} = -We\,\underset{\approx}{\dot{\gamma}}^{*} - (f-g)\underset{\approx}{I} \tag{3.16}$$

where, superscript $*$ indicates non-dimensionalised variables, λ is the relaxation time, R is the radius of the pipe, υ_m is the maximum velocity and $We = \frac{\lambda\upsilon_m}{R}$ is the Weissenberg number.

We now consider fully developed flow through a capillary for which, $\upsilon = \upsilon(\upsilon_z)$, $\upsilon_z = \upsilon_z(r)$, $P = P(z, r)$, $\underset{\approx}{\sigma} = \underset{\approx}{\sigma}(r)$. The equation of motion can be written as,

$$0 = -\frac{\partial P}{\partial r} - \frac{1}{r}\frac{\partial(r\sigma_{rr})}{\partial r} + \frac{\sigma_{\theta\theta}}{r} \tag{3.17}$$

$$0 = -\frac{\partial P}{\partial z} - \frac{1}{r}\frac{\partial(r\sigma_{rz})}{\partial r} \tag{3.18}$$

It can be easily shown that the transient network model predicts $\sigma_{rr} = \sigma_{\theta\theta}$ (refer equation (3.21) and (3.22)). Thus, from equation (3.17) and (3.18)

$$P(r,z) = F(r) + G(z) \tag{3.19}$$

and hence from equation (3.18)

$$\sigma_{rz} = -\frac{r}{2}\frac{\partial P}{\partial z} \tag{3.20}$$

For capillary flow, the constitutive equation (equation 3.16) can be written in component form as,

$$g\sigma^{*}_{rr} = -f + g \tag{3.21}$$

$$g\sigma^{*}_{\theta\theta} = -f + g \tag{3.22}$$

$$g\sigma^{*}_{zz} - 2We\,\sigma^{*}_{rz}\frac{\partial \upsilon^{*}_{z}}{\partial r^{*}} = -f + g \tag{3.23}$$

$$g\sigma_{zz} - We\,\sigma^{*}_{rr}\frac{\partial \upsilon^{*}_{z}}{\partial r^{*}} = -We\frac{\partial \upsilon^{*}_{z}}{\partial r^{*}} \tag{3.24}$$

Equation (3.20) together with equations (3.21) to (3.24) describes the flow of an entangled polymeric liquid through a capillary in terms of a transient network model framework.

The solution of this set of equations requires a description of the functions f and g. Ahn and Osaki (1994, 1995) proposed that the creation and loss rates could be defined as functions of the effective strain

$$f = \exp(a\gamma_e) \tag{3.25}$$

$$g = \exp(b\gamma_e) \tag{3.26}$$

$$\text{where, } \gamma_e = \frac{\sigma_{11} - \sigma_{22}}{2\sigma_{12}} \tag{3.27}$$

Deeper mechanistic considerations of the problem at hand suggest the following insights,

- Adsorption of chains on the wall must restrict their relaxation dynamics and hence make them more susceptible to being deformed/stretched as compared to chains in the bulk. Hence the dynamics of entanglement and disentanglement near the wall ought to be different than those in the bulk. In terms of the network model, this means that the f and g increase with deformation earlier than those at the wall.
- Consequently, the capillary can be divided into two domains, namely, the bulk and the wall. The wall domain can be assumed to be an annulus of diameter equal to that of the pipe and having a thickness of the order of the radius of gyration of the molecule [see figure (3.1)]. The wall domain is significant as long as the molecules are attached to the wall.
- At low rates of deformation the segment, creation and loss rates are nearly equal to their equilibrium values (i.e., $f = g = 1$). Above a certain rate of deformation the adsorbed chains being to deform and orient. This is expected to increase the rate of loss of entanglements. At still higher deformation rates, the adsorbed chains might begin to experience stretch; upon which the rate of re-entanglement would increase above its equilibrium value due an additional spring-like retraction of the chains. At still higher deformation rates the rates of creation and loss of entanglements are expected to remain constant.

- Desorption of the molecules from the wall does not happen even at nearly complete disentanglement. As discussed earlier, this will hold for strongly adsorbed molecules.

The above arguments suggest that the formation and loss rates should have an 'S' shaped functional nature with respect to the effective strain. We propose a new empirical function for creation and loss rates,

$$f = \frac{F_f}{2}\left(1 + erf\left(\frac{\gamma_e - \alpha_f}{\theta_f}\right)\right) \tag{3.28}$$

$$g = \frac{F_g}{2}\left(1 + erf\left(\frac{\gamma_e - \alpha_g}{\theta_g}\right)\right) \tag{3.29}$$

where $erf(x) = \frac{2}{\sqrt{\pi}}\int_0^x \exp(-\xi^2)d\xi$. The model parameters are $F_f, F_g, \theta_f, \theta_g$. The parameters α_f, α_g are fitted such that $f = g = 1$, at $\gamma_e = 0$.

The main difference between the above functions and Ahn-Osaki's exponential functions is that the creation and loss rates become asymptotically constant at high strains, at which the molecules might be sufficiently stretched. This behavior predicts a plateau at infinite shear rate, which is not possible with the Ahn-Osaki's exponential function. As mentioned earlier the creation and loss rate functions proposed here are purely empirical in nature. We proceed now to solve the capillary flow problem by using these functional forms and show that the wall slip can be successfully predicted.

3.4 Predictions

3.4.1 Flow curves:

The five simultaneous equations [equation (3.20) to equation (3.24)], i.e., the equation of motion and the constitutive equation can be elegantly simplified to give one main equation in terms of the effective strain as follows,

$$G_0\gamma_e\frac{f}{g} = -\frac{r}{2}\frac{\partial P}{\partial z} = \sigma_{rz} = r^*\sigma_w \tag{3.30}$$

(The derivation to obtain this equation is given in appendix I) where f and g are explicit functions of γ_e as discussed in the previous section. This is the main equation of

the model. It describes the relation between the shear stress and the strain on a flowing fluid element. As shown in appendix I, this equation holds not only for capillary flow but can be derived for other simple shear flows such as in cone & plate or couette geometries.

Te solution procedure for equation (3.30) is as follows. The capillary is divided into two domains, namely the annular wall region ($r = R - \delta$ to $r = R$) of thickness $\delta = 10^{-8}$ m to account for attached chains and the remaining bulk region ($r = 0$ to $r = R - \delta$). For the numerical solution of equation (3.30) the bulk region is divided into 100 nodes and the wall annular region divided into 4 nodes. Equation (3.30) is solved for obtaining the strain, γ_e, at each radial position with *bisection* method. In some calculations, the capillary is not divided into two domains but its cross section is directly divided into 100 nodes from $r = 0$ to $r = R$. The velocity at each radial position, r, is calculated from the effective strain by the following equation using a simple finite difference scheme.

$$\frac{\partial \upsilon_z^*}{\partial r} = \frac{g\gamma_e}{WeR} \tag{3.31}$$

Figure (3.2) shows the prediction of equation (3.30) for a typical set of model parameters. The shear stress-strain curve for the wall region can be seen along with creation and loss functions plotted with strain. The stress-strain curve for the wall region shows a non-monotonic behavior. As the effective strain increases, the stress increases first then goes through a maximum, followed by a minimum, after which it once again increases continuously. A plot of stress-shear rate also follows the same behavior, but is shifted on the abscissa. To solve the set of equations (3.30) and (3.31), using the f and g functions proposed in this chapter equation (2.28) and (3.29), six model parameters are required to be fitted. Out of which $F_f, F_g, \theta_f, \theta_g$ are required to obtain f and g functions while other parameters are λ and G_0. The G_0 is equivalent to the plateau modulus and other five parameters for bulk are obtained by fitting steady shear data. If the interfacial region is taken into account then an independent set of $F_f, F_g, \theta_f, \theta_g$ in the interfacial region is required to be described. We have taken λ and G_0 in the interfacial to be same as that in the bulk region.

The origin of the non-monotonic stress-strain curve lies in the comparative rates of entanglement and disentanglement of chains at the wall. Figure (3.2) also shows the

functions f and g which are described by equation (3.28) and equation (3.29). For low effective strain (low shear rates) the f and g values are small and close to their equilibrium value of unity. Thus, in the limit of zero strain the stress increases linearly with strain. With increasing effective strain (or shear rates) the strongly adsorbed chains at the wall stretch more easily than those in the flowing bulk. The rate of disentanglement increases rapidly once a certain effective strain is reached until the chains almost completely disentangle. This gives rise to a decrease in stress. Hence the flow curve shows a maximum. At higher shear rates the rate of entanglement also increases in the stretched chains, as more sites are available for possible junction formation. The rates of entanglement and disentanglement balance each other to produce a state in which the number of entanglement points is very small and the chains are stretched. This is similar to the 'marginal state' proposed by Brochard and de Gennes (1992). The rapid rise in disentanglement rate causes the stress to decrease first, which gives rise to the maximum in stress. At still higher strains the ratio f/g remains constant because of which the stress increases again roughly proportional to g_e. This gives rise to a minimum in the flow curve.

The effect of disentanglement of adsorbed chains can be seen directly by recognizing that the left side of equation (3.30). This equation can be written as $\frac{G_0\gamma_e f}{g} = G_0\gamma_e n$, where n is the normalized number of steady state network junctions. Thus, the Y-axis of figure (3.2) can be written as $G_0\gamma_e n$. This means that as the stress decreases after the maximum, it is n which decreases (i.e. disentanglement of chains). At larger strain, when n remains constant the increase in stress corresponds to an increase in γ_e.

For the interfacial region, equation (3.30) can also be written as

$$\sigma_{rz} = \frac{G_0\gamma_e f}{g} = (\phi\, n_0 kT)n\gamma_e \qquad (3.32)$$

where n_0 is the equilibrium number of entanglements of the adsorbed chains with the bulk chains per unit volume under no flow condition. $n_0 n$ are the total number of entanglements under full surface coverage (ϕ=1). Since the adsorption-desorption time scale is much smaller compared to the rheological time scale [Hill, 1998], ϕn_0 also

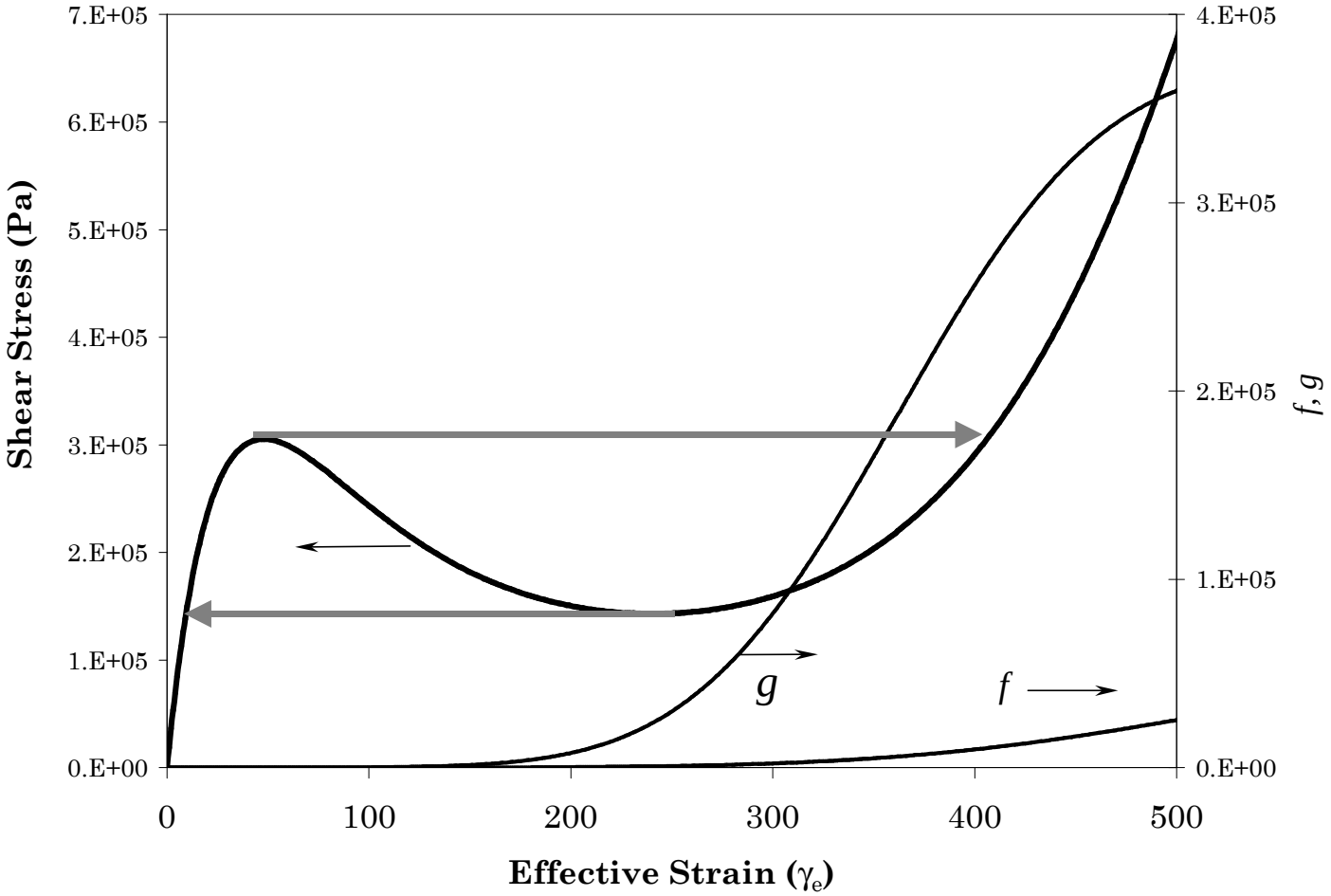

Figure 3.2. Prediction of equation (3.30) in annular (wall) region and in the bulk. Non-monotonic curve in the wall region shows hysteresis. Also, behavior of f and g functions proposed in this paper [equation (3.28) and (3.29)] are plotted on right hand side. These f and g functions are used to plot the stress-strain curve in the wall region.

denote the "equilibrium" number of entanglements under flow conditions. Equation (3.32) shows that the wall shear stress is directly proportional to the temperature and to the surface coverage ϕ. Both of these predictions are in qualitative agreement with the prediction of Brochard and de Gennes (1992).

Non-monotonic stress/shear rate curves have been predicted by other models as discussed in chapter two. For example, the Doi-Edwards model predicts a maximum in stress. A modification of this model by McLeish and Ball [1986, 1987] predicts both a stress maximum and a stress minimum. They found that above a critical shear stress there would be a radial discontinuity in the shear rate and they assumed that the stable interface would exist at the minimum possible radius from the center. Similarly, the Johnson-Segalman model also predicts a stress maximum and minimum [Kolakka *et al.*, 1988; Malkus *et al.*, 1990]. However, a fundamental difference between these predictions and our work is that the non-monotonic nature of the stress-strain (or strain rate) curves shown in figure (3.2) is due to disentanglement of chains at the wall and not in the bulk. In fact, our model may predict a similar curve for bulk chains at much higher stresses, the implications of which will be discussed later in this chapter.

Figure (3.2) can be used to predict the flow curve for the net flow through the capillary, i.e., the wall shear stress (σ_w) versus the apparent shear rate $\left(\dot{\gamma}_a = \frac{4Q}{\pi R^3}\right)$. Here the flow rate can be obtained by integrating equation (3.31), which shows that an increase in strain, γ_e, is analogous to an increase in flow rate, Q. The region of the non-monotonic stress-strain curve in figure (3.2) in which the stress decreases with strain is a domain of unstable flow. Thus, if capillary flow experiments are carried out under controlled flow rate conditions, it is possible to travel through the unstable region. In such a case the model would, in principle, provide a constitutive equation for predicting pressure drop oscillations. However, if the experiments are carried out under controlled pressure drop conditions, then the model predicts a sudden jump in flow rate at a critical wall shear stress. Moreover, a hysteresis effect is also predicted. With increasing shear stress a 'top-jump' is possible, while with decreasing shear stress the system would probably show a 'bottom-jump' as indicated in figure (3.2).

It is important to note that in general, a multi-valued flow curve does not necessarily predict all slip-characteristics such as flow enhancement and diameter dependence. For

example, a non-monotonic flow curve for the entire bulk flow does not predict diameter dependence (see discussions of chapter 2). However, a non-monotonic flow curve near a wall region is sufficient for predicting flow enhancement and diameter dependence of the net flow curve. We will discuss this point in more detail in next subsection. In other words, a difference in the dynamics of entanglement and disentanglement between bulk chains and wall chains is the fundamental origin of slip behavior.

Finally, it is interesting to note that the stress-strain plot of figure (3.2) is qualitatively very similar to those observed in mechanical testing of solid polymers. In the limit of zero strain, the stress is linearly proportional to strain similar to figure (3.2). The "yield" point in figure (3.2) occurs when the wall chains disentangle and stretch. At higher strains any further stretching of the disentangled chains requires increasing force, which is similar to the "strain-hardening" phenomenon.

3.4.2 Polymer solutions:

We begin quantitative comparisons between model and experiments by analyzing experimental data on polymer solutions. As an example, we consider the data of Cohen and Metzner (1982) for a 0.5 % aqueous hydrolyzed polyacrylamide (PAm) solution. The molecular weight of PAm is in the range of 0.8 to 4.5 million [Cohen, 1981]. The critical concentration C^* can be calculated following Kulicke *et al.* (1982),

$$C^* = 1.8\times10^{-25}\left(\left\langle R_g^2\right\rangle^{-3/2}\right)M \qquad (3.33)$$

Substituting the values of the radius of gyration as $\sqrt{\left\langle R_g^2\right\rangle} = \frac{10^{-10}M^{1/2}}{\sqrt{6}}$ in meters [Brandrup and Immergut, 1989], C^* is found to be between 0.13% to 0.3%, which indicates that $C > C^*$. That means the solution is sufficiently entangled to allow the modeling by a transient network formulation.

We will first consider the original Ahn and Osaki model [equation (3.25) and (3.26)] to solve the fully developed capillary flow problem. The Ahn Osaki model consists of four parameters namely, a, b, relaxation time λ, and modulus G_0. In order to obtain realistic values of these parameters we have fitted the Ahn-Osaki model to viscosity/shear rate data of Cohen (1981) for the PAm solution. Figure (3.3) shows the fit

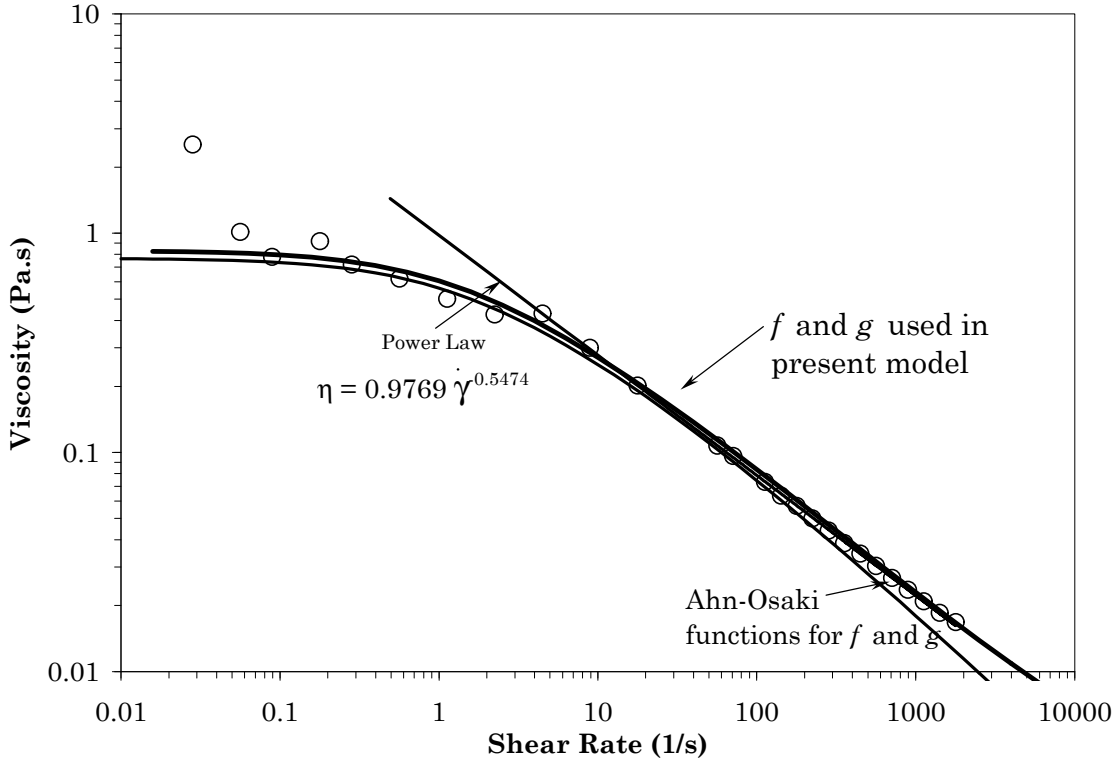

Figure 3.3. Fit of different models to viscosity-shear rate data of Cohen (1981). (1) Model parameters for Transient network model using Ahn-Osaki's functions are $G_0 = 0.128$, $\lambda = 6.0$, $a = 0.12215$ and $b = 0.1$, (2) Model parameters for Transient network model using equations 3.28 and 3.29 are $G_0 = 0.37$, $\lambda = 2.25$, $F_f = 50000$, $F_g = 3000$, $\theta_f = 20.$ and $\theta_g = 20.$ (3) For power law model $n = 0.453$ and $m = 0.977$.

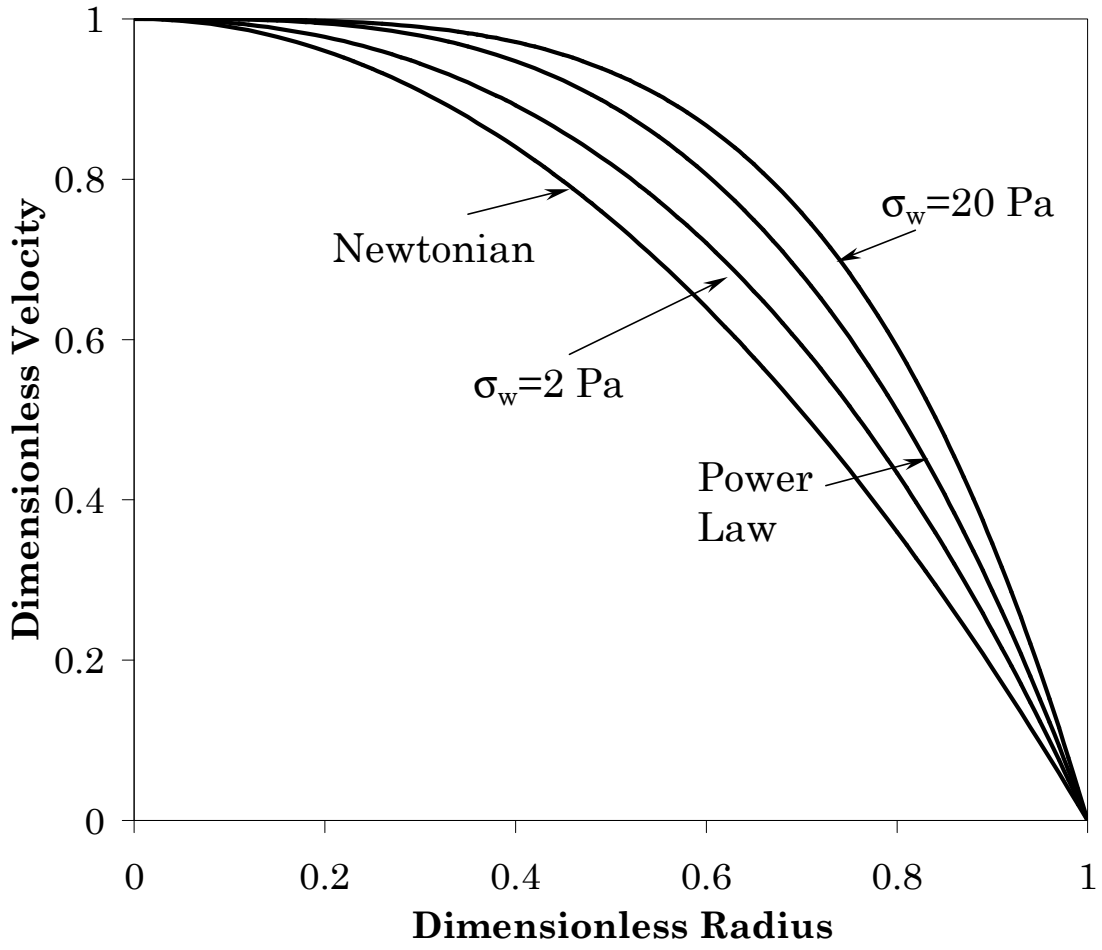

Figure 3.4. Velocity profiles predicted using model parameters for Ahn-Osaki's functions as given in figure (3.3). Power law model profile used in figure (3.3). In addition, Newtonian profile is also seen.

of a power law model (n~0.453) and that of the transient network model with Ahn and Osaki's f and g functions.

Figure (3.4) shows the predicted non-dimensional velocity profile for pipe flow using the Ahn-Osaki transient network model, the power law model and a Newtonian model at different pressure drops. As expected, the velocity profile predicted by the Newtonian and the power law models is pressure drop independent, whereas that predicted by the network model is pressure drop dependent. It can be seen from figure (3.4) that the velocity gradient at the wall for the network model increases with pressure drop.

Using the same model parameters, the volumetric flow rate Q is plotted against wall shear stress σ_w in figure (3.5). The prediction of the transient network model with Ahn and Osaki's f and g functions lie above the power law prediction, and are in better agreement with the experimental data. Thus, the network model shows an apparent *flow enhancement* at the same pressure drop over the power law model. This might be interpreted as slip-like behavior.

Although the above analysis predicts a pressure-drop dependence of the velocity profile, it fails to predict radius dependence of flow curves. This is easily seen by the following simple analysis. Equation (3.31) can be integrated to give,

$$Q = \frac{2\pi R^3}{\lambda}\int_0^1 r^*\left(\int_0^{r^*} g\gamma_e\, dr^*\right)dr^* \qquad (3.34)$$

It is clear that the apparent shear rate $\left(\dot{\gamma}_a = \frac{4Q}{\pi R^3}\right)$ is independent of R.

The above analysis indicates that if the dynamics of entanglement and disentanglement are same in the bulk and near the wall, the transient network model (or any other model) will fail to show a radius dependence of the flow curves. Also, though the model predicts an increasing velocity gradient with increasing pressure drop, it still does not show a non-zero 'slip' velocity very close to the wall as observed experimentally [Muller-Mohnssen *et al.*, 1987].

The above discussion suggests that the behavior of the network at the wall might be different from that in the bulk. We therefore conceptualize the capillary as being divided

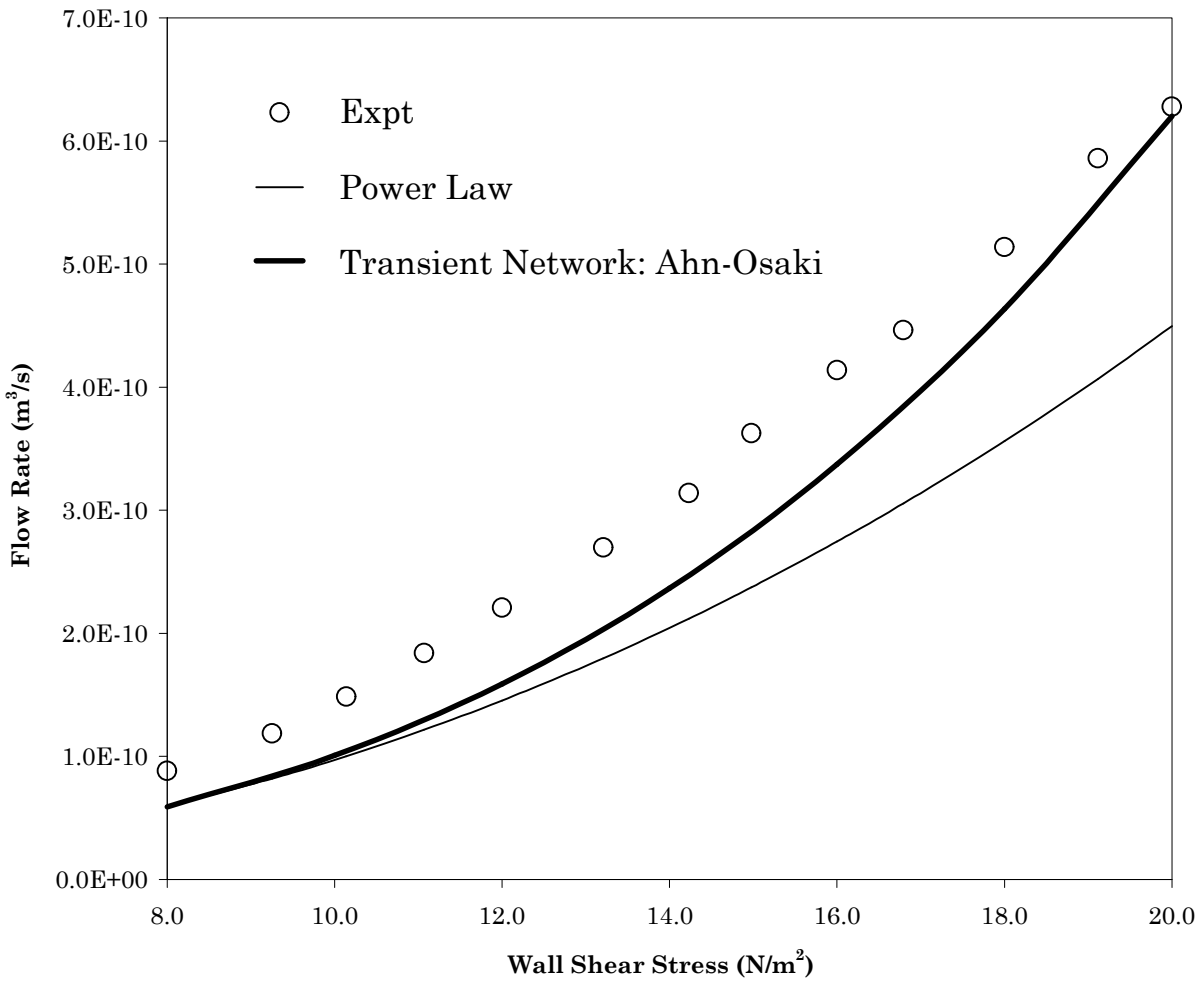

Figure 3.5. Prediction of flow rate vs. wall shear stress for power law model and Transient network model using Ahn-Osaki's functions. Model parameters are same as given in figure (3.3). Points represent experimental data [Cohen and Metzner, 1982].

into two domains, namely, an annular wall region having a thickness of the order of radius of gyration of the polymer molecule ($\sim 10^{-8}\,\mathrm{m}$), and the remaining space (bulk). It should be noted here that the significance of the annular region is only to take into account different dynamics of attached molecules from that of the bulk. As discussed in the theoretical section we assume that the dynamics of entanglement and disentanglement are given by equation (3.28) and (3.29) and that the model parameters $F_f, F_g, \dot{e}_f, \dot{e}_g$, the relaxation time λ and the modulus G_0 have different values in the bulk and in the wall region. In the present calculations, we have kept the values of λ and G_0 to be same in both the domains. Equations (3.30) and (3.31) are solved in the two regions with different model parameters while maintaining the continuity of the velocity and the shear stress at the boundary of the two domains. Figure (3.3) shows the fit of the transient network model using creation and loss functions given by equation (3.28) and (3.29) to the viscosity/shear rate data of Cohen (1981) for the PAm solution. We use the parameters obtained by this fit for the bulk domain during capillary flow. The reason for this is that the stress levels in cone-plate viscometric data are well below the critical stress, so that the dynamics of chains in the bulk and in the wall regions are the same. Therefore, although, in principle, the bulk and wall regions can exist for a cone-plate geometry, they are indistinguishable under the given experimental conditions.

Figure (3.6) shows model calculations of apparent shear rate $\left(\dot{\gamma}_a = \frac{4Q}{\pi R^3}\right)$ vs. wall shear stress ($\acute{o}_w$) compared with the experimental data of PAm [Cohen, 1981]. The parameters for the bulk domain are obtained as discussed above. The parameters in the annular wall domain are obtained by fitting to the experimental points for D=0.109 cm. Using the bulk and annular region parameters so obtained, the flow curves for other diameters are predicted and it can be seen that those are in good agreement with the experimental data.

Thus, the network model now shows diameter-dependent flow curves because of the consideration of two different domains. This can be easily shown by the following analysis. The total flow rate can be written as sum of contributions from the velocity in the bulk region and in the annular region.

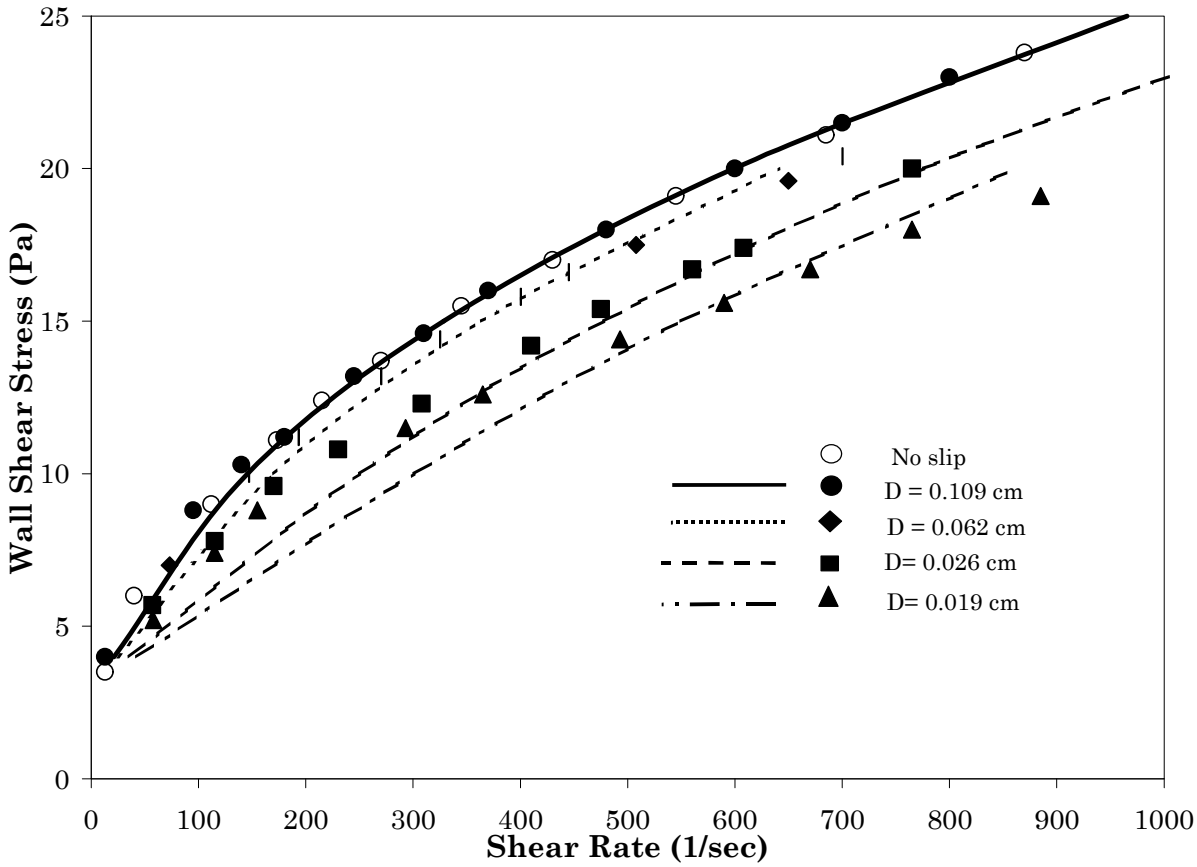

Figure 3.6. Wall shear stress vs. apparent shear rate plot for transient network model using equation 3.28 and 3.29. Points represent experimental data [Cohen and Metzner, 1982] and line represents model prediction. Model parameters used in bulk are same as given in figure (3.3). Wall parameters $F_f = 50000$, $F_g = 38000$, $\theta_f = 20.$ and $\theta_g = 15.5$ are used to fit flow curve for D=0.109 cm. Flow curves for other diameters are predicted.

$$Q_T = 2\pi \int_0^{r-\delta} r(\upsilon - \upsilon_b)\mathrm{d}r + \pi R^2 \upsilon_b \tag{3.35}$$

where υ_b is velocity at the boundary of the bulk and wall domain (slip velocity) and δ is the thickness of annulus. From equation (3.35), the apparent wall shear rate can be calculated as,

$$\dot{\gamma}_a = \frac{4Q_T}{\pi R^3} = \frac{4Q_B}{\pi R^3} + \frac{4\upsilon_b}{R} \tag{3.36}$$

where $Q_B = 2\pi \int_0^r r(\upsilon - \upsilon_b)\mathrm{d}r$ and $\frac{\upsilon_b}{R}$ can be calculated as,

$$\frac{\upsilon_b}{R} = \int_1^{1-\delta/R} \frac{g\gamma_e}{\lambda}\mathrm{d}r^* \tag{3.37}$$

At constant wall shear stress the integrand in equation (3.37) is a function of r^* only. Hence as R increases, $1-\frac{\delta}{R}$ increases and tends to unity at large R. Consequently, the change in $\frac{\upsilon_b}{R}$ decreases and tends to zero. Thus the model predicts significant diameter dependence for small diameter capillaries, but as the diameter increases the flow curves gradually become diameter-independent.

Flow enhancement and diameter dependence are only indirect evidences for slip. Comparison of the predicted velocity profiles with experimentally measured velocity profiles should provide a better test for the model. As an example of direct slip measurement for polymer solution, we compare our model calculations with the experimental data of Muller-Mohnssen *et al.* (1987) on the velocity profile of a 0.25 % aq. PAm solution. The C^* for this solution was found out to be 0.078 % using a similar estimation to that discussed earlier. The model parameters for bulk flow are obtained by fitting viscosity-shear rate data as shown in figure (3.7). Model parameters in the annular region are fitted so as to predict the slip shown by Muller-Mohnssen *et al.* (1987). Figure (3.8) shows good agreement between the predicted velocity profile and the experimental velocity profile. In the above calculations we have assumed the flow to occur through a capillary of equivalent diameter. Since the experimental data was for flow through a rectangular conduit, this might be the reason for a small difference between the model and the experimental data.

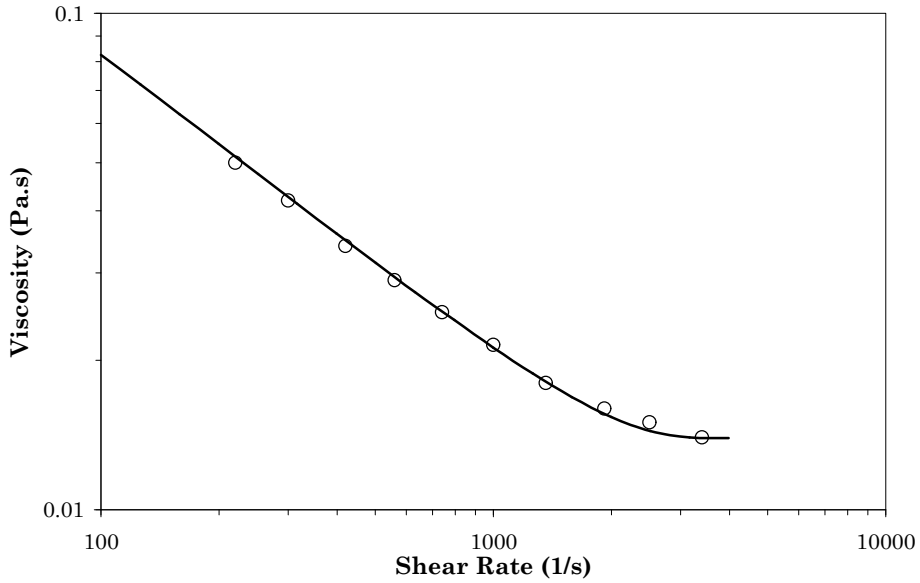

Figure 3.7. Fit for experimental viscosity-shear rate data [Muller-Mohnssen *et al.*, 1987] using Transient Network model [equation (3.28) and (3.29)]. Fitted model parameters are $G_0 = 0.77$, $\lambda = 8.5$, $F_f = 90$, $F_g = 65$, $\theta_f = 12.65$ and $\theta_g = 12.65$. Points represent experimental data and line represents model fit.

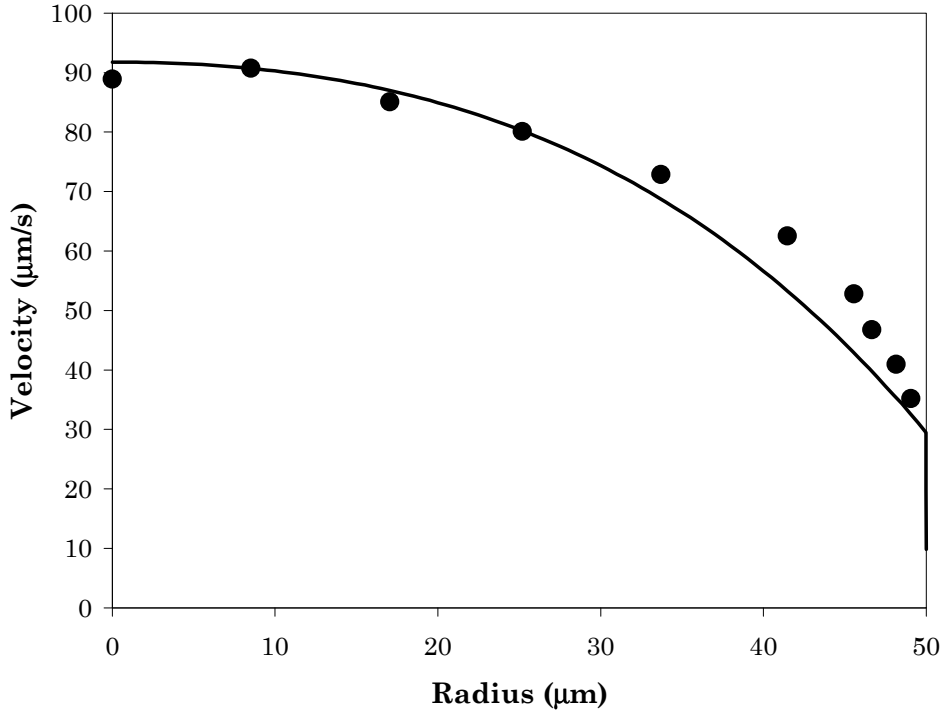

Figure 3.8. Comparison of velocity profile calculated by our model with the measured velocity profile [Muller-Mohnssen *et al.*, 1987]. Bulk parameters are same as given in figure 3.7. Wall parameters are $F_f = 900$, $F_g = 2000$, $\theta_f = 48.99$ and $\theta_g = 28.28$. Wall shear stress is σ_w=4.6 Pa. Points represent experimental data and line represents model fit.

Muller-Mohnssen *et al.* (1987) did not measure the pressure drop across the conduit and hence could not detect the presence or absence of any critical wall shear stress, at which a jump in flow rate occurs. Our model calculations predict a critical stress for their data to be 4.6 Pa. Cohen and Metzner's (1982) data does not show any critical wall shear stress. This could possibly be due to the fact that their capillary surface was pre-treated to decrease the adsorption of PAm chains on the wall. Equation (3.32) shows that a reduction in the grafting density can reduce the critical wall shear stress. For their data, it is possible that the critical stress was below the investigated range. It is also possible that a critical stress is completely absent. As discussed earlier, a multivalued stress is not a necessary condition for flow enhancement. In fact, our model parameters used for fitting to the Cohen and Metzner's (1982) data do not predict a multivalued stress function. Thus, the fact that the dynamics of chains at the wall differs from that of chains in the bulk is enough to predict flow enhancement and diameter dependent flow curves shown in figure (3.5) and figure (3.6).

3.4.3 Polymer melts:

Our network model can also be applied to data for an entangled polymer melts. Polymer melts are known to show a sudden enhancement in flow rate above a critical pressure drop in controlled stress capillary flow. The flow curves for various melts also show diameter dependence and stick-slip oscillations in controlled flow rate capillary flow.

Figure (3.9) shows the comparison of our model with the capillary flow data of Wang and Drda (1996a). Apparent shear rate (without correction) is plotted against wall shear stress for capillaries of different diameters. The model is fitted for D=1.04mm and flow rates for the lower diameter capillaries are predicted. Experimental data for a polyethylene melt shows a jump in apparent shear rate (or flow rate) at a critical shear stress of about 0.3 MPa. It can be seen that the magnitude of the jump increases with a decrease in diameter. The network model provides a good fit to the experimental data.

It is interesting to note that at very high shear stress some polymers show another first order transition in apparent shear rate. For example Wang and Drda (1997b) show a second criticality for LLDPE resin. They found that unlike the first jump in $\dot{\gamma}_a$, the second jump does not show diameter-dependent flow curves. Wang and Drda argue that

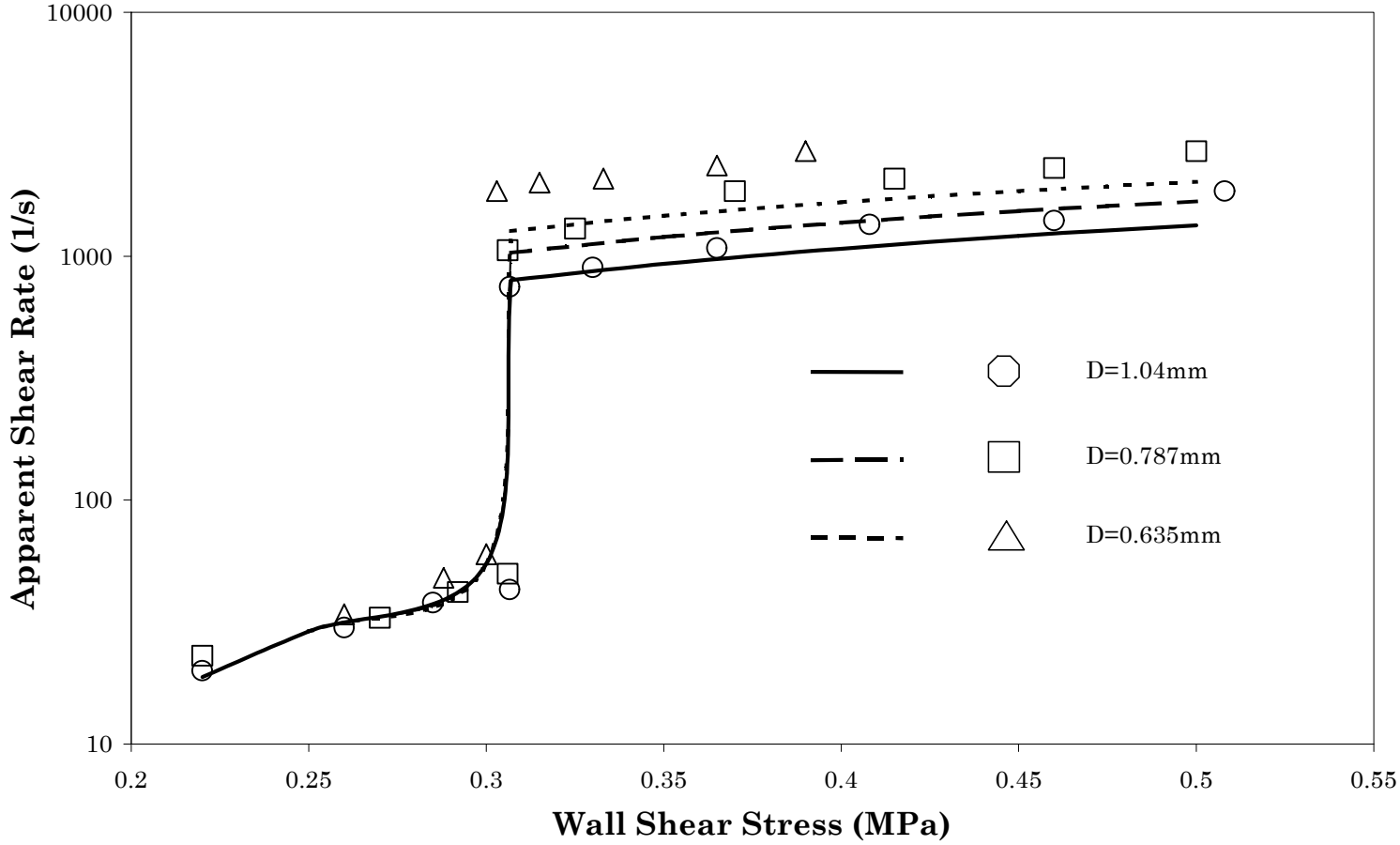

Figure 3.9. Comparison of model prediction for apparent shear rate vs. wall shear stress with polyethylene melt experimental data [Wang and Drda, 1996a]. Flow curve for D=1.04 mm is fitted using model parameters $F_f = 75$, $F_g = 100$, $\theta_f = 12{,}65$, $\theta_g = 12.65$ in the bulk region, and $F_f = 60000$, $F_g = 375000$, $\theta_f = 178.88$ and $\theta_g = 112.42$ in the wall region and $G_0 = 19200$, $\lambda = 8.5$. Flow curves for other diameters are predictions. Points represent experimental data and line represents model fit.

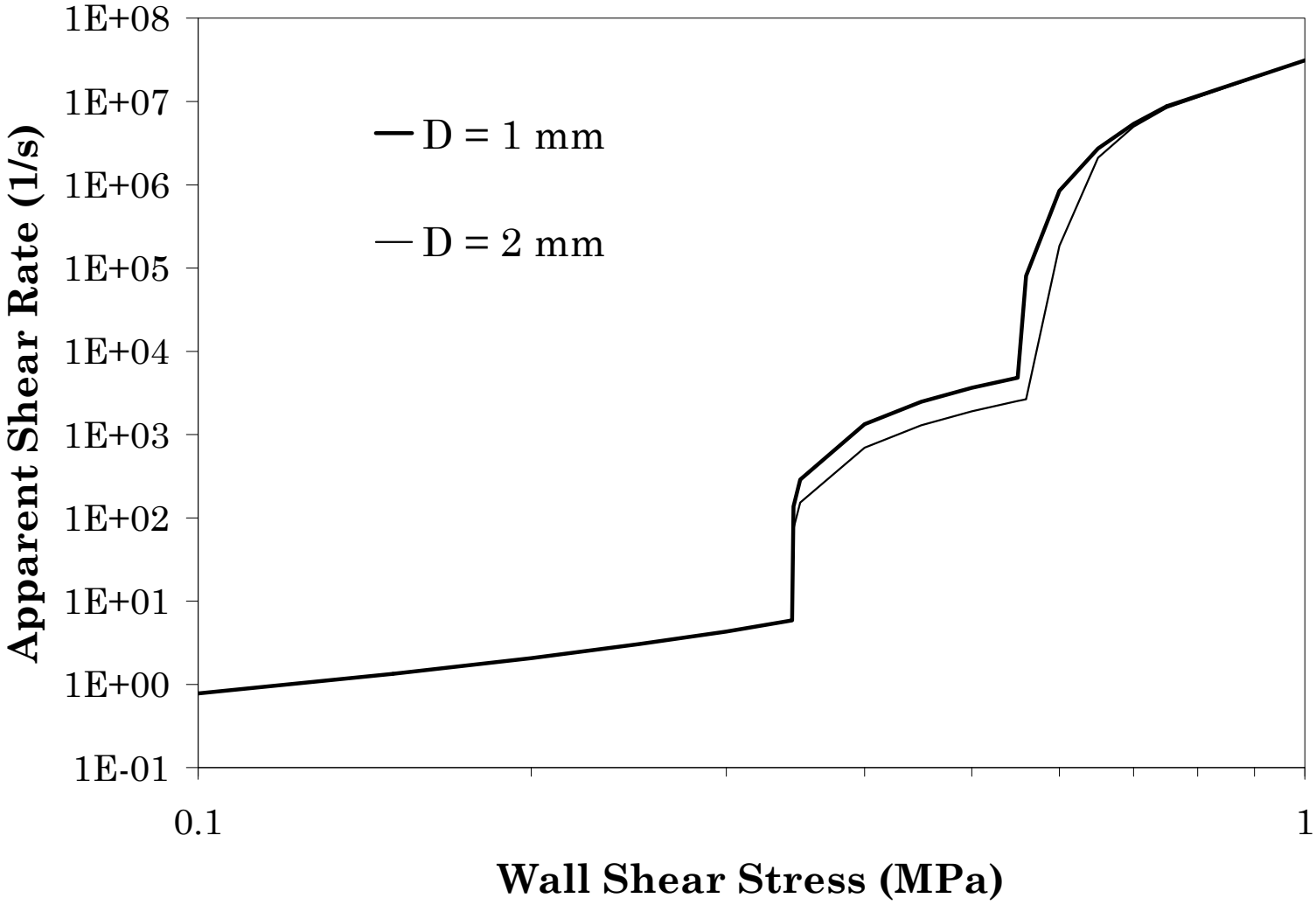

Figure 3.10. Prediction of two discontinuous flow rate transitions and their diameter dependence.

the second criticality in flow rate may be due to stretching of the bulk chains. Our model predicts bulk disentanglement and hence a second jump in flow rate at a much higher shear stress as shown in figure (3.10). Interestingly, our model also predicts diameter independent flow curves after the second criticality. This happens because the difference between the wall and the bulk chain dynamics vanishes with the disentangling of bulk chains. The capillary is now a single domain and hence predicts diameter-independent flow curves.

We note here that the diameter independence observed by Wang and Drda (1997) in the second flow rate jump need not necessarily arise due to bulk disentanglement. The second criticality could also arise from desorption of chains attached to the wall. Indeed, the chain desorption models suggest that pressure dependence of viscosity can effectively cancel out the diameter dependence of flow curves [Person and Denn, 1997].

It is particularly interesting to compare the predicted slip length from our model with that of the Brochard-de Gennes model. An experimental study of Leger *et al.* (1997b) showed three distinct regions of slip in agreement with Brochard-de Gennes (1992) model. These are; (*i*) A low shear rates regime in which the slip length is very small and constant with respect to slip velocity. (*ii*) An intermediate shear-rate regime above a critical velocity, in which a near-linear relationship (of slope unity in a log-log plot) exists between slip length and slip velocity. (*iii*) A high shear rate regime in which the slip length is much larger than the size of a surface-anchored polymer molecule. Our model predictions are shown in figure (3.11) and figure (3.12). Here slip length is calculated as $b = V_s / \kappa_{12}$, where V_s is the boundary (slip) velocity and κ_{12} is the velocity gradient in the bulk region at the boundary. The model successfully predicts these three regimes mentioned above. The slope of the b vs. V_s curve in the second regime is predicted to be unity, which is close to that obtained by Leger *et al.* (1997b). It can be seen from figure (3.11) that there exists a fourth regime in which the slip length *decreases* with slip velocity. This decrease in slip length is due to the shear thinning of bulk fluid. The velocity gradient in the bulk increases more than the corresponding increase in the slip velocity, resulting in decrease of slip length. As derived in chapter 2 b can be defined as

$$b = \frac{\eta_B}{\eta_I} a' \qquad (3.38)$$

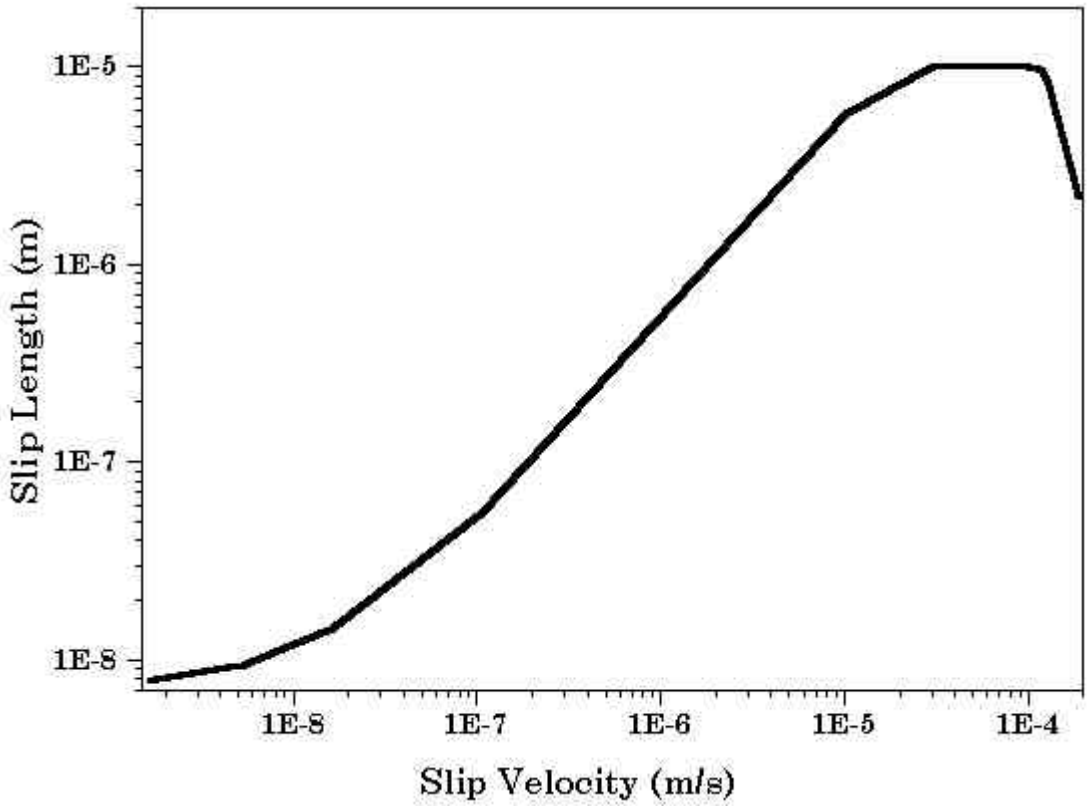

Figure 3.11 Slip-length vs. slip-velocity plot for model parameters same as in figure (3.8).

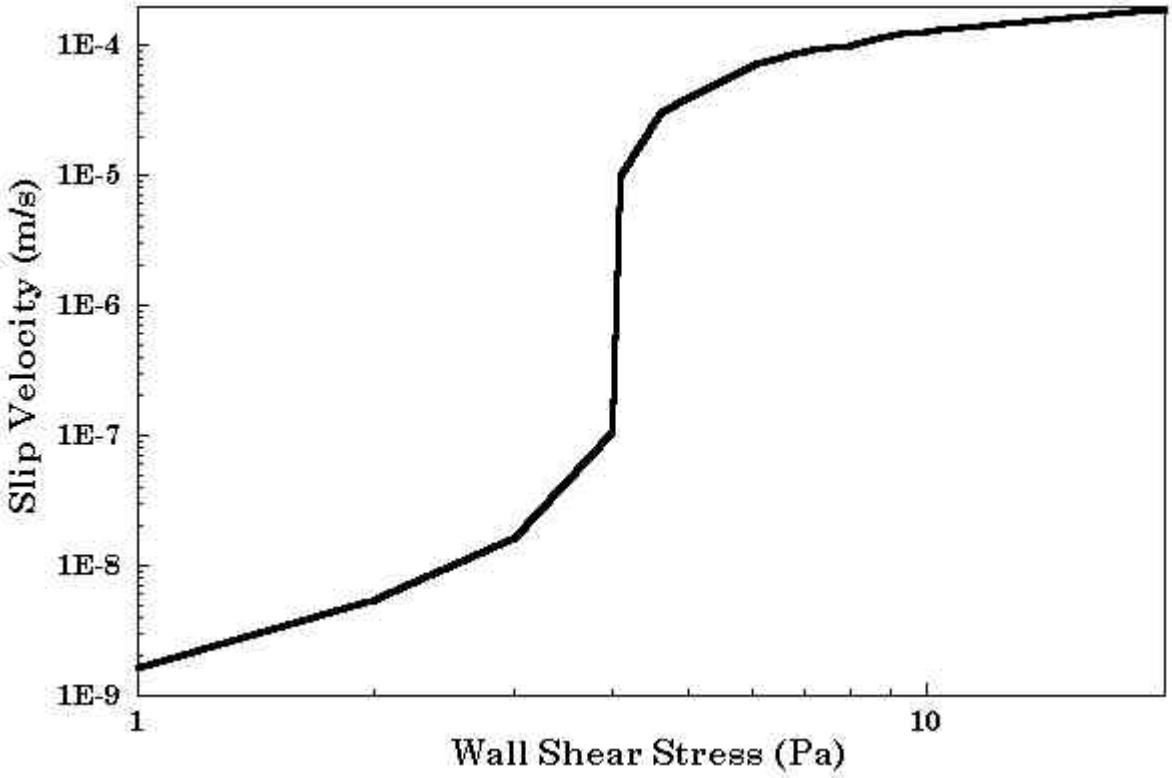

Figure 3.12 Slip-velocity vs. wall shear stress plot for model parameters same as in figure (3.8).

where η_B is the bulk viscosity, η_I is the interfacial viscosity and a' is the monomer length scale. At higher stresses η_B decreases due to the shear thinning nature while η_I remains constant (of the order of monomer viscosity after slip), which results in a decrease in b. The Brochard and de Gennes model predict the first three regions of slip-length but it does not predict the fourth region since the model does not consider dynamics of bulk molecules. Yang *et al.* (1998a) have indeed observed a decrease in b with stress. Recently Mhetar and Archer (1998a) have also seen a decrease in the slip length at higher shear stress in couette flow of polystyrene solution in diethyl phthalate. They interpreted this decrease to be a consequence of shear thinning, which can be related to bulk stretching and/or disentanglement.

3.4 Conclusion

We have attempted to unify various features of the slip phenomenon in one theoretical framework. Unification has been achieved for systems (solutions and melts) and for the underlying physical mechanisms (wall disentanglement, desorption and bulk disentanglement).

We have modeled the wall-slip phenomenon starting from the assumption of the existence of a dynamic network near the wall that is formed by entanglements between adsorbed chains and bulk chains. The network can be broken by either disentanglement of chains or by desorption of the wall chains. We have considered only the disentanglement mechanism in this chapter. We show that the model predicts flow rate enhancement, diameter-dependent flow curves, decrease in diameter dependence with increase in diameter, a discontinuous jump in flow rate for controlled pressure drop experiments and a second jump in flow rate at a higher stress. The model predicts a non-monotonic flow curve for severe disentanglement. The model also predicts four different regimes for the slip-length/slip velocity relation. Further, the critical stress is predicted to depend directly on the grafting density of adsorbed chains and on the temperature (provided no desorption occurs). The debonding mechanism will be considered in the next chapter.

CHAPTER 4

A UNIFIED MODEL

4.1 Introduction:

As discussed in chapter 2, the two most widely accepted slip mechanisms today are debonding and disentanglement. Hitherto it has been difficult to pinpoint which of these two mechanisms is actually responsible for the wall-slip for a given experimental data. Indeed the slip data for a polymer-wall pair, for instance polyethylene on stainless steel, has been explained using both types of models: debonding and disentanglement. Further more, the theoretical framework for these models is quite different making it even more difficult to say about the governing mechanism for slip. This situation motivates the formulation of a unified model that can predict the slip by both mechanisms and can discern the true mechanism based on physico-chemical parameters of the experiments.

The unified slip model developed in this chapter is an extension of the disentanglement model developed in the previous chapter. We have shown in chapter 3 that the model is naturally able to predict wall slip by an interfacial instability caused by a sudden disentanglement of the tethered chains from the bulk chains at a critical stress. The unified model developed here considers the dynamics of adsorption and desorption of chains at the wall in parallel with the entanglement-disentanglement dynamics. Since the adsorption-desorption processes strongly depend on the adhesive energy between the polymer and the wall, the model predicts slip to occur by debonding of chains at the wall for low adhesive energies and by disentanglement of chains at the wall for high adhesive energies. Thus, unification of the two mechanisms of slip is achieved in a single mathematical framework.

Our approach as outlined distinctly differs from earlier slip models. Hill (1998) developed a slip model by postulating only a debonding mechanism. Brochard and de Gennes (1992), Ajdari *et al.* (1994) and Brochard-Wyart *et al.* (1996) developed scaling models only by postulating disentanglement mechanisms. Hatzikiriakos and Kalogerakis (1994) developed a slip model based on the TN formalism, but considered

only the strain induced debonding of tethered segments above a critical strain. Thus, their model is specifically for debonding mechanism. Recently Yarin and Graham (1998) have proposed a slip model based on the proposition that the lifetime of a tethered chain under shear flow is proportional to the excess energy gained by the tethered molecule due to flow. In the case, where the detachment of tethered chains precedes disentanglement, they predict that the shear stress-slip velocity relationship becomes non-monotonic due to desorption of tethered chains. Thus, their model is essentially a debonding model. They also predict that when slip occurs by debonding, the slip length [see equation (2.1)] is independent of temperature thus implying that the temperature independence of the slip length may not be an appropriate criterion for assigning the slip to be disentanglement driven. This is contrary to the hypothesis of Wang and Drda (1996a), who infer that the temperature invariance of slip length along with the time-temperature superposition of slip data necessarily indicate slip by disentanglement. It is clear that none of the models developed so far have addressed the issue of the unification of the two mechanisms of slip in the same manner as the slip model described in this chapter.

The physical basis of the unified model has been partially developed in the previous chapter, in which the interfacial polymer layer between the wall and the bulk fluid was considered to be an annular region with a thickness of approximately one radius of gyration. We showed that the model predicts wall slip in polymer melts as well as solutions, thus unifying different systems showing slip. However, the model considered slip solely by the disentanglement of adsorbed chains, completely disregarding debonding. Our previous work forms a natural platform on which we build a new model, which will unify the two mechanisms of slip, i. e. debonding and disentanglement, into one self-consistent framework.

The model developed in this chapter is semi-empirical in nature and contains adjustable parameters arising from the phenomenological nature of the rates of creation and breakage of network. Although this approach does not throw light on the details of molecular dynamics of polymer chains near the wall, it has the inherent advantage of presenting a simpler constitutive equation that captures the essence of slip phenomena by either of the two physical mechanisms. Such a constitutive equation could be useful for providing numerical solutions to real engineering problems.

4.2 Model development

We begin by postulating the existence of an interfacial layer at the capillary wall, wherein the molecules are sparsely adsorbed on to the wall (mushroom region) and their tails are entangled with the bulk. The interfacial layer can be considered to be a transient network made up of two types of network junctions [see figure (3.1)]: one consisting of the junctions on the wall, where the molecules are adsorbed, and the other consisting of the entanglement points with the bulk chains. The nature of these two types of network junctions is different in terms of their energetics and dynamics, as will be discussed later. We postulate that when both these types of junctions remain intact, the no-slip boundary condition prevails. Slip occurs when any one of the types of junctions is destroyed. If the junctions at the wall are destroyed, then slip occurs by debonding. When the entanglement junctions are destroyed, slip occurs by disentanglement.

The physical basis of the unified model has been partially developed in the previous chapter. For the sake of continuity we will repeat some of the equations developed in chapter 3. We assume that a polymer molecule adsorbs at a single site on the wall and has a Gaussian configuration. Let P_w be the number of chains per unit area adsorbed on the wall, P be the number of bulk polymer molecules per unit area coming in contact with the bare wall and w be the number of the bare sites per unit area on the wall on which a molecule can adsorb. Then the adsorption-desorption process can be represented in the framework of a reversible chemical reaction as,

$$P_w \underset{k_a}{\overset{k_d}{\rightleftarrows}} P + w \tag{4.1}$$

where, k_a and k_d are kinetic rate constants for adsorption and desorption reactions, respectively. From equation (4.1),

$$\frac{d[P_w]}{dt} = k_a[P][w] - k_d[P_w] \tag{4.2}$$

Let w_t be the total number of sites per unit area on which a polymer molecule can adsorb, then,

$$w_t = P_w + w \tag{4.3}$$

Since the kinetics of adsorption and desorption are extremely fast as compared to the processes occurring on a rheological time scale [Hill, 1998], it is appropriate to assume that pseudo-equilibrium condition holds. Then from equation (4.2) and (4.3) we get,

$$\phi = \frac{[P_w]}{[w_t]} = \frac{k_a[P]}{k_a[P] + k_d} \tag{4.4}$$

Here ϕ is the fractional surface coverage. Since the concentration of the unattached polymer molecules near the wall is very high, it can be assumed to be approximately constant.

The kinetic coefficients in equation (4.4) can be defined as a product of the pre-exponential frequency factor and an activation term [similar to that used by Hill (1998)].

$$k_a[P] = A\frac{k_B T}{h}\exp\left(\frac{-\Delta E_a}{k_B T}\right),\ k_d = \frac{k_B T}{h}\exp\left(\frac{-\Delta E_d + \Delta E_m}{k_B T}\right) \tag{4.5}$$

where ΔE_a is the activation energy for adsorption, ΔE_d is the activation energy for desorption, ΔE_m is the elastic free energy of the attached molecule relative to the equilibrium (no-flow) state, h is the Plank's constant and A is a parameter that converts the second order rate constant k_a into a pseudo-first order rate constant. It is important to note that we have assumed the desorption rate to be proportional to the elastic (recoverable) energy of the adsorbed molecule.

The free energy of the attached molecule relative to the equilibrium (no-flow) state can be written as [Larson, 1988],

$$\Delta E_m = \frac{3}{2}k_B T\frac{\langle R^2\rangle}{\langle R^2\rangle_0} - \Delta E_{eq} \tag{4.6}$$

$$\Delta E_{eq} = \frac{3}{2}k_B T \tag{4.7}$$

Here subscript 0 represents unperturbed conditions (no flow). If it is assumed that the effective strain on the adsorbed molecule can be substituted by the effective elastic strain, then,

$$\gamma_e^2 \sim \left(\frac{\langle R^2\rangle}{\langle R^2\rangle_0} - 1\right) \tag{4.8}$$

where $\gamma_e = \frac{\sigma_{11} - \sigma_{22}}{2\sigma_{12}}$. For simplicity we assume that the constant of proportionality in equation (4.8) is unity. We feel that this is a reasonable assumption to make in the view of the fact that the network deforms affinely at low stress values. The approximation of substituting γ_e in place of the actual strain on a molecule allows one to derive a closed form constitutive relation for the shear stress as will be seen later. This approximation is further justified by the fact that the axial strain on molecules in laminar capillary flow is proportional to the normal stress [Philippoff, 1957], which is considered in γ_e. From equations (4.5) to (4.8), the kinetic rate constant for desorption can be written as,

$$k_d = \frac{k_B T}{h} \exp\left(-\frac{\Delta E_d}{k_B T} + \frac{3}{2}\gamma_e^2 \right) \tag{4.9}$$

The above form of the kinetic rate constant for desorption implicitly takes into account the effect of temperature. The desorption rate is proportional to the energy of the adsorbed molecule, which is directly proportional to the product of the tension in the molecule and the strain experienced by the adsorbed molecule. Note that at constant wall-shear stress, the tension in the adsorbed molecule remains independent of temperature but the strain in the molecule decreases with an increase in temperature due to increased stiffness.

Insertion of equations (4.9) and (4.5) into equation (4.4) gives the final expression for surface coverage,

$$\phi = \frac{A\exp\left(\frac{[\Delta E_{adh}]}{k_B T} \right)}{A\exp\left(\frac{[\Delta E_{adh}]}{k_B T} \right) + \exp\left(\frac{3}{2}\gamma_e^2 \right)} \tag{4.10}$$

where, ΔE_{adh} is the adhesive energy $(\Delta E_{adh} = \Delta E_d - \Delta E_a)$. Thus the fractional surface coverage is a function of the adhesive energy for any polymer-wall pair.

We have already discussed in chapter 3 the solution of the Transient Network (TN) model for the case of constant ϕ (= 1) leading to disentanglement driven wall slip in the capillary flow. Note that when adhesive energy is very high, equation (4.10) gives $\phi \approx 1$. Thus, the model naturally predicts that the slip would occur by disentanglement on a highly adhesive surface. It was assumed that the capillary could be divided into two

regions, an interfacial annular region of thickness equal to approximately one radius of gyration at the wall consisting the adsorbed molecules, and the remaining bulk region. It was further argued that the dynamics of entanglement and disentanglement of the adsorbed chains are different from those of the bulk chains. We showed that the constitutive equation reduces to two governing equations for the network model, which have to be solved independently in the annular wall region and in the bulk region. These equations are,

$$\sigma_{12} = \frac{G_0 \gamma_e f}{g} = (n_0 k_B T) n \gamma_e \tag{4.11}$$

$$\frac{\partial \upsilon_1^*}{\partial r} = \frac{g \gamma_e}{We \mathrm{R}} \tag{4.12}$$

where, superscript $*$ indicates non-dimensionalised variables $\left(\upsilon_1^* = \upsilon_1 / \upsilon_m\right)$, $We = \lambda \upsilon_m / R$ is the Weissenberg number, λ is the relaxation time, R is the radius of the capillary, υ_m is the maximum velocity, $n\,(= f/g)$ are the number of entanglements per unit volume under flow normalized with respect to the equilibrium number of entanglements n_0, and f and g are the rates of creation and the loss of entanglements, respectively.

If however, $\phi < 1$, which would imply desorption of chains, then as long as the interfacial network is intact the stress in the annular region is only due to the contribution from the segments of the adsorbed chains. Hence equation (4.11) for the annular region can be written as,

$$\sigma_{12} = \phi \frac{G_0 \gamma_e f}{g} = (\phi n_0 k T) n \gamma_e \tag{4.13}$$

Equation (4.12) and (4.13) can be solved provided the rates of entanglement and disentanglement under flow are known. In the present analysis we have used the f and g functions proposed by Ahn and Osaki (1994).

$$f = \exp(a\gamma_e),\ g = \exp(b\gamma_e) \tag{4.14}$$

The above functions when used in equation (4.13) yield a non-monotonic shear stress-shear rate relationship for $b > a$. A maximum in stress occurs at $\gamma_e = 1/(b-a)$. We have shown that such non-monotonic behavior represents severe disentanglement $(g > f)$ due to chain stretching. At the stress maximum, the chains undergo a transition in the

end to end distance, akin to the coil to stretch transition predicted by Brochard and de Gennes (1992).

Now let us consider the interfacial annular wall region. Equation (4.14) along with equations (4.12) and (4.13) constitute a set of equations that need to be solved in the annular wall region. It can be seen from equation (4.13) that in the annular region the contribution to the wall-shear stress is from three interdependent variables: (*i*) ϕ, the fractional surface coverage, which depends on the dynamics of adsorption and desorption and decreases with increase in γ_e and temperature, (*ii*) γ_e the effective strain, which represents the stretching of chains and (*iii*) f/g, which decreases with γ_e for severe disentanglement ($b > a$). Thus equation (4.13) can predict a non-monotonic local shear stress-shear rate relationship by two independent mechanisms. For low surface energy wall, the product $\phi\gamma_e$ will cause a stress maximum due to desorption of macromolecules (decrease in ϕ). For high surface energy wall the disentanglement of adsorbed chains will occur due to the chain stretching at constant fractional surface coverage ϕ and the stress maximum will occur due to the product $\gamma_e f/g$.

When strong slip occurs, either by a debonding or by a disentanglement mechanism, the network in the annular wall region is disrupted. We argue that in this region the stress transfer occurs primarily by friction between the bulk sliding over the bare wall in the case of debonding or between the bulk sliding over a carpet wall (carpet formed due to the stretched adsorbed chains on the wall) in the case of disentanglement. A 'friction law' can be written in a simple empirical form as proposed by de Gennes (1985)

$$V_s = k'\sigma_w \qquad (4.15)$$

where k' is the friction coefficient. The various forms of k' for bare wall and carpet wall with different surface coverages have been developed by Ajdari *et al.* (1994) and Brochard-Wyart *et al.* (1996). In the current model k' has been taken to be a fitting parameter.

We solve equations (4.11) and (4.12) in the bulk region, and equations (4.12) and (4.13) in the annular wall region before the onset of a strong slip. The model parameters common to the bulk and annular regions are G_0 and λ. However, the model parameters related to the entanglement and the disentanglement (a and b respectively) are

different in the bulk and wall regions. The physical picture behind this assumption is as follows. The bulk chains can relax by several mechanisms such as reptation, convective constraint release, fluctuations and chain stretching. However, a tethered chain cannot reptate as long as it is attached to the wall. Therefore it is probably more susceptible to getting orientated and stretched. Hence the inherent dynamics of tethered chains as represented by a and b in a network model is expected to be different than that of the bulk chains. The parameters related to kinetics of adsorption and desorption are A and ΔE_{adh}. A in equation (4.10) is treated to be a curve fitting parameter, while the adhesive energy ΔE_{adh} is taken from the available data in the literature. At the interface of both the regions, the continuity of the stress and velocity is maintained. After the stress maximum in the annular region, the interfacial region ceases to exist either due to loss of complete surface coverage or due to the stretched and fully disentangled chains. Therefore, after strong slip the slip boundary condition [equation (4.15)] is considered at the wall.

4.3 Results and Discussion:

4.3.1 Flow Curves:

As discussed earlier, the non-monotonic shear stress-shear rate relationship at the wall results in a first order transition in the flow rate (i.e. strong slip). The figure (4.1) shows a qualitative model prediction of wall shear stress vs. slip velocity before and after a strong slip. The slip velocity before the first order transition (weak slip) is the velocity at the interface of the annular region. This is calculated from the network model. After strong slip, the slip velocity is calculated from equation (4.15). The transient network model, when solved in the annular wall region predicts a non- monotonic wall shear stress as shown by curve I in figure (4.1). The non-monotonic nature can arise due to disentanglement or due to debonding. Curve II in figure (4.1) represents either the monomer-monomer friction (in the case of disentanglement) or the monomer-wall friction (in the case of debonding). In a controlled stress experiment the slip velocity will jump from curve I to curve II at the stress maximum. Such a first order transition in the slip velocity will result in a first order transition in the flow rate. If curve I merges with curve II without going through the maximum, then the model will predict a continuous slip without any first order transition. This phenomenon has been observed in the case

of some polymers such as LDPE. The exact nature of Curve I and II will depend on the dynamics in the polymer-wall interfacial region, which will be governed by the molecular structure of the polymer and the characteristics of the wall-polymer interaction.

Figure (4.2-a) shows a qualitative prediction of the fractional surface coverage (ϕ) and the non-monotonic wall-shear stress with respect to slip velocity. It can be seen that the fractional surface coverage (ϕ) remains constant while the wall-shear stress goes through a maximum. The decrease in wall-shear stress at constant ϕ indicates that the slip occurs by disentanglement for the high value of adhesive energy indicated in figure (4.2a). If the adhesive energy is decreased while keeping the other parameters constant, then the slip occurs by debonding. Figure (4.2b) shows wall-shear stress and ϕ as a function of the slip velocity at a lower value of the adhesive energy. Other parameters have been kept the same as in figure (4.2a). The surface coverage and the wall-shear stress rapidly decrease at the same slip velocity, confirming that the slip is due to debonding. Thus the model is able to predict the wall slip by both disentanglement and debonding mechanisms and unifies them into one mathematical framework. The critical model parameter, which governs the mechanism, is the adhesive energy.

An important prediction of the unified slip model is the temperature dependence of slip parameters namely, the slip length $b(T)$ and the critical wall shear stress $\sigma_w^*(T)$. As discussed in chapter two the slip length is defined as,

$$b = \begin{cases} \dfrac{\eta_B}{\eta_I} a & \cdots \text{disentanglement} \\ \\ \eta_B k' & \cdots \text{debonding} \end{cases} \tag{4.16}$$

where η_B is the bulk viscosity, η_I is the interfacial viscosity a is the monomer length scale and k' is the friction coefficient of ungrafted bare wall. Both interfacial and bulk viscosities are inversely proportional to temperature, while $k' = a_m^2/\zeta_m$ (a_m is the monomer length and ζ_m is the monomeric friction coefficient) is also inversely proportional to temperature [Yarin and Graham, 1998]. It can be clearly seen that the slip length is naturally independent of temperature for both mechanisms of slip. Thus,

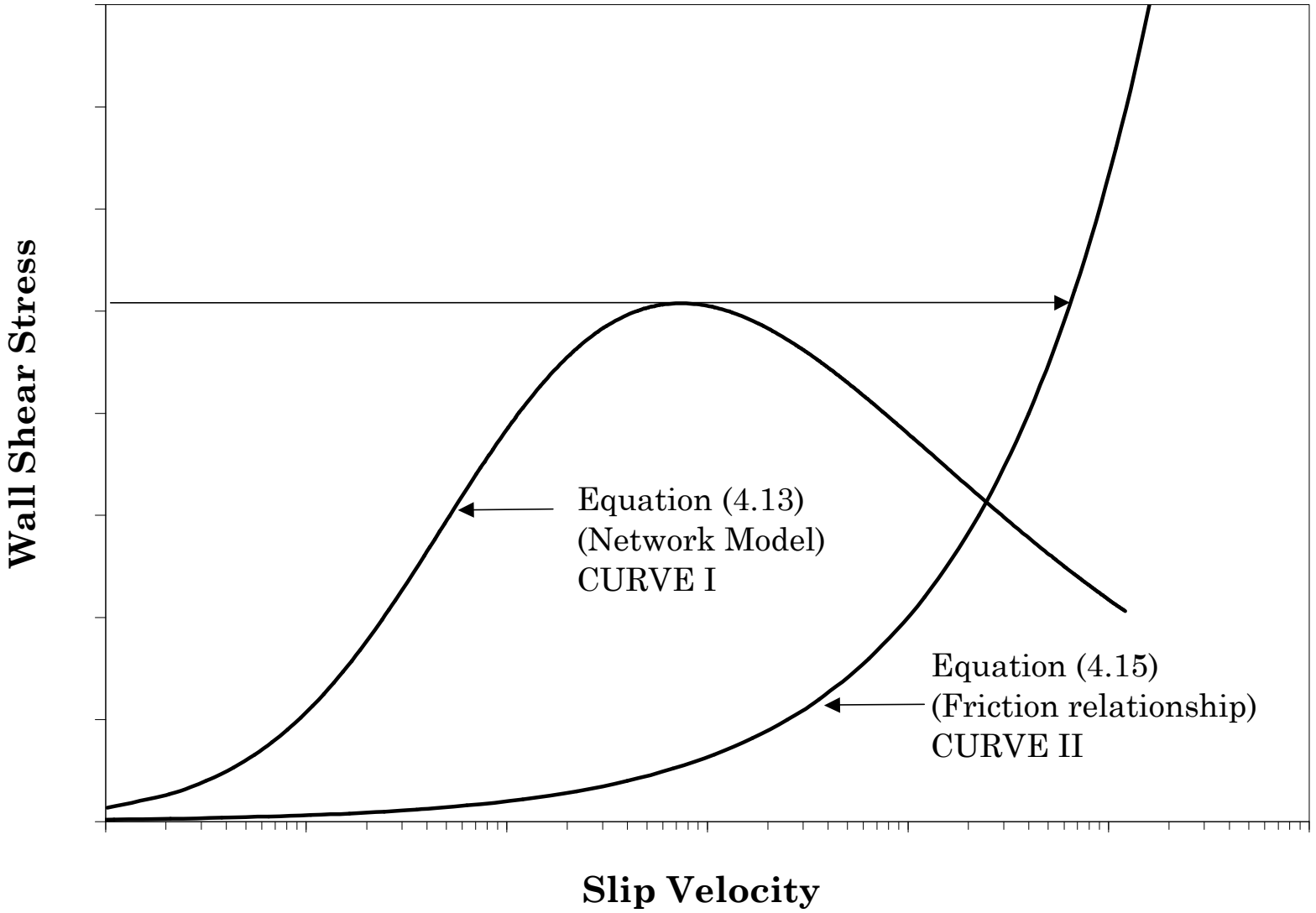

Figure 4.1 A schematic of wall slip mechanisms. Slip due to both debonding and disentanglement mechanism can be seen.

the temperature dependence of the slip length cannot be used to discuss the governing mechanism of slip.

In fact, the temperature dependence of the critical stress (not slip length) might be used to distinguish between the two slip mechanisms. The temperature dependence of stress arises from three factors: the temperature dependence of the network modulus, the activation terms in the adsorption-desorption kinetics and the temperature dependence of the stress induced desorption kinetics. It can be seen from equation (4.10) that the equilibrium (no flow condition) fractional surface coverage (ϕ) decreases with increase in temperature. In the presence of flow, the surface coverage tends to decrease further with increase in temperature. On the other hand, the modulus of the network tends to increase with temperature and the relaxation time decreases with increase in temperature. All these different temperature dependent factors influence the critical wall-shear stress. The parameter A in equation (4.10) plays a crucial role in determining the temperature dependence of critical wall-shear stress. The parameter A considers the concentration of unattached polymer chains in the vicinity of the bare wall. The value of parameter A can in principle be calculated from the equilibrium surface coverage data. A controls the equilibrium fractional surface coverage (ϕ_{eq}) such that ϕ_{eq} increases with increase in A. However, in the absence of any data on adsorption of chains from melts, we are forced to consider A as a curve fitting parameter in our model.

Figures (4.3a to 4.3c) show the critical wall-shear stress vs. desorption energy at two different temperatures and for various values of A. In general, three regions of temperature dependence can be seen in these figures. The first region corresponds to disentanglement, while the last two regions correspond to debonding. It can be seen that at high values of adhesive energies the critical shear stress is independent of the adhesive energy irrespective of the value of A. The governing mechanism in this region is disentanglement and the critical stress is also seen to be increasing with temperature as predicted by Brochard and de Gennes (1992) and our disentanglement model (chapter 3). The mechanism changes from disentanglement to debonding, as the adhesive energy is progressively decreased. In the third region, where slip occurs by debonding, the temperature dependence is surprisingly similar to that in the first region. In this region

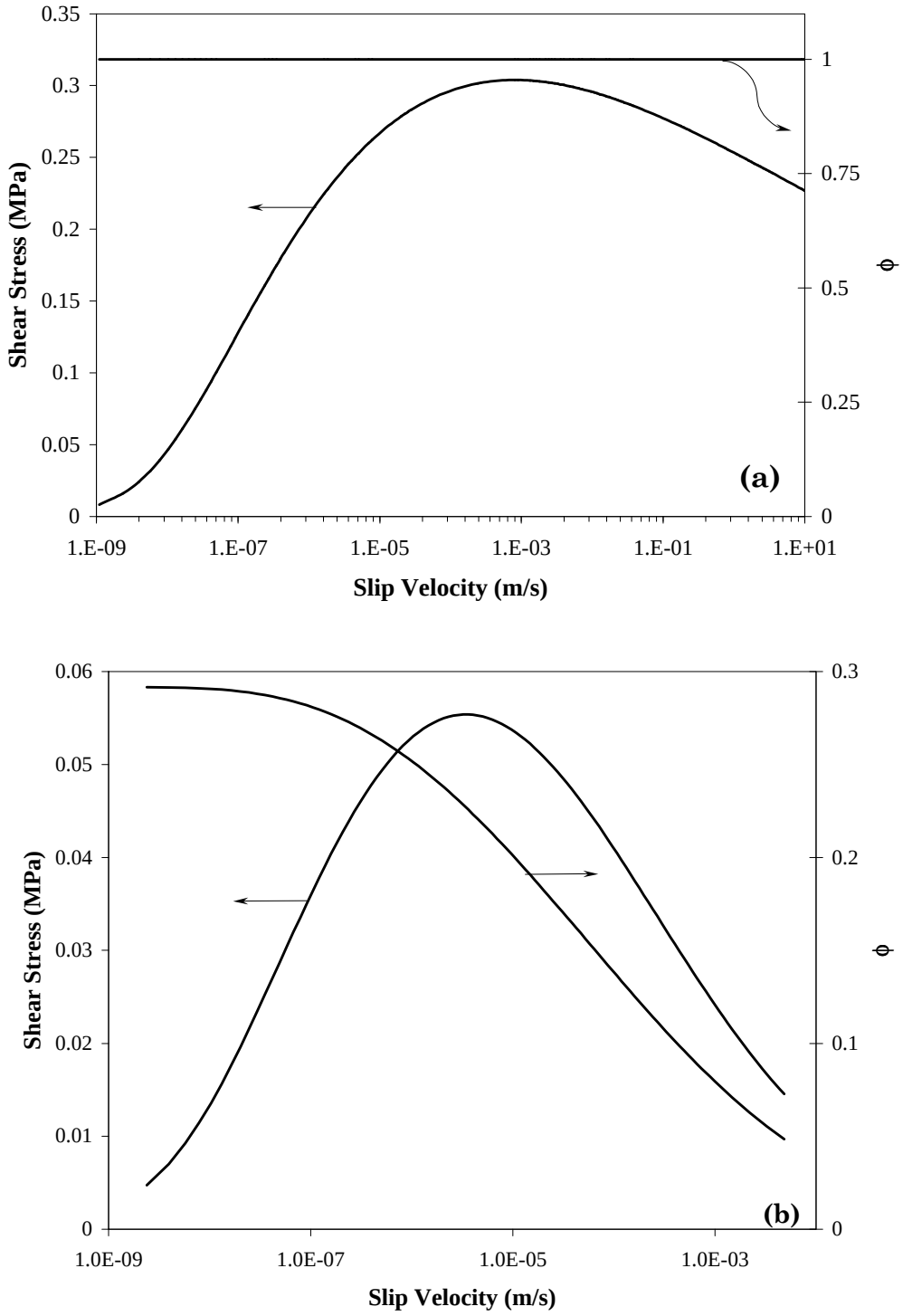

Figure 4.2 A plot of fractional surface coverage and shear stress vs. slip velocity. The slip mechanism is dependent on the adhesive energy of the wall-polymer pair. The model parameters are A=0.0047, T=473 K, n_0=1.265×10^{26} (G_0=0.547 MPa at 200^{0}C). In the interfacial region a=8.0, b=9.0 (a) At high surface energy (ΔE_{adh}=2.827×10^{-19} J/molecule) the non-monotonic behavior is due to disentanglement. The surface coverage remains constant. (b) If adhesive energy is decreased (ΔE_{adh}=2.921×10^{-20} J/molecule) keeping all other parameters constant, slip occurs due to debonding and stress and surface coverage drop simultaneously.

the critical wall-shear stress increases with temperature and this dependence is independent of the value of A. For very low values of the adhesive energy, a small amount of stretching is sufficient to cause debonding. However, the extent of stretching decreases with temperature and therefore higher stress is required for debonding to occur. Hence the critical shear stress increases with temperature. We wish to caution that in the third region the equilibrium fractional surface coverage is so low that the transient network model may not be really applicable.

The effect of parameter A is seen in the second region of figures (4.3-a to 4.3-c). In figure (4.3-a) it can be seen that as the mechanism changes from disentanglement to debonding in the second region, the temperature dependence of the critical stress also reverses. For lower values of A, i.e. for low ϕ_{eq}, the critical stress decreases with an increase in temperature. Such inverse temperature dependence was intuitively suggested by Wang and Drda (1997). Our model is the first to predict it mathematically. Thus, the temperature dependence of the critical stress could be an indicator of the governing slip mechanism. However, the parameter A determines the temperature dependence of critical stress. For high values of A, i.e., for high ϕ_{eq}, the critical stress increases with an increase in temperature over the full range of adhesive energies as seen in figure (4.3-c). Only for low values of A and for the intermediate values of adhesive energies, the temperature dependence of critical wall-shear stress is different for disentanglement and debonding mechanisms (see figure 4.3-b). We will show in the next chapter that experimental determination of the temperature dependence of critical stress on a fluoropolymer coated surface (of low adhesive energy) validates the inverse temperature dependence.

We have shown that our model successfully unifies the two mechanisms into one mathematical framework. It predicts that the adhesive energy between the polymer wall pair is the governing parameter determining the operative mechanism. It also predicts the temperature dependence of critical wall-shear stress. However, our model suffers from certain drawbacks owing to its inherent simplicity. For instance, the prediction of stress-slip velocity curve by the network model when $b > a$ does not show a minimum in stress. The stress decreases continuously in a manner predicted in the original Doi-Edwards model. The absence of a stress minimum in Doi-Edwards model is due to the

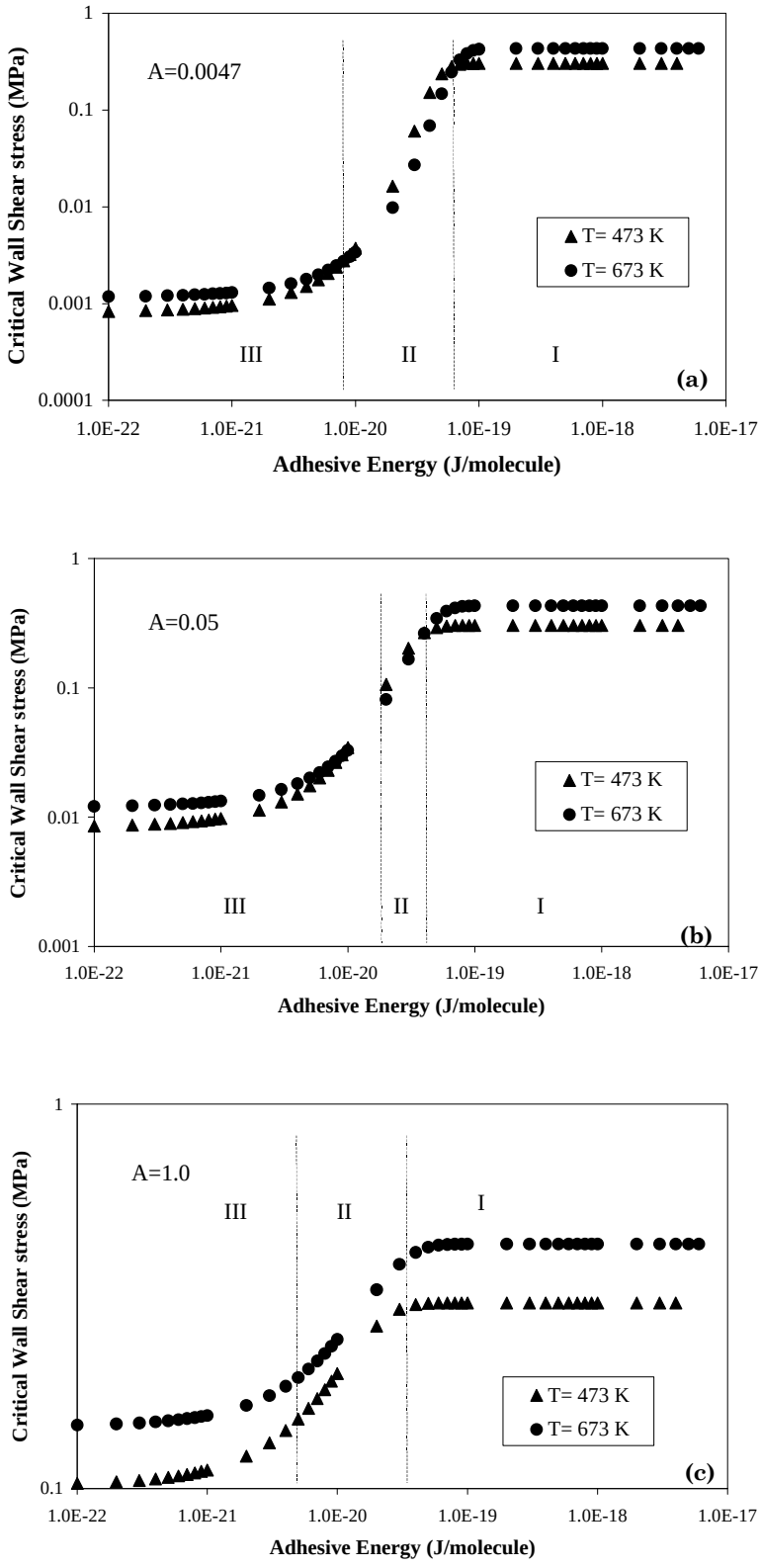

Figure 4.3 The temperature dependence of critical stress over the range of adhesive energies is shown. In the first and third regions, the temperature dependence is independent of A, while in the second region with increase in A the temperature dependence reverses. The first region corresponds to disentanglement, while the other two regions correspond to debonding. The model parameters are the same as in figure (4.2).

absence of chain stretching [Doi and Edwards, 1986]. The friction law takes care of the stress transfer to the tethered chains or on the bare wall in the strong slip region, which increases stress with slip velocity. In the present model, our major concern is identifying the stress at which the instability begins and not to develop a slip law in the strong slip region.

4.3.2 Comparison with experimental results:

We will now compare our model predictions quantitatively with some of the available experimental data on slip in polymer melts. The details regarding the model parameters have been already discussed in the previous section. To compare the experimental results with the model predictions the adhesive energy values reported in literature are used. Hill (1998) has reported the adhesive energy of the polyethylene-steel pair (difference between polymer-metal (wall) work of adhesion and polymer-polymer work of cohesion) to be 90 mJ/m^2. This adhesive energy can be converted into (energy)/(adsorption junction) or (energy)/(adsorbed molecule) by using the equilibrium surface coverage density based on an assumption that only a single junction on the wall is present in the circular area of 1nm radius. Figure (4.4) shows a quantitative fit of our model to the slip data for high-density polyethylene [Wang and Drda, 1996a]. For this high value of adhesive energy the model predicts slip to occur by a disentanglement mechanism. The network modulus G_0 is approximately of the order of the plateau modulus (for polyethylene, the plateau modulus is ~2.6 MPa). The model successfully predicts the first order transition in flow rate along with the diameter dependent flow curves. The diameter dependence originates from the difference in network dynamics in the bulk and interfacial region and can also be predicted for the case of a debonding mechanism by our model.

The model also successfully predicts the temperature dependence of critical wall-shear stress. Figure (4.5) shows the critical wall-shear stress plotted against temperature. The points show the experimental data for polybutadiene on a steel surface [Yang *et al.*, 1998b]. It can be seen that the model fits the experimental data quantitatively, when the disentanglement is assumed to be the governing mechanism. In this case the network modulus G_0 has been assumed to be the same as the plateau modulus of the polymer (G_0=1.0 MPa, or n_0= 2.314×10^{26} at 200^{0}C). Recently Anastasiadis and

Hatzikiriakos (1998) have measured the adhesive energies of various polymer-metal pairs using the pendent drop method. They have also compared the critical wall stress data with the adhesive energy. We feel that fitting our model to such data will give a better test of the unification hypothesis. We have considered the experimental data of LLDPE on steel and on Teflon® in this work. The experimental adhesive energy in units of (energy)/(area) has been converted to (energy)/(adsorbed molecule) as discussed earlier (See table 4.1). We begin by assuming that the system of LLDPE on steel shows slip due to disentanglement. The higher value of ΔE_{adh} for LLDPE-steel system and increase in critical wall shear stress with increase in temperature support this assumption. The model successfully fits the critical stress as shown in figure (4.6a). The constant fractional surface coverage confirms slip by disentanglement. Keeping all the other parameters constant, if the adhesive energy is changed to that for LLDPE on Teflon®, the model not only successfully predicts slip due to debonding but also predicts the experimentally observed critical wall-shear stress for the same system [see figure (4.6b)]

As it stands, the model has two curve fitting parameters, $(a-b)$ in the interfacial region and A. The network parameters for the chain dynamics in the interfacial region $(a-b)$ can be obtained from independent experimental data on confined melts. The parameter A can be obtained from equilibrium surface coverage data. G_0 is obtained from the plateau modulus while the bulk parameters like a, b and λ are to be fitted to viscometric data. If this is done, then no curve fitting parameters will be required and the model will become fully predictive.

4.4 Conclusion

In this chapter a unified slip model is developed, which shows slip by either mechanism, disentanglement or debonding depending on the adhesive energy. It is shown that in the case of either of the mechanisms prevailing, a local non-monotonic shear stress-shear rate behavior near the wall is necessary to show the first order transition in flow rate, which is the signature of stick-slip transition. The non-monotonic behavior near the wall. (annular wall region) arises through a coil to stretch transition for a high surface energy wall (disentanglement), while it arises through the desorption of the adsorbed

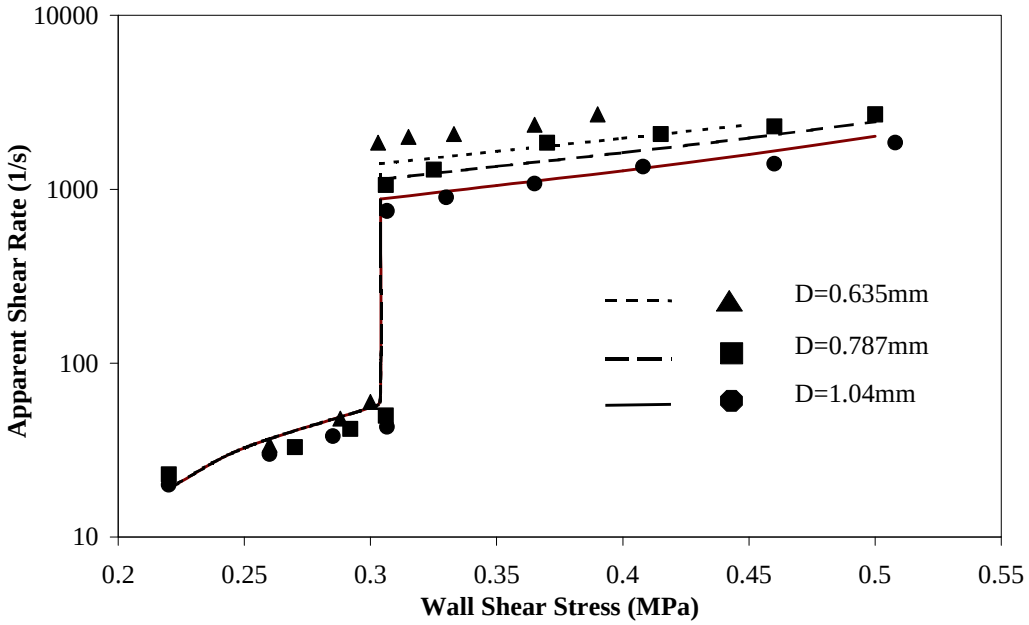

Figure 4.4 A Comparison of the model prediction for apparent shear rate vs. wall shear stress with polyethylene melt experimental data [Wang and Drda, 1996a]. The flow curve for D=1.04 mm is fitted using model parameters same as that in figure (4.3a) with λ=0.1s, in bulk, region a=8.0, b=8.0 and k'=7×10^{-7}. Flow curves for other diameters are predictions. Points represent the experimental data and the line represents the model fit.

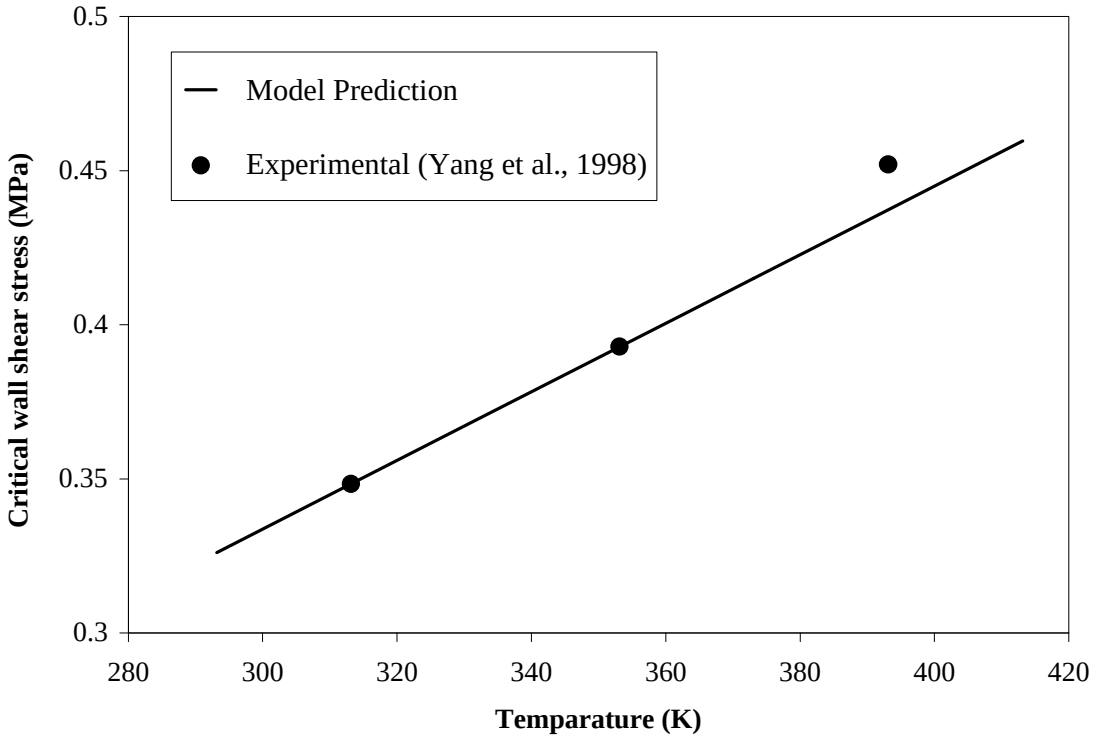

Figure 4.5 A comparison of the model prediction for critical wall shear stress vs. temperature experimental data [Yang *et al.*, 1998b]. The model parameters are, A=0.0047, T=313 K, ΔE_{adh} = 2.827×10^{-19} J/molecule, n_0=2.314×10^{26} (G_0=1MPa at 40^{0}C). In the interfacial region a=8.0, b=9.056.

Table 4.1 The adhesive energy and critical wall shear stress data for various wall-polymer pairs from Anastasiadis and Hatzikiriakos (1998).

Ploymer-wall system	The adhesive energy given in (energy)/(area)	Converted form of adhesive energy in (energy/molecule)	Corresponding critical wall shear stress
LLDPE-steel	22.6 dyne/cm	7.098E-20 J/molecule	0.1 MPa
LLDPE- Teflon®	9.3 dyne/cm	2.921E-20 J/molecule	0.027 MPa

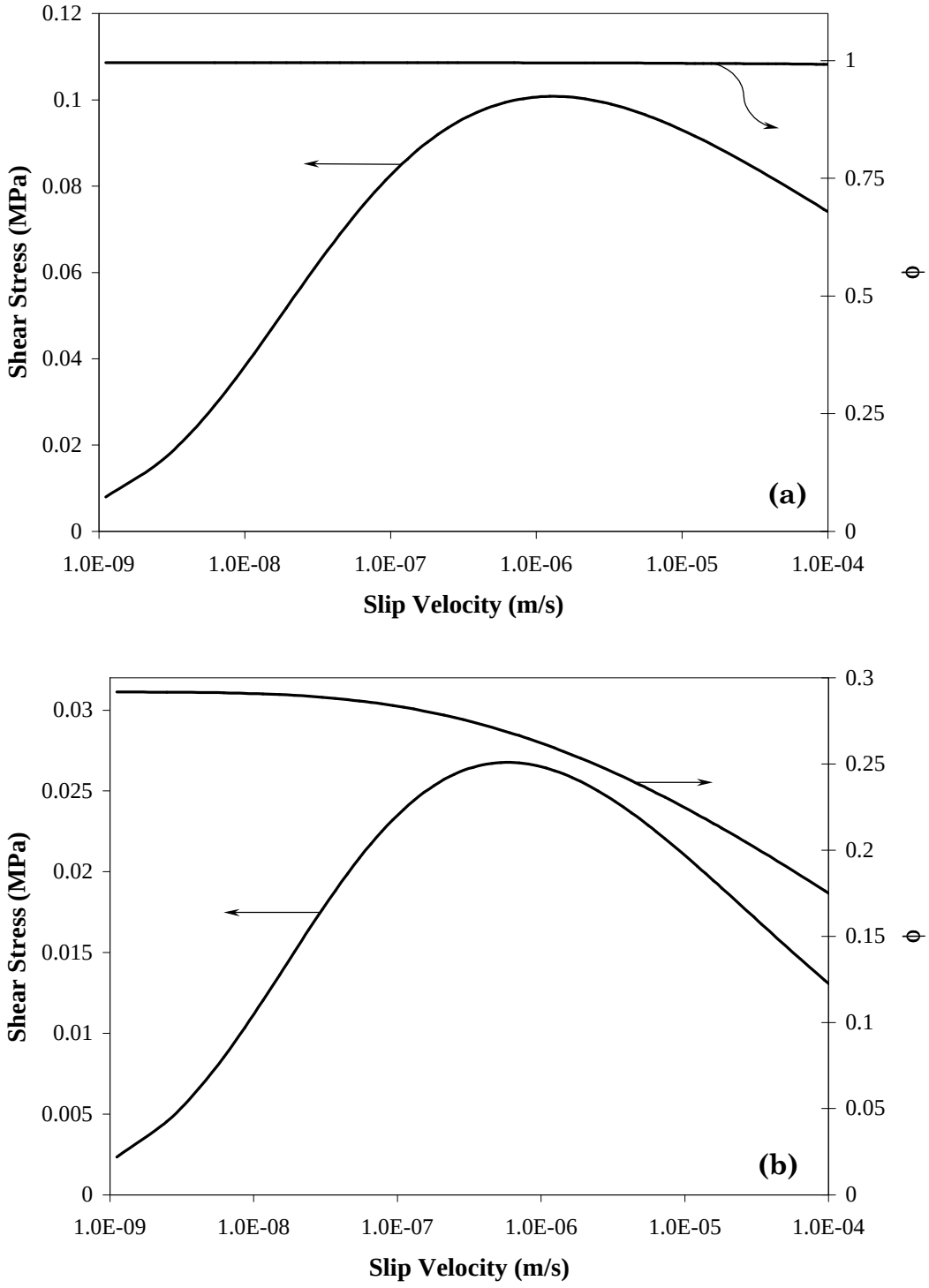

Figure 4.6 Comparison of adhesive energy and critical wall shear stress [Anastasiadis and Hatzikiriakos, 1998]. The model parameters are A=0.0047, T=473 K, n_0=1.265×10^{26} (G_0=0.547 MPa at 200^{0}C). In the interfacial region a=8.0, b=11.0. (a) For adhesive energy corresponding to LLDPE-steel (ΔE_{adh}=7.098×10^{-20} J/molecule). The slip is considered to be by disentanglement. (b) For adhesive energy corresponding to LLDPE-Teflon® (ΔE_{adh}=2.921×10^{-20} J/molecule) the model correctly predicts critical stress by debonding.

molecules for a low energy wall. After a strong slip (in both the cases), the stress transfer is assumed to arise from friction between the bulk molecules and the wall. In the case of debonding, the wall is bare while in the case of disentanglement the wall is carpeted.

The model predicts diameter dependence of the flow curves for both disentanglement and debonding mechanisms. We believe that the diameter dependence arises from different flow behaviors (network dynamics) in the bulk and near the wall region. For the case of disentanglement the model shows direct dependence of critical wall-shear stress on temperature, while for debonding, this dependence is determined by the equilibrium surface coverage.

CHAPTER 5

EXPERIMENTAL DETERMINATION OF TEMPERATURE DEPENDENCE OF CRITICAL STRESS FOR SLIP DUE TO DEBONDING

5.1 Introduction:

As discussed earlier, the strong wall slip (stick-slip) observed during melt extrusion occurs either by disentanglement or by debonding processes [Wang, 1999]. However, there are no clear guidelines for discerning the governing mechanism of slip under a given set of experimental conditions. It has been hypothised that slip occurs by disentanglement for high adhesive energy surfaces and by debonding for low adhesive energy surfaces. The unified model proposed in the previous chapter provides a quantitative basis for this hypothesis. Furthermore, our model predicts that the temperature dependence of critical stress could be an important criterion for discerning the correct mechanism of slip prevailing under a given set of experimental conditions.

The critical shear stress predicted by disentanglement models [see, chapter 2; Brochard and de Gennes, 1992] indicate that,

$$\sigma_w^* \propto \Sigma T \qquad (5.1)$$

where Σ is the number of chains per unit area grafted to the wall (grafting density) and T is the absolute temperature. Equation (5.1) shows that the critical wall shear stress (σ_w^*) increases with increase in temperature when slip is due to disentanglement. Wang and Drda (1996a) indeed observed such a dependence for controlled stress extrusion of HDPE in steel die and hence they related the observed slip phenomenon to disentanglement. They ruled out the possibility of debonding and postulated that since debonding is an activation process, the critical stress for debonding should decrease with increase in temperature. This postulate, which was predicted by our unified model also, has not been experimentally confirmed so far.

In this chapter, we experimentally determine the critical stress for slip on a low adhesive energy surface at various temperatures. A fluoropolymer coated low energy surface ensures that slip occurs due to a debonding mechanism. We use a cone and plate geometry with cone coated with fluoroelastomer coating. We find that the critical stress for slip on this surface decreases with an increase in temperature. We also show that the unified model successfully predicts the observed temperature dependence. In next section we discuss various instabilities observed in cone and plate viscometers. In section 5.3, the detailed experimental plan is discussed. Finally, the experimental observations and the unified model prediction for this system are discussed in section 5.4.

5.2 Instabilities in cone and plate viscometers

The cone and plate geometry is the most commonly used geometry to measure the viscoelastic properties of the polymeric liquid. Figure (5.1a) shows a schematic of cone and plate geometry. The fluid is confined between the cone and the plate. The angle β between cone and plate is generally very small and in the range 1^0 to 6^0. The cone is rotated at the angular velocity ω, and the shear rate (ω/β) is independent of radius. At low shear rates, the flow in this geometry is undisturbed, but at higher shear rates, the instabilities arise mainly due to existence of the free surface, secondary flows and elasticity of the fluid. Several instabilities are seen in cone and plate geometry. These include centrifugal expulsion (inertial disturbances), elasticity driven meniscus distortion, elastic instability, ect., at the interface [Larson, 1992; Powell, 1998]. Out of all these instabilities, elastic instability is seen for lightly entangled or un-entangled liquids such as Boger fluids [Larson, 1992]. This instability develops over a very long time scale and hence is out of scope of present work.

5.2.1 Centrifugal expulsion (inertial disturbances)

The flow in the cone and plate geometry becomes instable when the material being sheared is thrown out of the gap. Centrifugal effects produce secondary flow, which become important when Reynolds number Re>800 [Clegg, 1968; Larson, 1992]. Here Reynolds number is given by $4\rho\kappa_{12}\beta^2 R^2/\eta$, where ρ is density of the material, κ_{12} is the shear rate, R is plate radius and η is shear viscosity. Tanner and Keentok (1983)

argued that the inertial forces must be kept less than the capillary forces, which holds the meniscus in the gap. They further argued that the inertial expulsion occurs when $ReCa$ exceeds $80/3$. Here Ca is the Capillary number and is given by $R\omega\eta/\sigma$, where σ is the surface tension of the liquid. Based on above theories Larson (1992) postulates that with R=2 cm and β=0.04 rad, inertial expulsion occurs at the shear rate roughly about 650 s^{-1}.

5.2.2 Meniscus distortion:

It can be seen from figure (5.1b) that though the material in the gap is sheared and stressed, the free meniscus surface has the stress free condition $\hat{n}\cdot\underset{\approx}{\sigma}\cdot\hat{t}=0$, here $\hat{n}$ is unit vector normal to free surface, $\hat{t}$ is the unit vector tangent to the free surface and $\underset{\approx}{\sigma}$ is the stress tensor. This causes a strong discontinuity in the velocity field at the rim (free surface). This results in sharp increase in stress at upper and lower contact lines [Wang, 1999]. At higher shear rates, the stress built-up becomes significant such that it leads to meniscus distortion. Generally, two types meniscus distortions are seen. One is irregular nonaxisymmetric distortion while the other is an axisymmetric indentation of the meniscus [Larson 1992].

The irregular, nonaxisymmetric distortion is observed at moderate Weissenberg number and the corresponding shear rate is close to the onset at which severe shear thinning starts. The ratio N_1/σ_{12} (where N_1 is first normal stress difference and σ_{12} is shear stress) is a critical parameter. At the onset of the meniscus distortion phenomena, a sharp increase in slope of N_1/σ_{12} is observed when it is plotted with shear stress σ_{12}. It is speculated that the distortion occurs due to azimuthally spaced eddies that penetrates the rotation axis of the cone [Larson, 1992; Kulicke and Porter, 1979].

The second one that is axisymmetric indentation of the meniscus is located half way between cone and plate. It lowers the effective shearing surface area. Tanner and Keentok (1983) observed that the instability occurs when the second normal stress difference (N_2) is negative and large in magnitude. Lee *et al.* (1992) argued that even first normal stress difference (N_1) is very large as compared to second normal stress (N_2), this type of fracture is not observed.

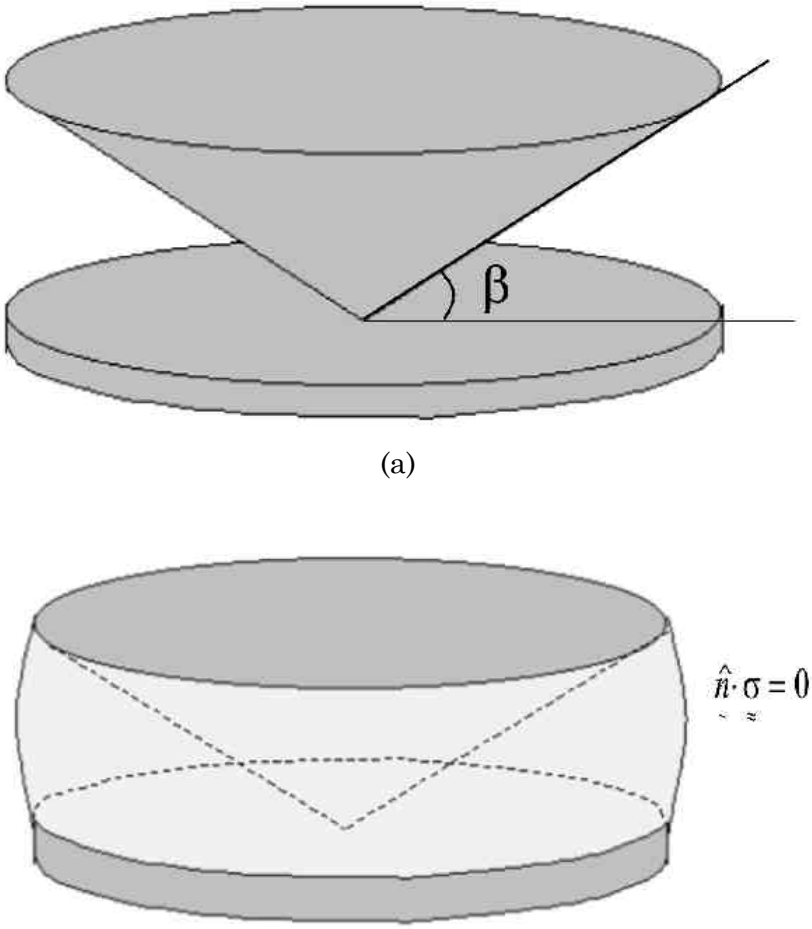

(a)

(b)

Figure 5.1 (a) Schematic of cone and plate geometry. (b) At the free surface stress is zero which gives rise to discontinuous boundary condition.

5.3 Experimental:

5.3.1 Materials:

The material used in this study was linear low density polyethylene (Dowlex 2045) from Dow Chemicals having M_w=116400 and M_n=34300. The molecular weight information was obtained by using 150C Waters GPC fitted with three detectors: light scattering, viscosity and refractive index (RI). The carrier solvent trichlorobenzene was pumped at a flow rate of 1 ml/min at 160 ^{0}C in the injector and column compartments.

5.3.2 Apparatus:

A Bohlin cone and plate controlled-stress rheometer (CVO 50) was used for the rheological measurements. A 5.4^0 truncated cone of 15 mm diameter was used. The cone and plate were of stainless steel. The measurements were carried out by using a bare cone as well as a fluoropolymer coated cone. The cone was coated by dipping it in a 5 % solution of the fluoroelastomer (SUMMIT, Sumitomo Corporation, Japan) in acetone for two hours. The wetted cone was dried in an open atmosphere till a thin layer of the fluoroelastomer was formed on the cone. The cone was then kept at 60 ^{0}C for two hours to remove the acetone and then at 220 ^{0}C for 12 hours to cure the coating. All experiments were carried out under controlled stress conditions at four temperatures namely, 150 ^{0}C, 170 ^{0}C, 190 ^{0}C and 210 ^{0}C.

Extrusion experiments were carried out using a CEAST Rheovis 2100 rate controlled capillary rheometer at the temperatures mentioned above. LLDPE was extruded through a case hardened steel die of 1.0 mm diameter, L/D 40 and an entry angle of 60^0. Extrusion experiments were also carried out by using a coated die, for which the internal surface was coated with the same fluoroelastomer. Coating was carried out following the procedure recommended by Wang and Drda (1997a). A 5% solution of the fluoroelastomer in acetone was made to flow through the capillary for several times followed by drying the capillary at 220^{o}C for 12 hours.

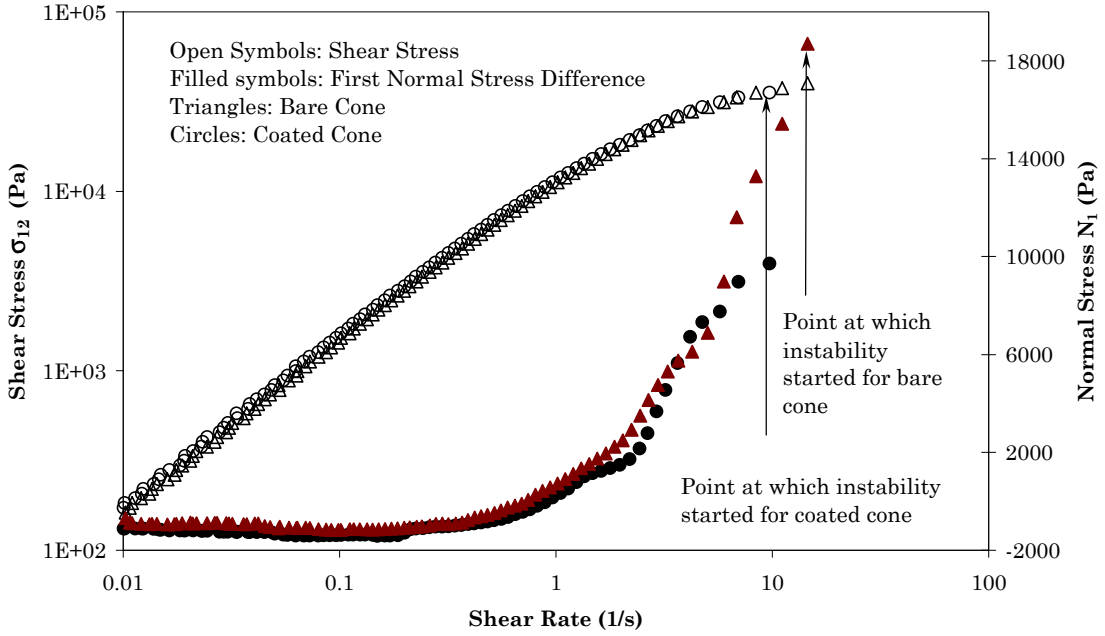

Figure 5.2 Shear stress and first normal stress difference plotted against shear rate. It can be seen that at the onset of instability N_1 increases more rapidly for the bare cone. T=150 ^{0}C.

Figure 5.3 The photograph of the plate immediately after the instability has occured in the cone and plate rheometer. The left picture (a) is from the plate where the coated cone was used, while the right picture (b) corresponds to a bare cone. The sample with the coated cone is almost free from distortions relative to the bare cone case.

5.4 Results and Discussion

Irrespective of the nature of the cone (bare or coated) all the experiments showed a steady and continuous increase in shear rate with shear stress followed by a sudden increase in rpm of the cone at a critical shear stress. The data in figure (5.2) at 150 ^{0}C shows the observed instabilities for bare and coated fixtures (cones). Such instabilities in curvilinear viscometric flows are known to arise due to any of the failure mechanisms namely, centrifugal expulsion, elasticity driven meniscus distortion or slip [Powell, 1998] as discussed earlier.

It was observed during our experiments that at all temperatures the sudden increase in shear rate in the case of a bare cone occurred consistently at higher stresses than that for the coated cone. It was also observed that the first normal stress difference at the onset of instability increased much more rapidly for the bare cone than for the coated cone. Figure (5.2) shows the shear stress and normal stress data at 150 ^{0}C.

Figure (5.3) shows photographs of the sample left on the plate after the sudden increase in the apparent shear rate in experiments in which both coated and uncoated cones where used. The photograph is of the experiment done at 170 ^{0}C. It can be seen that when the bare cone was used, the sample is cracked and was partly thrown out of the gap, while in the case of experiments with a coated cone the sample was almost devoid of any distortions. The Reynolds number at the onset of instability can be calculated from the expression discussed earlier. The Reynolds number can be given by $4\rho\kappa_{12}\beta^2 R^2/\eta$. Taking the density of LLDPE to be 935 kg/m^3 [Billmeyar, 1984], we get $Re \approx 10^{-5}$, which is much lower than the critical Reynolds number for expulsion $Re_c \approx 800$. Although the material in the bare cone can be seen to be expelled out from the gap, the possibility for the centrifugal expulsion can be ruled out since the Reynolds number is much lower than the critical Reynolds number for expulsion [Larson, 1992]. In figure (5.4) the ratio of first normal stress difference (N_1) and shear stress (σ_{12}) is plotted against the shear stress (σ_{12}). It can be seen that at the onset of distortion for the bare cone, N_1/σ_{12} increases sharply as compared to that for the coated cone. Such sharp increase in the slope for the bare cone can be related to the surface distortion phenomena (elasticity driven meniscus distortion) [Larson, 1992]. We believe that the

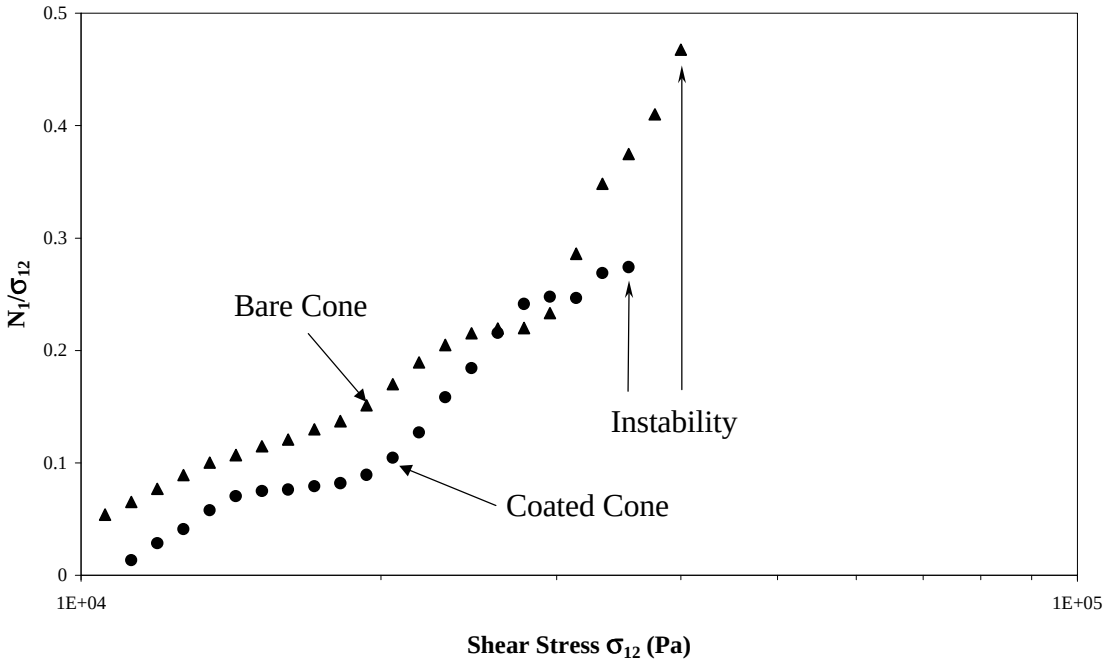

Figure 5.4 N_1/σ_{12} vs shear stress (σ_{12}), plotted for the data shown in figure 5.1. It can be seen that at the onset of instability N_1/σ_{12} increases more rapidly for the bare cone than that for the coated cone.

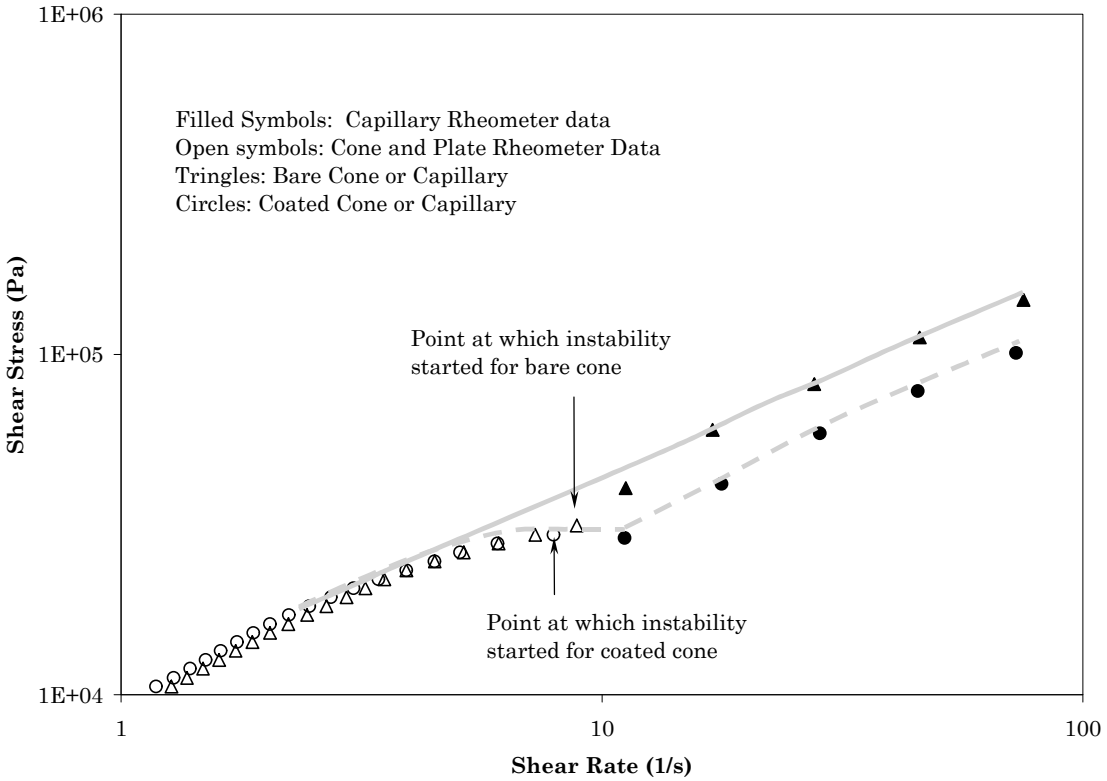

Figure 5.5 Flow curves for coated and uncoated surfaces (cone and capillary die) at 170°C. The flow curves obtained from an uncoated cone smoothly merge with those obtained from an uncoated capillary die. The flow curve for a coated cone overlaps with that for the uncoated cone up to the point of slip, after which the flow curve in the coated die is always below that for the uncoated die.

instability in bare cone is initiated by meniscus distortion resulting finally in expulsion and/or cracking at very high speeds. For the case of the coated cone, the slope of N_1/σ_{12} curve at the point of instability is much smaller than that of bare fixtures and also the instability occurred at lower shear stress (or shear rate). Hence, we believe that the instability in the coated cone case is most probably driven by slip.

As an independent conformation, we performed similar experiments on the capillary rheometer. Figure (5.5) shows the data at 170 ^{0}C obtained from a capillary rheometer (using coated and bare dies) and from cone and plate rheometer (using coated and bare cones). It can be seen that the stress at which the slip occurred on the coated cone is the same at which the flow curve for the coated extrusion die separated from the flow curve of the bare extrusion die. A similar separation of flow curves for coated and bare surfaces have been observed by Xing and Schreiber (1996) and by Koran and Dealy (1999).

The above experimental observations lead us to believe that it is possible to measure the critical stress for slip due to adhesive failure by conducting controlled stress experiments on a fluoropolymer-coated cone. We have measured the critical stress for slip as a function of temperature. Figure (5.6) shows the shear stress plotted against shear rate for various temperatures. The critical wall shear stress is then plotted against temperature in figure (5.7). It can be seen that the critical stress for adhesive failure (slip) decreases with an increase in temperature. This temperature dependence of critical stress for coated surfaces is opposite to that observed by Wang and Drda (1996a) for uncoated steel dies. We believe that the results presented here are the first observations of temperature dependence of critical stress for slip occurring due to debonding. This observation provides further evidence that the temperature dependence of critical stress could indeed be used to discern the true mechanism of slip.

Our unified slip model developed in the previous chapter predicts this behavior. The stress in the interfacial region (i.e, wall shear stress) in given by,

$$\sigma_{12} = \phi \frac{G_0 \gamma_e f}{g} = (\phi n_0 kT) n \gamma_e \qquad (5.2)$$

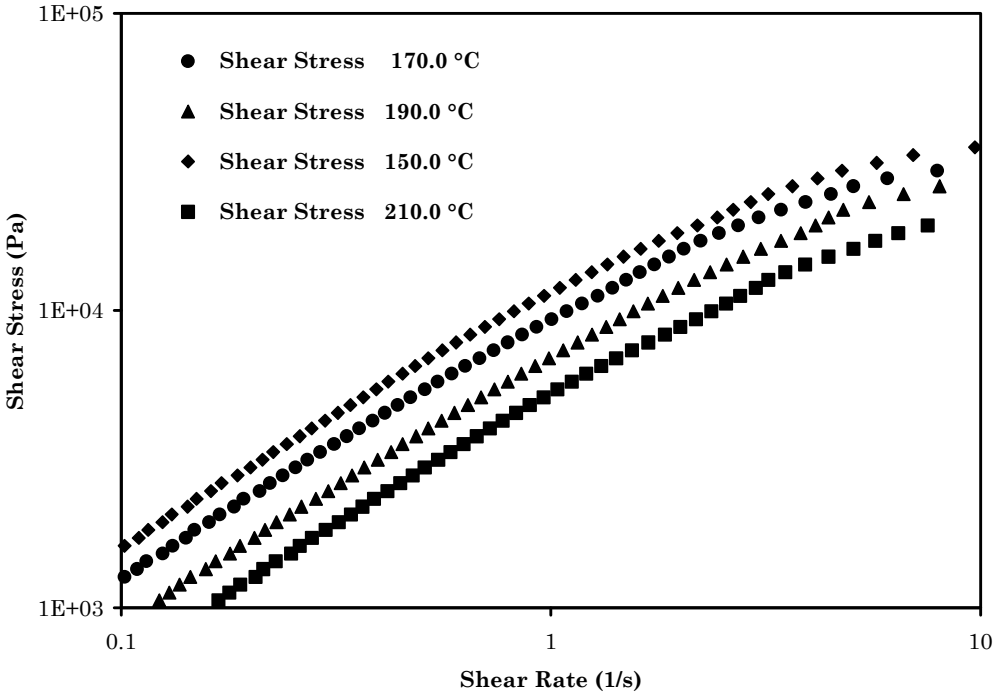

Figure 5.6 The plot inserted within the figure shows shear stress plotted against shear rate for the coated cone up to the point of instability (slip).

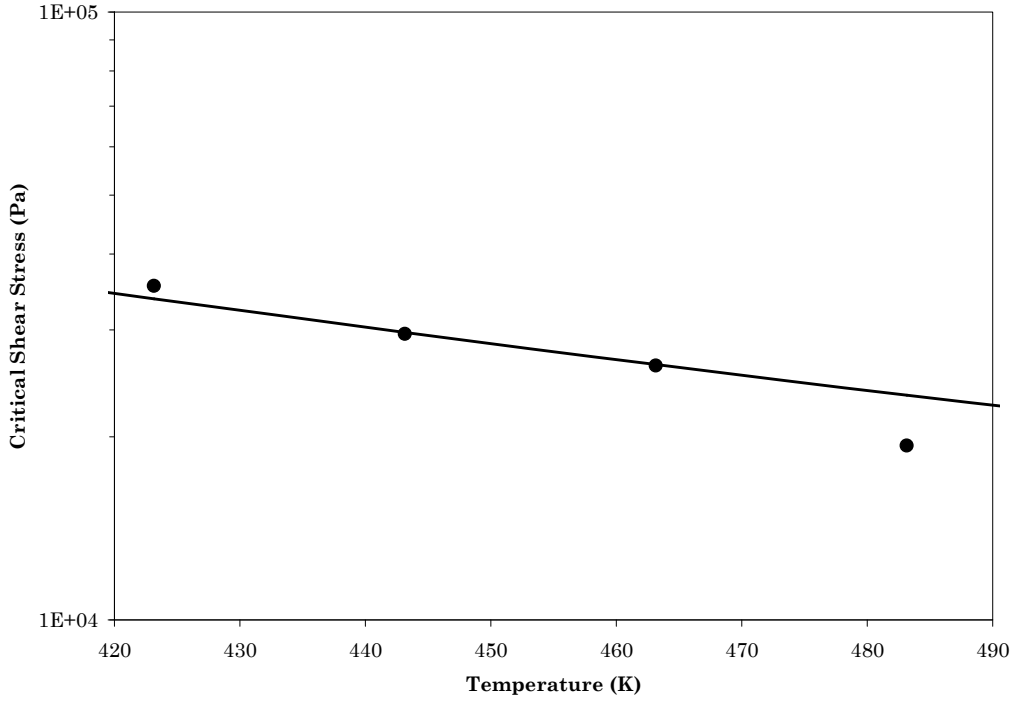

Figure 5.7 The critical stress for debonding is plotted against temperature. The points show experimental data, while the line shows the model prediction. The model parameters are, A=0.0025, ΔE_{adh} = 2.921E-20 J/molecule, n_0=2.057E+26. In the interfacial region a=8.0, b=11.25.
where

$$\phi = \frac{A\exp\left(\frac{[\Delta E_{adh}]}{kT}\right)}{A\exp\left(\frac{[\Delta E_{adh}]}{kT}\right) + \exp\left(\frac{3}{2}\gamma_e^2\right)} \tag{5.3}$$

is the fractional surface coverage, ΔE_{adh} is the adhesive energy, $\gamma_e = (\sigma_{11} - \sigma_{22})/2\sigma_{12}$ is the effective strain, $n\,(= f/g)$ are the number of entanglements per unit volume under flow normalized with respect to the equilibrium number of entanglements n_0, and f and g are the rates of creation and the loss of entanglements given by,

$$f = \exp(a\gamma_e)\ ,\ g = \exp(b\gamma_e) \tag{5.4}$$

Here, A, a and b are adjustable model parameters. The effective strain γ_e is directly proportional to shear rate. We have shown that the stress-effective strain (σ_{12} vs. γ_e) curve shows a non-monotonic behavior due to either a decrease in ϕ (i.e., debonding) or due to decrease in n (i.e., disentanglement). The critical stress for slip can be calculated from the non-monotonic stress curve as the value of the maximum stress before it begins to decrease.

The important model parameter in the unified model is the adhesive energy. The adhesive energy for the LLDPE-Teflon® system (the difference between polymer-metal work of adhesion and polymer-polymer work of cohesion) is known to be 9.3 dyne/cm [Anastasiadis and Hatzikirikos, 1998]. This adhesive energy is converted into (energy)/(adsorption junction) or (energy)/(adsorbed molecule) for the calculations of the unified model. The maximum shear-stress is calculated using equation (5.2) for various temperatures. Figure (5.6) shows a quantitative theoretical fit for the temperature dependence data observed experimentally in the case of coated surfaces. We have already shown in the previous chapter that the same unified model also predicts an increase in critical stress with temperature for slip occurring by disentanglement on high-energy surfaces (polyethylene on bare steel walls). Thus, the unified model provides the first successful prediction of the correct temperature dependence of critical stress for slip occurring due to disentanglement and due to debonding.

5.5 Conclusion

We have presented an experimental verification of the temperature dependence of critical shear stress for slip when the operative mechanism is debonding. The critical stress for polyethylene slipping on fluoropolymer surfaces was found to decrease with increase in temperature, which is opposite to the increase in critical stress with temperature observed for polyethylene slipping on uncoated steel surfaces [Wang and Drda, 1996a]. The unified slip model proposed in chapter 4 predicts both the trends correctly by simply using the correct adhesive energy values for the two surface-polymer pairs. We have shown correctly for the first time that the temperature dependence of critical stress can be used to discern the true mechanism of wall-slip for any polymer-wall pair.

CHAPTER 6

A MOLECULAR MODEL FOR WALL SLIP

6.1 Introduction:

The previous chapters have attempted to develop a simpler empirical model for predicting strong slip. The model is successful because it can predict many of the experimentally observed characteristics features of the stick-slip instability. Furthermore, the model elegantly unifies the two apparently different mechanisms of slip, debonding and disentanglement. A key physical insight into the development of the unified model is that it adopts the transient network formalism for describing the dynamics of entangled polymeric fluid and also that it intuitively proposes a different dynamics for polymer molecules near the wall compared to those in the bulk. Consequently, the major drawback of the unified model is that it is incapable of answering exactly *why* and *how* does the chain dynamics of polymer chains near the wall differ from the bulk chain dynamics. In order to answer these very important fundamental questions, one needs to understand the molecular picture; in other words, a molecular model is required. In this chapter, we propose a molecular model that is based on the tube model of entangled polymers. The molecular model is developed for an idealized and simplified picture of polymer chains end-tethered to the highly adhesive wall. The most important prediction of the model is that it identifies a key molecular relaxation process that is responsible for stick-slip. The model is fully predictive and requires no adjustable parameters. The only information required is purely molecular properties of the polymer.

The Doi-Edwards tube model is undoubtedly the most successful molecular theory for polymeric liquids. In an entangled polymeric liquid, non-crosslinked polymeric chains form a fine mesh due to their entanglements with each other. The transient network formalism is one way of modeling this picture. In 1967, Edwards presented a different picture of the entangled system. He proposed that the molecule could be considered to be confined in a mesh of constraints posed by the surrounding molecules. Edwards called

this unique configuration of the molecule the *primitive path* and surrounding constraints to be the *tube*. A key advance in this concept came in a seminal paper by de Gennes in 1971. He proposed that the molecule can not move laterally due to constraints imposed by the tube, but imagined that the molecule can move to and fro along the contour of the tube made of crosslinked chains performing a one dimensional diffusion. He called this movement of the molecule along the contour of the tube as *reptation*. In a series of seminal papers Doi and Edwards generalized this idea to non-crosslinked, non-permanent set of obstacles, a situation observed in entangled melts and solutions of linear flexible and rod like polymers [Doi and Edwards, 1978a, b, c, 1979]. This family of models is generally called the *tube model*.

6.2 Background on Tube Model

6.2.1 Doi-Edwards (DE) Theory

The Doi-Edwards theory deals with the large-scale motions of linear chains in an entangled system. Each chain is confined in a tube. The centerline of the tube tracks the current chain conformation. The diameter of the tube is governed by the mesh size, and it is a mean distance the chain should move laterally to meet the constraint imposed by other entanglements. The centerline of the tube, the primitive path of the chain, is assumed to be a random walk sequence of N_0 steps with step length a. The mean square end-to-end distance $\left\langle R^2 \right\rangle_0$ of the tube (chain) under equilibrium is then,

$$\left\langle R^2 \right\rangle_0 = N_0 a^2 \tag{6.1}$$

$$L_0 = N_0 a \tag{6.2}$$

where L_0 is the contour length or path length of the tube. The step length of the primitive path (a) and the diameter of the tube are independent of chain length (molecular weight) and are comparable in magnitude. In the Doi-Edwards theory, they are taken to be equal to each other. It is assumed that the motion of center of gravity of the chain is governed by its diffusion along the curvature of the tube. When the chain end emerges out from the current tube, it takes an instantaneous random direction. The chain thus creates a new primitive path with random orientations at the emerging end vacating the currently occupied tube at the other end. The time required to vacate the

original tube is known as disentanglement time or the reptation time τ_d [Graessley, 1982].

Consider the melt to be deformed rapidly such that the chains are stretched affinely and the stress is built up. Primarily the relaxation of stress occurs in two steps, retraction and reptation. Due to the possibility of movement along the contour of the tube, the molecule retracts quickly to achieve an equilibrium path length to relax its stress related to its stretch. Though the molecule regains its equilibrium contour length by retraction, it is still orientated in the direction of deformation and its end-to-end distance is higher that the equilibrium end-to-end distance, which contributes to the stress. The relaxation of this stress can be achieved by randomization of the orientation, which occurs through the process of reptation. The process of retraction is very fast as compared to the reptation and occurs over a time scale τ_r known as the Rouse relaxation time or retraction time. In the original theory of Doi and Edwards, the retraction process was ignored and the theory assumes a constant equilibrium path length.

Consider a strand in the primitive path having a unit vector $\underset{\sim}{u}$. The expression for the stress tensor $\underset{\approx}{\sigma}$ is written as,

$$\underset{\approx}{\sigma} = 3cN_0 k_B T \left\langle \underset{\sim}{u}\,\underset{\sim}{u} \right\rangle = G_0 \left\langle \underset{\sim}{u}\,\underset{\sim}{u} \right\rangle \tag{6.3}$$

where c is the number of chains per unit volume, k_B is Boltzmann's constant, T is absolute temperature and G_0 is the elasticity modulus or Young's modulus of the network. Now if an instantaneous deformation $\underset{\approx}{E}$ is applied, the deformation will carry a vector $\underset{\sim}{u}$ into $\left(\underset{\approx}{E}.\underset{\sim}{u}\right)$ and consequently the stress tensor is given as,

$$\underset{\approx}{\sigma} = 3cN_0 k_B T \left\langle \left(\underset{\approx}{E}.\underset{\sim}{u}\right)\left(\underset{\approx}{E}.\underset{\sim}{u}\right) \right\rangle \tag{6.4}$$

It should be noted that for any $\underset{\approx}{E}$, $\left|\underset{\approx}{E}.\underset{\sim}{u}\right| > 1$. The retraction process is a fast process, which brings the number of monomers per unit length of the tube to its equilibrium value. The retraction of the chain brings its path length to an equilibrium value of L_0. It can be shown that the number of subchains decrease in the retraction process and

becomes $N_0\left\langle\left|\underset{\approx}{E}.\underset{\sim}{u}\right|\right\rangle^{-1}$ and the length of subchain increases to $a\left\langle\left|\underset{\approx}{E}.\underset{\sim}{u}\right|\right\rangle$ [Marrucci, 1984]. After the retraction the stress is given by [Marrucci, 1984],

$$\underset{\approx}{\sigma} = G_0 \frac{1}{\left\langle\left|\underset{\approx}{E}.\underset{\sim}{u}\right|\right\rangle}\left\langle\frac{\left(\underset{\approx}{E}.\underset{\sim}{u}\right)\left(\underset{\approx}{E}.\underset{\sim}{u}\right)}{\left|\underset{\approx}{E}.\underset{\sim}{u}\right|}\right\rangle = G_0\,\underset{\approx}{Q} \tag{6.5}$$

where $\underset{\approx}{Q}$ is the geometric universal tensor. Further, $\langle\cdots\rangle = \frac{1}{4\pi}\int_0^{2\pi}\int_0^{\pi}\cdots\sin\theta\, d\theta\, d\phi$ and this averaging is to be performed over isotropic, equilibrium orientation distribution function. The second relaxation step occurs over a longer time and corresponds to randomization of the retracted chain through the reptation by vacating the deformed tube.

Doi (1980b) considered a chain having a path length L_0, with s_0=0 at the center of the chain and s_0 varies from $-L_0/2$ at one end to $L_0/2$ to other end. Then the orientational order parameter tensor $\underset{\approx}{S}(s_0,t)$ can be defined as,

$$\underset{\approx}{S}(s_0,t) = \left\langle \underset{\sim}{w}(s_0,t)\,\underset{\sim}{w}(s_0,t) - \frac{1}{3}\underset{\approx}{I}\right\rangle \tag{6.6}$$

where $\underset{\sim}{w}(s_0,t)$ is the unit vector of the segment at s_0 location along the chain, and $\underset{\approx}{I}$ is the unit tensor. The macroscopic stress can be calculated from $\underset{\approx}{S}(s_0,t)$ as,

$$\underset{\approx}{\sigma}(t) = \frac{G_0}{L_0}\int_{-L_0/2}^{L_0/2}\underset{\approx}{S}(s_0,t)\,ds_0 \tag{6.7}$$

The orientational order parameter tensor $\underset{\approx}{S}(s_0,t)$ may be expressed as [Doi, 1980b],

$$\underset{\approx}{S}(s_0,t) = \int_{-\infty}^{t}\frac{\partial G(s_0,t',t)}{\partial t'}\underset{\approx}{Q}\left[\underset{\approx}{E}(t,t')\right]dt' \tag{6.8}$$

$G(s_0,t',t)$ is the probability that the tube segment located at s_0 at time t' survives until time t y, (Doi, 1980b; Marrucci, 1986)

$$\frac{\partial G(s_0,t',t)}{\partial t} = D_{rep}\frac{\partial^2 G(s_0,t',t)}{\partial {s_0}^2} - \langle \upsilon(s_0,t)\rangle\frac{\partial G(s_0,t',t)}{\partial s_0} \tag{6.9}$$

where the first term on the right is the diffusion term, which corresponds to Brownian motion between chain and tube. $D_{rep} = L_0^2/(\pi^2\tau_d)$ is the longitudinal diffusion coefficient of the chain. The diffusion term represents the reptation process by which the primitive chain escapes into the randomly oriented tube. The second term is the convective term and corresponds to the tangential motion of the tube relative to the center of the chain.

$\langle \upsilon(s_0,t) \rangle$ is the pre-averaged tangential velocity and arises due to the continuous retraction of the chain under continuous deformation in direction towards the center of the chain. The boundary and initial conditions for equation (6.9) are,

$$\begin{aligned} &G(s_0,t) = 1 \qquad \cdots \textit{when} \quad t = t' \qquad \textit{initial condition} \\ &G(s_0,t',t) = 0 \qquad \cdots \textit{at} \quad s_0 = \pm\frac{L_0}{2} \end{aligned} \tag{6.10}$$

$\langle \upsilon(s_0,t) \rangle$ is given by,

$$\langle \upsilon(s_0,t) \rangle = \underset{\approx}{\kappa}(t) : \int_0^{s_0} \underset{\approx}{S}(s',t)\, ds' \tag{6.11}$$

Since $\langle \upsilon(s_0,t) \rangle$ is always positive for steady flow and $\frac{\partial G}{\partial s_0}$ is always negative the net effect of the convective term will be to suppress the reptative diffusion process [Mead *et al.*, 1995; Mead and Leal, 1995]. The equations (6.7) to (6.11) form a set of equations, which form a constitutive model of Doi and Edwards. The original model of Doi and Edwards assumes independent alignment approximation (IAA), which allows the individual parts of the primitive chain to deform affinely. With IAA, $\langle \upsilon(s_0,t) \rangle = 0$ and the above equations are considerably simplified. The model requires only two parameters to be fitted independently that must be obtained from the rheological data. These parameters are the plateau modulus and the reptation time. The predictions of this model are exceptionally good for slow and small deformations. The most important prediction of the tube model is the molecular weight (M) dependence of the zero shear viscosity (η_0). The theory predicts the dependence to be $\eta_0 \propto M^3$ in comparison with experimental observation $\eta_0 \propto M^{3.4}$. The theory predicts non-linear relaxation modulus for linear molecules in excellent agreement with experiments. The Doi-Edwards equation poorly predicts the shear stress relaxation after a reversing double-step strain. The response improves considerably after removing independent alignment approximation [Doi, 1980a]. The model predicts overshoot in shear stress in the startup

of steady shear flow. The detailed list of various predictions of Doi-Edwards model can be found out elsewhere [Larson, 1988; Doi and Edwards, 1986].

An important failure of the model is that it predicts a severe shear-thinning behavior. The stress undergoes a maximum at a shear rate $\kappa_{12} \sim 1/\tau_d$ and approaches zero at higher shear rate. In addition, though the model predicts shear stress over shoot in the startup of steady shear, the first normal stress difference increases monotonically with time and does not show any overshoot. Various other drawbacks of the model are discussed elsewhere [Larson, 1988; Mead *et al.*, 1998]. One of the most important features of the Doi-Edwards model is that it considers relaxation of stretch and relaxation of orientation independently. As the model assumes the relaxation of stretch to occur over infinitesimal time, the chains can be considered to be orientated but not stretched in any flow situation. Although it is sufficient to assume a reptation-dominant stress relaxation mechanism for $\kappa_{12}\tau_d \leq 1$, the assumption fails for higher shear rates where chain stretching can occur.

6.2.2 The tube model with chain stretching (DEMG Model)

In 1988, Marrucci and Grizzuti accounted for local chain stretching and consequently the retraction process by considering new curvilinear co-ordinate 's'. As discussed earlier the curvilinear co-ordinate s_0, $\left(-L_0/2 \leq s_0 \leq L_0/2\right)$ spans the primitive chain at equilibrium. In the DEMG model, it is assumed that chain is now arbitrarily stretched and s, $\left(-L/2 \leq s \leq L/2\right)$ spans the new co-ordinates of the chain. A material point of the chain originally located at s_0 has been displaced to s and the function $s(s_0)$ defines the deformation and can be obtained from [Marrucci and Grizzuti, 1988; Pearson *et al.*, 1991]

$$\frac{\partial s(s_0,t)}{\partial t} = \left\langle \upsilon(s,t) \right\rangle + 3N_0 D_{rep} \frac{\partial q(s_0,t)}{\partial s_0}, \qquad where \quad q(s_0,t) = \frac{\partial s(s_0,t)}{\partial s_0} \tag{6.12}$$

$$\begin{aligned} q &= 1 \qquad \cdots at \quad t = t' \\ q &= 1 \qquad \cdots at \quad s_0 = \pm\frac{L_0}{2} \end{aligned} \tag{6.13}$$

Due to incorporation of this effect, equations (6.7) and (6.11) get modified to,

$$\left\langle \upsilon(s_0,t) \right\rangle = \underset{\approx}{\kappa}(t) : \int_0^s \underset{\approx}{S}(s',t)\, ds' \tag{6.14}$$

$$\underset{\approx}{\sigma}(t) = \frac{G_0}{L_0} \int_{-L_0/2}^{L_0/2} q^2 \, \underset{\approx}{S}(s_0, t) \, ds_0 \qquad (6.15)$$

Thus equation (6.8) to (6.10), (6.12) and (6.15) constitute the set of equations for tube model with segmental stretch. In recognition of the contribution of Marrucci and Grizzuti for generalizing the Doi-Edwards model for segmental stretching the model is designated as the DEMG model. The incorporation of the stretching in the reptation model improves its response in the transient mode showing the overshoot for the first normal stress difference in startup of steady shear flow above shear rate $\tau_r \sim 1/\kappa_{12}$. However, under the steady shear, the predictions of DEMG are as bad as DE (Doi-Edwards) theory showing a maximum in shear stress. In DEMG model, q does exceed unity initially after startup of a fast shearing flow and produces an overshoot in the first normal stress difference. However, the shear flow rotates the chain in the flow direction, which decreases the S_{12}, decreasing $\langle \upsilon \rangle$ and hence q and stress collapses back towards the DE value. It is apparent from the DEMG theory that the reptation is dominant for shear rates $\kappa_{12}\tau_d < 1$ and the stretching is dominant (in transient flow) for shear rates $\kappa_{12}\tau_r > 1$. This means for high molecular weight polymers ($\tau_d >> \tau_r$) there is a wide range of shear rates in the regime $1/\tau_d < \kappa_{12} < 1/\tau_r$, where the flow is not slow enough so that chain relaxes by reptation and not fast enough so as to stretch the chains. Hence, a non-linear relaxation mechanism must exist in the middle region of shear rates so that the shear stress increases monotonically with κ_{12} as observed experimentally.

Before the development of the systematic approach to incorporate chain stretching in the tube model by Marrucci and Grizzuti (1988) and Pearson *et al.* (1991), several tentative attempts to incorporate chain stretching have been made [Lin, 1985; McLeish and ball, 1986]. These models predicted a non-monotonic flow curve for steady shearing. Because of lack of knowledge of the relaxation mechanisms for the middle region ($1/\tau_d < \kappa_{12} < 1/\tau_r$), such non-monotonic prediction was misunderstood for the cause of spurt effect. However, various experimental studies have now conformed the existence of monotonic shear stress-shear rate behavior over a broad range of shear rates [Mead *et al.*, 1998; Bearcea *et al.*, 1993]. Apart from the linear polymers, the tube stretching is also very important for branched polymers. In that case, the retraction of the cross bar that connects two branch points becomes very sluggish. This case is out of scope of

present work and discussion can be found elsewhere [McLeish and Larson, 1998; McLeish and Milner, 1999]

6.2.3 Constraint release tube models

In 1996, Marrucci introduced an important relaxation mechanism addressing the issue of the renewal of the topological obstacles by the relative motion among chains due to flow (convection). This mechanism is known as convective constraint release (CCR). CCR is expected to occur when the mesh of constraints is flowing faster than the primitive chain. Considering the fact that the two mechanisms of relaxation (reptation and CCR) operate in parallel, their frequencies must be summed to get the overall effect [Marrucci, 1996]. For steady state, Ianniruberto and Marrucci (1996) proposed that the overall relaxation time becomes,

$$\frac{1}{\tau} = \frac{1}{\tau_d} + \beta \underset{\approx}{\kappa} : \underset{\approx}{\sigma} \tag{6.16}$$

where β is an arbitrary parameter. Based on the concept of Marrucci, Mead *et al.* (1998) developed a most refined constitutive model that considers both CCR and chain end fluctuations. The importance of the fluctuations was been recognized by Doi (1981), when he showed that the molecular weight dependence of η_0 significantly improves after accounting for chain end fluctuations. Mead *et al.* (1998) accounted for all these effects and proposed a contour variable model. They corrected the equation (6.9) and (6.12) for CCR and chain end fluctuations as,

$$\frac{\partial G(s_0,t',t)}{\partial t} = D_{rep}\frac{\partial^2 G(s_0,t',t)}{\partial {s_0}^2} - \langle \upsilon(s_0,t)\rangle \frac{\partial G(s_0,t',t)}{\partial s_0} - f(q)\left[\left(\frac{\langle \upsilon\rangle - \dot{s}}{s}\right)_{s=L/2}\right] G - \frac{G}{\tau_\xi(s_0)} \tag{6.17}$$

$$\frac{\partial s(s_0,t)}{\partial t} = \langle \upsilon(s,t)\rangle + 3N_0 D_{rep}\frac{\partial q(s_0,t)}{\partial s_0} - \frac{1}{2}\left[\left(\frac{\langle \upsilon\rangle - \dot{s}}{s}\right)_{s=L/2}\right](s - s_0) \tag{6. 18}$$

The second last term of equation (6.17) describes the effect of CCR on the orientation probability function, while the last term of equation (6.18) incorporates CCR into the equation for tube stretch. Both these terms are evaluated at the chain end, because constraints are released only when the end of a neighboring chain is convected through

the tube of the test chain. $f(q)$ is the *switch function* and that is used to reduce the dominance of the CCR, when the corresponding segment is stretched. Mead *et al.* (1998) proposed the self-consistent form of switch function, $f = \exp(-q)$. The last term of equation (6.17) is the fluctuation term, where $\tau_\xi(s_0)$ is the fluctuation time and is given by,

$$\tau_\xi(s_0) = \left(\frac{\tau_r}{4}\right)\exp\left(\vartheta\frac{N_0}{2}\xi^2\right) \tag{6.19}$$

where $\xi = 1 - 2|s(s_0)|/L$ and ϑ was estimated to be ~1.5. Equations (6.7), (6.8), (6.10), (6.13) to (6.15) and (6.17) to (6.19) constitute the contour variable model [Mead *et al.*, 1998]. This model is able to predict most of the experimental observations, including the important steady state behavior, which shows a monotonic flow curve up to moderate M/M_e values. The model requires three parameters, plateau modulus $[G_N^0 = (15/4)G_0]$, reptation time (τ_d) and retraction time $(\tau_r = \tau_d/3N_0)$, which can be calculated from viscometric data.

Another mechanism of relaxation that is active at low shear rates is the constraint release (CR). The physical basis of this mechanism is as follows. If the chains constituting the tube reptate away creating a *hole* in the tube, the probe chain undergoes a large-scale lateral motion (jump) with respect to its backbone [Graessley, 1982; Watanabe, 1999]. A series of such jumps provide a Rouse-like chain relaxation process, which is called constraint release. In the case of linear monodispersed entangled system, relaxation due to reptation always dominates over the relaxation due to constraint release. Hence, while modeling the dynamics of the monodispersed linear polymers the relaxation due to constraint release is often neglected. However, this becomes important for polydisperse polymers, blends and branched polymers for which there is a significant difference between the orientation relaxation time scales of different topological components of the fluid.

Consider a long chain with N_1 segments embedded in a *sea* of shorter entangled chains with N_2 segments. The mean waiting time for the local jump is equal to the reptation time of the surrounding chain and can be written as $\tau_w = \Lambda(z)\tau_d(N_2)$, where $\Lambda = \left(\pi^2/12\right)^z$, and z is the average number of constraints per cell. The constraint

release time scale is then given by $\tau_{CR}(N_1, N_2) = 2\tau_w N_2^{\,2}/\pi^2$ [Graessley, 1982]. In the case of star–linear blend, the arms of the star cannot reptate and hence the dominant relaxation mechanism is CR. If the star arm has N_1 segments and is dissolved in a sea of linear polymer of N_2 segments, the constraint release relaxation time is given by $\tau_{cr}(N_1, N_2) \approx N_1^{\,2}\left(\min(N_1, N_2)\right)^{-0.5}\tau_d(N_2)$ provided $N_1 > 10$.

If the probe chain with N_1 segments is small ($N_1 < 10$) and is embedded in a sea of chains having N_2 segments, then the surrounding N_2 chains behave as a permanent network. In this situation, the probe chain can renew its configurations only by retracting its tail in its own tube, which leads to exponentially long relaxation times [Ajdari, *et al.*, 1994; Brochard *et al.*, 1994]. This relaxation time for arm retraction is given by $\tau_{AR}(N_1) \approx N_1^{\,-1}\tau_d(N_1)\exp(\nu N_1)$, where value ν is of the order of unity.

6.3 A molecular model development for slip

On the basis of the various relaxation mechanisms discussed in the previous section, we will now develop a molecular theory for slip on a high adhesive wall. In a real extrusion system, polymer chains in the vicinity of a wall adsorb to form loops and tails, which are entangled with the free bulk chains. The bulk and the adsorbed chains have polydispersity in terms of molecular weights and loop sizes. In this section, we develop a tube model for the simplified case of monodispersed end-tethered molecules of N segments per molecule, which are entangled with monodispersed bulk chains of P segments per molecule. We will call the grafted wall region as the 'interfacial' region and the region away from the wall as the 'bulk'. We restrict our model development to the mushroom regime at the wall in which the tethered chains do not overlap with each other. Thus, the tube constraining a tethered chain is formed only by the bulk chains. The P chains of the bulk flow past the wall with a (unknown) slip velocity V_s as shown in figure (6.1a).

The picture in figure (6.1a) is equivalent to the case of a probe chain that is pulled by one end at a velocity V_s through a stationary melt [Ajdari et al., 1994; Mhetar and

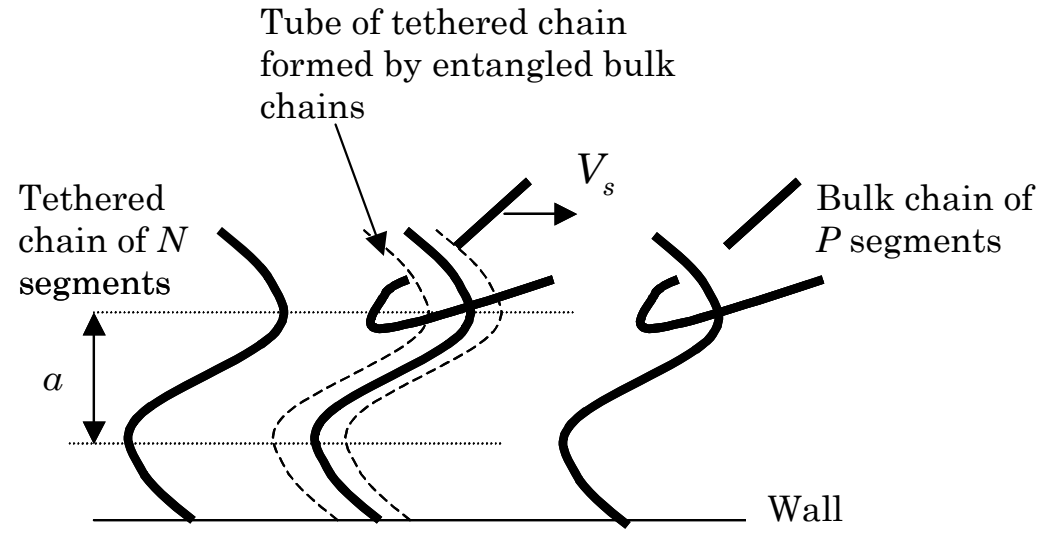

Figure 6.1a The bulk chains flowing with macroscopic velocity V_s are entangled with the tethered chains. The bulk chains form the tube of the tethered chains.

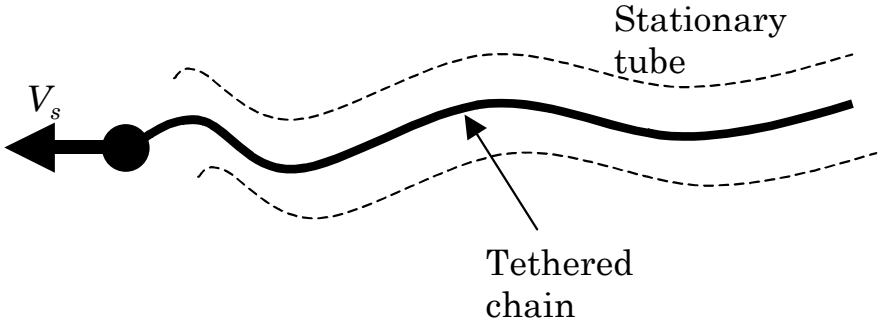

Figure 6.1b The probe chain (tethered chain) is pulled at one end (tethered end) with velocity V_s through the bulk chains.

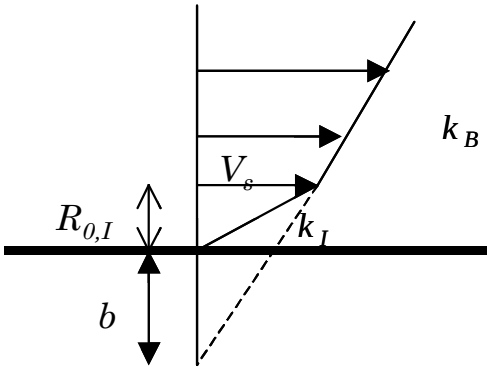

Figure 6.1c A schematic showing the interfacial region of thickness R_0. The slip length $b = V_s / k_B$ can also be seen in the sketch.

Archer, 1998a] (see figure 6.1b). Whereas the bulk experiences a shear rate κ_B, the interfacial region experiences an effective shear rate κ_I at the same wall shear stress. Depending on the magnitude of κ_I, a slip length b can be defined as shown in figure (6.1c). We make an attempt to develop a tube model that can quantitatively predict the interfacial shear rate κ_I, the slip velocity V_s and the slip length b at a given value of the bulk shear rate κ_B (or wall shear stress) with the knowledge of only molecular parameters.

To begin with, it must be noted that there are several important differences between the modes of stress relaxation in a flowing bulk chain and those in a stationary tethered chain. The relaxation mechanisms of a tethered chain are similar in many ways to those of an arm of a star polymer [Ajdari, *et al.*, 1994]. Firstly, the dominant stress relaxation mechanism for a bulk chain at low shear rates is reptation, whereas a tethered chain cannot reptate at all. Secondly, constraint release (CR) becomes an important mechanism for relaxation of a tethered chain since the bulk chains, which form the tube of the tethered chain, can reptate and release the constraints on the tethered chain. This results in a local random jump in the conformation of the tethered chain [Graessley, 1982], which relaxes its stress. On the other hand, the contribution of constraint release for monodispersed bulk chains is negligible [Marrucci, 1996]. Thus, the principle mechanism of stress relaxation for a tethered molecule at low shear rates ($\kappa_I < \tau_{cr,I}^{-1}$) is constraint release, where $\tau_{cr,I}$ is the tube renewal time due to CR of the tethered chains with N segments by bulk chains with P segments.

In the shear rate range $\tau_{r,I}^{-1} > \kappa_I > \tau_{cr,I}^{-1}$, the dominant relaxation mechanism is CCR, where $\tau_{r,I}$ is the retraction time of the tethered chain. In the CCR mechanism, the constraints on a test chain are released when the end of the chain that forms the tube is convected through the tube of the test chain. The convection velocity is the same as the motion along the contour that sets in by the continuous retraction process discussed earlier. For the case of bulk chains, the CCR relaxation occurs over the time scale of the order $O(1/\kappa_B)$, where κ_B is the bulk shear rate [Marrucci, 1996], which is the same time scale over which the bulk chain is being deformed by flow. Hence, the bulk chains can randomize the flow-induced orientation of other bulk chains by CCR. However, when the test chain is a tethered molecule in the mushroom regime, the rate at which

its constraints are released by CCR is determined by the convective velocity of the ends of the *bulk* chains, which form the tube of the tethered chain. Since the bulk chains experience a different shear rate κ_B, the CCR relaxation time scale for a tethered chain is of the order $O(1/\kappa_B)$. On the other hand, the time scale over which the tethered chain experiences deformation is of the order $O(1/\kappa_I)$. Thus, when $\kappa_I >> \kappa_B$, the tethered chains will preferentially orient in the flow direction. In other words, the subdued CCR in the vicinity of the wall is unable to prevent the orientation of the tethered chains. We postulate that this is the physical mechanism at a molecular level that is responsible for sudden orientation and slip.

Above the shear rate $\kappa_I \sim \tau_{r,I}^{-1}$, the chain relaxes mainly by fluctuations and partly by retraction. The contribution to stress comes from chain stretching. Tethering at one end slows down the retraction process. The retraction time for a tethered chain is four times larger than that of a free chain of the same molecular weight [Graessley, 1982]. The frequency of fluctuations of the contour length is maximum at the free end and decreases inwards in such a way that there are no fluctuations at the tethered end.

Thus, a deformed tethered chain can relax its stress by retraction, constraint release (CR), convective constraint release (CCR) and fluctuations. We will now apply the CV model to the interfacial region, which consists of tethered molecules grafted on the wall in the mushroom regime. Let the undeformed reference coordinate of the contour length of the tethered chain be s_0 with the first segment (tethered) at $s_0 = 0$ and the free end at $s_0 = L_{0,I}$, where $L_{0,I}$ is the equilibrium contour length of the tethered molecule. Let s be the contour length variable for deformed tethered chain, which varies from tethered end $s = 0$ to the free end $s = L_I$. The segment renewal probability $G_I(s,q)$ for the tethered chain at time θ and at position s under steady state flow is given by,

$$\frac{\partial G_I(s,\theta)}{\partial \theta} = D_I \frac{\partial^2 G_I(s,\theta)}{\partial s^2} - \langle \upsilon_1(s) \rangle \frac{\partial G_I(s,\theta)}{\partial s} - f(q_I)\left[2\frac{\langle \upsilon_2 \rangle}{L_B}\right] G_I(s,\theta) - \frac{G_I(s,\theta)}{\tau_{\xi,I}(s)} \tag{6.20}$$

The first term on the right hand side of equation (6.20) indicates tube renewal by dominating relaxation model either CR or Arm retraction (AR) depending on the

molecular weight of the tethered chain. The diffusivity for the tethered chains can be written as [Watanabe, 1999] $D_I = 2L_I^{\,2}/(\pi^2\tau_I)$. The dominating relaxation mode for $N > N_c$ is CR so that $\tau_I = \tau_{cr,I}$, i. e., the diffusion is controlled by CR process. For $N < N_c$ the diffusion is due to arm retraction so that $\tau_I = \tau_{AR,I}$. For a tethered chain of N segments entangled with bulk chain having P segments, the CR time scale depends on the values of N and P. The CR time scale for $N > N_c$ is given by [Brochard-Wyart, *et al.*, 1994, Ajdari *et al.*, 1994] $\tau_{cr,I}(N) \approx N^2\left(\min(P,N)\right)^{-0.5}\tau_d(P)$. For $N < N_c$, arm retraction is dominant with a relaxation time given by $\tau_{AR,I}(N) \approx N^{-1}\tau_d(N)\exp(\nu N)$, where τ_d is the reptation time of a free chain with N segments and the numerical factor of ν is taken to be unity. The value of critical number of segments N_c does not exceed 10 [Brochard-Wyart, *et al.*, 1994].

The second term in equation (6.20) indicates convection of the mesh relative to the chain at an average relative velocity $\langle \upsilon_1(s) \rangle$ between the chain and its mesh. The third term gives the tube renewal by CCR wherein the constraints on the tethered chain are released by convection of the chain end of bulk chains of contour length L_B at an average velocity $\langle \upsilon_2 \rangle$ that arises due to continuous retraction. $\langle \upsilon_1(s) \rangle$ and $\langle \upsilon_2 \rangle$ are defined later in equation (6.25) and equation (6.27). The last term is the fluctuation contribution to tube renewal, where $\tau_{\xi,I}(s_0)$ is the fluctuation time-scale, q_I is the local stretch ($q_I = \dfrac{ds}{ds_0}$) and $f(q_I)$ is the switch function. The fluctuation time-scale for the tethered chain is given by,

$$\tau_{\xi,I}(s) = \left(4\tau_r(N)\right)\exp\left(\vartheta N \xi_I^{\,2}\right) \qquad (6.21)$$

where $\xi_I = 1 - 2\left|s(s_0)\right|/L_I$ and ϑ is 1.5. The pre-factor of 4 multiplying the retraction time τ_r of N chain accounts for the effect of tethering one end of the chain [Graessley, 1982]. The switch function is used to reduce the dominance of the CCR, when the corresponding segment is stretched. We have used here the self-consistent switch function as described by Mead *et al.* (1998) namely $f(q_I) = q_I^{\,-1}$.

At steady state, the segmental stretch q_I is given by,

$$\frac{\partial q_I(s_0)}{\partial s_0} = \frac{1}{6ND_{rep,N}}\left[2\frac{\langle \upsilon_2 \rangle}{L_B}\right](s - s_0) - \frac{\langle \upsilon_1(s_0) \rangle}{3ND_{rep,N}} \qquad (6.22)$$

$$\text{where, } q_I = 1 \qquad \cdots at \quad s_0 = L_{0,I}$$

In equation (6.22), $D_{rep,N} = {L_I}^2 / (\pi^2 \tau_d(N))$ is the reptative diffusion coefficient and $\tau_d(N)$ $(= 3N\tau_r(N))$ is the reptation time of a free chain with N segments.

The initial and boundary conditions for the tube renewal probability in equation (6.20) can be arrived at from the following discussion. It can be seen from equation (6.21) that the magnitude of fluctuations decreases exponentially from the free end to the tethered end. Since the maximum fluctuations at the free end, do not allow the end-segment to remain in the tube, $G_I(\theta) = 0$ at the free end. In addition, since the other tube renewal mechanisms namely, CR and CCR, are uniform over the entire tube length, while the fluctuations are negligible at the tethered end, the boundary condition at the tethered end should be $\frac{dG_I(\theta)}{ds_0} = 0$. Thus,

$$\left.\begin{aligned} G_I(s_0) &= 1 \quad at \quad \theta = 0 \\ G_I(\theta) &= 0 \quad at \quad s_0 = L_{0,I} \\ \frac{dG_I(\theta)}{ds_0} &= 0 \quad at \quad s_0 = 0 \end{aligned}\right\} \qquad (6.23)$$

The net relative velocity between the segments of the tethered chain and its tube consists of two components, the one, which sets in due to the continuous retraction process, is given by,

$$\langle \upsilon_I(s_0) \rangle = \underset{\approx}{\kappa}_I : \int_0^s \underset{\approx}{S}_I(s')\, ds' \qquad (6.24)$$

and the other, which arises from the macroscopic velocity V_s of the tethered chain relative to the stationary tube formed by bulk chains [see figure (6.1b)]. Since $\langle \upsilon_I \rangle$ is always positive [Mead *et al.*, 1995], the direction of relative movement of the segments is always towards the tethered end, which is parallel to the direction of the slip velocity V_s. Hence, the net average relative velocity between the tethered molecule and its mesh is given by,

$$\langle \upsilon_1(s_0) \rangle = V_s + \langle \upsilon_I(s_0) \rangle \tag{6.25}$$

$\underset{\approx}{S}_I(s')$ in equation (6.24) is the orientational order parameter tensor for the tethered chain and is given by,

$$\underset{\approx}{S}_I(s_0) = \int_0^{\infty} \frac{\partial G_I(s_0,\theta)}{\partial \theta} \underset{\approx}{Q}_I \left[\underset{\approx}{E}_I(\theta) \right] d\theta \tag{6.26}$$

Here $\underset{\approx}{E}_I(\theta)$ is the deformation tensor for the tethered chains, which for shear flow is given by $E_I = \kappa_I \theta$, $\underset{\approx}{Q}_I$ is the geometric universal tensor $\underset{\approx}{Q}_I = \left\langle \left(\underset{\approx}{E}_I . \underset{\sim}{u} \right) \left(\underset{\approx}{E}_I . \underset{\sim}{u} \right) \Big/ \left| \underset{\approx}{E}_I . \underset{\sim}{u} \right| \right\rangle \Big/ \left\langle \left| \underset{\approx}{E}_I . \underset{\sim}{u} \right| \right\rangle - \underset{\approx}{I}/3$, where $\langle\ \rangle$ is the average over the isotropic distribution of unit vectors $\underset{\sim}{u}$ and $\underset{\approx}{I}$ is the unit tensor.

As discussed earlier, the CCR relaxation of tethered chains is determined by the velocity of the end segments of the bulk chain. This velocity is calculated by

$$\langle \upsilon_2 \rangle = \langle \upsilon_B(s_0) \rangle = \underset{\approx}{\kappa}_B : \int_0^{L_B/2} \underset{\approx}{S}_B(s') \, ds' \tag{6.27}$$

where, the bulk shear rate κ_B and the integral are to be calculated from the constitutive equation for bulk chains [Equations. (6.7), (6.8), (6.10), (6.13) to (6.15) and (6.17) to (6.19) discussed in the earlier section] at the same wall shear stress.

Further, the shear stress in the interfacial region is given by,

$$s_{12,I} = \frac{15}{4} G^0_{N,I} \frac{1}{L_{0,I}} \int_0^{L_{0,I}} {q_I}^2 S_{12,I}(s_0) \, ds_0 \tag{6.28}$$

where, $G^0_{N,I}$ is the plateau modulus of the interfacial region at the wall.

The calculation of the stress in the interfacial region from equation (6.28) requires an additional relationship between the slip velocity V_s and the effective shear rate experienced by the tethered molecules κ_I. We use a simple relationship in analogy to that proposed earlier by Wang (1999) [see figure (6.1c)],

$$V_s = R_{0,I} \kappa_I \tag{6.29}$$

where, $R_{0,I} = a\sqrt{N}$ is equilibrium end-to-end distance of a tethered molecule, which is also equal to the thickness of the grafted layer on the wall in the mushroom regime [Leger *et al.*, 1999]. This assumption can be expected to remain valid as long as the tethered chain does not stretch extensively. Thus, we can expect overprediction of V_s after strong slip.

Besides the slip velocity, one also requires knowledge of the plateau modulus of the interfacial region, which is expected to depend on the surface coverage of the tethered chains. Consider a small volume of height approximately equal to the entanglement spacing a shown by the dotted lines in figure (6.1a). Let there be ν chains grafted on this area such that the chains per unit area are $\Sigma = \nu / \text{area}$. Then the number of entanglements (or segments) in this volume element of height a is $\nu/(a \times \text{area}) = \Sigma / a$. Consequently, the plateau modulus is given by

$$G^o_{N,i} = \frac{\Sigma}{N_A\, a} RT \tag{6.30}$$

where, N_A is the Avogrado's number, R is the universal gas constant and T is the absolute temperature. Substituting equation (6.30) into equation (6.28) gives,

$$\sigma_{12,I} = \frac{15}{4}\frac{\Sigma kT}{a}\left\{\frac{1}{L_{oI}}\int_0^{L_{0I}} {q_I}^2 S_{12,I}(s_0)\,ds_0\right\} \tag{6.31}$$

Finally, the main equation that couples the dynamics of the interfacial and bulk regions is the continuity of shear stress between these regions. Thus,

$$s_{12,B} = s_{12,I} \tag{6.32}$$

Equations, (6.7), (6.8), (6.10), (6.13) to (6.15) and (6.17) to (6.19) for bulk along with equations (6.20) to (6.32) for interfacial region form the complete set of coupled integro-differential equations, which must be solved for predicting the flow curves of the tethered chains. The model parameters are: the number of entanglements per chain for the bulk molecules (P), the number of entanglements per chain for the tethered molecules (N), the reptation time (τ_d) of the bulk chain, the plateau modulus of the

bulk ($G^0_{N,B}$) and the surface coverage (Σ). The first two parameters require the knowledge of entanglement molecular weight M_e, which has been well documented in the literature [Durliat *et al.*, 1997]. The next two parameters can be determined from independent rheological experiments and are also documented in the literature for several polymers [Fetters *et al.*, 1994]. The last parameter (Σ) can be controlled by modifying the polymer-surface chemistry. The relationship between CR timescale and the reptation timescale has been discussed earlier. The retraction timescale for a free polymer chain can be estimated as $\tau_r(N) = 3N^{-1}\tau_d(N)$. All these timescales can also be found elsewhere [Ajdari, *et al.*, 1994; Graessley, 1982, Brochard-Wyart, *et al.*, 1994]. The wall shear stress in all of the calculations presented below has been non-dimensionalized using the bulk plateau modulus. Similarly, the slip velocity has been non-dimensionalized using the reptation time of the bulk chain and the equilibrium contour length of the bulk chain unless specified otherwise. Thus, P, N and Σ are the only parameters required to obtain the solution. The set of equations for the steady shear flow of contour variable model as well as slip model along with the detailed procedure to solve both of them is described in Appendix II.

6.4 Predictions:

All calculations presented in this section have been carried out for the case of a Polydimethylsiloxane (PDMS) melt, for which very precise experimental data on wall-slip is available from the recent work of Leger and co-workers (1996a, 1996b, 1999) and Durliat *et al.* (1997). From the experimental data of Leger and coworkers (1996a), the reptation time of PDMS chain having molecular weight 970,000 kg/kgmol is estimated to be 0.5632 sec. The plateau modulus of PDMS melt is known to be 0.18 MPa, its molecular weight between entanglements (M_e) is 13522 kg/kgmol and the segment length between entanglements can be estimated to be $a = 7.855\,\text{nm}$ [Fetters, *et al.*, 1994].

6.4.1 Flow curves

We will first examine the flow curves of the tethered chains and the influence of molecular weight of the tethered chain on the flow curves. In figure (6.2), the molecular weight of the bulk chain is kept constant while the molecular weight of the tethered chain is varied. The non-dimensional shear stress is plotted against non-dimensional

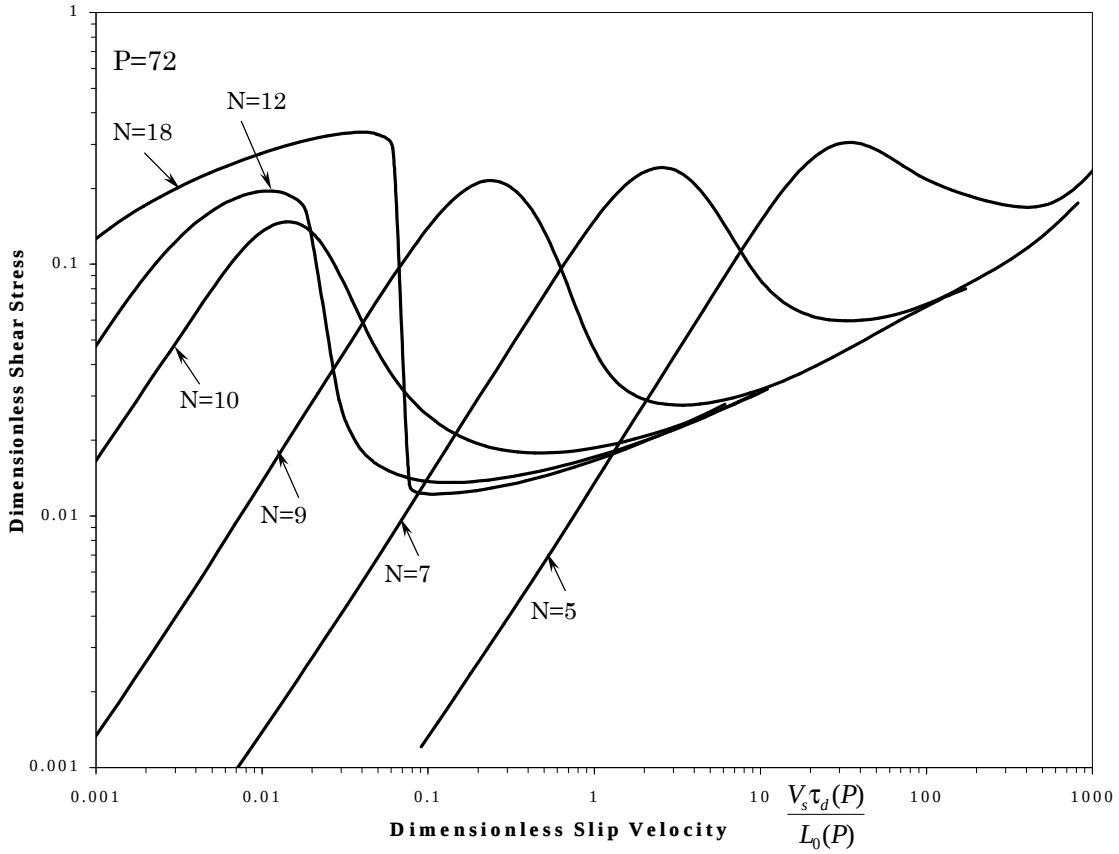

Figure 6.2 Dimensionless shear stress is plotted against dimensionless slip velocity for various values of N keeping P constant. It can be seen that as N decreases the severity of non-monotonicity and the jump in slip velocity decreases.

slip velocity in figure (6.2) for various values of N while keeping constant $P = 72$ and surface coverage $\Sigma = 3\times10^{17}\ 1/\mathrm{m}^2$. This choice of the surface coverage essentially renders the interfacial plateau modulus equal to that of the bulk and has been chosen arbitrarily to demonstrate the main predictions of the model. However, all of the trends in figure (6.2) are observed for other values of Σ also. The flow curve for the bulk chains shows a slight non-monotonic nature for $1/\tau_{d,B} < \kappa_B < 1/\tau_{r,B}$ for high value P [Mead *et al.*, 1998]. The small amount of non-monotonicity is in agreement with the nature of the CV model and indicates that a further relaxation mechanism is still missing in this shear rate range. An improvement of the CCR mechanism has been recently proposed [Ianniruberto and Marrucci, 2000], which is expected to make the flow curve fully monotonic.

For the tethered chains, it can be seen that the shear stress becomes increasingly non-monotonic as N increases. This clearly implies that the instability in the net flow has its origin in the interfacial region close to the wall. The maximum in the flow curve corresponds to a critical wall shear stress and a critical slip velocity (or a corresponding critical shear rate) at which the instability sets in. Figures (6.2) further shows that the shear stress increases monotonically in the low shear rate region $\kappa_I \tau_{cr,I} = V_s \tau_{cr,I} / R_{0,I} < 1$, indicating that the deformed tethered chain relaxes faster (due to CR) than the rate at which it is deformed. In the high shear rate region above $(V_s \tau_{r,I} / R_{0,I}) \sim 1$ the contour length of the chain starts increasing and consequently the stress increases monotonically with shear rate due to stretching. In the intermediate shear rate region, the shear stress becomes non-monotonic for high P and N values. In this region, the main relaxation mechanism is CCR. Clearly, the CCR is ineffective in completely randomizing the orientation of the tethered chains. This happens, as hypothised earlier, because the CCR time scale, which is determined by the retraction velocity of bulk chains, is longer than the time scale over which the tethered chains experience deformation ($\kappa_I \tau_{CCR,I} \sim \kappa_I L_B / \langle \upsilon_2 \rangle \sim \kappa_I / \kappa_B > 1$). Thus, the subdued CCR relaxation of the tethered chains cannot prevent their flow-induced orientation above the critical shear rate. As a result, the bulk chains suddenly lose their entanglements with the tethered chains and slip with a high slip velocity.

The critical shear stress at which the flow curve becomes non-monotonic decreases with increase in N due to the slowing down of the AR relaxation with molecular weight.

However, this trend does not continue for large values of $N > N_c$ when the CCR relaxation starts influencing the CR mechanism. For very small values of N the fluctuations of the contour length also relax the orientation of the chain. The relaxation due to fluctuations is highly effective in low molecular weight chains compared to that in high molecular weight chains [Ianniruberto and Marrucci, 2000]. This means that the low molecular weight tethered chains are less susceptible to orientation than the higher molecular weight tethered chains.

6.4.2. Scaling:

If τ is a typical relaxation time of the tethered chain, then the orientation of the chain would begin when the Weissenberg number $\kappa_I \tau \sim 1$. Thus, if the dominant relaxation mode were constraint release then

$$V_s^* = \left\langle R_o^2 \right\rangle^{1/2} \kappa_I \sim \frac{\left\langle R_o^2 \right\rangle^{1/2}}{\tau_{CR,I}} \sim \frac{N^{0.5}}{P^3 N^{1.5}} = P^{-3} N^{-1} \tag{6.33}$$

This scaling law demonstrated in figure (6.3a) for the case of $G_{N,I}^0 / G_{N,B}^0 = 0.05$ and $N < P$, agrees with that predicted by the Brochard *et al.* (1996) scaling model. Leger *et al.* (1996b) have experimentally validated this scaling, although in their experiments $N \geq P$ for which the above scaling should in fact be replaced by

$$V_s^* = \left\langle R_o^2 \right\rangle^{1/2} \kappa_I \sim \frac{\left\langle R_o^2 \right\rangle^{1/2}}{\tau_{CR,I}} \sim \frac{N^{0.5}}{P^{2.5} N^2} \sim P^{-2.5} N^{-1.5} \tag{6.34}$$

For the case of $N < N_c \sim 10$, the arm retraction is dominating mode of relaxation [Brochard-Wyart, *et al.*, 1994], and the scaling for the critical slip velocity can be given by

$$V_s^* = \left\langle R_o^2 \right\rangle^{1/2} \kappa_I \sim \frac{\left\langle R_o^2 \right\rangle^{1/2}}{\tau_I} \sim \frac{N^{0.5}}{N^2 e^N} \sim N^{-1.5} e^{-N} \tag{6.35}$$

For higher values of $G_{N,I}^0 / G_{N,B}^0$ (i.e., for higher surface coverage) the dependence of the critical slip velocity on P and N becomes complicated as shown in figure (6.3b). This is possibly due to the combined effect of the different relaxation mechanisms, which interact to produce a scaling, that does not agree with any one of the specific relaxation mechanisms.

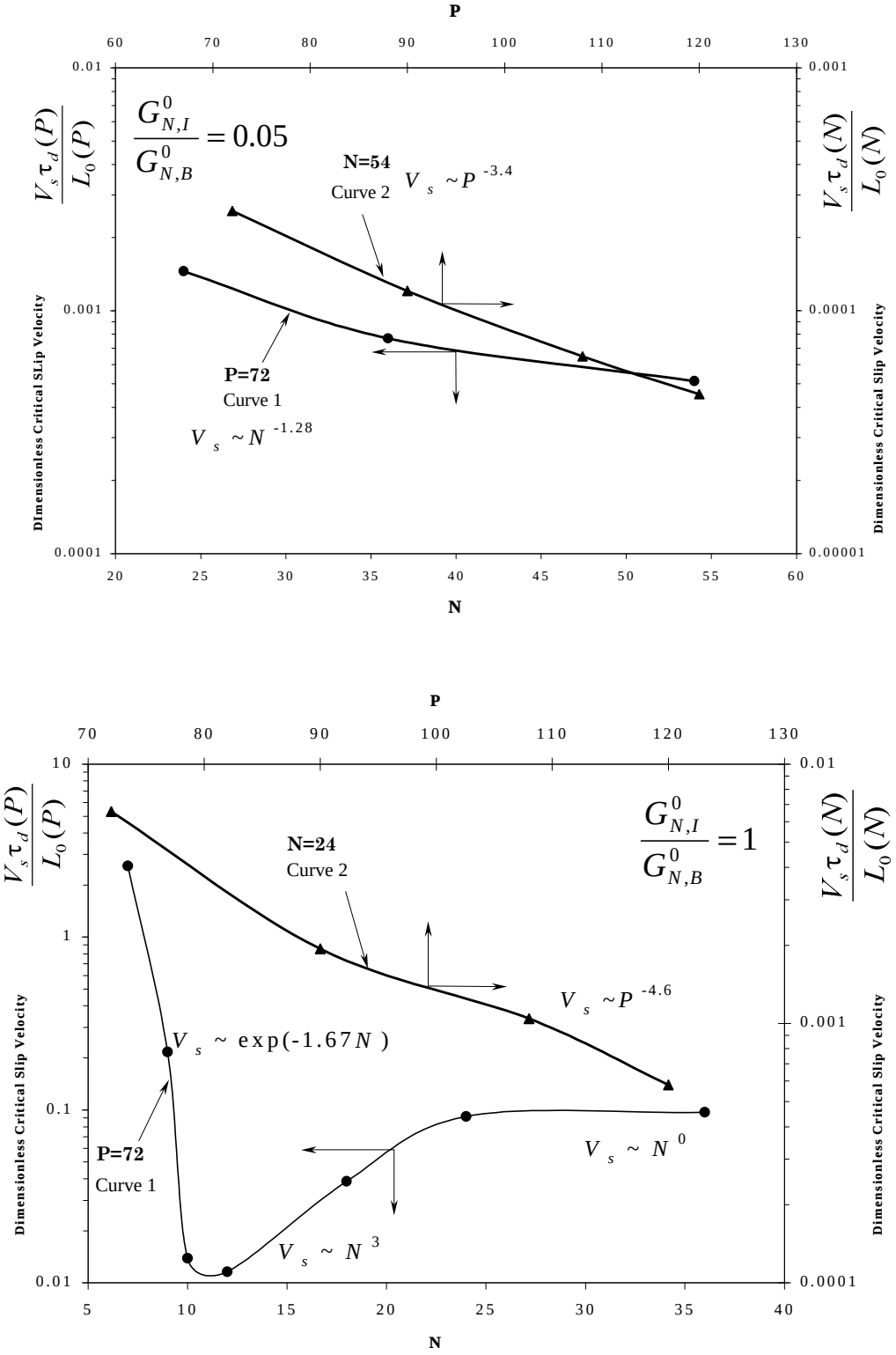

Figure 6.3 The critical slip velocity (at the onset of instability) is plotted against number segments of tethered and bulk chain for two plateau modulus ratios. (a) $G^0_{N,I}/G^0_{N,B} = 0.05$ and (b) $G^0_{N,I}/G^0_{N,B} = 1$.

6.4.3. Coil-to-stretch transition:

In figure (6.4), we plot the shear stress and contour length of the tethered molecule against slip velocity for the case of $P = 72$ and $N = 7$. For simplicity, we divide the slip velocity in three regions, first in which the stress increases with slip velocity, the second, where the stress decreases with slip velocity, and the third, where the stress again increases with slip velocity. In the third region, the numerical scheme adopted in this work poses some difficulties with respect to convergence at high slip velocities due to the change in the nature of the partial differential equation (equation 6.20) from parabolic to hyperbolic. The dashed line in this region simply indicates the possible trend in the increase in shear stress at the high slip velocities. In a controlled stress extrusion experiment, the thick arrows shown in figure (6.4) indicate the hysteresis associated with the slip instability. For a rate-controlled extrusion process, the second region of negative slope will correspond to an unstable region, where flow and pressure oscillations are expected to prevail. It is interesting to see that in this region while the stress becomes non-monotonic, the contour length of the tethered molecule increases by a factor of only about two. In the first and second region, though the contour length of the tethered molecule does not increase, the end-to-end distance of the tethered chain should obviously increases with the orientation of the molecule. Thus, the jump in slip velocity is associated with a 'coil-to-stretch' transition in which the tethered chain suddenly increases its end-to-end distance at a critical shear stress without increasing its segmental contour length substantially.

In figure (6.5) the shear component of the orientational order parameter tensor S_{12} is plotted against the non-dimensionalized length scale along the segmental contour length s_0/L_0 for various locations 1 to 3 on the shear stress curve of figure (6.4). For the corresponding curves in figure (6.5), S_{12} is always zero at $s_0/L_0 = 1$. This implies that the segmental orientation is always random at the chain end, which is due to the fluctuations of the last segments. For all the curves 1 to 3 in figure (6.5), the value of S_{12} increases towards the tethered end indicating that the orientation increases near the tethered end. Point 1 in figure (6.4) is in the region where AR is the dominating relaxation mechanism. The molecule has little orientation at this point and hence shows low values of S_{12} in the corresponding curve in figure (6.5). At point 2, in figure (6.4) the value of S_{12} attains a maximum at the tethered end, which consequently leads to the

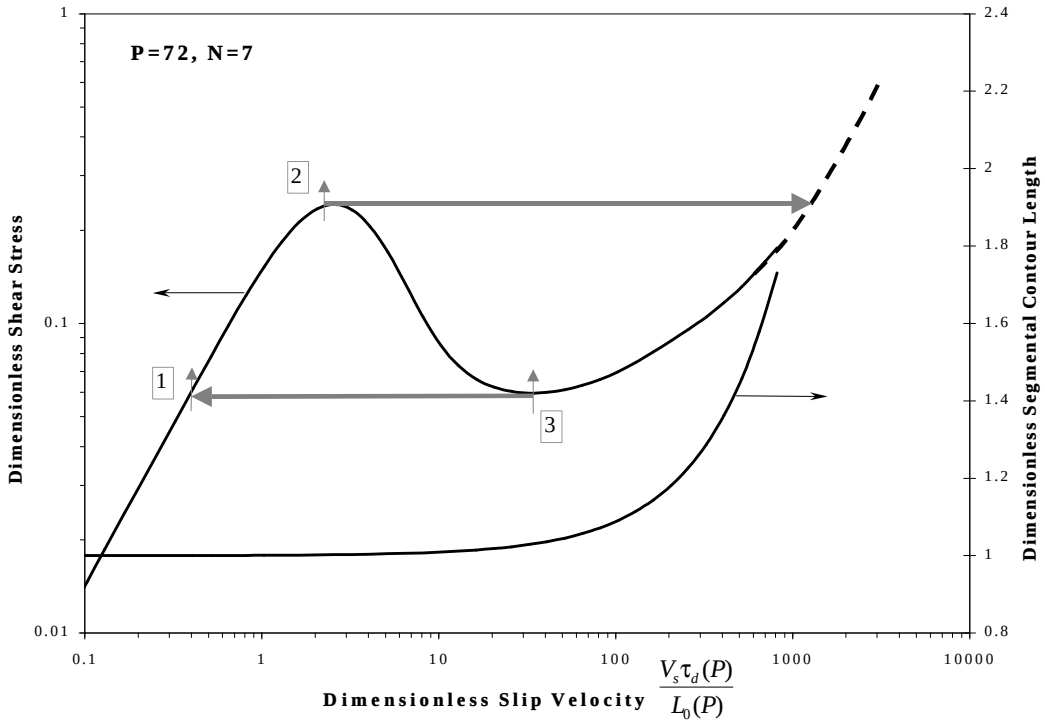

Figure 6.4 Dimensionless shear stress and segmental contour length are plotted against dimensionless slip velocity for P=72 and N=7. The hysteresis loop in the stress-controlled mode can be seen. The part of the curve with a negative slope indicates instability

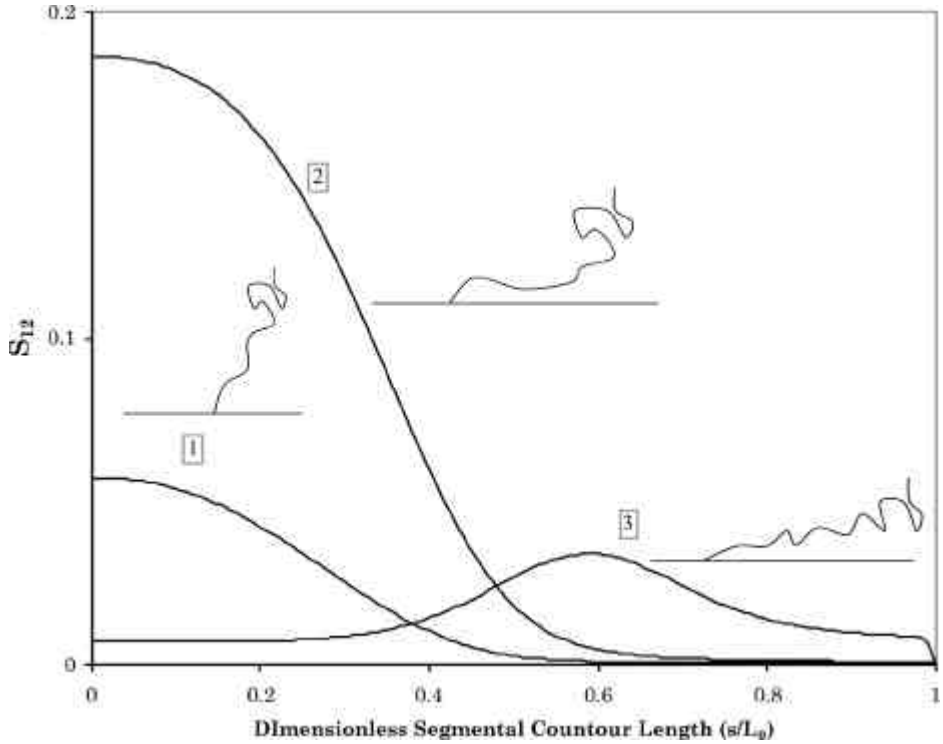

Figure 6.5 The shear component of the orientational order parameter tensor is plotted against the segmental contour length variable. The curves 1 to 3 correspond to various locations described on the shear stress-slip velocity curve of figure (6.4).

maximum in stress. Further increase in shear rate after the stress maximum, corresponding to point 3 in figure (6.4), shows a decrease in the value of S_{12} as seen in the curve 3 of figure (6.5). This implies a strong orientation of the segments near the tethered end. Any further increase in shear rate increases the contour length since $\kappa_I > \tau_{r,I}^{-1}$. This picture of the orientation of a tethered molecule is very similar to that proposed by Ajdari *et al.* (1994) and Mhetar and Archer (1998).

6.4.4. Comparison with experimental data:

We now compare the predictions of our model with the experimental data of Léger and coworkers (1996a, 1996b, 1999) and Durliat *et al.* (1997). These experiments were performed using monodispersed end-grafted PDMS chains of molecular weight 96000 kg/kgmol that are grafted on a wall to give a surface coverage of $\Sigma = 0.0055/(5\times10^{-10})^2 = 2.2\times10^{16}$ chains/m². The grafted wall is in contact with a monodispersed melt of molecular weight 970000 kg/kgmol. Velocities were measured at a distance of 70 nm from the wall, which is of the order of the end-to-end distance of the bulk chains $\left(\left\langle R_{o,B}^2\right\rangle^{1/2} = 67\ \text{nm}\right)$. The values of the various model parameters for PDMS have been listed earlier. At the experimental surface coverage of $\Sigma = 2.2\times10^{16}$ chains/m², the interfacial plateau modulus takes the value of 0.0115 MPa according to equation (6.30).

Figure (6.6) shows the slip length ($b = V_s / k_B$) plotted against slip velocity for two values of the interfacial plateau modulus namely, $G_{N,I}^0 = 0.0115$ MPa and $G_{N,I}^0 = G_{N,B}^0 = 0.18$ MPa. The bulk shear rate is taken as that value which gives the same shear stress in the bulk as that in the interfacial region (equation 3.32). The points in figure (6.6) show the experimental data while the lines shows the tube model prediction for the two values of the interfacial plateau modulus. The present model substantially overpredicts the critical slip length if the interfacial plateau modulus value calculated from equation (6.30) were to be used. The slip length decreases as the interfacial plateau modulus increases. This is because as the number of entanglements in the interfacial region increase, the shear stress that can be borne by the tethered chains at a given slip velocity increases, thereby increasing the bulk shear rate and

consequently decreasing the slip length. Thus it appears that the actual number of entanglements in the interfacial region is far more than that calculated from equation (6.30). Another possible reason for the over prediction of slip length could be that the bulk rheological behavior of the slightly polydisperse PDMS of $P = 72$ might not be accurately predicted by CV model. Only the zero-shear viscosity data on this polymer was available, whereas for a fair comparison, complete rheogram would be needed. We proceed now assuming $G^0_{N,I} = G^0_{N,B}$ for which quantitative match to the experimental data is obtained before strong-slip. Above the critical slip velocity, the slip length is overpredicted by the model. The reason for this is most probably the fact that equation (6.29) is not expected to be valid after strong slip because of the strong orientation of the tethered molecules.

The model prediction of the critical slip velocity in figure (6.6) has been corrected to account for the fact that the experimental data is actually for a case where the surface coverage is greater than the overlap coverage by a factor of 7. Even at this surface coverage, the bulk chains penetrate the grafted layer sufficiently to avoid entanglements between the tethered chains [Durliat *et al.*, 1997; Léger *et al.*, 1999]. In this region of surface coverage the critical slip velocity is known to increase linearly with the surface coverage, while the slip length essentially remains locked at the value corresponding to that at the overlap coverage [Durliat *et al.*, 1997; Léger *et al.*, 1999; Brochard-Wyart, *et al.*, 1996]. The solid line in figure (6.6) shows the predictions of the model when extended to surface coverage above the overlap. Thus, the model almost quantitatively predicts the experimental critical slip velocity data.

Another interesting feature of figure (6.6) is that the slip length before the critical slip velocity is of the order of 2 to 3 μm, which when compared to the coil size of the tethered molecule $\left\langle R^2_{o,I} \right\rangle^{1/2} = 0.0209\,\mu\text{m}$, clearly indicates that the bulk chains have a finite non-zero slip velocity even before the strong slip. Thus, there is a 'weak-slip' region before the strong-slip region such that the no-slip boundary condition fails even before the strong-slip sets in. This behavior is very similar to that observed recently by Munstedt *et al.* (2000) for the extrusion of polyethylene through a slit die.

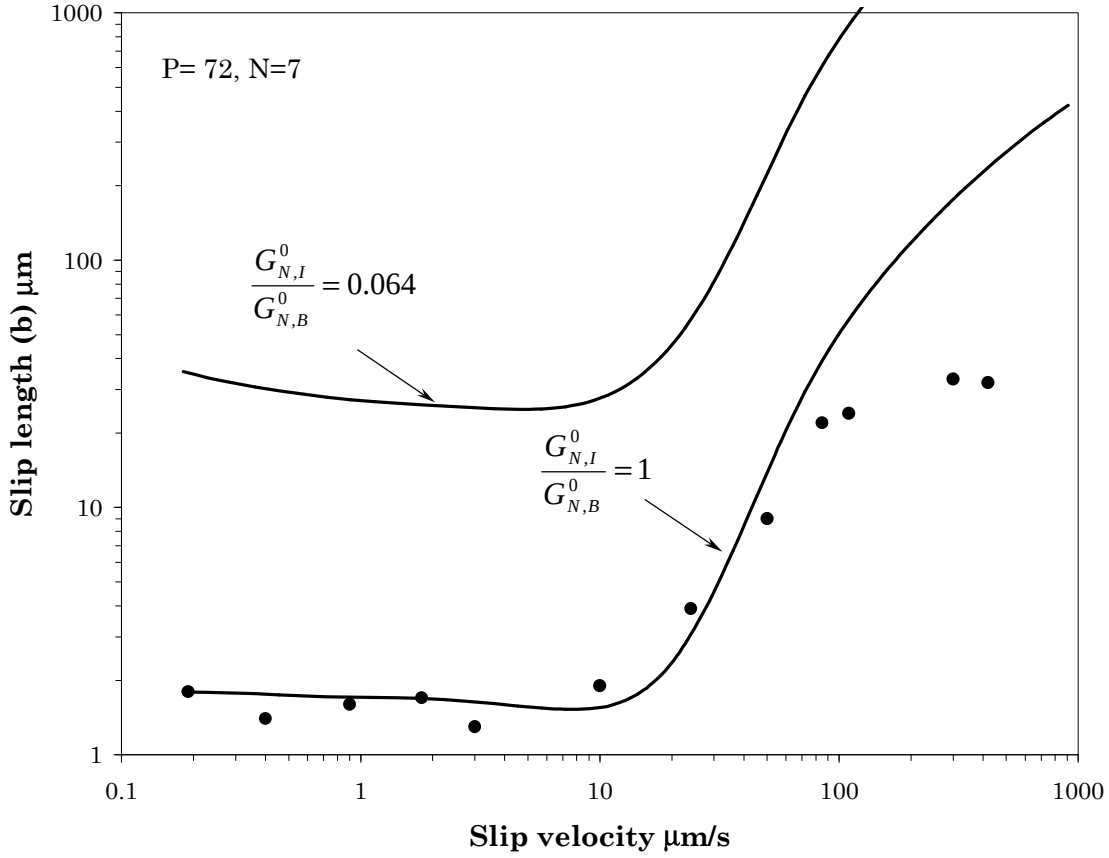

Figure 6.6 Comparison of experimental data with model prediction. The experimental data is by Durliat *et al.*, (1997) and is for PDMS melt with $P \sim 72$ and $N \sim 7$. The upper curve is corresponds to $G^0_{N,I} = 0.0115$ and $G^0_{N,I} / G^0_{N,B} = 0.064$ while for $G^0_{N,I} = G^0_{N,B}$, a good fit with the experimental data can be seen.

6.5 Conclusions and Discussions

We have developed a molecular model for tethered chains in the mushroom region. The model predicts a discontinuous strong slip that arises from sudden disentanglement of the tethered chains from the flowing bulk chains. The formulation of the model is based on the contour variable tube model. We have considered all possible modes of the relaxation applicable to a tethered chain namely, constraint release, convective constraint release, fluctuations and retraction. The most important concept proposed in the model is that the tethered molecules experience a suppressed CCR relaxation; because of which they are easily oriented by shear flow above a critical shear rate and critical shear stress. This, we believe, is the main molecular mechanism that drives strong slip by sudden disentanglement and has not been recognized in any of the previous scaling models for slip. Our model also differs from previous scaling models by virtue of its potential ability to quantitatively predict slip parameters based solely on molecular information.

There are several other important predictions of the model. The tendency to show stick-slip instability increases with molecular weight of the bulk molecules and of the tethered molecules. Shorter tethered molecules do not orient easily compared to longer molecules. Thus, extrusion of a material containing small molecular weight chains or extrusion through a die coated with small chains will not show stick-slip instability. The scaling laws predicted by the model for the critical stress and the critical slip velocity agree with those predicted by the earlier scaling models. However, our model also predicts different scaling laws for cases of very low and very high N. The model predicts that the stick-slip transition is caused by a coil-to-stretch transition of the tethered molecules, which is also in agreement with the earlier scaling models [Brochard and de Gennes, 1992]. Our model quantitatively predicts the critical slip velocity at which strong slip occurs, but requires much larger number of entanglements per unit volume in the interfacial region in order to quantitatively match the experimental slip length in the weak-slip region. This issue needs further exploration. The model also predicts two regions for the slip length, a weak slip region for low shear rates and a strong-slip region for high shear rates. Thus, the model suggests that the conventional no-slip boundary condition may not be valid for a large range of extrusion shear rates.

Finally, it is important to mention the limits within which our present model is applicable. We have so far considered the specific case of monodispersed bulk and end-tethered chains. In a real system, both the bulk and tethered chains would have a distribution in chain lengths. The relaxation due to CR and CCR would be faster in a polydisperse material due to presence of shorter chains. This would decrease the time-scale for the randomization process of the tethered molecules and thereby prevent their orientation. Thus, polydispersity would decrease the non-monotonicity of flow curve as observed experimentally [Myerholtz, 1967]. A real system is further complicated by the fact that a single bulk molecule can tether to multiple sites on the solid wall, giving rise to loops and tails. We have not addressed the dynamics of the loops and their influence on slip in this paper. The present tube model needs to be further refined to account for polydispersity and dynamics of loops on slip. The present model also does not consider the effects of other molecular architectural parameters such as long-chain branching. We hope however, that the new molecular insights that we have provided in the wall slip phenomenon will stimulate further theoretical and experimental work to understand this phenomenon in complicated systems.

CHAPTER 7

SUMMARY AND CRITICAL EVALUATION OF THESIS

In this work, we have proposed semi-empirical and molecular models to predict slip by disentanglement and debonding mechanisms. We believe that the spurt phenomenon is interfacial in nature and either the disentanglement or the debonding of the tethered chains at the interface is responsible for the same. In chapter 3 we developed a disentanglement model that is based on an empirical transient network (TN) theory. We divided the flow in a capillary (or in any shear flow geometry) into two regions namely, interfacial and bulk. The interfacial region is a layer of fluid immediately next to the solid boundary and having a width of chain dimensions. Entanglements between the tethered chains and bulk chains form a dynamic network near the wall. We solve the TN model independently in both the regions keeping the stress and the velocity continuity at the boundary of the two regions. We argue that the dynamics of adsorbed chains is different from that of the bulk molecules. We show that the transient network model predicts disentanglement of the adsorbed molecules from the bulk chains at a critical wall-shear stress. The model also successfully predicts a first order transition in the flow rate at the critical wall-shear stress. Further, it predicts a direct proportionality between the temperature and the critical wall-shear stress, which is similar to the prediction made by Brochard and de Gennes (1992). Finally, the model also predicts the diameter dependence of the flow curves, hysteresis and the possibility of periodic oscillations in flow rate and pressure during extrusion. We show that the model predicts wall slip in polymer melts as well as in concentrated solutions, thus unifying different systems showing slip. However, the model considers only the disentanglement of adsorbed chains, completely disregarding debonding.

In chapter 4 we proposed a unified model that accounts for both disentanglement and debonding into one self-consistent mathematical framework. The activation processes of adsorption and desorption are considered to occur at the wall in parallel to the stretching of the adsorbed chains. The model predicts slip occurring by either mechanisms, debonding or disentanglement depending on the adhesive energy of the

wall-polymer pair. It is shown that the stick-slip transition occurs due to a local non-monotonic flow behaviour near the wall irrespective of the mechanism of slip. The model predictions of the critical wall shear stress are in good agreement with experiments for various adhesive energies of wall polymer pair. The model further predicts that the temperature dependence of the critical wall shear stress for debonding is different than that of disentanglement mechanism under certain experimental conditions. The unified model encompasses different systems (viz. entangled solutions and melts) and diverse mechanisms (viz. disentanglement and debonding) under a common mathematical framework. To validate the predictions of unified model, we have measured the critical stress for sudden slip due to debonding at various temperatures using a cone and plate viscometer with fluoroelastomer-coated cone. This experimental investigation was presented in chapter 5. The temperature dependence of the critical stress for instability (slip) on a coated cone is found out to be inversely dependent on temperature. This is expected for the case of debonding, which is known to be an activation process. The unified slip model successfully predicts the observed temperature dependence quantitatively.

The disentanglement and unified slip models are semi-empirical in nature and contain adjustable parameters arising from the phenomenological nature of the rates of creation and breakage of network. While this approach does not throw light on the fundamental issues regarding molecular dynamics of polymer chains near the wall, it has the inherent advantage of presenting a simpler constitutive equation that captures the essence of slip phenomena by either of the two physical mechanisms. Such a constitutive equation could be useful for providing numerical solutions to real engineering problems. Thus, while the unified model provides an “engineering model” that can be useful for predicting slipping flows, it is mainly a phenomenological model consisting of several model parameters that have to be determined through independent rheological experiments. It is desirable to develop a truly molecular model that can predict slip on the basis of only molecular information without the need for any other adjustable parameters.

Using the tube theory of entangled polymeric liquids, we developed in chapter 6 a molecular model for tethered chains in the mushroom region. The tube model was developed on the basis of the contour variable model, which is a refined version of the original Doi-Edwards tube model. We consider all possible modes of the relaxation

applicable to a tethered chain namely, constraint release (CR), convective constraint release (CCR), fluctuations and retraction. The most important concept proposed in the model is that the tethered molecules experience a suppressed CCR relaxation; because of which they are easily oriented by shear flow above a critical shear rate and critical shear stress. The model predicts a discontinuous slip that arises from sudden disentanglement of the tethered chains from the flowing bulk chains.

We show that the tendency to show stick-slip instability increases with molecular weight of the bulk molecules and of the tethered molecules. Shorter tethered molecules do not orient easily compared to longer molecules. For low values of the interfacial modulus the model predicts the critical slip velocity to be $V_s^* \sim P^{3.4} N^{-1}$, where P is the number of segments of the bulk molecule while N is the number of segments of the tethered molecule. For the values of interfacial modulus comparable to bulk modulus the tube model predicts a more complicated scaling. The model predicts that the stick-slip transition is caused by a coil-to-stretch transition of the tethered molecules such that the end segments of the tethered chains are always more randomized compared to the tethered end. The critical stress is predicted to be directly proportional to the absolute temperature and the grafting density of tethered chains. All of these predictions are also in agreement with the earlier scaling models [Brochard and de Gennes, 1992]. The model also predicts two regions for the slip length, a weak slip region for low shear rates and a strong-slip region for high shear rates. Our model quantitatively predicts the critical slip velocity at which strong slip occurs, but requires much larger number of entanglements per unit volume in the interfacial region in order to quantitatively match the experimental slip length in the weak-slip region.

The important characteristics of all these models that predict stick-slip instability is the existence of the local non-monotonic shear stress-slip velocity relationship. In case of disentanglement mechanism, the stretching (orientation) of the tethered molecules increases auto-catalyatically with stress to give rise to such non-monotonic relationship. While in the case of debonding, the sudden desorption of the tethered chains suddenly decrease the stress to give rise to such relationship. In the present work, we predict such relationship using both the approaches, empirical and molecular.

The molecular model in this work has been developed for the simplest case of end-grafted tethered chains at very small surface coverage (in the *mushroom* regime).

However, the model can, in principle, be extended to more realistic situations wherein the grafting density is high so that different tethered chains could entangle with each other, or could form loops and tails on the wall, or could be entangled with a polydisperse melt. These refinements are out of the scope of the present work and would naturally constitute a major part of a separate work. We hope that the new molecular insights proposed in this work will stimulate further theoretical and experimental work to understand this phenomenon in complicated systems.

APPENDIX I

DERIVATION OF EQUATION (3.30)

The constitutive equation for Transient Network model is given as,

$$g\underset{\approx}{\sigma}^{*}+We\overset{\nabla}{\underset{\approx}{\sigma}}^{*}=-We\,\underset{\approx}{\dot{\gamma}}^{*}-\left(f\text{-}g\right)\underset{\approx}{I} \tag{AI.1}$$

For shear flow we have, $\underset{\sim}{\upsilon}=\underset{\sim}{\upsilon}(\upsilon_1)$, $\upsilon_1=\upsilon_1(x_2)$, $\underset{\approx}{\sigma}=\underset{\approx}{\sigma}(r)=\begin{pmatrix}\sigma_{11} & \sigma_{12} & 0\\ \sigma_{21} & \sigma_{22} & 0\\ 0 & 0 & \sigma_{33}\end{pmatrix}$ and

$\underset{\approx}{\dot{\gamma}}=\dfrac{d\upsilon_1}{dx_2}\begin{pmatrix}0 & 1 & 0\\ 1 & 0 & 0\\ 0 & 0 & 0\end{pmatrix}$. Hence, we get,

$$g\sigma_{22}^{*}=-f+g \tag{AI.2}$$

$$g\sigma_{33}^{*}=-f+g \tag{AI.3}$$

$$g\sigma_{11}^{*}-2We\,\sigma_{12}^{*}\frac{\partial\upsilon_1^{*}}{\partial x_2^{*}}=-f+g \tag{AI.4}$$

$$g\tau_{12}^{*}-We\,\sigma_{22}^{*}\frac{\partial\upsilon_1^{*}}{\partial x_2^{*}}=-We\frac{\partial\upsilon_1^{*}}{\partial x_2^{*}} \tag{AI.5}$$

From equation (AI.2) and (AI.3) it can be seen that $\sigma_{22}^{*}=\sigma_{33}^{*}=\dfrac{-f+g}{g}$. Inserting this in equation (AI.4) we get,

$$We\frac{\partial\upsilon_1^{*}}{\partial x_2^{*}}=\frac{\sigma_{11}^{*}-\sigma_{22}^{*}}{2\sigma_{12}^{*}}g \tag{AI.6}$$

This can be written as,

$$\frac{\partial\upsilon_1^{*}}{\partial x_2^{*}}=\frac{\gamma_e g}{We} \tag{AI.7}$$

Now using equation (AI.5) and (AI.7) we get,

$$\sigma_{12}^{*}=\gamma_e\frac{f}{g} \tag{AI.8}$$

Equation (AI.7) and (AI.8) give a final set of constitutive equations to be solved.

APPENDIX II

SET OF EQUATION FOR CONTOUR VARIABLE AND SLIP MODEL AND PROCEDURE TO SOLVE THE SAME

AII.1 Set of equations for Contour Variable model

We present the set of equations of contour variable model for steady shear flow: For a detailed description of the equations, the reader is referred to the original CV model [Mead *et al.*, 1998]. Under the steady state, the constitutive equation for shear stress s_{12} consists of a set of coupled integro-differential equations given by,

$$\sigma_{12,B} = \frac{15}{4} G^0_{N,B} \frac{1}{L_{0,B}} \int_{-L_{0,B}/2}^{L_{0,B}/2} {q_B}^2 S_{12,B}(s_0)\, ds_0 \tag{AII.1}$$

$$\frac{\partial q_B(s_0)}{\partial s_0} = \frac{1}{6PD_{rep,P}} \left[2 \frac{\langle \upsilon_B \rangle|_{s_0 = L_B/2}}{L_B} \right] (s - s_0) - \frac{\langle \upsilon_B(s) \rangle}{3PD_{rep,P}} \tag{AII.2}$$

$$S_{12,B}(s) = \int_0^\infty \frac{\partial G_B(s,\theta)}{\partial \theta} Q_{12,B}\left[\underset{\approx}{E}_B(\theta) \right] d\theta \tag{AII.3}$$

$$\frac{\partial G_B(s,\theta)}{\partial \theta} = D_{rep,P} \frac{\partial^2 G_B(s,\theta)}{\partial s^2} - \langle \upsilon_B(s) \rangle \frac{\partial G_B(s,\theta)}{\partial s} - f(q_B) \left[2 \frac{\langle \upsilon_B \rangle|_{s_0 = L_B/2}}{L_B} \right] G_B(s,\theta) - \frac{G_B(s,\theta)}{\tau_{\xi,B}(s)} \tag{AII.4}$$

In the above equations, subscript B stands for bulk chains, the bulk molecule is assumed to have P segments and hence $D_{rep,P} = {L_B}^2 / (\pi^2 \tau_d(P))$ is the longitudinal diffusivity of bulk chain, $G_B(s,\theta)$ is the segment renewal probability for the bulk chain at time θ and at position s, $G^o_{N,B}$ is the high frequency plateau modulus of the bulk chains, $L_{0,B} = aP$ is the equilibrium contour length of a bulk chain, a is the tube diameter or the length of a segment, $S_{12,B}$ is the shear component of the orientational

order parameter tensor $\underset{\approx}{S}_B$, s_0 is the undeformed reference coordinate of the contour length ($s_0 = \pm L_{0,B}/2$ at the chain ends and $s_0 = 0$ at the center), s is the reference coordinate of the deformed contour length, q_B is the segmental stretch ratio ($q_B = \partial s / \partial s_0$). The continuous retraction velocity of a bulk chain along its contour directed towards its center is give by,

$$\left\langle \upsilon_B(s) \right\rangle = \underset{\approx}{\kappa}_B : \int_0^s \underset{\approx}{S}_B(s')\,ds' = \kappa_{12,B} \int_0^s S_{12,B}(s')\,ds' \qquad \text{(AII.5)}$$

$\underset{\approx}{E}_B(\theta)$ is the deformation tensor for bulk chains, $\underset{\approx}{Q}_B$ is the geometric universal tensor $\underset{\approx}{Q}_B = \left\langle \left(\underset{\approx}{E}_B . \underset{\sim}{u} \right) \left(\underset{\approx}{E}_B . \underset{\sim}{u} \right) \Big/ \left| \underset{\approx}{E}_B . \underset{\sim}{u} \right| \right\rangle \Big/ \left\langle \left| \underset{\approx}{E}_B . \underset{\sim}{u} \right| \right\rangle - \underset{\approx}{I}/3$, $\langle\ \rangle$ is the average over the isotropic distribution of unit vectors $\underset{\sim}{u}$, $\underset{\approx}{I}$ is the unit tensor, $t_{x,B}$ is the fluctuation time scale of the bulk chains and is given by,

$$\tau_{\xi,B}(s) = \left(\tau_r(P)/4\right) \exp\left(0.5\vartheta P \xi_B^{\,2}\right) \qquad \text{(AII.6)}$$

where $x_B = 1 - 2|s|/L_B$, $J = 1.5$, $\tau_r(P)$ is the retraction time of the bulk chain with P segments.

The initial and boundary conditions for the above equations (AII.2) and (AII.4) are,

$$\left.\begin{aligned}
&G_B(s_0) = 1 \quad at \quad \theta = 0 && \text{(initial condition)} \\
&G_B(\theta) = 0 \quad at \quad s_0 = \pm L_{0,B}/2 && \text{(due to fluctuations at chain end)} \\
&\frac{dG_B(\theta)}{ds_0} = 0 \quad at \quad s_0 = 0 && \text{(symmetry at the centre of chain)} \\
&q_B = 1 \quad at \quad s_0 = \pm L_{0,B}/2 && \text{(the chain ends are always random)}
\end{aligned}\right\} \qquad \text{(AII.7)}$$

We will now summarize the procedure to be followed to solve such set integro-differential equations that also can be found elsewhere [Mead *et al.*, 1998; Marrucci and Grizzuti, 1988; Mead *et al.*, 1995; Mead and Leal, 1995]. For any given choice of shear rate $\kappa_{12,B}$, $Q_{12,B}$ is calculated as a function of θ for once and for all. After that the following trial-error loop is needed to be solved.

1. Assign some value to $S_{12,B}(s_0)$ and consider $s = s_0$.

2. Calculate the value of $\langle \upsilon_B(s) \rangle$ using equation (AII.5).
3. Integrate equation (AII.2) for s using tri-diagonal matrix system.
4. Now using the corrected value of s go to step 2 and then step 3 until s converges.
5. Integrate equation (AII.4) to calculate $G(s,\theta)$.
6. Using equation (AII.3) calculate $S_{12,B}$, compare it with the assigned value in step 1, if the error is not below the allowed limit, then start from step 1 with the corrected values of $S_{12,B}$. Recycle the loop until $S_{12,B}$ converges.
7. Using equation (AII.1) calculate the shear stress.

AII.2 Set of equations for slip model

The segment renewal probability is given by,

$$\frac{\partial G_I(s,\theta)}{\partial \theta} = D_I \frac{\partial^2 G_I(s,\theta)}{\partial s^2} - \langle \upsilon_1(s) \rangle \frac{\partial G_I(s,\theta)}{\partial s} - f(q_I)\left[2\frac{\langle \upsilon_2 \rangle}{L_B}\right] G_I(s,\theta) - \frac{G_I(s,\theta)}{\tau_{\xi,I}(s)} \quad \text{(AII.8)}$$

where, $D_I = 2L_I{}^2 / (\pi^2 \tau_I)$.

$N > N_c \quad \tau_I = \tau_{cr,I}\,;\ \tau_{cr,I}(N) \approx N^2 \left(\min(P,N)\right)^{-0.5} \tau_d(P)$

$N < N_c \quad \tau_I = \tau_{AR,I}\,; \tau_{AR,I}(N) \approx N^{-1} \tau_d(N) \exp(\nu N)$.

$$\frac{\partial q_I(s_0)}{\partial s_0} = \frac{1}{6ND_{rep,N}}\left[2\frac{\langle \upsilon_2 \rangle}{L_B}\right](s - s_0) - \frac{\langle \upsilon_1(s_0) \rangle}{3ND_{rep,N}} \quad \text{(AII.9)}$$

$$\tau_{\xi,I}(s) = \left(\tau_r(N)\right) \exp\left(\vartheta N \xi_I{}^2\right) \quad \text{(AII.10)}$$

The boundary conditions for equations (AII.8) and (AII.9) are,

$$\left.\begin{aligned} G_I(s_0) &= 1 \quad at \quad \theta = 0 \\ G_I(\theta) &= 0 \quad at \quad s_0 = L_{0,I} \\ \frac{dG_I(\theta)}{ds_0} &= 0 \quad at \quad s_0 = 0 \\ q_I &= 1 \quad at \quad s_0 = L_{0,I} \end{aligned}\right\} \tag{AII.11}$$

$$\left\langle \upsilon_I(s_0) \right\rangle = \kappa_{12,I} \int_0^s S_{12,I}(s')\, ds' \tag{AII.12}$$

$$V_s = R_{0,I}\, \kappa_{12,I} \tag{AII.13}$$

$$\left\langle \upsilon_1(s_0) \right\rangle = V_s + \left\langle \upsilon_I(s_0) \right\rangle \tag{AII.14}$$

$$\underset{\approx}{S_I}(s_0) = \int_0^\infty \frac{\partial G_I(s_0,\theta)}{\partial \theta} \underset{\approx}{Q_I}\left[\underset{\approx}{E_I}(\theta)\right] d\theta \tag{AII.15}$$

$$\underset{\approx}{Q_I} = \left\langle \left(\underset{\approx}{E_I}.\underset{\sim}{u} \right) \left(\underset{\approx}{E_I}.\underset{\sim}{u} \right) \Big/ \left| \underset{\approx}{E_I}.\underset{\sim}{u} \right| \right\rangle \Big/ \left\langle \left| \underset{\approx}{E_I}.\underset{\sim}{u} \right| \right\rangle - \underset{\approx}{I}/3 \tag{AII.16}$$

$$\left\langle \upsilon_2 \right\rangle = \left\langle \upsilon_B(L_B/2) \right\rangle \Big|_{\sigma_{12,B}=\sigma_{12,I}} \tag{AII.17}$$

$$G^o_{N,i} = \frac{\Sigma}{N_A a} RT \tag{AII.18}$$

$$s_{12,I} = \frac{15}{4} G^0_{N,I} \frac{1}{L_{0,I}} \int_0^{L_{0,I}} {q_I}^2 S_{12,I}(s_0)\, ds_0 \tag{AII.19}$$

Description of various parameters can be seen in chapter 6. The procedure to solve the above slip model is similar to that of CV model but more complicated because of simultaneous solving of bulk as well as interfacial region at same stress.

In the model described above the constitutive equations for the bulk and the interfacial regions are coupled. The coupling arises from the fact that the retraction velocity required for the CCR relaxation of tethered chains has to be calculated from the constitutive equation of bulk while simultaneously maintaining the stress continuity between the two regions. The numerical procedure required to solve the coupled equations is briefly described below. For a given value of κ_I, the value of shear stress in the interfacial region is initially predicted from equations (AII.8) to (AII.19) assuming

$\langle v_2 \rangle$=0. The equations (AII.8) to (AII.19) can be solved similar to that of CV model for bulk described in the earlier section. $\langle v_2 \rangle$ is then calculated from the bulk constitutive equation at the same shear stress by inverting equations (AII.1) to (AII.7) numerically. Next, this value of $\langle v_2 \rangle$ is now used to solve the constitutive equation for the interfacial region to predict a new value of the stress. This procedure is repeated until the shear stress and $\langle v_2 \rangle$ converge between previous and current iterations. An alternative procedure would be to first choose a value of the bulk shear rate $\kappa_{12,B}$ and calculate $\langle v_2 \rangle$ and stress in the bulk using equations (AII.1) to (AII.7). Next, the interfacial shear rate $\kappa_{12,I}$ and consequently, the slip velocity, are calculated by using equations (AII.8) to (AII.19) for a range of values of $\kappa_{12,B}$ and then predicting stress which then matches with that predicted by bulk equations. In either procedure a numerical inversion of the integro-differential equations is required. We find that the numerical scheme is robust until a high value of interfacial shear rate ($\kappa_{12,I} > 1/\tau_{r,I}$) after which the convergence is seriously affected due to the change of the nature of equations from parabolic to hyperbolic. It is important to note that the input variables to the problem are either the bulk shear rate or the wall shear stress, while the predicted variables are the interfacial shear rate, the slip velocity and the slip length. Thus, the input variables are the same as the *control* variables used in extrusion (or simple shear) experiments and the predicted variables are the same as those *measured* from experiments.

APPENDIX III

FORTRAN PROGRAMS

AIII.1 Programs in chapter 3

```
c MAIN1.FOR

$debug

c This is the main program to solve equation 3.30 (chapter 3) in the
c capillary. The transient network model is solved in both annular wall
c region and in the bulk independently. The variables f1f, f1g, t1, t2 are
c the fitting parameters required to calculate the f and g functions from
c equation 3.28 and 3.29 in the bulk domain. Similarly f1fw, f1gw, t1w, t2w
c are for interfacial or wall domain. go is the network modulus and common
c for both the domains. pu and pd are the maximum and minimum values of
c shear stress on shear stress vs. effective strain (non-monotonic) plot.
c gu and gd are the effective strain corresponding to pu and pd
c respectively. These maximum and minimum values are obtained from the
c program max-min.for

        implicit double precision (a-h,o-z)
        open(1,file='yerr1.inp')
        open(2,file='yerr2.inp')
        open(4,file='yerr3.inp')
        open(3,file='yerr.dat')

        read(1,*)go, f1f, f1g
        read(1,*)t1, t2
        read(2,*)go, f1fw, f1gw
        read(2,*)t1w, t2w, r1, trzw

c Subroutine trans if to find out values of gf and gg in such a way that
c f1f and f1g are unity at gam=0

        call trans(f1f, t1, gf)
        call trans(f1g, t2, gg)

        read(4,*)gu, pu
        read(4,*)gd, pd
        close(1)
        close(2)

        gam=0.0
        n=0

c r1 is the radius of the capillary and the trzw is wall shear stress
        cc=trzw/r1

c The system of equations for bulk region

c r is the radial distance from center of the capillary
```

```
        r=0.00
        write(3,*) r, abs(gam)
 5      n=n+1
        write(*,*) n
        nn=0
        r=r1*n/100.0
        if (n.eq.100) then
        goto 15
        else
        endif
        gaml=-0.00
        ugam=-0.00-15000000.
 10     nn=nn+1
        call ct(ffl, gaml, go, f1f, f1g, t1, t2, r, cc, gg, gf)
        call ct(ffu, ugam, go, f1f, f1g, t1, t2, r, cc, gg, gf)
        ygam=(gaml+ugam)/2
        call ct(ffm, ygam, go, f1f, f1g, t1, t2, r, cc, gg, gf)
        if ((ffl*ffm).le.0) then
        gaml=gaml
        ugam=ygam
        else
        gaml=ygam
        ugam=ugam
        endif
        ww=abs(ugam-gaml)
        if (abs(ugam-gaml).le.1e-3) then
        gam=(ugam+gaml)/2
        write(3,*) r, abs(gam)
        write(*,*) r
        goto 5
        else
        if (((ffu.le.0).and.(ffl.le.0)).or.((ffu.ge.0).and.(ffl.ge.0)))
     &  then
        pause
        else
        endif
        goto 10
        endif

c TN Equation system for interfacial domain of 1e-8 m thickness

 15     n1=-1
        r=(r1-1e-8)
        gam=0.00
        call trans(f1fw, t1w, gfw)
        call trans(f1gw, t2w, ggw)
 20     n1=n1+1

        nn1=-1
        cc1=cc*r1
        r=r+(1e-8)*n1/4.0
        if (cc1.lt.pd) then
        gaml=-0.00
        ugam=-gd
        write(*,*)'RIGHT'
        else
        gaml=-gd
        ugam=-gd-15000000.
        write(*,*)'WRONG'
        endif
 25     nn1=nn1+1
```

```
      call ct(ffl, gaml, go, f1fw, f1gw, t1w, t2w, r, cc, ggw, gfw)
      call ct(ffu, ugam, go, f1fw, f1gw, t1w, t2w, r, cc, ggw, gfw)
      ygam=(gaml+ugam)/2
      call ct(ffm, ygam, go, f1fw, f1gw, t1w, t2w, r, cc, ggw, gfw)
      if ((ffl*ffm).le.0) then
      gaml=gaml
      ugam=ygam
      else
      gaml=ygam
      ugam=ugam
      endif
      ww=abs(ugam-gaml)
      if (ww.le.1e-3) then
      gam=(ugam+gaml)/2
      write(3,*) r, abs(gam)
      if (r.ge.r1) goto 50
      goto 20
      else
      goto 25
      endif
 50   stop
      end


      subroutine ct(ff, gam, go, f1f, f1g, t1, t2, r, cc, gx, gy)
      implicit double precision (a-h,o-z)
      gamy=abs(gam)+gy
      call errorf(gamy, erf, t1)
      f=f1f*(1+erf)/2.
      gamx=abs(gam)+gx
      call errorf(gamx, erf, t2)
      g=f1g*(1+erf)/2.
      ff=(cc*r*g)+gam*go*f
      return
      end


c The subroutine to calculate the error function

      subroutine errorf(game, erf, t)
      implicit double precision (a-h,o-z)
      if (game.lt.0.0) then
      i11=0
      else
      i11=1
      endif
      x=abs(game)/(2*sqrt(t))
      tni=(exp(-((0)**2))+exp(-(x**2)))*0.5
      xx=0
 9    if (abs(xx-x).le.1e-3) goto 10
      xx=xx+x/10000.0
      tni=tni+exp(-(xx**2))
      goto 9
 10   tni=tni*x/10000.0
      erf=2*tni/(sqrt(3.14159265359))
      if (i11.eq.0) then
      erf=-erf
      game=-abs(game)
      else
      endif
      return
```

```
        end


        subroutine trans(f1, t, g)
        implicit double precision (a-h,o-z)
        tt1=-0
        tt2=-1500000000.0
        call errorf(tt1, erf, t)
        ff1=(2/f1)-1-erf
        call errorf(tt2, erf, t)
        ff2=(2/f1)-1-erf
  1     ttm=(tt1+tt2)/2.0
        call errorf(ttm, erf, t)
        ffm=(2/f1)-1-erf
        if ((ff1*ffm).lt.0) then
        tt2=ttm
        ff2=ffm
        else
        tt1=ttm
        ff1=ffm
        endif
        if (abs(tt1-tt2).le.1e-6) then
        ttm=(tt1+tt2)/2
        g=ttm
        else
        goto 1
        endif
        return
        end
```

```
c MAX-MIN.FOR

$debug

c Program to evaluate a maximum and minimum in the effective strain and
c shear stress plot. a is effective strain while b is shear stress. c and d
c are dummy variables.

        implicit double precision (a-h, o-z)
        dimension a(805), b(805)
        open(1,file='fg.dat')
        open(2,file='yerr3.inp')
        do i=1,802
        read(1,99) a(i), b(i), c, d
        enddo
 99     format(4(e12.5,1x))
        do i=2,801
        if (b(i).lt.b(i-1)) goto 10
        enddo
  10    l=i
        if (i.ge.801) goto 40
        do j=l, 801
        write(*,*) b(j), b(j-1)
        if (b(j).gt.b(j-1)) goto 20
        enddo
  20    m=j
        write(2,*) a(l), b(l)
        write(2,*) a(m), b(m)
        close(2)
  40    stop
```

```
        end
```

```
c MAIN2.FOR

$debug

c Main program 2 which solves equation 3.31 in capillary geometry.
c Program variables and subroutines are same as that in MAIN1.FOR
c tlam is the relaxation time (lambda), v(i) is velocity
c rr is the radius of the capillary, q is flow rate
c (4.0*q/(3.14159265359*(r1**3))) is apparent shear rate

        implicit double precision (a-h,o-z)
        dimension v(120), gam(120), r(120)
        open(1,file='yerr.dat')
        open(2,file='velo.dat')
        open(4,file='yerr2.inp')
        open(5,file='yerr1.inp')
        read(4,*)go, f1fw, f1gw
        read(4,*)t1w, t2w, r1, trzw
        read(5,*)go, f1f, f1g
        read(5,*)t1, t2
        close(5)
        close(4)
        tlam=8.5
        do i=1,104
        read(1,*) r(i), gam(i)
        enddo
        dr=abs(r(10)-r(11))
        rr=dr*100.0
        we=tlam
        dr1=0.25*1e-8
        v(104)=0.
        write(2,*) r(104), v(104), v(104)

        call trans(f1gw, t2w, gg)
        write(*,*) gg
        do i=104,102,-1
        call gv(gam(i-1), g, f1gw, gg, t2w)
        der=(gam(i-1))*g/we
        write(*,*) i, der
        v(i-1)=v(i)+dr1*der
        enddo

        call trans(f1g, t2, gg)
        do i=101,2,-1
        call gv(gam(i-1), g, f1g, gg, t2)
        der=(gam(i-1))*g/we
        v(i-1)=v(i)+dr*der
        write(*,*) r(i-1), der
        enddo
        do i=103, 1,-1
        write(2,*) r(i), v(i)/v(1), v(i)
        enddo
        close(1)
        close(2)

c subroutine flowr performs an integration on v(i) to calculate
c the flow rate.
```

```
      call flowr(v, r, q)
      write(*,*) q, trzw, (4.0*q/(3.14159265359*(r1**3)))
      stop
      end


      subroutine errorf(game, erf, t)
      implicit double precision (a-h,o-z)
      if (game.lt.0.0) then
      i11=0
      else
      i11=1
      endif
      x=abs(game)/(2*sqrt(t))
      tni=(exp(-((0)**2))+exp(-(x**2)))*0.5
      xx=0
9     if (abs(xx-x).le.1e-3) goto 10
      xx=xx+x/10000.0
      tni=tni+exp(-(xx**2))
      goto 9
10    tni=tni*x/10000.0
      erf=2*tni/(sqrt(3.14159265359))
      if (i11.eq.0) then
      erf=-erf
      game=-abs(game)
      else
      endif
      return
      end


      subroutine gv(gam, g, f1g, gg, t)
      implicit double precision (a-h,o-z)
      gamx=gam+gg
      call errorf(gamx, erf, t)
      g=f1g*(1+erf)/2.
      return
      end


      subroutine trans(f1, t, g)
      implicit double precision (a-h,o-z)
      tt1=-0
      tt2=-1500000000.0
      call errorf(tt1, erf, t)
      ff1=(2/f1)-1-erf
      call errorf(tt2, erf, t)
      ff2=(2/f1)-1-erf
 1    ttm=(tt1+tt2)/2.0
      call errorf(ttm, erf, t)
      ffm=(2/f1)-1-erf
      if ((ff1*ffm).lt.0) then
      tt2=ttm
      ff2=ffm
      else
      tt1=ttm
      ff1=ffm
      endif
      if (abs(tt1-tt2).le.1e-6) then
      ttm=(tt1+tt2)/2
      g=ttm
```

```
        write(*,*)'########@@@@@@@@@@$$$$$$$$ CONGRATS '
        else
        goto 1
        endif
        return
        end


        subroutine flowr(v, r, q)
c Simpson's rule is used to integrate velocity to calculate flow rate.
        implicit double precision (a-h,o-z)
        dimension v(120), r(120)
        q1=(r(104)*v(104)+r(101)*v(101))/2.
        q1=q1+r(103)*v(103)+r(102)*v(102)
        q1=0.25*(1e-8)*2.*q1*3.14159265359
        q2=(r(101)*v(101)+r(1)*v(1))/2.
        do i=2,100
        q2=q2+r(i)*v(i)
        enddo
        q2=q2*abs(r(10)-r(11))*2.*3.14159265359
        q=q1+q2
        return
        end
```

AIII.2 Programs in chapter 6

```
c QO.FOR
$debug

c This program calculates shear component geometric universal tensor using
c equation (6.5). st is the time variable.

        open(1, file='qo.inp')
c For time t=0 to t=0.1, dt is taken to be 1e-4, while time t=0.1 to t=100
c dt is taken to be 0.01

        do 1 ixi=1, 1000
        st=(ixi-1)*1e-4
        pi=3.14159265359
        gg1=0.0
        gg2=0.0

        do 12 j=2,100
        x=(j-1)*pi/100.
        a=((sin(x))**2)*cos(x)
        b=st*((cos(x))**2)*sin(x)
        c=st*sin(2.*x)
        d=1.+((st*cos(x))**2)
        ff1=sqrt(d)
        ff2=b/sqrt(d)
        do 22 jj=2,100
        si=sin(2*(jj-1)*pi/100.)
        f1=sqrt(c*si+d)
        ff1=ff1+f1
        f2=(a*si+b)/f1
        ff2=ff2+f2
 22     enddo
        ff1=ff1*(pi/50.)
        ff2=ff2*(pi/50.)
```

```
c        write(*,*) ff1, ff2, x/pi
         gg1=gg1+(sin(x))*ff1
         gg2=gg2+ff2
 12      enddo
         gg1=gg1*pi/100.0
         gg1=gg1/(4.*pi)
         gg2=gg2*pi/100.0
         gg2=gg2/(4.*pi)

         q=gg2/gg1
         write(*,*) st, q
         write(1,*) q
 1       enddo

         do 21 ixi=10, 10000
         st=0.01*(ixi+1)
         pi=3.14159265359
         gg1=0.0
         gg2=0.0
         do 102 j=2,100
         x=(j-1)*pi/100.
         a=((sin(x))**2)*cos(x)
         b=st*((cos(x))**2)*sin(x)
         c=st*sin(2.*x)
         d=1.+((st*cos(x))**2)
         ff1=sqrt(d)
         ff2=b/sqrt(d)
         do 202 jj=2,100
         si=sin(2*(jj-1)*pi/100.)
         f1=sqrt(c*si+d)
         ff1=ff1+f1
         f2=(a*si+b)/f1
         ff2=ff2+f2
 202     enddo
         ff1=ff1*(pi/50.)
         ff2=ff2*(pi/50.)
         gg1=gg1+(sin(x))*ff1
         gg2=gg2+ff2
 102    enddo

         gg1=gg1*pi/100.0
         gg1=gg1/(4.*pi)
         gg2=gg2*pi/100.0
         gg2=gg2/(4.*pi)

         q=gg2/gg1
         write(*,*) st, q
         write(1,*) q
 21      enddo
         stop
         end
```

```
c BULK.FOR

$debug
c Program to solve the Contour Variable Model (Bulk flow)
c This is set of equations AII.1 to AII.7
c s0 is the undeformed length scale along the tube contour
c s is the deformed length scale along the tube contour
c q=ds/ds0; scap and stot are shear component of the orientational
c order parameter tensors, qq=dq/ds0
c pp is the ratio of retraction time to reptation time
c q0 is the shear component of geometric universal tensor

        parameter (n=101)
        dimension s0(n),q(n),scap(n),stot(n),v(n),g(n),sp(n),pg(n)
        dimension a(n), b(n), c(n), r(n), q0(11000), gg(n), s(n), qd(n)
        dimension qq(n), ftz(n)

        open(2, file='qo.inp')
        open(4, file='bulk.dat')
        open(3, file='conv.dat')

c Reading a file containing shear component of geometric universal tensor.
        do i=1, 10992
        read(2,*) q0(i)
        enddo

c chk and chk1 are the permissible errors used for convergence
        chk=1e-4
        chk1=1e-5

        do i=1,n
        stot(i)=0.0
        s0(i)=0.5*((i-1.)/(n-1.))
        s(i)=s0(i)
        enddo

c segn is the number of segments in a linear chain of the bulk
        pp=(1./(3.*segn.))

c g is the segmental renewal probability and i is the spatial co-ordinate
c on the chain, i=n corresponds to chain end while i=0 corresponds to
c the center of the chain
        do i=1,n
        g(i)=1.0
        q(i)=1.0
        enddo
        g(n)=0.0

        pi2=9.869604401089
        ds0=0.5/(n-1.)

c wi is the Weissenberg number based on constraint release time scale
c scap and stot are shear component of orientational order parameter tensor
c scap is the previous value while stot is the current value
        i=10
        do 1102 n101=-3, -3
        do 1100 n102=0, 9
        j3j=0
        wi=10.0**(n101+(n102/10.0))
 1000   write(*,*) abs(scap(i)-stot(i)), i, j3j
        j3j=j3j+1
```

```
        do 32 ii=1, n
        scap(ii)=stot(ii)
        stot(ii)=0
  32    enddo

        j1j=0

 1111   do i=1,n
        qd(i)=q(i)
        enddo
        j1j=j1j+1
        s(1)=0

c v is the convection velocity and can be estimated using equation AII.5
c Simpson's rule is used to perform an integration
        v(1)=0
        do i=2,n
        v(i)=v(i-1)+ds0*(qd(i-1)*scap(i-1)+qd(i)*scap(i))/2.0
        enddo

c Calculation of stretch s wrt s0. The code for solving equation AII.2
c Equation AII.2 is discritised in such way that it can solved using
c tridigonal system. a, b, c and r are variable constructed to solve
c tridiagonal matrix system

 2222   sm=s(n)
        do i=1,n-2
        a(i)=1.0
        c(i)=1.0
        b(i)=-2.0-(ds0**2.)*0.5*pi2*wi*pp*(v(n)/(s(n)))
        r(i)=0.-(ds0**2.)*pi2*wi*pp*v(i+1)
     &  -(ds0**2.)*0.5*pi2*wi*pp*(v(n)/(s(n)))*s0(i+1)
        enddo
        r(n-2)=r(n-2)-ds0
        b(n-2)=b(n-2)+1.0
        call tridag(a, b, c, r, sp, n-2)
        s(1)=0.0
        do i=2, n-1
        s(i)=sp(i-1)
        enddo
        s(n)=s(n-1)+ds0
c        write(*,*) abs(s(n)-sm)

        if (abs(s(n)-sm).gt.1e-5) goto 2222
        q(n)=1.0
        qq(1)=0
        do i=2, n-1
        q(i)=(s(i)-s(i-1))/ds0
        enddo
        q(1)=q(2)
        if (j1j.gt.50) chk1=5e-3
        if (j1j.gt.150) chk1=5e-2
        if (j1j.gt.250) goto 37
        do i=1,n
        if (abs(q(i)-qd(i)).gt.chk1) then
c        write(*,*) 'abs(qd(i)-q(i)), i', abs(qd(i)-q(i)),i,qd(i),q(i)
        goto 1111
        else
        endif
        enddo
```

```
 37     do i=1, n-1
        qq(i+1)=(q(i+1)-q(i))/ds0
        enddo

c To calculate fluctuation timescale
        do i=1,n
        ptz=4.0*exp(0.0-(0.25/pp)*((1.-(s(i)/s(n)))**2))
        ftz(i)=ptz/(wi*pp)
        enddo

c To calculate memory function g(i); i:space; j: time. g is calculated
c using equation AII.4. This equation is also discritised so as to
c solve by tridigonal system.
c As mentioned in program qo.for, for time t=0 to t=0.1, dt is taken to be
c 1e-4, while time t=0.1 to t=100, dt is taken to be 0.01
        dt=1e-4
        alp=dt/(ds0**2.0)
        beta=dt/ds0

        do 101 i=2, n-1
        a(i-1)=-(alp/(2.*wi*pi2*(q(i)**2.)))-(beta*
     &  ((qq(i)/(wi*pi2*(q(i)**3.)))+ (v(i)/q(i)))/4.)
        c(i-1)=a(i-1)+(beta*((qq(i)/(wi*pi2*(q(i)
     &  **3.)))+ (v(i)/q(i)))/2.)
        b(i-1)=1.-a(i-1)-c(i-1)
        b(i-1)=b(i-1)+dt*0.5*((1./q(i))*(v(n)/s(n))+ftz(i))
  101   enddo
        b(1)=b(1)+a(1)

        do 4 j=1, 1000

        if (j.eq.1) then
        do i=1,n
        g(i)=1.0
        enddo
        g(n)=0
        else
        endif

        do i=1,n
        pg(i)=g(i)
        enddo

        do 6 i=2, n-1
        r(i-1)=(1-alp/
     &   (wi*(q(i)**2)*pi2))*pg(i)+((alp/(2.*wi*(q(i)**2)*pi2))+
     &  (beta*((qq(i)/(wi*pi2*(q(i)**3.)))+ (v(i)/q(i)))/4.))*pg(i-1)+
     &  ((alp/(2.*wi*(q(i)**2)*pi2))-
     &  (beta*((qq(i)/(wi*pi2*(q(i)*3.)))+ (v(i)/q(i)))/4.))*pg(i+1)
        r(i-1)=r(i-1)-dt*0.5*((1./q(i))*(v(n)/s(n))+ftz(i))*pg(i)
  6     enddo

        call tridag(a, b, c, r, gg, n-2)
        g(n)=0.0
        do 7 i=1,n-2
        g(i+1)=gg(i)
        stot(i+1)=stot(i+1)-(g(i+1)-pg(i+1))*q0(j+1)
  7     enddo
        g(1)=g(2)
        stot(1)=stot(1)-(g(1)-pg(1))*q0(j+1)
  4     enddo
```

```
      do i=1,n
      stot(i)=stot(i)+(g(i)-pg(i))*q0(1001)/2.
     &  -100.0*(g(i)-pg(i))*q0(1001)/2.
      enddo

      dt=0.01
      alp=dt/(ds0**2.0)
      beta=dt/ds0

      do 106 i=2, n-1
      a(i-1)=-(alp/(2.*wi*pi2*(q(i)**2.)))-(beta*
     &  ((qq(i)/(wi*pi2*(q(i)**3.)))+ (v(i)/q(i)))/4.)
      c(i-1)=a(i-1)+(beta*((qq(i)/(wi*pi2*(q(i)
     &  **3.)))+ (v(i)/q(i)))/2.)
      b(i-1)=1.-a(i-1)-c(i-1)
      b(i-1)=b(i-1)+dt*0.5*((1./q(i))*(v(n)/s(n))+ftz(i))
106   enddo
      b(1)=b(1)+a(1)

      do 14 j=1001, 10991

      do i=1,n
      pg(i)=g(i)
      enddo

      do 16 i=2, n-1
      r(i-1)=(1-alp/
     &   (wi*(q(i)**2)*pi2))*pg(i)+((alp/(2.*wi*(q(i)**2)*pi2))+
     &  (beta*((qq(i)/(wi*pi2*(q(i)**3.)))+ (v(i)/q(i)))/4.))*pg(i-1)+
     &  ((alp/(2.*wi*(q(i)**2)*pi2))-
     &  (beta*((qq(i)/(wi*pi2*(q(i)*3.)))+ (v(i)/q(i)))/4.))*pg(i+1)
      r(i-1)=r(i-1)-dt*0.5*((1./q(i))*(v(n)/s(n))+ftz(i))*pg(i)
16    enddo

      call tridag(a, b, c, r, gg, n-2)
      g(n)=0.0
      do 17 i=1,n-2
      g(i+1)=gg(i)
      stot(i+1)=stot(i+1)-(g(i+1)-pg(i+1))*q0(j+1)
17    enddo
      g(1)=g(2)
      stot(1)=stot(1)-(g(1)-pg(1))*q0(j+1)
      if (abs(g(n/2)-pg(n/2)).lt.1e-12) goto 98
14    enddo

      do i=1,n
      stot(i)=stot(i)+(g(i)-pg(i))*q0(9992)/2.
      enddo
98    if (j3j.eq.20) goto 35
      do 33 i=1,n
      if (abs(scap(i)-stot(i)).gt.chk) goto 1000
33    enddo
35    chk=scap(1)*1.e-2
      if (chk.lt.1e-5) chk=1e-5

      write(*,*) scap
      str=(stot(1)*(q(1)**2.)+stot(n)*(q(n)**2.))/2.0
      do i=2,n-1
      str=str+stot(i)*(q(i)**2.)
      enddo
```

```
c Calculation of stress
        stress=(15./2.)*str*ds0
        write(4,*) wi, stress
        write(3,*) wi,  stress, v(n)
        write(*,*) wi, stress
        if (n101.eq.3) goto 1102
 1100   enddo
 1102   enddo

        stop
        end


c Subroutine for solving a program for solving the tridigonal matrix system
        subroutine tridag(a, b, c, r, u, n)
c        implicit double precision (a-h,o-z)
        real a(501), b(501), c(501), r(501), u(501), gam (501)
        if (b(1).eq.0)pause 'tridag failed 1'
        bet=b(1)
        u(1)=r(1)/bet
        do 1 i=2,n
        gam(i)=c(i-1)/bet
        bet=b(i)-a(i)*gam(i)
        if (bet.eq.0)pause 'tridag failed 2'
        u(i)=(r(i)-a(i)*u(i-1))/bet
 1      enddo

        do i=n-1, 1, -1
        u(i)=u(i)-gam(i+1)*u(i+1)
        enddo
        return
        end
```

```
c INTERFACIAL.FOR
c This program is to solve contour variable model for the interfacial
c region. This is set of equations AII.8 to AII.19. Various variables used
c in this program are identical to that in the earlier program BULK.FOR.
c
$debug
        implicit double precision (a-h,o-z)
        parameter (n=101)
        dimension s0(n),q(n),scap(n),stot(n),v(n),g(n),sp(n),pg(n)
        dimension a(n), b(n), c(n), r(n), q0(11000), gg(n), s(n), qd(n)
        dimension qq(n), ftz(n)
        open(2, file='qo.inp')
        open(3, file='sl.dat')
        open(4, file='INTERFACIAL.dat')

c Reading a file containing shear component of geometric universal tensor.
        do i=1, 10992
        read(2,*) q0(i)
        enddo

c rat is the ratio of interfacial modulus to bulk modulus
        rat=1.0

c chk and chk1 are the permissible errors used for convergence
        chk=1e-6
        chk1=1e-5
```

```
        do i=1,n
        stot(i)=0.0
        s0(i)=((i-1.)/(n-1.))
        s(i)=s0(i)
        enddo
        pp=90.
        p=54.
c p is the number of segments of tethered chain while pp is that of bulk
        pt=pp/p
        fac=(p**(-0.9))*(pp**3.4)
        e=0.75*(pp**3.4)/(p**(0.9))

c g is the segmental renewal probability and i is the spatial co-ordinate
c on the chain, i=n corresponds to chain end while i=0 corresponds to
c tethered end
        do i=1,n
        g(i)=1.0
        q(i)=1.0
        enddo
        g(n)=0.0

        pi2=9.869604401089
        ds0=1.0/(n-1.)
        alp1=2.*(p**1.5)

c vss and vss1 is the convection velocity given by equation (AII.17)
        vss=1.0
        i=10
        do 1102 n101=-1,0
        do 1100 n102=0,9
        j3j=0

c wi is the Weissenberg number based on constraint release time scale
c scap and stot are shear component of orientational order parameter tensor
c scap is the previous value while stot is the current value

        wi=10.0**(n101+(n102/10.0))
        stress1=0
 1000   write(*,*) abs(scap(i)-stot(i)), i, j3j, chk
        j3j=j3j+1
        vss=abs(vss)
        do 32 ii=1, n
        scap(ii)=stot(ii)
        stot(ii)=0
  32    enddo
        j1j=0

 1111   do i=1,n
        qd(i)=q(i)
        enddo

        j1j=j1j+1
        s(1)=0

2222   sm=s(n)

c v is the convection velocity and can be estimated using equation AII.14
c Simpson's rule is used to perform an integration
        v(1)=1.0/sqrt(p)
        do i=2,n
        v(i)=v(i-1)+ds0*(qd(i-1)*scap(i-1)+qd(i)*scap(i))/2.0
```

```
        enddo

c To calculate stretch s wrt s0. The code for solving equation AII.9
c Equation AII.9 is discritised in such way that it can solved using
c tridigonal system. a, b, c and r are variable constructed to solve
c tridiagonal matrix system

c       To calculate stretch s wrt s0
        do i=1,n-2
        a(i)=1.0
        c(i)=1.0
        b(i)=-2.0-(ds0**2.)*pi2*wi*(vss*alp1/s(n))/(6.*fac)
        r(i)=0.-(ds0**2.)*pi2*wi*v(i+1)/(3.*fac)
     &  -(ds0**2.)*pi2*wi*(vss*alp1/s(n))*s0(i+1)/(6.*fac)
        enddo
        r(n-2)=r(n-2)-ds0
        b(n-2)=b(n-2)+1.0
        call tridag(a, b, c, r, sp, n-2)
        s(1)=0.0
        do i=2, n-1
        s(i)=sp(i-1)
        enddo
        s(n)=s(n-1)+ds0

        if (abs(s(n)-sm).gt.1e-5) goto 2222
        q(n)=1.0
        qq(1)=0
        do i=2, n-1
        q(i)=(s(i)-s(i-1))/ds0
        enddo
        q(1)=q(2)
        if (j1j.gt.50) chk1=5e-3
        if (j1j.gt.150) chk1=5e-2
        if (j1j.gt.250) goto 37
        do i=1,n
        if (abs(q(i)-qd(i)).gt.chk1) then
c        write(*,*) 'abs(qd(i)-q(i)), i', abs(qd(i)-q(i)),i,qd(i),q(i)
        goto 1111
        else
        endif
        enddo
 37     do i=1, n-1
        qq(i+1)=(q(i+1)-q(i))/ds0
        enddo

c To calculate fluctuation timescale (equation AII.10)

        do i=1,n
        ptz=exp(0.0-(1.5*p)*((1.-(s(i)/s(n)))**2))
        ftz(i)=e*ptz/wi
        enddo

c To calculate memory function g(i); i:space; j: time. g is calculated
c using equation AII.8. This equation is also discritised so as to
c solve by tridigonal system.
c As mentioned in program qo.for, for time t=0 to t=0.1, dt is taken to be
c 1e-4, while time t=0.1 to t=100, dt is taken to be 0.01

        dt=1e-4
        alp=2.*dt/(ds0**2.0)
        beta=dt/ds0
```

```
      do 101 i=2, n-1
      a(i-1)=-(alp/(2.*wi*pi2*(q(i)**2.)))-(beta*
     &  ((qq(i)/(wi*pi2*(q(i)**3.)))+ (v(i)/q(i)))/4.)
      c(i-1)=a(i-1)+(beta*((qq(i)/(wi*pi2*(q(i)
     &  **3.)))+ (v(i)/q(i)))/2.)
      b(i-1)=1.-a(i-1)-c(i-1)
      b(i-1)=b(i-1)+dt*((1./q(i))*(vss*alp1/s(n))+ftz(i))
101   enddo
      b(1)=b(1)+a(1)

      do 4 j=1, 1000

      if (j.eq.1) then
      do i=1,n
      g(i)=1.0
      enddo
      g(n)=0
      else
      endif

      do i=1,n
      pg(i)=g(i)
      enddo

      do 6 i=2, n-1
      r(i-1)=(1-alp/
     &  (wi*(q(i)**2)*pi2))*pg(i)+((alp/(2.*wi*(q(i)**2)*pi2))+(beta*
     &  ((qq(i)/(wi*pi2*(q(i)**3.)))+(v(i)/q(i)))/4.))*pg(i-1)+
     &  ((alp/(2.*wi*(q(i)**2)*pi2))-(beta*((qq(i)/(wi*pi2*(q(i)*3.)))
     &  + (v(i)/q(i)))/4.))*pg(i+1)
      r(i-1)=r(i-1)-dt*((1./q(i))*(vss*alp1/s(n))+ftz(i))*pg(i)
6     enddo

      call tridag(a, b, c, r, gg, n-2)
      g(n)=0.0
      do 7 i=1,n-2
      g(i+1)=gg(i)
      stot(i+1)=stot(i+1)-(g(i+1)-pg(i+1))*q0(j+1)
7     enddo
      g(1)=g(2)
      stot(1)=stot(1)-(g(1)-pg(1))*q0(j+1)
4     enddo

      do i=1,n
      stot(i)=stot(i)+(g(i)-pg(i))*q0(1001)/2.
     &  -100.0*(g(i)-pg(i))*q0(1001)/2.
      enddo

      dt=0.01
      alp=2.*dt/(ds0**2.0)
      beta=dt/ds0

      do 106 i=2, n-1
      a(i-1)=-(alp/(2.*wi*pi2*(q(i)**2.)))-(beta*
     &  ((qq(i)/(wi*pi2*(q(i)**3.)))+ (v(i)/q(i)))/4.)
      c(i-1)=a(i-1)+(beta*((qq(i)/(wi*pi2*(q(i)
     &  **3.)))+ (v(i)/q(i)))/2.)
      b(i-1)=1.-a(i-1)-c(i-1)
      b(i-1)=b(i-1)+dt*((1./q(i))*(vss*alp1/s(n))+ftz(i))
106   enddo
```

```
        b(1)=b(1)+a(1)

        do 14 j=1001, 10991

        do i=1,n
        pg(i)=g(i)
        enddo

        do 16 i=2, n-1
        r(i-1)=(1-alp/
     &  (wi*(q(i)**2)*pi2))*pg(i)+((alp/(2.*wi*(q(i)**2)*pi2))+(beta*
     &  ((qq(i)/(wi*pi2*(q(i)**3.)))+(v(i)/q(i)))/4.))*pg(i-1)+
     &  ((alp/(2.*wi*(q(i)**2)*pi2))-(beta*((qq(i)/(wi*pi2*(q(i)*3.)))
     &  + (v(i)/q(i)))/4.))*pg(i+1)
        r(i-1)=r(i-1)-dt*((1./q(i))*(vss*alp1/s(n))+ftz(i))*pg(i)
  16    enddo

        call tridag(a, b, c, r, gg, n-2)
        g(n)=0.0
        do 17 i=1,n-2
        g(i+1)=gg(i)
        stot(i+1)=stot(i+1)-(g(i+1)-pg(i+1))*q0(j+1)
  17    enddo
        g(1)=g(2)
        stot(1)=stot(1)-(g(1)-pg(1))*q0(j+1)
        if (abs(g(n/2)-pg(n/2)).lt.1e-12) goto 98
  14    enddo

        do i=1,n
        stot(i)=stot(i)+(g(i)-pg(i))*q0(10992)/2.
        enddo
  98    if (j3j.eq.20) goto 35
        do 33 i=1,n
        if (abs(scap(i)-stot(i)).gt.chk) goto 1000
  33    enddo
  35    chk=scap(1)*1.e-3
        if (chk.lt.1e-6) chk=1e-6

        do i=1,n
        if (stot(i).lt.0.0) stot(i)=0.0
        enddo
        write(*,*) stot

        str=(stot(1)*(q(1)**2.)+stot(n)*(q(n)**2.))/2.0
        do i=2,n-1
        str=str+stot(i)*(q(i)**2.)
        enddo
        vs=wi*v(1)/(pp*sqrt(p))

c Calculation of stress

        stress=(15./4.)*str*ds0
        write(*,*) wi, vs, stress, s(n)

        call correction(rat*stress, rate, vss1)

        vss1=vss1*rate/wi
        if (abs(stress-stress1).gt.1e-5) then
        stress1=stress
        if (j3j.gt.100) goto 1121
        vss=vss1
```

```
        goto 1000
        else
        endif

        write(4,99) wi, vs, rat*stress, s(n)
        write(3,*) vs, vs/rate

 1100   enddo
 1102   enddo
 99     format(4(e12.5,1x))
 1121   stop
        end

        subroutine tridag(a, b, c, r, u, n)
        implicit double precision (a-h,o-z)
        dimension a(501), b(501), c(501), r(501), u(501), gam (501)
        if (b(1).eq.0)pause 'tridag failed 1'
        bet=b(1)
        u(1)=r(1)/bet
        do 1 i=2,n
        gam(i)=c(i-1)/bet
        bet=b(i)-a(i)*gam(i)
        if (bet.eq.0)pause 'tridag failed 2'
        u(i)=(r(i)-a(i)*u(i-1))/bet
 1      enddo

        do i=n-1, 1, -1
        u(i)=u(i)-gam(i+1)*u(i+1)
        enddo
        return
        end

c Subroutine correction connects system if equations for bulk and system of
c equations for interfacial region through equation AII.17
c This subroutine calculates a convection velocity of chain in the bulk to
c be used in the system of equations for interfacial region as a CCR
c velocity at the same shear stress

        subroutine correction(stress, rate, velo)
        implicit double precision (a-h,o-z)
        parameter (m=52)
        dimension str2(m), str3(m), gam1(m), gam(m), con1(m), con(m)
        open(1, file='conv90.dat')

        do i=1, 51
        read(1,*) gam1(i), str3(i), con1(i)
        enddo
        str2(1)=str3(1)
        gam(1)=gam1(1)
        con(1)=con1(1)
        l=1
        j=1
 3      j=j+1
        if (j.gt.m) goto 4
        if (str2(l).lt.str3(j)) then
        l=l+1
        str2(l)=str3(j)
        gam(l)=gam1(j)
        con(l)=con1(j)
        goto 3
        else
```

```
      goto 3
      endif
4     if (stress.gt.str2(l)) pause

      if (stress.lt.str2(1)) then
      rate=gam(1)+(stress-str2(1))
     &  *((gam(2)-gam(1))/(str2(2)-str2(1)))
      velo=con(1)+(stress-str2(1))
     &  *((con(2)-con(1))/(str2(2)-str2(1)))
      else
      endif

      j=1
6     if (stress.gt.str2(j+1)) then
      j=j+1
      goto 6
      else
      rate=gam(j)+(stress-str2(j))
     &  *((gam(j+1)-gam(j))/(str2(j+1)-str2(j)))
      velo=con(j)+(stress-str2(j))
     &  *((con(j+1)-con(j))/(str2(j+1)-str2(j)))
      endif
      close(1)
      return
      end
```

Reference:

Adewale, K. P. and Leonov, A. I., 1997, "Modeling spurt and stress oscillations in flows of molten polymers", *Rheol. Acta*, **36**, 110-127.

Agarwal, U. S., Dutta, A. and Mashelkar, R. A., 1994, "Migration of macromolecules under flow: The physical origin and engineering implications", *Chem. Eng. Sci.*, **49**, 1693-1717.

Ahn, K. H. and Osaki, K., 1994, "A network model predicting the shear thickening behavior of poly(vinyl alcohol)/sodium borate aqueous solution", *J. Non-Newtonian Fluid Mech.*, **55**, 215-227.

Ahn, K. H. and Osaki, K., 1995, "Mechanism of shear thickening investigated by a network model", *J. Non-Newtonian Fluid Mech.*, **56**, 267-288.

Ajdari, A. F., Brochard-Wyart, F., de Gennes, P. G., Leibler, L., Viovy, J. L. and Rubenstein, M., 1994, "Slippage of an entangled polymer melt on a grafted surface", *Physica A*, **204**, 17-39.

Akay, G., 1983, "Unstable capillary flow of reinforced polymer melts", *J. Non-Newtonian Fluid Mech.*, **13**, 309-323.

Anastasiadis, S. H. and Hatzikiriakos, S. G., 1998, "The work of adhesion of polymer /wall interfaces and its association with the onset of wall slip", *J. Rheol.*, **42**, 795-812.

Bagley E. B., Cabott, I. M. and West, D. C., 1958, "Discontinuity in the flow curve of polyethylene", *J. App. Phys.*, **29**, 109-110.

Bagley, E. B. and Schreiber, H. P., 1961, "Effect of die entry geometry on polymer melt fracture and extrudate distortion", *Trans. Soc. Rheol.*, **5**, 329-353.

Bagley, E. B. and Schreiber, H. P., 1969, "Elasticity effects in polymer extrusion", in Rheology, Vol. 5 (F. R. Eirich, ed.), Academic, New York, 1969, 93-125.

Bagley, E. B., 1961, "Some elastic effects in polymer flow", *Trans. Soc. Rheol.*, **5**, 355-368.

Ballanger, T. F., Chen, I-J, Crowder, J. W., Hagler, G. E., Boguc, D. C. and White, J. L., 1971, "Polymer melt flow instabilities in extrusion: investigation of the mechanism and material and geometric variables", *Trans. Soc. Rheol.*, **15**, 195-215.

Barnes, H. A., 1995, "A review of the slip (wall depletion) of polymer solutions, emultions and particle suspensions in viscometers: its causes, character and cure", *J. Non-Newtonian Fluid Mech.*, **56**, 221-251.

Barone, J. R. and Wang, S. Q., 2000, "Adhesive wall slip on organic surfaces", *J. Non-Newt. Fluid Mech.*, **91**, 31-36.

Barone, J. R. and Wang, S. Q., 2001, "Rheo-optical observations of sharkskin formation in slit-die extrusion", *J. Rheol.*, **45**, 49-60.

Barone, J. R., Plucktaveesak, N. and Wang, S. Q., 1998, "Interfacial molecular instability mechanism for sharkskin phenomenon in capillary extrusion of linear polyethylenes", *J. Rheol.*, **42**, 813-832.

Beaufils, P., Vergnes, B. and Agassant, J. F., 1989, "Characterization of the sharkskin defect and its development with the flow conditions," *Int. Polym. Proc.*, **4**, 78-84.

Benbow, J. J. and Lamb, P., 1963, "New aspects of melt fracture", *S. P. E. Trans.*, **3**, 7-17.

Bercea, M., Peiti, C., Simionescu, B. and Navard, P., 1993, "Shear rheology of semidilute poly(methyl methacrylate) solutions", *Macromolecules*, **26**, 7095-7096.

Bergem, N., 1976, "Visualization Studies of Polymer Melt Flow Anomalies in Extrusion," in *Proceedings of the VIIth International Congress on Rheology*, Stockholm, Sweden, pp. 50-54.

Billmeyar, F. W., 1984, *Textbook of polymer science*, John Wiley and Sons, New York.

Bird, R. B., Armstrong, R. C. and Hassager, O., 1987, *Dynamics of polymeric liquids, Vol 2, Kinetic Theory*, John Wiley and Sons, New York.

Bird, R. B., Armstrong, R. C. and Hassager, O., 1987, *Dynamics of polymeric liquids, Vol 1, Fluid Mechanics*, John Wiley and Sons, New York.

Black, W. B. and Graham, M. D., 1996, "Wall-slip and polymer-melt flow instability", *Phys. Rev. Lett.*, **77**, 956-959.

Boudreaux, E. and Cuculo, J. A., 1977, "Polymer flow instability: A review and analysis", *J. Macromol. Sci.- Rev. Macromol. Chem.*, **C16**, 39-77.

Brasseur, E., Fyrillas, M. M., Georgiou, C. G. and Crochet, M. J., 1998, " The time dependent extrudate swell problem of an Oldroyd-B fluid with slip along the wall", *J. Rheol.*, **42**, 549-566.

Brochard, F. and de Gennes, P. G., 1992, "Shear-dependent slippage at a polymer/solid interface", *Langmuir*, **8**, 3033-3037.

Brochard-Wyart, F., Ajdari, A., Leibler, L., Rubinstein, M. and Viovy, J. L., 1994, "Dynamics of stars and linear chains dissolved in a polymeric melt", .*Macromolecules*, **27**, 803-808.

Brochard-Wyart, F., Gay C. and de Gennes, P. G., 1996, "Slippage of polymer melts on grafted surfaces", *Macromolecules*, **29**, 377-382.

Burton, R. H., Folkes, M. J., Narh, K. A. and Keller, A., 1983, "Spatial variation in viscosity in sheared polymer melts", *J. Mater. Sci.*, **18**, 315-320.

Chan, C. -M. and Feng, J., 1997, "Mechanisms for viscosity reduction of polymer blends: blends of fluoroelastomer and high-density polyethylene", *J. Rheol.*, **41**, 319-333.

Chauveteau, G., 1982, "Rodlike solutions through fine pores: influence of pores size on rheological behavior", *J. Rheol.*, **26**, 111-142.

Chauveteauet, G., Tirrel, M. and Omari, A., 1984, "Concentration dependence of effective viscosity of polymer solutions in small pores with repulsive or attractive walls" *J. Colloid Interface Sci.*, **100**, 41-54.

Chen, Y., Kalyon, D. M. and Bayramli, E., 1993, "Effects of surface roughness and the chemical structure of materials of construction on wall slip behavior of linear low density polyethylene in capillary flow", *J. Appl. Poly. Sci.*, **50**, 1169-1177.

Cheng, D. C. –H., 1968, "The effect of secondary flow on the viscosity measurement using the cone-and-plate viscometer", *Chem. Eng. Sci.,* **23**, 895-899.

Clegg P. L., 1957, in *Rheology of Elastomers*, Mason, P. and Wookey, N. (Eds.), Pergamon, New York.

Cogswell, F. N., 1977, "Stretching flow instabilities at the exit of extrusion dies," *J. Non-Newtonian Fluid Mech.*, **2**, 37-47.

Cohen, Y. and Metzner, A. B., 1982, "Slip phenomena in polymer solutions flowing through small channels", *AICHE Symp. Ser No. 212*, **78**, 77-85.

Cohen, Y. and Metzner, A. B., 1985, "Apparent slip flow of polymer solutions", *J. Rheol.*, **29**, 67-102.

Cohen, Y., 1981, "The behavior of polymer solutions in non-uniform flows", Ph.D. thesis, University of Delware, Newark, U. S. A.

Constantin, D., 1984, "LLDPE melt rheology: extensibility and extrusion defects", *Polym. Eng. Sci.*, **24**, 268-274.

de Dennes, P. G., 1971, "Reptation of a polymer chain in the presence of fixed obstacles", *J. Chem. Phys.*, **55**, 572-579.

de Gennes, P. G., 1979, Ecoulements viscometriques de polymers enchevetres", *C R Acad Sci Paris Ser B*, **288**, 219-220.

de Gennes, P. G., 1985, "Wetting: statics and dynamics", *Rev. Mod. Phys.*, **57**, 827-863.

De Smedt, C. and Nam, S., 1987, "The processing benefits of fluoroelastomer application in LLDPE", *Plast. Rubber Process Appl.*, **8**, 11-16.

de Vargas, L. and Manero, O., 1989, "On the slip phenomenon of polymeric solutions through capillaries", *Polym. Engng. Sci.*, **29**, 1232-1236.

Dealy, J. M. and Giacomin, A. J., 1998, “Sliding Plate and Sliding Cylinder Rheometers”, in *Rheological Measurements*, Collyer, A. A., Clegg D. W. (Eds.), Chapman & Hall, London, pp. 237-259.

Deeprasertkul, C., Rosenblatt, C. and Wang, S. Q., 1998, "Molecular characters of sharkskin phenomenon in metallocence linear low density polyethylenes", *Macromol. Chem & Phys.*, **199**, 2113-2118.

Deiber, J. A. and Schowalter, W. R., 1991, “On the comparison of simple non-monotonic constitutive equations with data showing slip of well-characterized polybutadines”, *J. Non-Newtonian Fluid Mech.*, **40**, 141-150.

Den Otter J. L., 1970, “Mechanics of Melt fracture,“ *Plastics Polymers*, **38**, 155-168.

Den Otter, J. L., 1971, “Some investigations of melt fracture”, *Rheol Acta*, **10**, 200-207.

Denn, M. M., 1990, “Issues in viscoelastic fluid mechanics”, *Annu. Rev. Fluid Mech.*, **22**, 13-34.

Denn, M. M., 2001, “Extrusion instabilities and wall slip”, *Annu. Rev. Fluid Mech.*, **33**, 265-287.

Dhori, P.K., Jeyaseelan, R.S., Giacomin, A.J. and Slattery, J.C., 1997, “Common line motion III: implications in polymer extrusion”, *J. Non-Newtonian Fluid Mech.*, **71**, 231-243.

Doi, M. and Edwards, S. F., 1978a, “Dynamics of concentrated polymer systems, Part 1. Brownian motion in the equilibrium state”, *J. Chem. Soc. Faraday Trans. II*, **74**, 1789-1801.

Doi, M. and Edwards, S. F., 1978b, “Dynamics of concentrated polymer systems, Part 2. Molecular motion under flow”, *J. Chem. Soc. Faraday Trans. II*, **74**, 1802-1817.

Doi, M. and Edwards, S. F., 1978c, “Dynamics of concentrated polymer systems, Part 3. The constitutive equation”, *J. Chem. Soc. Faraday Trans. II*, **74**, 1818-1832.

Doi, M. and Edwards, S. F., 1979, “Dynamics of concentrated polymer systems, Part 4. Rheological properties”, *J. Chem. Soc. Faraday Trans. II*, **75**, 38-54.

Doi, M. and Edwards, S. F., 1986 *The theory of polymer dynamics*, Oxford University Press, London.

Doi, M., 1980a, “Molecular Rheology of concentrated polymer systems. I”, *J. Polym. Sci. Part B, Polym. Phys.*, **18**, 1005-1020.

Doi, M., 1980b, “A constitutive equation derived from the model of Doi and Edwards for concentrated polymer solutions and Polymer melts”, *J. Polym. Sci. Part B, Polym. Phys.,* **18**, 2055-2067.

Doi, M., 1980c, "Stress relaxation of polymeric liquids after double-step strain", *J. Polym. Sci. Part B, Polym. Phys.*, **18**, 1891-1905.

Doi, M., 1981, "Explanation for the 3.4 power law of viscosity of polymeric liquids on the basis of the tube model", *J. Polym. Sci., Polym. Lett. Ed.*, **19**, 265-273.

Durliat, E., Hervet, H. and Leger, L., 1997, "Influence of grafting density on wall slip of a polymer melt on a polymer brush", *Europhys. Lett.*, **38**, 383-388.

Dutta, A. and Mashelkar, R. A., 1983, "Hydrodynamic changes due to polymer migration in very dilute solution", *Rheol. Acta*, **22**, 455-461.

Dutta, A., Ravetkar, D. and Mashelkar, R. A., 1987, "On flow length requirement for stress induced polymer migration in fine capillaries", *Chem. Engng. Commun.*, **53**, 131-147.

Edwards, S. F., 1967, "The statistical mechanics of polymerized material", *Proc. Phys. Soc.*, **92**, 9-16.

Fetters, L. J., Lohse, D. J., Richter, D., Witten, T. A., Zirkel, A., 1994, "Connection between Polymer Molecular Weight, Density, Chain Dimensions, and Melt Viscoelastic Properties", *Macromolecules*, **27**, 4639-4647.

Focquet, K. and Blong, T. J., 1998, "Processing aids: Fluoropolymers to improve the conversions of polyolefins", in *Plastics Addivities*, Pritchard G. (Eds), Chapman and Hall, London, U.K., pp 519-525.

Garvey, B. S., Whitlock, M. H. and Freese, J. A., 1942, "Processing characteristics of synthetic tire rubber", *Ind. Eng. Chem.*, **34**, 1309-1312.

Giacomin, A. J., Samurkas, T., Dealy, J. M., 1989, "A novel sliding plate rheometer for molten plastics" *Polym. Eng. Sci.*, **29**, 499-504.

Graessley, W. W., 1982, "Entangled linear, branched and network polymer systems-molecular theories", *Adv. Polym. Sci.*, **47**, 67-117.

Graham, M. D., 1999, "The sharkskin instability of polymer melt flows", *Chaos*, **9**, 154-163.

Green, M. S. and Tobolsky, A. V., 1946, "Theory of relaxing polymeric media", *J. Chem. Phys.*, **14**, 80-92.

Halley, P. J. and Mackay, M. E., 1994, "The effect of metals on the processing of LLDPE through a slit die", *J. Rheol.*, **38**, 41-51.

Hatzikiriakos, S. G. and Dealy, J. M., 1991 "Wall slip of molten high-density polyethylene. I. Sliding plate rheometer studies", *J. Rheol.*, **35**, 497-523.

Hatzikiriakos, S. G. and Dealy, J. M., 1993, "Effects of interfacial conditions on wall slip and sharkskin melt fracture of HDPE", *Int. Polym. Process.*, **8**, 36-43.

Hatzikiriakos, S. G. and Kalogerakis, N., 1994, "A Dynamic slip model for molten polymers based on a network kinetic theory", *Rheol. Acta,* **33**, 38-47.

Hatzikiriakos, S. G., 1995, "A multimode interfacial constitutive equation for molten polymers", *J. Rheol.*, **39**, 61-71.

Hatzikiriakos, S. G., 2000, "Gross melt fracture elimination during the extrusion of polyolefins", in *Proceedings of XIIIth International Congress on Rheology*, Cambridge, Vol.3 pp 143-145.

Hatzikiriakos, S. G., Hong, P., Ho, W. and Stewart, C. W., 1995, "The effect of Teflon coating in polyethylene melt extrusion", *J. Appl. Polym. Sci.*, **55**, 595-603.

Hatzikiriakos, S. G., Kazatchkov, I. B. and Vlassopoulos, D., 1997, "Interfacial phenomena in the capillary extrusion of metallocene polyethylenes", *J. Rheol.*, **41**, 1299-1316.

Hatzikiriakos, S. G., Stewart, C. W. and Dealy, J. M., 1993 "Effect of surface coatings on wall slip of LLDPE", *Int. Polym. Process.*, **8**, 30-35.

Henson, D. J. and Mackay, M. E., 1995, "Effect of gap on the viscosity of monodisperse polystyrene melts: slip effects", *J. Rheol.*, **39**, 359-373.

Hill, D. A., 1998, "Wall slip in polymer melts: A pseudo-chemical model", *J. Rheol.*, **42**, 581-601.

Hill, D. A., Hasegawa, T. and Denn, M. M., 1990, "On the apparent relation between adhesive failure and melt fracture", *J. Rheol.*, **34**, 891-918.

Hunter, J. K. and Slemrod, M., 1983, "Viscoelastic fluid flow exhibiting hysteretic phase changes" *Phys. Fluids*, **26**, 2345-2351.

Huseby, T. W., 1966, "Hypothesis on a Certain Flow Instability in Polymer Melts", *Trans. Soc. Rheol.*, **10**, 181-190.

Ianniruberto, G and Marrucci, G., 1996, "On the compatibility of the Cox-Merz rule with the model of Doi and Edwards", *J. Non-Newtonian Fluid Mech.*, **65**, 241-246.

Ianniruberto, G. and Marrucci, G., 2000, "Progress in describing the CCR mechanism in entangled polymers *,* in *Proceedings of XIIIth International Congress on Rheology*, Cambridge, Vol 2, pp 102-104.

Ianniruberto, G., Marrucci, G., 2000, "Convective orientational renewal in entangled polymers", *J. Non-Newtonian Fluid Mech.*, **95**, 363-374.

Janssen, L. P. M. B., 1980, "A thermodynamic approach to the understanding of slip phenomena", *Rheol. Acta*, **19**, 32-37.

Kalashnikov, V. N. and Valsov, S. A., 1978, "On scale-dependent effect in laminar flow of dilute polymer solutions in tubes", *Rheol. Acta*, **17**, 296-302.

Kalika, D. S. and Denn, M. M., 1987, "Wall slip and extrudate distortion in linear low-density polyethylene", *J. Rheol.*, **31**, 815–834.

Kazatchkov, I. B., Bohnet, N., Goyal, S. K. and Hatzikiriakos, S. G., 1999, "Influence of molecular structure on the rheological and processing behavior of polyethylene resins", *Polym. Engng. Sci.*, **39**, 804-815.

Kazatchkov, I. B., Hatzikiriakos, S. G. and Stewart, C. W., 1995, "Extrudate distortion in the capillary/slit extrusion of a molten polypropylene", *Polym. Engng. Sci.*, **35**, 1864-1871.

Kissi, N. El. and Piau, J. M., 1990, "The different capillary flow regimes of entangled polydimethylsiloxane polymers: macroscopic slip at wall, hysteresis and cork flow", *J. Non-Newtonian Fluid Mech.*, **37**, 55-94.

Kissi, N. El. and Piau, J-M., 1996a, "Slip and friction of polymer melt flows", in *Rheology for Polymer Melt Processing*, Piau, J-M., Agassant, J-F. (Eds.), Elsevier Science: Amsterdam, pp 357-388.

Kissi, N. El. and Piau, J-M., 1996b, "Stability phenomena during polymer melt extrusion", in *Rheology for Polymer Melt Processing*, Piau, J-M., Agassant, J-F. (Eds.), Elsevier Science: Amsterdam, pp 389-420.

Kissi, N. El., Leger, L., Piau, J.-M. and Mezghani, A., 1994, "Effect of surface properties on polymer melt slip and extrusion defects", *J. Non-Newtonian Fluid Mech.*, **52**, 249-261.

Kolakka, R. W., Malkus, D. S., Hansen, M. G., Ierley, G. R. and Worthing, R. A., 1988, "Spurt Phenomena of the Jonson-Segalman fluid and related models", *J. Non-Newtonian Fluid Mech.*, **29**, 303-335.

Kolnaar, J. W. H. and Keller, A., 1994 "A temperature window of reduced flow resistance in Polyethylene with implications for melt flow rheology: 1. The basic effect and principal parameters", *Polymer*, **35**, 3863-3873.

Kolnaar, J. W. H. and Keller, A., 1996, "A singularity in the melt flow of Polyethylene with wider implications for polymer flow rheology", *J. Non-Newtonian Fluid Mech.*, **67**, 213-240.

Koran, F. and Dealy J. M., 1999a, "A high pressure sliding plate rheometer for polymer melts", *J. Rheol.*, **43**, 1279-1290.

Koran, F. and Dealy J. M., 1999b, "Wall slip of polyisobutylene: Interfacial and pressure effects", *J. Rheol.*, **43**, 1291-1306.

Kulicke, W. M. and Porter, R. S., 1979, "Irregularities in steady flow for non-Newtonian fluids between cone and plate", *J. Appl. Polym. Sci.*, **23**, 953-965.

Kulicke, W. M., Kniewske, R. and Klien, J., 1982, "Preparation characterization solution properties and rheological behavior of polyacrylamide", *Prog. Polym. Sci.*, **8**, 373-468.

Kurtz, S. J., 1984, "Die geometry solutions to sharkskin melt fracture," in *Advances in Rheology*, Mena, B., Garcia-Rejon, A. and Rangel Nafaile, C., (Eds.), UNAM press, Mexico, pp. 399-407.

Larson, R. G., 1988, "Constitutive equations for Polymer melts and solutions", Butterworths series in chemical engineering, Boston.

Larson, R. G., 1992, "Instabilities in viscoelastic flows", *Rheol. Acta*, **31**, 213–263.

Lau, H. C. and Schowalter, W.R., 1986, "A model for adhesive failure of viscoelastic fluids during flow", *J. Rheol.*, **30**, 193-206.

Laun, H. M., 1982, "Elastic properties of polyethylene melts at high shear rates with respect to extrusion", *Rheol. Acta*, **21**, 464-469.

Lee, C. S., Tripp, B. C. and Magda, J. J., 1992, "Does N_1 or N_2 control the onset of edge fracture?", *Rheol. Acta*, **31**, 306-308.

Lee, K. and Mackley, M. R., 2000, "The significance of slip in matching polyethylene processing data with numerical simulation", *Journal of Non-Newtonian Fluid Mech.*, **94**, 159-177.

Leger, L., Hervet, H. and Massey, G., 1996b, "Slip at wall", in *Rheology for Polymer Melt Processing*, Piau, J-M., Agassant, J-F. (Eds.), Elsevier Science: Amsterdam, pp 337-355.

Leger, L., Hervet, H. and Massey, G., 1997b, "The role of attached polymer molecules in wall slip", *Trends in Polym. Sci.*, **5**, 40-45.

Leger, L., Hervet, H., Auroy, P., Boucher, E. and Massey, G., 1996a, "The reptation model: tests through diffusion measurements in polymer melts", in *Rheology for Polymer Melt Processing*, Piau, J-M., Agassant, J-F. (Eds.), Elsevier Science: Amsterdam, pp 1-16.

Leger, L., Hervet, H., Massey, G. and Durliat, E., 1997a, "Wall slip in polymer melts", *J. Phys.: Condens Matter*, **9**, 7719-7740.

Leger, L., Raphael, E. and Hervet, H., 1999, "Surface-anchored polymer chains: their role in adhesion and friction", *Adv. Polym. Sci.*, **138**, 185-225.

Liang, R. F. and Mackley, M. R., 2001, "The gas-assisted extrusion of molten polyethylene", *J. Rheol.*, **45**, 211-226.

Lim, F. J. and Schowalter, W. R., 1989, "Wall Slip of Narrow Molecular Weight Distribution Polybutadienes", *J. Rheol.*, **33**, 1359-1382.

Lin, Y.-H., 1985, "Explanation for stick slip melt fracture in terms of molecular dynamics in polymer melts", *J. Rheol.*, **29**, 605-637.

Lo, H. H. K., Chan, C. M. and Zhu, S. H., 1999, "Characterization of the lubricant layer formed at the interface between the extrudate and the die wall during the extrusion of high density polyethylene and fluoroelastomer blends by XPS, SIMS and SEM", *Polym. Eng. Sci.*, **39**, 721-32.

Mackley, M. R., Marshall, R. T. J. and Smeulders, J. B. A. F., 1995 "The multipass rheometer", *J. Rheol.*, **39**, 1293-1309.

Mackley, M. R., Rutgers, R. P. G. and Gilbert, D. G., 1998, "Surface instabilities during the extrusion of linear low density polyethylene", *J. Non-Newtonian Fluid Mech.*, **76**, 281-297.

Malkus, D.S., Nohel, J.A. and Plohr, B.J., 1990, "Dynamics of shear flow of a non-Newtonian fluid", *J. Comp. Phys.*, **87**, 464-487.

Marrucci, G. and Grizzuti, N., 1988, "Fast flows of concentrated polymers: predictions of the tube model on chain stretching", *Gaz. Chim. Ital.*, **118**, 179-185.

Marrucci, G., 1984, "Molecular modeling of flows of concentrated polymers" in *Advances in transport processes*, Vol. V, Mujamdar, A. S. and Mashelkar, R. A. (Eds.), John Wiley & Sons. pp 1-36.

Marrucci, G., 1986, "The Doi-Edwards model without independent alignment", *J. Non-Newtonian Fluid Mech.*, **21**, 329-336.

Marrucci, G., 1996, "Dynamics of entanglements: A non-linear model consistent with the Cox-Merz rule" *J. Non-Newtonian Fluid Mech.*, **62**, 279-289.

Marrucci, G., Bhargava, S. and Cooper, S. L., 1993, "Models of shear thickening behavior in physically crosslinked networks", *Macromolecules*, **26**, 6483-6488.

McLeish, T. C. B. and Ball, R. C., 1986, "A molecular approach to the spurt effect in polymer melt flow", *J. Polym. Sci.: Part B: Polym. Phys.*, **24**, 1735-1745.

McLeish, T. C. B., 1987, "Stability of the interface between two dynamic phases in capillary flow of linear polymer melts", *J. Polym. Sci.: Part B: Polym. Phys.*, **25**, 2253-2264.

McLeish, T. C. B. and Larson, R. G., 1998, "Molecular constitutive equations for a class of branched polymers: the pom-pom polymer", *J. Rheol.*, **42**, 81-110.

McLeish, T. C. B. and Milner, S. T., 1999, "Entangled dynamics and melt flow of branched polymers", *Adv. Polym. Sci.*, **143**, 195-256.

Mead, D. W. and Leal, L. G., 1995, "The reptation model with segmental stretch I. Basic equations and general properties", *Rheol. Acta*, **34**, 360-383.

Mead, D. W., Larson, R. G. and Doi, M., 1998, "A molecular theory for fast flow of entangled polymers", *Macromolecules*, **31**, 7895-7914.

Mead, D. W., Yavich, D. and Leal, L. G., 1995, "The reptation model with segmental stretch II. Steady flow properties", *Rheol. Acta*, **34**, 339-359.

Mendez-Sanshez, A. F., Perez-Gonzalez, J., de Vargas, L. and Tejero, J., 1999, "Two fluid model of the apparent slip phenomenon in Poiseuille flow", *Rev. Mexicana de Fisica*, **45**, 26-30.

Metzner A. B., Cohen, Y. and Rangel-Nafaile, C.,1979, "Inhomogeneous flows of non-Newtonian fluids: generation of spatial concentration gradients", *J. Non-Newtonian Fluid Mech.*, **5**, 449-462.

Mhetar, V. and Archer, L. A., 1998a, "Slip in entangled polymer solutions", *Macromolecules*, **31**, 6639-6649.

Mhetar, V. and Archer, L. A., 1998b, "Slip in Entangled Polymer Melts. 1. General Features", *Macromolecules*, **31**, 8607-8616.

Mhetar, V. and Archer, L. A., 1998c, "Slip in Entangled Polymer Melts. 2. Effect of Surface Treatment", *Macromolecules*, **31**, 8617-8622.

Migler, K. B., Massey, G., Hervet, H., Leger, L., 1994, "The slip transition at the polymer-solid interface" *J. Phys.: Condens Matter*, **6**, A301-A304.

Molenaar, J. and Koopmans, R. J., 1994, "Modeling polymer melt-flow instabilities", *J. Rheol.*, **38**, 99-109.

Mooney, M., 1931, "Explicit formulas for slip and fluidity", *J. Rheol.*, **2**, 210-222.

Moynihan, R. H., Baird, D. G. and Ramanathan, R., 1990, "Additional observations on the surface melt fracture behavior of linear low-density polyethylene", *J. Non-Newtonian Fluid Mech*., **36**, 225-263.

Muller-Mohnssen, H., Lobl, H. P. and Schauerte, W., 1987, "Direct determination of apparent slip for a ducted flow of polyacrylamide solutions", *J. Rheol.*, **31**, 323-336.

Muller-Mohnssen, H., Weiss, D. and Tippe, A., 1990, "Concentration dependent changes of apparent slip in polymer solution flow", *J. Rheol.*, **34**, 223-244.

Munstedt, H., Schmidt, M. and Wassner, E., 2000, "Stick and slip phenomena during extrusion of polyethylene melts as investigated by laser-Doppler velocimetry", *J. Rheol.*, **44**, 413-427.

Myerholtz, R. W., 1967, "Oscillating flow behavior of high density polyethylene", *J. Appl. Polym. Sci.*, **11**, 687-698.

Nam, S., 1987, "Mechanism of fluoroelastomer processing aid in extrusion of LLDPE," *Int. Polym. Proc.*, **1**, 98–101.

Nason, H. K., 1945, "A high temperature, high pressure rheometer for plastics", *J. Appl. Phys.*, **16**, 338-343.

Omari A., Moan, M. and Chauveteau, G., 1989a, "Hydrodynamic behavior of semirigid polymer at solid liquid interface", *J. Rheol.*, **35**, 89-92.

Omari A., Moan, M. and Chauveteau, G., 1989b, "Wall effects in the flow of flexible polymer solutions through small pores", *Rheol. Acta*, **28**, 520-526.

Pao, Y.-H., 1962, "Theories for the flow of dilute solutions of polymers and of non-diluted liquid polymers", *J. Polym. Sci.,* **61**, 413-448.

Pao, Y.-H., 1964, "Clarification of some aspects of the non-linear theory for viscoelastic flow", *J. Polym. Sci.* B, **2**, 437-439.

Pearson, 1985, Mechanics of polymer processing, Elsevier applied science publishers, London, U.K.

Perez-Gonzalez, D., Perez-Trejo, L., de Vargas, L. and Manero, O., 1997, "Inlet instabilities in the capillary flow of polyethylene melts", *Rheol. Acta*, **36**, 677-685.

Perez-Gonzalez, J., de Vargas, L, Pavlinek, V., Hausnerova, B. and Saha, P, 2000, "Temperature-dependent instabilities in the capillary flow of a metallocene linear low-density polyethylene melt", *J. Rheol.*, **44**, 441-451.

Perez-Gonzalez, J., De Vergas, L and Tejero, G., 1992, "Flow development of Xanthan solutions in capillary rheometers", *Rheol. Acta*, **31**, 83-93.

Pearson, D. S., Herbolzheimer, E., Grizzuti, N. and Marrucci, G., 1991, "Transient behavior of entangled polymers at high shear rates", *J. Polym. Sci. Part B, Polym. Phys.*, **29**, 1589-1597.

Person, T. J. and Denn, M. M., 1997, "The effect of die materials and pressure-dependent slip on the extrusion of linear low density polyethylene", *J. Rheol.*, **41**, 249-265.

Petrie, C. J. S. and Denn, M. M., 1976, "Instabilities in Polymer processing", *AIChE J.*, **22**, 209-236.

Petruccione, F. and Biller, P., 1988, "A numerical stochastic approach to network theories of polymeric fluids", *J. Chem. Phys.*, **89**, 577-582.

Philippoff, W., 1956, "On normal stresses, flow curves, flow birefringence, and normal Stresses of polyisobutylene solutions. Part I. Fundamental principles", *Trans. Soc. Rheol.*, **1**, 95-107.

Piau, J. M., Kissi, N. El. and Tremblay, B., 1990, "Influence of upstream instabilities and wall slip on melt fracture and sharkskin phenomena during silicones extrusion through orifice dies", *J. Non-Newtonian Fluid Mech.*, **34**, 145-180.

Piau, J.-M., Nigen, S. and Kissi, N. El., 2000, “Effect of die entrance filtering on mitigation of upstream instability during extrusion of polymer melts”, *J. Non-Newtonian Fluid Mech.*, **91**, 37-57.

Piau, J-M., Kissi, N. El. and Toussaint, F. and Mezghani, A., 1995, “Distortions of polymer melt extrudates and their elimination using slippery surfaces”, *Rheol. Acta*, **34**, 40-57.

Plucktaveesak, N., Wang, S. Q. and Halasa, A., 1999, "Interfacial flow transition in entangled polymer solutions", *Macromolecules*, **32**, 3045-3050.

Powell, R.L., 1998, “Rotational viscometry”, in *Rheological Measurements*, Collyer, A. A. and Clegg, D. W. (Eds.), Chapman &Hall, London, U.K., pp. 260–296.

Pudjijanto, S. and Denn, M. M., 1994, “A stable "island" in the slip-stick region of linear low-density polyethylene”, *J. Rheol.*, **38**, 1735-44.

Ramamurthy, A. V., 1974, “Flow Instabilities in a Capillary Rheometer for an Elastic Polymer Solution”, *Trans. Soc. Rheol.*, **18**, 431-452.

Ramamurthy, A. V., 1986, “Wall slip in viscous fluids and influence of materials of construction,” *J. Rheol.*, **30**, 337–357.

Ranganathan, M., Mackley, M. R. and Spittler, P. H. J., 1999, The application of the multipass rheometer to time dependent capillary flow measurements of a polyethylene melt” *J. Rheol.*, **43**, 443-451.

Rofe, C. J., de Vargas, L., Perez-Gonzalez, J., Lambert, R. K. and Callaghan, P. T., 1996, “Nuclear magnetic resonance imaging of apparent slip effects in xanthan solutions”, *J. Rheol.*, **40**, 1115-1128.

Rosenbaum, E. E., Randa, S. K, Hatzikiriakos, S. G., Stewart, C. W., Henry, D. L. and Buckmaster, M., 2000, “Boron nitride as a processing aid for the extrusion of polyolefins and fluoropolymers”, *Polym. Eng. Sci.*, **40**, 179-190.

Rudin, A., Schreiber, H. P. and Duchesne, D., 1990, “Use of fluorocarbon elastomers as processing additives for polyolefins”, *Polym. Plast. Technol. Eng.*, **29**, 199–234.

Rutgers, R. and Mackley, M., 2000, “The correlation of experimental surface extrusion instabilities with numerically predicted exit surface stress concentrations and melt strength for linear low density polyethylene”, *J. Rheol.*, **44**, 1319-1334.

Rutgers, R. P. G., Mackley, M. R. and Gilbert, D., 1998, “Surface instabilities during extrusion of linear low density polyethylene”, in *Dynamics of Complex Fluids*, Adams, M. J., Mashelkar, R. A., Pearson, J. R. A., Rennie, A. R. (Eds), Imperial College Press-The Royal Society: London, pp 30-37.

Sabia, R. and Mullier, M. S., 1962, "On the discontinuity in the flow curve of polyethylene", *J. Appl. Polym. Sci.*, **6***,* S.42.

Schreiber, H. P., Bagley, E. B. and Birks, A. M., 1960, " Filament distortion and die entry angle effects in polyethylene extrusion", *J. Appl. Polym. Sci.*, **4**, 362-363.

Shaw, M. T. and Wang, L., 2000, "Sharkskin melt fracture: recent findings using model geometries", in *Proceedings of XIIIth International Congress on Rheology*, Cambridge, Vol.3, pp170-173.

Shore, J. D., Ronis, D., Piche, L. and Grant, M., 1996, "Model for melt fracture in the capillary flow of polymer melts", *Phys. Rev. Lett.*, **77**, 655-658.

Sornberger, G., J. C. Quantin, R. Fajolle, B. Vergnes, and J. F. Agassant, 1987, "Experimental study of the sharkskin defect in LLDPE," *J. Non-Newtonian Fluid Mech.*, **23**, 123–135.

Stewart, C. W., 1993, "Wall slip in the extrusion of linear polyolefins", *J. Rheol.*, **37**, 499-513.

Tanaka, F. and Edwards, S. F., 1992, "Viscoelastic properties of physically crosslinked networks . 1. Transient network theory", *Macromolecules*, **25**, 1516-1523.

Tanner, R. I. And Keentok, M., 1983, "Shear Fracture in Cone-Plate Rheometry", *J. Rheol.*, **27**, 47-57.

Tapadia, P. S., Joshi, Y. M., Lele, A. K. and Mashelkar, R. A., 2000, "Influence of stereoregularity on the wall slip phenomenon in polypropylene", *Macromolecules*, **33***,* 250-252.

Tirrel, M. and Malone, M. F., 1977, "Stress induced diffusion of macromolecules", *J. Polym. Sci. Polym. Phys. Ed.*, **15**, 1569-1583.

Todd, J. E., 1972, "Stabilization of polymer types", in *Plasticisers, stabilizers and fillers*, Ritchie, P. D., Critehley, S. W. and Hill, L. (Eds.), Lliffe Books, London, U.K.pp 239-252.

Tomos, B. A., 1949, "Detection of wall effects in laminar flow of solutions of linear polymer", *J. Colloid Sci.*, **4**, 511.

Tordella, J. P., 1963, "Unstable flow of molten polymers: a second site of melt fracture", *J.App. Polym. Sci.*, **7**, 215-229.

Tordella, J. P., 1969, "Unstable flow of molten polymers", in *Rheology*, Vol. 5 , Eirich, F. R. (Ed.), Academic, New York, 1969, 57-92.

Utracki, L. A. and Gendron, R., 1984, "Pressure oscillation during extrusion of polyethylenes. II", *J. Rheol.*, **28**, 601-623.

van Bilsen, H. M. M., Fischer, H., Kolnaar, J. W. H. and Keller, A.., 1995, "A temperature window of reduced flow resistance in Polyethylene: In Situ WAXS", *Macromolecules*, **28**, 8523-8527.

Venet C. and Vergnes, B., 1997, "Experimental characterization of sharkskinin polyethylenes", *J. Rheol.*, **41**, 873-892.

Venet C. and Vergnes, B., 2000, "Stress distribution around capillary die exit: an interpretation of the onset of sharkskin defect", *J. Non-Newtonian Fluid Mech.*, **93**, 117-132.

Vinogradov, G. V., Malkin, A. Y., Yanovski, Y. G., Yarlykov, N. V. and Berezhnaya G. V., 1972, "Viscoelastic properties and flow of narrow polybutadines and polyisoprenes", *J. Polym. Sci. A2*, **10**, 1061-1084.

Vinogradov, G. V., Protasov, V. P. and Dreval, V. E., 1984, "The rheological behavior of flexible-chain polymers in the region of high shear rates and stresses, the critical rate and process of spurting, and supercritical conditions of their movement at T>Tg", *Rheol. Acta*, **23**, 46-61.

Vrahopoulou E. P. and McHugh, A. J., 1987 "Theory with non-Gaussian chain segments", *J. Rheol.*, **31**, 371-384.

Wales, J. L. S., 1969, "Apparatus for measurement of flow birefringence of polymer melts at high shear stresses", *Rheol Acta*, **8**, 38-44.

Wang, S. Q., 1992, "Transient network theory for shear thickening fluids and physically crosslinked systems", *Macromolecules*, **25**, 7003-7010.

Wang, S. Q., Drda, P. A. and Y. W. Inn, 1996 "Exploring molecular origins of sharkskin, partial slip, and slope change in flow curves of linear low density polyethylene," *J. Rheol.*, **40**, 875-898.

Wang, S.-Q. and Drda, P. A., 1996a, "Super fluid like Stick-Slip transition in capillary flow of linear Polyethylene melt. 1. General Features", *Macromolecules*, **29**, 2627-2632.

Wang, S.-Q. and Drda, P. A., 1996b, "Stick-slip transition in capillary flow of polyethylene. 2. Molecular weight and low temperature anomaly", *Macromolecules*, **29**, 4115-4119.

Wang, S-Q. and Drda, P. A., 1997a, "Stick slip transition in capillary flow of linear polyethylene: 3. Surface conditions", *Rheol Acta*, **36**, 128-134.

Wang, S-Q. and Drda, P. A., 1997b, “Molecular instabilities in capillary flow of polymer melts: interfacial stick-slip transition, wall slip and extrudate distortion,” *Macromol. Chem. Phys.*, **198,** 673-701.

Wang, S-Q., 1999, “Molecular transitions and dynamics at polymer/wall interfaces: origins of flow instabilities and wall slip”, *Adv. Polym. Sci.*, **138**, 227–275.

Watanabe, H., 1999, “Viscoelasticity and dynamics of entangled polymers”, *Prog. Polym. Sci.*, **24**, 1253-1403.

White, J. L., 1973, “Critique on flow patterns in polymer fluids at the entrance of a die and instabilities leading to extrudate distortion”, *Appl. Polym. Sci. Symp.*, **20**, 115-174.

Xing, K. C. and Schreiber, H. P., 1996, “Fluoropolymers and their effect on processing linear low-density polyethylene”, *Polym. Eng. Sci.*, **36**, 387-393.

Yang, X., Halasa, A., Ishida H. and Wang, S. Q., 1998b, "Experimental study of interfacial and constitutive phenomena in fast flow. 1. Interfacial instabilities of monodisperse polybutadiene", *Rheol. Acta*, **37**, 415-423.

Yang, X., Halasa, A., Ishida H. and Wang, S. Q., 1998c, "Experimental study of interfacial and constitutive phenomena in fast flow. 2. Barrel corrections to capillary flow of monodisperse polybutadiene", *Rheol. Acta*, **37**, 424-429

Yang, X., Ishida H. and Wang, S. Q., 1998a "Wall slip and absence of interfacial flow instabilities in capillary flow of various polymer melts", *J. Rheol.*, **42**, 63-80.

Yarin, A. L. and Graham, M. D., 1998, “A model for slip at polymer/solid interface”, *J. Rheol.*, **42**, 1419-1504.

SUMMARY

In this work, we present various semi-empirical as well as molecular models to predict slip by disentanglement and debonding mechanisms. We believe that the spurt phenomenon is interfacial in nature and either the disentanglement or the debonding of the tethered chains at the interface is responsible for the same. We initially propose a disentanglement model that is based on transient network (TN) theory. We divide a capillary (or any shear flow geometry) into two regions namely, interfacial and bulk. The interfacial region is at the solid boundary having a width of molecular dimension. A dynamic network near the wall is formed by entanglements between tethered chains and bulk chains. We solve the TN model independently in both the regions keeping the stress and the velocity continuity at the boundary of both the regions. We argue that the dynamics of adsorbed chains is different from that of the bulk molecules. We show that the transient network model predicts disentanglement of the adsorbed molecules from the bulk chains at a critical wall-shear stress. The model also successfully predicts a first order transition in the flow rate at the critical wall-shear stress. Further, it predicts a direct proportionality between the temperature and the critical wall-shear stress, which is similar to the prediction made by Brochard and de Gennes (1992). Finally, the model also predicts the diameter dependence of the flow curves, hysteresis and the possibility of fluctuations in flow rate and pressure during extrusion. We show that the model predicts wall slip in polymer melts as well as solutions, thus unifying different systems showing the slip. However, the model considers the slip solely by the disentanglement of adsorbed chains, completely disregarding debonding.

We then propose a unified model that accounts for both disentanglement and debonding into one self-consistent mathematical framework. The activation processes of adsorption and desorption are considered to occur at the wall in parallel to the stretching of the adsorbed chains. The model predicts the slip by either mechanism, debonding or disentanglement depending on the adhesive energy of the wall-polymer pair. It is shown that the stick-slip transition occurs due to the local non-monotonic flow behaviour near the wall irrespective of the mechanism of slip. The model predictions of the critical wall shear stress are in good agreement with experiments for various adhesive energies of wall polymer pair. The model further predicts that the temperature dependence of the

critical wall shear stress for debonding is different than that of disentanglement mechanism under certain experimental conditions. The unified model encompasses different systems (viz. entangled solutions and melts) and diverse mechanisms (viz. disentanglement and debonding) in a common mathematical framework. To validate the predictions of unified model, we measure the critical stress for sudden slip due to debonding for various temperatures using cone and plate viscometer with fluoroelastomer-coated cone. The temperature dependence of the critical stress for instability (slip) on a coated cone is found out to be inversely dependent on temperature. This is expected for the case of debonding, which is known to be an activation process. The unified slip model successfully predicts the observed temperature dependence quantitatively.

Both these models (disentanglement and debonding) developed using TN theory are semi-empirical in nature and contains adjustable parameters arising from the phenomenological nature of the rates of creation and breakage of network. While this approach does not throw light on the details of molecular dynamics of polymer chains near the wall, it has the inherent advantage of presenting a simpler constitutive equation that captures the essence of slip phenomena by either of the two physical mechanisms. Such a constitutive equation could be useful for providing numerical solutions to real engineering problems. While the unified model provides an "engineering model" that can be useful for predicting slipping flows, it is mainly a phenomenological model consisting of several model parameters that have to be determined through independent rheological experiments. It is desirable to develop a truly molecular model that can predict slip on the basis of only molecular parameters and no other adjustable parameters.

Using the tube theory of entangled polymeric liquid, we develop a molecular model for tethered chains in the mushroom region. We make use of the contour variable tube model, which is the most refined version in the series of the tube models. We consider all possible modes of the relaxation applicable to a tethered chain namely, constraint release (CR), convective constraint release (CCR), fluctuations and retraction. The most important concept proposed in the model is that the tethered molecules experience a suppressed CCR relaxation; because of which they are easily oriented by shear flow above a critical shear rate and critical shear stress. The model predicts a discontinuous

slip that arises from sudden disentanglement of the tethered chains from the flowing bulk chains.

We show that the tendency to show stick-slip instability increases with molecular weight of the bulk molecules and of the tethered molecules. Shorter tethered molecules do not orient easily compared to longer molecules. And hence the die having small tethered chains will not show the transition. For low values of the interfacial modulus the model predicts the critical slip velocity to be $V_s^* \sim P^{3.4} N^{-1}$, where P is number of segments in the bulk molecule while N is number of segments in the tethered molecule, which is in agreement with previous models. But for the values of interfacial modulus comparable to bulk modulus model predicts complicated scaling. The model further predicts that the stick-slip transition is caused by a coil-to-stretch transition of the tethered molecules, which is also in agreement with the earlier scaling models [Brochard and de Gennes, 1992]. The model also predicts two regions for the slip length, a weak slip region for low shear rates and a strong-slip region for high shear rates. Our model quantitatively predicts the critical slip velocity at which strong slip occurs, but requires much larger number of entanglements per unit volume in the interfacial region in order to quantitatively match the experimental slip length in the weak-slip region. We hope that the new molecular insights proposed in this work will stimulate further theoretical and experimental work to understand this phenomenon in complicated systems.

ABSTRACT

Commercial plastic extrusion processes are severely limited by the occurrence of instabilities above a critical production rate. There are different types of instabilities observed in an extrusion process. In this work, we are primarily concerned with the stick-slip instability, which occurs above a critical wall shear stress during extrusion and is characterized by fluctuations in flow rate and pressure drop as well as the *bamboo-like* distorted extrudate surface. The stick-slip instability is believed to occur because of a sudden slip of the polymer chains at the die wall either due to disentanglement or debonding mechanism. In this work we attempt to theoretically understand this phenomenon through empirical and molecular models.

Initially, we use the framework a transient network theory, which is suitable for describing dynamics of entangled liquids to model the slip phenomenon. We consider the case of polymers flowing over a high adhesive energy surface. We argue that the dynamics of chain entanglement and disentanglement at the wall is different from that in the bulk. We show that the severe disentanglement in the interfacial region can give rise to non-monotonic flow curve locally in that region. This model can predict all features of wall slip such as discontinuous increase in flow rate, diameter dependent flow curves, hysteresis and the possibility of pressure and flow rate oscillations.

Next, we generalize the above model into a unified slip model, which predicts wall slip by either disentanglement or by debonding mechanism, depending upon the adhesive energy of the wall-polymer pair. The model predictions of the critical wall shear stress are in good agreement with experiments for various adhesive energies of the wall-polymer pair. The model predicts that the temperature dependence of the critical wall shear stress for debonding is different than that of disentanglement mechanism under certain experimental conditions. To validate the predictions of unified model, we measure the critical stress for sudden slip due to debonding for various temperatures using cone and plate viscometer with fluoroelastomer-coated cone. The temperature dependence of the critical stress for instability (slip) on a coated cone is found out to be inversely dependent on temperature, which expected for the case of debonding.

While the phenomenological models developed in the first part of this work are able to predict various macroscopic experimental observations of slip, it is desirable to

understand the key molecular dynamics that are responsible for slip. Towards this end we develop, in the final part of this thesis, a parameter-free tube model for predicting the stick-slip phenomenon. The model, which is based on the contour variable model [Mead *et al.*, 1998, *Macromolecules*, **31**, 7895], considers the dynamics of the tethered chains, which are grafted on a high-energy wall and which are entangled with the bulk chains flowing past them. We show that the restricted relaxation modes of the tethered molecule give rise to discontinuous slip instability. More specifically, the slow relaxation of the tethered chains due to the subdued constraint release by the convecting bulk chains (CCR) plays a crucial role in determining the nature of the flow curve near the wall. The restricted CCR experienced by a tethered chain is unable to randomize its flow-induced orientation above a critical shear rate or stress. This decreases the resistance to flow for the bulk chains, which suddenly slip past the oriented tethered chains. The model correctly predicts the molecular weight dependence of the slip length, critical slip velocity and critical wall shear stress. It also quantitatively predicts the slip length and the critical slip velocity for a PDMS melt, for which valuable molecular level experimental data are available in the literature.

Publications based on the work done in this thesis

1. Joshi, Y. M., Lele, A. K. and Mashelkar R. A., 2000, "Slipping fluids: A unified transient network model", *J. Non-Newtonian Fluid Mech.*, **89**, 303-335.
2. Joshi, Y. M., Lele, A. K., and Mashelkar R. A, 2000, "A Unified wall slip model", *J. Non-Newtonian Fluid Mech.*, **94** 135-149.
3. Joshi, Y. M., Tapadia, P. S., Lele, A. K. and Mashelkar R. A., 2000, "Temperature dependence of the critical stress for wall-slip by debonding", *J. Non-Newtonian Fluid Mech.*, **94** 151-157.
4. Joshi, Y. M., Lele, A. K. and Mashelkar R. A., 2001, "A molecular model for wall slip: Role of convective constraint release", *Macromolecules*, in press.